Hilje M. Doekes

Microbial Evolution at Multiple Scales

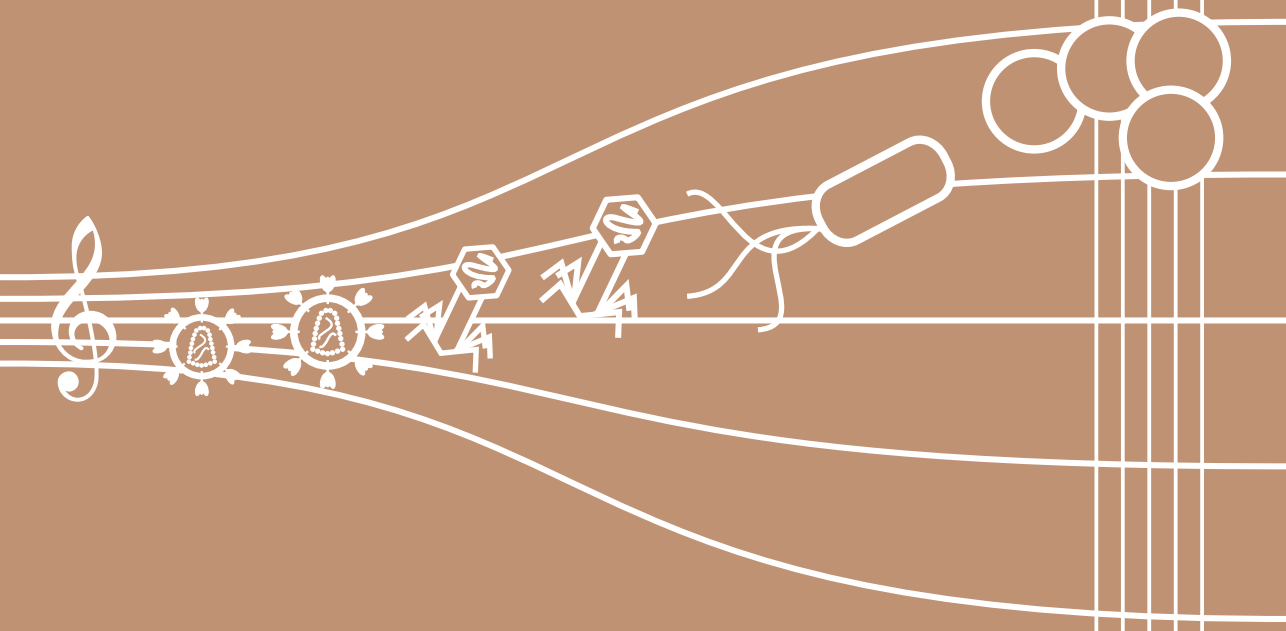

Microbial Evolution

at

Multiple Scales

Hilje M. Doekes

Hilje M. Doekes
Microbial Evolution at Multiple Scales
PhD thesis, Utrecht University

Cover: *A scale of microbes*, design by Leo de Visser and Hilje Doekes
Printing: Ridderprint | www.ridderprint.nl
ISBN: 978-94-6416-031-4

Microbial Evolution at Multiple Scales

Evolutie van Microben op Verschillende Schalen
(met een samenvatting in het Nederlands)

Proefschrift

ter verkrijging van de graad van doctor aan de Universiteit Utrecht op gezag van de rector magnificus, prof.dr. H.R.B.M. Kummeling, ingevolge het besluit van het college voor promoties in het openbaar te verdedigen op woensdag 23 september 2020 des middags te 4.15 uur

door

Hilje Marijke Doekes

geboren op 7 mei 1989 te Utrecht

Promotor: Prof. dr. R.J. de Boer

Copromotor: Dr. R. Hermsen

The studies described in this thesis were financially supported by the
Human Frontiers Science Program (HFSP), grant number RGY0072/2015.

Thesis assessment committee:

Prof. dr. S. Gandon	Centre d'Ecologie Fonctionelle et Evolutive, CNRS Montpellier, France
Prof. dr. J.S. Weitz	Georgia Institute of Technology, Atlanta, United States of America
Prof. dr. L. Chao	University of California at San Diego, United States of America
Prof. dr. F.J. Weissing	University of Groningen, the Netherlands
Dr. D.E. Rozen	Leiden University, the Netherlands

Contents

1

Introduction

1.1. Preface

Microbial evolution...

Microbes are found in all known habitats on earth, from the deep ocean to the human gut. They play an important role in shaping the world's ecosystems. Microbial consortia are for instance responsible for nutrient cycling in oceans and soils (Arrigo, 2005; van der Heijden *et al.*, 2008), while pathogenic microbes modulate biodiversity by controlling the populations of their host organisms (Thingstad *et al.*, 2014; Eck *et al.*, 2019).

While microbes are small and seemingly less complex than multicellular life forms, they are by no means simple or uninteresting. Many microbes live in dense, complex communities, in which they compete with others for nutrients and space (Hibbing *et al.*, 2010; Ghoul and Mitri, 2016). To survive and thrive in these communities, microbes display a wide variety of "social" behaviours (West *et al.*, 2006; Nadell *et al.*, 2009; Díaz-Muñoz *et al.*, 2017). For instance, they cooperate with each other by secreting public goods (Nadell *et al.*, 2016; Kramer *et al.*, 2020), engage in "microbial warfare" to harm or kill competitors (Riley and Wertz, 2002b; Granato *et al.*, 2019), or communicate their presence through the secretion of signalling molecules (Nealson *et al.*, 1970; Mukherjee and Bassler, 2019). These behaviours are not reserved to free-living organisms: even bacterial viruses engage in virus-virus communication (Erez *et al.*, 2017; Abedon, 2019).

Like any life form, the microbes displaying these intriguing behaviours arose through Darwinian evolution. If we wish to understand the complex behaviours of microbes, we need to study the selection pressures driving their evolution.

... at multiple scales

The environments in which microbes live are often highly variable, either over space, over time, or both. Most microbial communities are spatially structured (Nadell *et al.*, 2016; Yanni *et al.*, 2019), and interactions in these communities happen over small length scales (Dal Co *et al.*, 2020). Natural selection results from a range of processes, such as competition and cooperation, that all happen at potentially different scales. To understand the evolution of microbes in structured environments, we should take these different scales into account.

When studying the evolution of pathogens, a different distinction in levels of selection can be made. At the within-host level, pathogens adapt to their current host individual. At the epidemiological level, however, pathogens are selected for their ability to spread through a population of hosts. The selection pressures at these two levels are not necessarily aligned, and evolution depends on the balance

between the contributions of the two levels to selection (Coombs *et al.*, 2007; Mideo *et al.*, 2008). Especially for pathogens that cause long-lasting infections, such as the human immunodeficiency virus (HIV), the distinction between the within-host and epidemiological level is also a distinction between time scales, with within-host evolution occurring at much shorter time spans than epidemiological adaptation (Levin and Bull, 1994; Lythgoe *et al.*, 2013).

The title of this thesis - "Microbial evolution at multiple scales" - was chosen for two reasons. First, because in this thesis we use mathematical and computational modelling to study microbial evolution as the multilevel or multiscale process it often is. Second, because while doing so we will consider examples of multiple "scales of microbe": human viruses, bacterial viruses, and bacteria.

Before we dig in, the remainder of this chapter provides some background on how the spatial structure of microbial communities affects the evolution of social behaviours (and *vice versa*), how the effect of population structure on natural selection can be mathematically described, and how pathogen evolution is shaped by within- and between-host selection pressures.

1.2. Evolution of microbial interactions in spatially structured populations

Most microbes live in complex, spatially structured populations (Nadell *et al.*, 2016; Ghoul and Mitri, 2016). In those populations, the local environment of an organism strongly varies with its location, both in terms of abiotic (*e.g.*, oxygen level) as well as biotic conditions (*e.g.*, severity of competition for nutrients). Below, and throughout this thesis, we will focus on these biotic factors. On one hand, spatial structures dictate with whom an organism competes and otherwise interacts, thus shaping its evolution. On the other hand, the spatial structure of a population depends on the characteristics of the organisms that compose it. By interacting with their environment, organisms shape their own environment, and the way they do so depends on their evolved characteristics. This feedback between ecology and evolution may give rise to structures and corresponding selection pressures at scales larger than that of single organisms (Hogeweg, 1994; Johnson and Boerlijst, 2002; Lion and van Baalen, 2008); we will describe several examples below.

The spatial structure of microbial communities arises from various processes (Yanni *et al.*, 2019). Firstly, replication is a local process. In many environments the dispersal of microbes is furthermore limited, such that offspring remain close to their parent cells. This leads to positive genetic assortment (Tolker-Nielsen and Molin, 2000; Millet *et al.*, 2014; Mitri *et al.*, 2016). Secondly, social interactions, such as

the secretion of anticompetitor toxins and public goods, also affect spatial structure (*e.g.*, reviewed by Nadell *et al.* (2016)). We will consider these two examples in some more detail, focusing on the feedback between (the evolution of) the behaviour and spatial structure.

1.2.1. Interference competition through the secretion of anticompetitor toxins

Microbes have evolved a stunning variety of mechanisms to harm or kill competitors (Granato *et al.*, 2019). According to current knowledge, the most common of these "microbial warfare" mechanisms is the production of anticompetitor toxins: almost all known bacterial species produce at least one such toxin (Klaenhammer, 1988; Riley and Wertz, 2002a; Gonzalez and Mavridou, 2019; Granato *et al.*, 2019). From early on, it was recognised that spatial structure is a key determinant of the outcome of toxin-mediated interference competition. In 1981, Chao and Levin showed that while in liquid culture a toxin-producing *Escherichia coli* strain could invade a non-producing sensitive strain only if its initial frequency was above a certain threshold, no such minimal initial density was required on agar plates. The same result has recently been found for streptomycin-producing *Streptomyces griseus* (Westhoff *et al.*, 2020). In well-mixed liquid cultures, the toxin produced by a small population of toxin-producing cells is spread out over the entire culture, and hence occurs in low concentrations that are hardly harmful to the susceptible cells. Since toxin production is metabolically costly (Chao and Levin, 1981; Kerr *et al.*, 2002; Maldonado-Barragán and West, 2020), under these circumstances the toxin-producing strain is outcompeted by the faster-growing sensitive strain. In spatially structured cultures, however, the toxin acts locally and even a small initial population of toxin-producing cells can produce sufficient toxin to locally gain an advantage over the sensitive strain. In simple environments, such as agar plates, this will usually result in competitive exclusion of the sensitive strain by the toxin-producing strain (Chao and Levin, 1981; Durrett and Levin, 1997; Westhoff *et al.*, 2020).

Modelling work on more complex environments, such as biofilms, has suggested that toxin-mediated interference competition can also result in a spatial structure consisting of strongly segregated patches of toxin-producing and sensitive cells (Figure 1.1a; Bucci *et al.* (2011); Yanni *et al.* (2019)), a structure also observed in experimentally grown biofilms (Tait and Sutherland, 2002). In these models, a number of bacteria is seeded on a surface, and is then allowed to replicate. Nutrients are assumed to flow in from above, and bacterial growth is limited by the local nutrient availability. Cells that experience very low nutrient concentrations for a long time die, forming a bottom layer of inert material on which the biofilm can continue to grow. If the biofilm is seeded with a low number of initial cells, over time local protrusions arise that consist of a single type of bacteria (toxin-producing

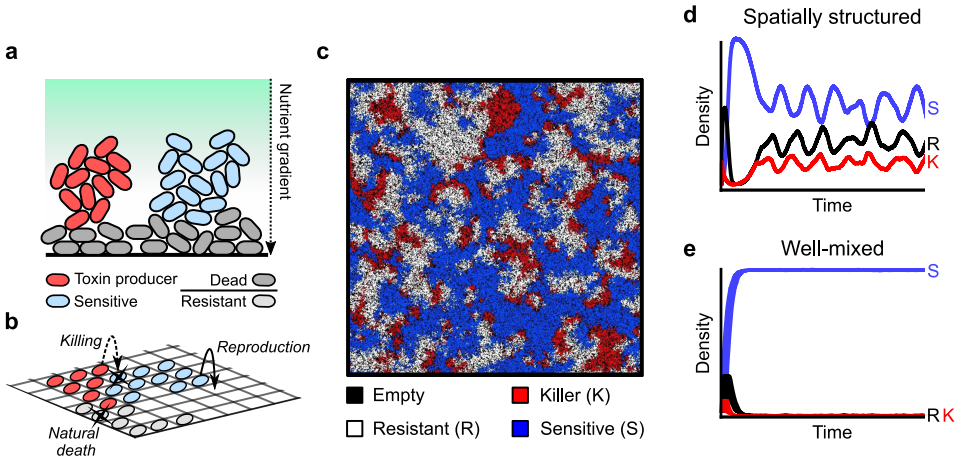

Figure 1.1. Individual-based models of spatially structured populations of toxin-producing, sensitive, and resistant bacteria. (a) In a biofilm model, spatially segregated protrusions of toxin-producing and sensitive bacteria can coexist (Bucci *et al.*, 2011). (b) 2D simulation model capturing the main interactions between toxin-producing, sensitive, and resistant bacteria. (c) Snapshot of the simulation lattice of model (b) showing KRS-dynamics (Kerr *et al.* (2002); see also chapter 4). (d-e) Spatial structure strongly affects the eco-evolutionary dynamics. In a spatially structured population toxin-producing, resistant, and sensitive cells coexist, while in a well-mixed population the sensitive strain dominates the population.

or sensitive). The distance between these protrusions is such that the effect of the toxin on sensitive cells is sufficiently small, allowing the two strains to coexist.

Once a toxin-producing strain has locally become highly frequent, natural selection will favour mutants that retain resistance to the toxin, but no longer produce it, hence avoiding the metabolic costs of toxin production (Kerr *et al.*, 2002; Weber *et al.*, 2014). Such resistant cells are "cheaters" compared to the toxin-producing strain: they benefit from the action of the toxin without contributing to its production. The emergence of resistant cheater strains leads to non-transitive dominance, similar to the game of rock-paper-scissors: toxin-producing cells locally outcompete sensitive cells, resistant cells locally outcompete toxin-producing cells, and sensitive cells locally outcompete resistant cells (because they avoid the metabolic costs of resistance) (Kerr *et al.*, 2002). Models of these interactions in a spatially structured population have shown that such interactions cause wave-like spatial patterns to emerge, in which the three types continuously chase each other (Figure 1.1b–c; Durrett and Levin (1997); Reichenbach *et al.* (2007)). In these dynamical patterns,

the three species stably coexist (Figure 1.1d). When pattern formation is prevented by continuously mixing the population, coexistence is no longer possible and the sensitive strain fixes in the population (Figure 1.1e). Hence, the evolution of toxin production and resistance depends crucially on local interactions and the spatial structure of populations. At the same time, the spatial structure arises from the interactions between toxin-producing, resistant, and sensitive cells.

1.2.2. Cooperation through the secretion of public goods

Next to anticompetitor toxins, many microbes also secrete a variety of "public goods" that promote the growth of not only the secreting cell, but also cells in the vicinity (Nadell *et al.*, 2016; Estrela *et al.*, 2019). The best-studied public goods are the siderophores produced by *Pseudomonas aeruginosa*: iron-scavenging molecules that allow bacteria to take up this trace element. Production of siderophores is metabolically costly (Griffin *et al.*, 2004), and non-siderophore-producing cheater strains are readily found in nature (de Vos *et al.*, 2001; Butaitė *et al.*, 2017). As with the evolution of toxin production, spatial structure plays a major role in explaining the evolution of such cooperative public good production.

Cooperative behaviour is usually subdivided in two types: *mutualistic* behaviour that benefits other individuals but also benefits the actor, and *altruistic* behaviour that benefits other individuals while reducing the actor's fitness (West *et al.*, 2006; Nadell *et al.*, 2009). Explaining the evolution of cooperation, and especially altruism, has been a central question in social evolutionary theory for a long time (Hamilton, 1964; Wilson, 1975). In general, social evolutionary theory predicts that altruistic behaviour can evolve only if the interactions between individuals are structured in some way, such that the altruistic behaviour preferentially benefits other altruists (Hamilton, 1964; Wilson, 1975; Fletcher and Doebeli, 2009). As argued in the beginning of this section, such assortment can easily arise in microbial communities from local reproduction and limited dispersal, such that the offspring of altruists (which likely also display altruistic behaviour) tend to be physically close to the parent cells. Indeed, simulation studies have shown that public good production can readily evolve in spatially structured microbial populations, but only if the interaction range of the public good is smaller than or similar to the spatial scale of assortment (Allison, 2005; Nadell *et al.*, 2010; Allen *et al.*, 2013).

1.2.3. Evolution of altruism and multilevel selection theory

To further illustrate how spatial population structure can shape the evolution of altruism, let us consider D.S. Wilson's trait-group model for the evolution of altruism (Figure 1.2; Wilson (1975)). In this model, organisms can express an altruistic behaviour ("altruists"), or not ("cheaters"). Consider a population of N organisms that are distributed over m groups with group sizes $n_1, n_2, \ldots, n_m$ ($\sum_{k=1}^{m} n_k = N$).

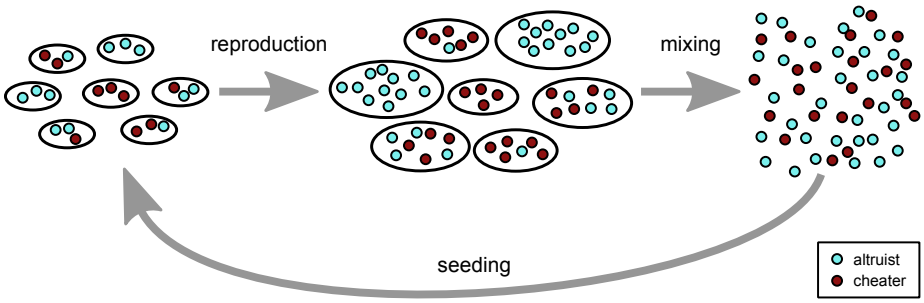

Figure 1.2. Illustration of trait-group model for the evolution of altruism (Wilson, 1975).

Within these groups, the organisms engage in interactions that determine their fitness, defined as the number of offspring that they will contribute to the next generation. Specifically, the fitness of an organism depends on its own type, with altruists paying a fitness cost compared to cheaters, and on the fraction of altruists in its group, with the fitness of all organisms in a group increasing with this fraction. All reproduction events are summarised in a single reproduction step, replacing each organism with its offspring (the parent organisms are assumed to die in this process). Reproduction is asexual and for simplicity we ignore mutations, such that the offspring of altruists are always altruists, and the offspring of cheaters are always cheaters. After this reproduction step, the population is mixed, and new founder organisms are randomly chosen to seed the next iteration of the model (Fig 1.2).

What selection pressures act on the altruists in this simple model? Within any single group, the fitness of cheaters is higher than the fitness of altruists, because the cheaters are exposed to the same environment as the altruists and do not pay the fitness cost. The *within-group selection* is hence clearly negative. However, if the positive effects of altruistic behaviour are large enough, the mean fitness of organisms in groups with a large fraction of altruists is higher than the mean fitness of organisms in groups with a small fraction of altruists. In other words, the *between-group selection* is positive. The overall selection on altruism depends on the balance between the selection pressures at these two levels (Wilson, 1975; Okasha, 2006).

These notions of within- and between-group selection can be mathematically formalised. Fifty years ago, George R. Price derived a highly general mathematical description of natural selection (Price (1970)). Considering a population of organisms that differ in some trait ϕ, Price showed that the change in the population

mean value of ϕ over some time step (*e.g.*, one generation) due to selection is equal to the selection differential

$$S \equiv \mathrm{Cov}\,(\phi, w)\,, \tag{1.1}$$

where w is the relative fitness of organisms (see Box 1.1 for a derivation). Price's equation provides a formalisation of what it means for a trait to be under positive or negative selection: if the trait-value ϕ positively covaries with fitness, selection will favour higher trait-values.

Turning back to Wilson's trait-group model, we let ϕ be equal to 1 if an organism is an altruist, and 0 if it is a cheater. We let ϕ_{jk} denote the ϕ-value of the j^{th} organism in the k^{th} group, and similarly write w_{jk} for the relative fitness of this organism. The fraction of altruists in a group k is then given by $\Phi_k \equiv \frac{1}{n_k}\sum_{j=1}^{n_k}\phi_{jk}$, and the mean fitness of organisms in group k is $v_k \equiv \frac{1}{n_k}\sum_{j=1}^{n_k} w_{jk}$.[1] We write $\overline{\phi}$ for the population mean of ϕ (see Box 1.1). Following Price (1972) and Wade (1985), we can now derive

$$\begin{aligned} S = \mathrm{Cov}\,(\phi, w) &= \overline{\phi w} - \overline{\phi}\,\overline{w} \\ &= \frac{1}{N}\sum_{k=1}^{m}\sum_{j=1}^{n_k}\phi_{jk}w_{jk} - \left(\frac{1}{N}\sum_{k=1}^{m}\sum_{j=1}^{n_k}\phi_{jk}\right)\left(\frac{1}{N}\sum_{k=1}^{m}\sum_{j=1}^{n_k} w_{jk}\right). \end{aligned}$$

Adding and substracting $\frac{1}{N}\sum_{k=1}^{m} n_k \Phi_k\, v_k$ and some regrouping yields

$$\begin{aligned} S &= \frac{1}{N}\sum_{k=1}^{m} n_k\left(\frac{1}{n_k}\sum_{j=1}^{n_k}\phi_{jk}w_{jk} - \Phi_k v_k\right) + \sum_{k=1}^{m}\frac{n_k}{N}\Phi_k v_k - \left(\sum_{k=1}^{m}\frac{n_k}{N}\Phi_k\right)\left(\sum_{k=1}^{m}\frac{n_k}{N}v_k\right), \\ &= \underbrace{\sum_{k=1}^{m}\frac{n_k}{N}\mathrm{Cov}_k\left(\phi_{jk}, w_{jk}\right)}_{\text{mean within-group selection}} + \underbrace{\mathrm{Cov}_{\mathrm{g}}\left(\Phi_k, v_k\right)}_{\text{between-group selection}}\,, \end{aligned} \tag{1.2}$$

where Cov_k denotes the covariance within the k^{th} group, and $\mathrm{Cov}_{\mathrm{g}}$ is the between-group covariance, in which each group's contribution is weighted by its size. The first term of the right-hand side of Eq 1.2 is the mean over all groups of the covariance between phenotype and fitness within that group (with groups weighted by their size). It hence describes within-group selection. The second term, on the other hand, is the covariance between the mean ϕ-value in a group (*i.e.*, the fraction of altruists) and the mean fitness of the organisms in that group. It hence describes between-group selection.

[1] To be precise, v_k is the mean of the relative fitness of organisms in group k, where relative fitness is calculate compared to the whole population. If $v_k > 1$, the mean fitness of organisms in group k is higher than the mean fitness of the whole population.

1

Box 1.1: The Price Equation (Price, 1970)

Consider a population of N parent entities, each of which is characterised by some characteristic ϕ_i ($i = 1, 2, \ldots, N$). This characteristic might be a continuous phenotypic value of the entities, such as a bacterium's investment in public good production or a pathogen's virulence, an indicator variable that is 1 if the entity displays a certain behaviour (*e.g.*, altruism) and 0 if it does not, or a measure of allelic dosage. Let $\overline{\phi} = \frac{1}{N}\sum_{i=1}^{N}\phi_i$ denote the mean value of ϕ in the population. We will describe how this population mean changes in a given time interval Δt, which we call a generation. For simplicity, we will here assume that entities reproduce asexually and that the generations do not overlap, the framework can however readily be extended to relax these assumptions (see *e.g.*, Day and Bonduriansky (2011); Frank (2012); Gardner (2020)).
Let W_i be the fitness of parent i, defined as its number of offspring in the next generation. We let ϕ_i' represent the mean value of ϕ among the offspring of parent i, and write $\phi_i' = \phi_i + \Delta\phi_i$. The term $\Delta\phi_i$ describes the part of the ϕ-value that is not faithfully inherited from parent to offspring, and hence captures *transmission biases*. The mean value of ϕ in the offspring population is now given by

$$\overline{\phi}_{\mathrm{o}} = \frac{1}{N}\sum_{i=1}^{N}\frac{W_i}{\overline{W}}\phi_i', \tag{1.3}$$

where $\overline{W}$ is the mean fitness of the parent entities, and $\frac{W_i}{\overline{W}}$ is the relative contribution of entity i to the offspring population; we denote this relative fitness by w_i, and note that $\sum_{i=1}^{N} w_i = 1$. We can now write the change in the mean phenotype $\Delta\overline{\phi} = \overline{\phi}_{\mathrm{o}} - \overline{\phi}$ as

$$\begin{aligned}
\Delta\overline{\phi} &= \frac{1}{N}\sum_{i=1}^{N} w_i(\phi_i + \Delta\phi_i) - \frac{1}{N}\sum_{i=1}^{N}\phi_i \\
&= \frac{1}{N}\sum_{i=1}^{N} w_i\phi_i - \overline{w}\frac{1}{N}\sum_{i=1}^{N}\phi_i + \sum_{i=1}^{N} w_i\Delta\phi_i \\
&= \overline{w\phi} - \overline{w}\,\overline{\phi} + \overline{w\Delta\phi} \\
&= \mathrm{Cov}(\phi, w) + \overline{w\Delta\phi}
\end{aligned} \tag{1.4}$$

Eq 1.4 is the Price equation. The first term in its right-hand side describes the effect of fitness differences between parents, it is therefore also called the *selection differential*. The second term describes the effects of non-faithful inheritance, and is therefore also called the *transmission term*.

As an aside, note that Eq 1.2 is a special case of the law of total covariance, where the conditional variable describes what group an organism is in.

What does Eq 1.2 tell us? Firstly, it provides general conditions for the evolution of altruism: the positive between-group selection should outweigh the negative within-group selection: $\mathrm{Cov}_{\mathrm{g}}(\Phi_k, v_k) > -\sum_{k=1}^{m} \frac{n_k}{N} \mathrm{Cov}_k(\phi_{jk}, w_{jk})$. Secondly, it helps us understand how assortment affects the evolution of altruism (Okasha, 2006). Assortment at the within-group level reduces the variation within-groups, while increasing the variation between groups. Since covariances increase with increasing variation, increasing assortment reduces the within-group selection while increasing the between-group selection, and hence favours the evolution of altruism.

Lastly, Eq 1.2 provides a means to measure selection at the within- and between-group level. Chuang *et al.* (2009) did so in an experimental model system of two *E. coli* strains: a public good producer and a cheater. They inoculated cultures with a range of different initial ratios between the public-good producer and the cheater, and then monitored how the relative frequency of the public-good producer changed over time. Within single cultures, the frequency of public-good producers always declined, *i.e.*, the first term in the right hand side of Eq 1.2 was negative. Over the whole population, however, the frequency of public-good producers increased, *i.e.*, the term in the left hand side of Eq 1.2 was positive. Hence, the between-group selection had to be positive and substantial. This study neatly demonstrates how within- and between-group selection act in different directions. Varying the inoculum size furthermore allowed a direct test of the prediction that increased variation in the initial composition of groups - which corresponds to increased assortment[2] - promotes the evolution of altruism; this was indeed found to be the case (Chuang *et al.*, 2009).

In summary, we have seen that the evolution of toxin-based competition and cooperation among microbes is strongly affected by spatial structure. The effects of spatial structure can be mathematically described by decomposing the selection differential in a within-group and a between-group component (Eq 1.2). While we derived this decomposition in the light of Wilson's trait-group model, Eq 1.2 is generally valid for any population that is subdivided in groups. It does however require that the groups of organisms in the evolving population are distinct and non-overlapping. In chapter 5, we derive a similar decomposition of selection pressures for populations in continuous space.

[2]If public-good producers and cheaters are initially mixed at a 1:1 ratio and the inoculum size is large, the initial frequency of public-good producing cells is very similar for all cultures, *i.e.*, $\Phi_k \approx 0.5$ for all cultures k. The between-culture variation is then small, and the within-culture variation is large (within-culture variation is maximal if $\Phi_k = 0.5$). If the inoculum size is small, by chance populations are more often initialised with either a large or small frequency of public-good producers. This increases the between-culture variation and decreases within-culture variation.

So far, we have focused on the effects of spatial structure on microbial evolution. Next, we will turn our attention to another form of multilevel structure.

1.3. Multilevel pathogen evolution and the transmission-virulence trade-off

Pathogens that infect multicellular hosts adapt to their host at multiple distinct levels. At the epidemiological level, pathogens are selected on their ability to spread between hosts. At the within-host level, however, they are selected on other characteristics, such as rapid host cell exploitation or immune escape. To understand the evolution of these pathogens, we should consider the interplay between these two levels of selection.

For a pathogen to be successful over long time scales, it has to be able to spread between host individuals. Selection at this between-host level acts on epidemiological characteristics such as transmission rate and virulence (defined here as the infection-induced host mortality rate). In an unrestricted setting, pathogens are expected to evolve an infinite transmission rate and a zero virulence, because this would allow them to spread infinitely fast from host to host while also maximising the time spent in a single host (Anderson and May, 1982; Alizon *et al.*, 2009). However, restrictions are often assumed to exist in the form of a *transmission-virulence trade-off* (Anderson and May, 1982; Bremermann and Pickering, 1983) in which the transmission rate and virulence are positively associated. This trade-off captures the idea that in order to obtain a high transmission rate, the pathogen density in the transmitting host should be high, which in turn causes damage to the host and hence leads to a high virulence. Under a transmission-virulence trade-off, evolution at the epidemiological level is expected to select those pathogen strains (*i.e.*, those transmission rate-virulence combinations) that maximise the baseline reproduction ratio R_0 [3] (Anderson and May, 1982; Alizon *et al.*, 2009; Shirreff *et al.*, 2011).

While the existence of a trade-off between transmission and virulence seems very reasonable, these trade-offs are difficult to measure experimentally (Alizon *et al.*, 2009). Nevertheless, some evidence supporting the existence of transmission-virulence trade-offs does exist (reviewed by Alizon *et al.* (2009)). For instance, in mixed-strain infection experiments of mice with rodent malaria the virulence (measured as the damage inflicted to the host's red blood cells) was positively correlated with transmission success (de Roode *et al.*, 2005; Bell *et al.*, 2006). Furthermore, large cohort studies of HIV infection showed that both HIV virulence (measured as the inverse of time until the onset of AIDS) and transmission rate increase with

[3] R_0 is defined as the number of new infections caused by an infected individual in an otherwise susceptible host population.

the set-point viral load: the relatively stable concentration of viral particles in the blood during chronic infection (Fraser *et al.*, 2007).

Many epidemiological evolutionary models assume that host individuals are infected by a single genetic variant of the pathogen. In reality, however, hosts often carry more than one variant as a result of super-infection or the generation of pathogen variation by mutations during within-host replication (Read and Taylor, 2001; Cressler *et al.*, 2016). The latter effect is especially prominent in rapidly replicating pathogens with mutation-prone genetic replication mechanisms, such as HIV, and gives rise to a within-host quasispecies that is shaped by mutations and selection (Maldarelli *et al.*, 2013). Variation in the pathogen population within a single host opens the door to within-host evolution. Selection at this level acts on within-host pathogen characteristics such as immune evasion and within-host replication capacity (RC) (Ganusov *et al.*, 2011; Troyer *et al.*, 2005; Kouyos *et al.*, 2011).

While selection at the within-host level does not act directly on the epidemiological characteristics of a pathogen, it might still have major implications for evolution at the between-host level. Firstly, extensive within-host evolution can obscure the heritability of epidemiological characteristics, because mutations might accumulate that are selectively neutral at the within-host level but affect transmission rate or virulence. Secondly, the epidemiological characteristics might be correlated with within-host characteristics that are under selection. For instance, positive associations between RC and virulence have been found in HIV (Quinones-Mateu *et al.*, 2000; Kouyos *et al.*, 2011), rodent malaria (de Roode *et al.*, 2005; Bell *et al.*, 2006), and *Daphnia*-infecting bacteria (Ben-Ami *et al.*, 2008; Ben-Ami and Routtu, 2013). Such a link between within-host replication capacity and virulence is conceivable: a pathogen that replicates rapidly within a host is likely to cause more damage to that host. This leads to conflicting selection pressures at the two different levels: within-host selection favours pathogen strains with high RC and hence high levels of virulence, while between-host selection favours strains with intermediate levels of virulence that optimise between-host transmission. Especially if pathogens cause long-lasting chronic infections this conflict in selection pressures can have great consequences, possibly preventing the long-term adaptation of the pathogen to between-host transmission (Levin and Bull, 1994).

To better understand pathogen evolution under selection at these different levels, nested dynamical models can be used that link a model of within-host dynamics to an epidemiological model (Figure 1.3; Sasaki and Iwasa (1991); Gilchrist and Sasaki (2002); Mideo *et al.* (2008)). As an example, we will here consider the multilevel evolution of HIV (following Lythgoe *et al.* (2013)).

Consider n genetic variants of HIV (which we will call strains for short) that differ in their within-host replication rate γ. We initiate new infections with a

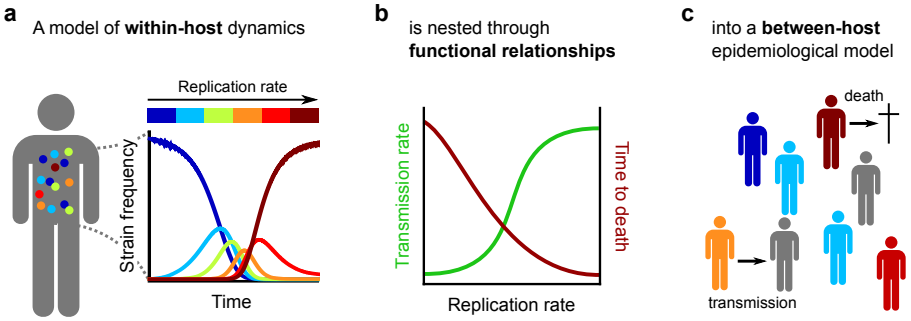

Figure 1.3. Nested dynamical model of pathogen evolution. (a) A mechanistic or population genetic model is used to describe within-host dynamics of different pathogen strains. (b) The within-host model is nested in a between-host model by defining functional relationships between the within-host pathogen population and epidemiological characteristics. In the example shown here, the replication rate of the dominant pathogen strain affects the transmission rate and life expectancy of the host. These curves are based on observations of the relationship between the set-point viral load of an HIV-infection and infectiousness and time until the onset of AIDS (Fraser *et al.*, 2007, 2014). (c) The epidemiological model describes the population dynamics of hosts and between-host transmission.

single strain, and ignore super-infection. Let $\mathbf{x}_k(\tau) = (x_{k,1}(\tau), x_{k,2}(\tau), \dots, x_{k,n}(\tau))$ describe the relative frequency of each strain in a host initially infected with strain k, as a function of the time since infection, τ. The within-host dynamics can then be modelled using a simple quasispecies equation:

$$\frac{\mathrm{d}\mathbf{x}_k}{\mathrm{d}\tau} = M\,\boldsymbol{\gamma}\,\mathbf{x}_k - \Omega\mathbf{x}_k, \quad \text{with} \quad \Omega = \sum_{i=1}^{n} \gamma_i \mathbf{x}_{k,i}, \tag{1.5}$$

where $\boldsymbol{\gamma} = (\gamma_1, \dots, \gamma_n)$ is the vector of replication rates, M is a mutation matrix, and the term $-\Omega\mathbf{x}_k$ ensures that $\sum_{i=1}^{n} x_{k,i} = 1$ (Eigen (1971); see also chapter 2). In Figure 1.3a, example dynamics of this model are shown, using a hill-climbing mutation matrix (*c.f.*, Lythgoe *et al.* (2013)).

The within-host model is nested into a model of the epidemiological dynamics by defining functional relationships that describe how the strain distribution within a host affects the epidemiological parameters of that host. We describe the rate at which a type-k individual transmits strain i as $\beta_{ki}(\tau) = f(\mathbf{x}_k(\tau))\, x_{k,i}(\tau)$, and similarly define a link between host mortality and $\mathbf{x}_k(\tau)$. Figure 1.3b shows examples of such functions, inspired by the observed relationships in HIV between the

within-host replicative capacity, set-point viral load, transmission rate and virulence (Quinones-Mateu *et al.*, 2000; Kouyos *et al.*, 2011; Fraser *et al.*, 2007, 2014). Using these expressions for transmission rate and host mortality of type-k individuals, we can then use a standard multi-type epidemiological model (Diekmann and Heesterbeek (2000)) to describe the between-host level dynamics.

Using this approach, Lythgoe *et al.* (2013) showed that the evolution of HIV should typically be expected to be "short-sighted" (*c.f.*, Levin and Bull (1994)), such that within-host evolution over short time scales prevents epidemiological adaptation over longer time scales. Even if within-host selection is based on relatively small differences in within-host replication rate, within-host selection is expected to completely dominate the evolutionary process, selecting strains with high within-host replication rate, but relatively small population-level fitness (Lythgoe *et al.* (2013), see also Figure 2.5 in chapter 2). Similar results were found by van Dorp *et al.* in more complex simulation models of the evolution of HIV through immune escape mutations in heterogeneous host populations (van Dorp *et al.*, 2014, 2020).

Surprisingly, these model predictions do not coincide with epidemiological observations. The distribution of set-point viral loads in HIV-infected individuals lies close to the value that maximises the R_0 of the infection, suggesting that HIV might have evolved to optimise its transmission in human populations (Fraser *et al.*, 2007). Given the expectations for short-sighted within-host evolution, it is still an open question how HIV might have adapted to selection pressures at the epidemiological scale (Fraser *et al.*, 2014). In chapter 2, we explore a possible answer to this question.

In summary, pathogen evolution is often a multilevel process, that may give rise to conflicting selection pressures at the within- and between-host levels. To understand the evolution of chronic pathogens, both the within- and between-host level (and hence different temporal scales) should be considered. Understanding how chronic pathogens avoid short-sighted evolution remains a major challenge (Fraser *et al.*, 2014; Lythgoe *et al.*, 2017).

1.4. Thesis outline

In this thesis, we use mathematical and computational models to study microbial evolution as the multilevel process it is.

Chapter 2 deals with the effect of latent reservoirs on the evolution of HIV. These reservoirs consist of long-lived immune cells in which the virus is dormantly present, forming a stark contrast with the fast viral proliferation observed in most infected cells. We use a nested dynamical model to study how these latent reservoirs

affect the evolution of the virus both within single hosts and at the population level, especially in the light of the transmission-virulence trade-off and short-sighted evolution (as introduced in section 1.3).

In **chapter 3** we consider a different type of viruses, namely bacteriophages, and study the evolution of a recently discovered phage-encoded communication system (Erez *et al.*, 2017). When phages of the SPbeta group infect a bacterium, they induce the secretion of a small signalling peptide. The concentration of this peptide subsequently affects the infection strategies adopted by other phages in later infections. This communication system seems to allow the phages to adjust their infection strategy to the availability of susceptible hosts (Erez *et al.*, 2017; Hynes and Moineau, 2017; Abedon, 2017). Using a mathematical model, we describe under what circumstances such peptide-based communication between bacteriophages can evolve (and when not), and what communication strategies are then selected.

The phage-encoded signalling peptide studied in chapter 3 conveys a message about the number of infections that recently took place in the vicinity; it measures "local infection density". Regulation by local density cues is also frequently found in bacteria, for instance controlling the production of costly anticompetitor toxins (Cornforth and Foster, 2013; Gonzalez and Mavridou, 2019). Bacteria employing such density-dependent regulation produce toxins only if the local cell density is high. In **chapter 4**, we use a spatially structured individual-based simulation model to capture the effects of spatial structure on the evolution of toxin production and regulation by local cell density, and investigate the selection pressures driving the evolution of density-dependent toxin production.

In **chapter 5**, we shift focus from modelling specific behaviours to the general question of how the effects of spatial structure on evolution can be captured. Extending Price's multilevel decomposition of the selection differential (Eq 1.2), we present a new framework that describes the contribution of different length scales to evolution in spatially structured populations that do not necessarily consist of distinct groups. This framework allows us to decompose selection into components that act within and among local environments for any length scale.

The specific evolutionary questions addressed in chapters 2–4 are interesting in their own right. Studying the evolution of specific behaviours however also helps to shape our intuition about multilevel evolutionary processes in general. The general discussion in **chapter 6** integrates the findings of chapters 2–5, highlighting several common themes and identifying promising directions for future work.

2

Effect of the latent reservoir on the evolution of HIV at the within- and between-host levels

Hilje M. Doekes, Christophe Fraser, Katrina A. Lythgoe

PLoS Computational Biology 35(1): e1005228 (2017)

Abstract

The existence of long-lived reservoirs of latently infected CD4+ T cells is the major barrier to curing HIV, and has been extensively studied in this light. However, the effect of these reservoirs on the evolutionary dynamics of the virus has received little attention. Here, we present a within-host quasispecies model that incorporates a long-lived reservoir, which we then nest into an epidemiological model of HIV dynamics. For biologically plausible parameter values, we find that the presence of a latent reservoir can severely delay evolutionary dynamics within a single host, with longer delays associated with larger relative reservoir sizes and/or homeostatic proliferation of cells within the reservoir. These delays can fundamentally change the dynamics of the virus at the epidemiological scale. In particular, the delay in within-host evolutionary dynamics can be sufficient for the virus to evolve intermediate viral loads consistent with maximising transmission, as is observed, and not the very high viral loads that previous models have predicted, an effect that can be further enhanced if viruses similar to those that initiate infection are preferentially transmitted. These results depend strongly on within-host characteristics such as the relative reservoir size, with the evolution of intermediate viral loads observed only when the within-host dynamics are sufficiently delayed. In conclusion, we argue that the latent reservoir has important, and hitherto under-appreciated, roles in both within- and between-host viral evolution.

Author Summary

During HIV infection, a small proportion of infected cells containing integrated proviral DNA enter a long-lived resting phase, thus creating latent reservoirs of virus. These reservoirs are a major barrier to curing HIV and have been studied intensively in this light. Latent reservoirs might also affect viral dynamics during untreated infection, because they provide an archive of old viral variants that can re-enter circulation at a later time upon activation of latently infected cells. We developed a mathematical model to investigate how reservoir dynamics affect the evolution of the virus within single hosts, and find that the presence of a latent reservoir can severely delay within-host evolutionary dynamics. This delay increases with the relative size of the reservoir and the rate at which latently infected cells proliferate. By nesting this within-host model into an epidemiological model of host population dynamics, we show that the presence of latent reservoirs can also influence the population-level evolution of the virus. In contrast to predictions made by previous models we find that population-level adaptation to maximise transmission between hosts, rather than within-host fitness, can occur, but only if adaptation of the virus within hosts is sufficiently slowed down by the presence of latent reservoirs.

2.1. Introduction

Shortly after the introduction of anti-retroviral therapy (ART) to treat HIV infected individuals, viral reservoirs, in the form of long-lived CD4+ T cells containing integrated proviral DNA, were identified in infected patients (Chun *et al.*, 1997; Finzi *et al.*, 1997). These reservoirs are established soon after infection (Chun *et al.*, 1998a; Whitney *et al.*, 2014), are long-lived (Siliciano *et al.*, 2003), and virus can re-emerge from the reservoirs after months or even years of latency (Chun *et al.*, 1998b). As such, latent reservoirs represent the major barrier to curing HIV (Chun and Fauci, 2012; Eisele and Siliciano, 2012). Although reservoirs of latent viruses have been extensively studied in the light of treatment and viral eradication, including several modelling studies (see Alizon and Magnus (2012) and Perelson and Ribeiro (2013) for recent reviews), we have little understanding of how latent reservoirs influence viral dynamics during untreated infection, and in turn how this might affect viral evolution at the epidemiological scale.

Viral lineages in the reservoir are expected to be evolutionarily very stable because proviruses only replicate when the host cell divides, and since this uses the host-cell replication machinery, mutation rates are extremely low. The reservoir is therefore likely to provide an archive of "ancestral" viral strains that were circulating earlier during the infection. If these archived viruses are reactivated months, or even years, after infection, their presence might have a profound influence on within- and between-host dynamics. Using a population-genetic modelling approach Kelly *et al.* (1996; 2003) showed that cycling through the reservoir can lower the within-host neutral rate of HIV evolution. In a model of drug resistance, Ward and White (2012) furthermore showed that a latent reservoir can provide memory of non-resistant viral strains for up to several years after treatment is started, and recently, Immonen and Leitner (2014) showed that substitution rates among within-host HIV lineages are overdispersed, which is consistent with the circulating of virus through a reservoir. Using a simulation model of within-host dynamics, it has also been predicted that due to recombination a significant fraction of circulating viral strains will have fragments of their genome that have been latent for some time during infection (Immonen *et al.*, 2015). Moreover, there has been speculation that the transmission of ancestral strains could explain the lower rates of HIV evolution observed at the epidemiological scale compared to within individuals (Pybus and Rambaut, 2009; Lythgoe and Fraser, 2012; Alizon and Fraser, 2013; Vrancken *et al.*, 2014), and the unexpectedly high heritability of HIV set-point viral load despite considerable within-host evolution between transmission events (Lythgoe *et al.*, 2013; Fraser *et al.*, 2014).

Here, we present a quasispecies model of within-host HIV evolutionary dynamics that incorporates a latently infected reservoir. Of note, we find that the presence

of a latent reservoir can severely delay the within-host evolution of the virus. The extent of this delay is primarily determined by the replication rates of competing strains, the activation rate of latently infected cells, the relative size of the reservoir compared to the number of active infected cells (which we estimate from published data to be between 0.06 and 3.1; data used from Chun *et al.* (1997); Ibáñez *et al.* (1999); Andreoni *et al.* (2000); Ngo-Giang-Huong *et al.* (2001); Koelsch *et al.* (2008); Chomont *et al.* (2009)), and the extent to which cells within the reservoir proliferate. Since it is reasonable to speculate that all of these factors vary considerably among infected individuals, the influence of the reservoir in different individuals is likely to be very heterogeneous, and, if recombination is pervasive and selection pressures differ across the HIV genome, might also vary among sites (Immonen *et al.*, 2015).

Next, we nest the within-host model into a standard model of HIV epidemiological dynamics, enabling us to determine the effects of within-host evolution, and importantly the reservoir, on between-host evolutionary dynamics. If viral strains differ in their within-host fitness, variants with a higher *in vivo* replication rate will be favoured within a given host. Indeed, the replicative capacity of viral populations (as measured by *in vitro* competition assays) has been found to increase over the course of an HIV infection, albeit slowly (Troyer *et al.*, 2005; Kouyos *et al.*, 2011). It was also shown that individuals infected with a virus with a high replicative capacity tend to have a high viral load and vice versa (Kouyos *et al.*, 2011; Quinones-Mateu *et al.*, 2000), with the replicative capacity either predicted from the Pol sequence of the circulating virus [28] or measured by an *in vitro* competition assay (Quinones-Mateu *et al.*, 2000). Furthermore, in a study of 149 transmission pairs a weak positive correlation was found between the replicative capacity conferred by the Gag sequence of the virus that initiated an infection and the set-point viral load (spVL) (Prince *et al.*, 2012), the relatively stable concentration of viral particles in the blood during the chronic phase of HIV infection. The spVL, in turn, is a predictor of the severity of infection, or virulence, since individuals with a high set-point tend to progress to AIDS faster (Mellors *et al.*, 1996; de Wolf *et al.*, 1997).

As well as being a predictor for the duration of infection, set-point viral load is also correlated with the transmission rate (Quinn *et al.*, 2000; Lingappa *et al.*, 2010). Hence, infected individuals with a low set-point viral load (who, because of the correlations described above, are likely infected with a strain that has a low replicative capacity) will live long but will infect few other individuals because their transmission rate is low, while individuals with a high viral load will have a high transmission rate during the infection but will also cause few new infections because progression to AIDS is fast. Under this trade-off between duration of the infection and the transmission rate, it has been calculated that the transmission potential (defined as the number of new infections caused by an infected individual over the entire infectious period) is maximised when set-point viral loads are intermediate,

i.e., $\log(\text{spVL}) \approx 4.5$ (Fraser *et al.*, 2007; Blanquart *et al.*, 2016). The distribution of set-point viral loads found in populations of infected individuals is centered around these intermediate values, suggesting that HIV virulence might have evolved to maximise between-host transmission (Fraser *et al.*, 2007; Blanquart *et al.*, 2016; Shirreff *et al.*, 2011). This is surprising, since HIV evolves rapidly within hosts and durations of infections are long, and so the virus should be expected to evolve to maximise within-host fitness (*e.g.*, replication rate) at the expense of between-host fitness, an outcome known as 'short-sighted' evolution (Levin and Bull, 1994). Previous mathematical and computational studies have explored this interplay between within- and between-host selection, either by including within-host selection for high replication rate, which was in turn directly coupled to higher virulence as described above (Lythgoe *et al.*, 2013), or by including within-host selection for immune escape mutations in a heterogeneous host population and hence allowing the virus to adapt to each new host (van Dorp *et al.*, 2014). In both cases, for realistic within-host selection pressures and mutation rates, the within-host selection process was found to dominate between-host selection, and hence between-host level adaptation was not predicted to occur.

Here, we find that delays in within-host dynamics caused by the presence of a reservoir can have a large impact on how the virus evolves at the epidemiological level, and can, under certain parameter conditions, be substantial enough to explain evolution towards intermediate levels of virulence that maximise transmission. We therefore contend that it is important to consider reservoir dynamics not only in patients on antiretroviral therapy, but also in untreated individuals with ongoing active viral replication. Understanding how the virus evolves under different levels of selection is crucial if we want to better describe the course of epidemics, and predict the evolutionary impacts of potential intervention measures.

2.2. Results

First, we investigate the effect of the latent reservoir on the within-host evolution of HIV by studying a model of within-host evolutionary dynamics, before nesting the within-host model into an epidemiological framework.

2.2.1. Within-host dynamics

Model

We developed a mathematical model that describes the cycling of viral strains through an active compartment and a latent reservoir (Figure 2.1). The active compartment represents infected actively replicating CD4+ T cells, while the reservoir represents long-lived latently infected CD4+ T cells. Extending the model pro-

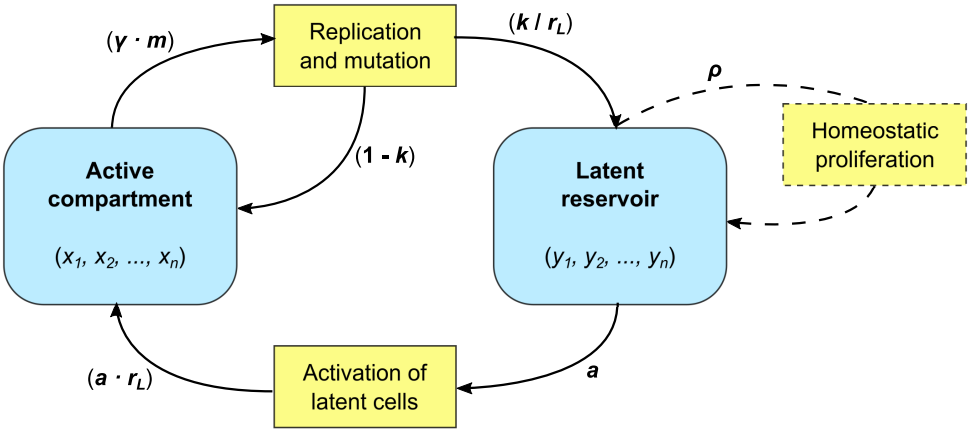

Figure 2.1. Schematic overview of the within-host model. The frequency of n different strains in the active compartment and latent reservoir (x_j and y_j respectively; $j = 1, \ldots, n$) are tracked. In the active compartment, strain-j virus replicates with strain-specific replication rate γ_j and can mutate into other strains i with probability m_{ij}. A small fraction, k, of newly infected cells become resting cells and move into the latent reservoir. Latent cells are reactivated at rate a per day. The effect of cells moving between the two compartments on the strain frequencies in these compartments depends on the relative size of the reservoir compared to the active compartment, r_L. The relative reservoir size is assumed to be constant throughout infection, maintained by a balance between inflow and outflow of cells, or by proliferation of latently infected cells if the outflow rate from the reservoir exceeds the entry rate. Specifically, the homeostatic proliferation rate is given by $\rho = a - \frac{k}{r_L}$ (see Methods for derivation). See Table 2.1 for model parameter values.

posed by Lythgoe *et al.* (2013), we use two coupled quasi-species equations (Eigen, 1971) to describe the frequency of the different viral strains in these compartments. We chose to consider viral frequencies rather than the absolute number of infected cells since tractable models that produce realistic profiles of infection and can also accommodate the distribution of viral loads found among infected individuals do not currently exist (Lythgoe *et al.*, 2016). A full description and derivation of the model are given in the Methods. In short, viral replication takes place in the active compartment at a strain-dependent replication rate, and with mutation occurring during replication. Most of the newly infected cells are assumed to directly feed back into the active compartment. However, upon infection a small fraction, k, of these cells enter a long-lived resting phase and become part of the reservoir. Cells in the reservoir are reactivated at rate a per day, at which point they re-enter the active compartment.

Since we describe the frequency of viral strains, rather than the absolute number

of infected cells, we have to account for a potential size difference between the two compartments. For example, if there are more actively infected than latently infected cells, then a single cell carrying a specific strain that moves from the reservoir to the active compartment will have a smaller effect on the viral strain frequency distribution in the active compartment than it had on the frequency distribution in the reservoir. We therefore define the relative reservoir size r_L to be the ratio between the number of latently infected cells (absolute size of the reservoir) and the number of actively infected cells (absolute size of the active compartment), and use this parameter to translate changes in the frequency distribution in one compartment to the appropriate changes in the other compartment (see Figure 2.1). *In vivo* measurements indicate that the reservoir is filled up quickly after infection, both in human patients (Chun *et al.*, 1998a) and in rhesus monkeys (Whitney *et al.*, 2014). Because viral load remains relatively constant during the chronic phase of an HIV infection, we assume that the size of the active compartment and the reservoir, and therefore also the relative reservoir size, are constant during chronic infection. Since with existing data it is only possible to estimate the relative reservoir size during chronic infection (see below), we furthermore make the simplifying assumption that the relative reservoir size in acute and late infection is the same as during chronic infection. We will however show that relaxing this assumption has almost no effect on the results.

In the absence of proliferation of cells in the reservoir, the assumption of a constant reservoir size is met if the inflow of new latently infected cells equals the outflow by reactivation. If, however, parameters are chosen such that the outflow exceeds the inflow, we make the implicit assumption that the proliferation of cells within the reservoir maintains its size. The homeostatic proliferation rate is then given by $\rho = \text{outflow rate} - \text{inflow rate} = a - \frac{k}{r_L}$ (see Methods for derivation). Note that we neglect mutation during homeostatic proliferation, since the integrated latent HIV DNA will be replicated by the host cell machinery, which has high copying fidelity.

A full overview of the model parameters and their values is shown in Table 2.1. Within the active compartment, viral replication rates are assumed to be close to 1 replication cycle per day (Perelson *et al.*, 1996). To model mutation and selection, we consider two scenarios: (i) a within-host selection model where the fastest replicating strain (strain n) has a 5% fitness advantage over the least fit strain (strain 1), reflected in an increased replication rate, and (ii) a within-host neutral model where all strains are of equal within-host fitness (but not necessarily of equal between-host fitness). For the first scenario we follow Lythgoe *et al.* (2013) and use a fitness landscape with a single peak in which strain j can only mutate into strain $(j-1)$ or $(j+1)$. Since this selection and mutation regime will lead to a monotonically increasing fitness trajectory, we call this a "hill-climb" fitness

Table 2.1. Model parameters

Parameter	Description	Value
γ_j	Replication rate of viral strain j (per day)	Variable, $[1.00 - 1.05]$
m_{ij}	Probability that strain j mutates into strain i during replication	5×10^{-5} iff $\|i - j\| = 1$ for the selection model
		5×10^{-3} iff $i = j + 1$ and 5×10^{-5} iff $i = j - 1$ for the within-host neutral model
k	Probability that a newly infected cell becomes latent	Variable, $[0 - 0.02]$
a	Activation rate of latent cells (per day)	Variable, $[0 - 0.01]$
r_L	Relative size of the latent reservoir	Variable, $[0.01 - 2]$
ρ	Homeostatic proliferation rate of latent cells (per day)	$a - \frac{k}{r_L}$
T_j	Duration of a type-j infection in the absence of natural mortality (years)	Variable, $[1.9 - 21.4]$
$\alpha_j(\tau)$	Time-dependent infectivity profile of individuals originally infected with strain j	Variable
B	Rate at which new susceptible individuals enter the host population (individuals per year)	200
ν	Natural death rate of hosts independent of infection status (per year)	0.02

landscape. These mutations happen with probability $5{\times}10^{-5}$ at replication (Mansky and Temin, 1995; Gao *et al.*, 2004). For the second scenario, we let "strain" j represent a bin of all viral strains that have acquired $(j-1)$ neutral mutations compared to the ancestral founder strain. Strain n then represents all viral strains carrying $\geq n$ mutations and is absorbing, meaning no mutations take place from strain n to strain $(n-1)$. We consider a 300bp region of the genome (a typical

read length in next generation sequencing studies) in which $1/3$ of all mutations are assumed to be both synonymous and neutral, and hence the probability of acquiring a neutral mutation is 5×10^{-3}, while the probability of reversion is again 5×10^{-5}. Because we consider at most 16 strains (*i.e.*, acquisition of at most 15 neutral mutations) we ignore saturation effects. Finally, we vary the probability of newly infected cells becoming latent, k, and the activation rate of latently infected cells, a. The probability of latency, k, is typically chosen to be 0.005 or less, and is never larger than 0.02, meaning that the vast majority of new cell infections lead to actively infected cells. The activation rate a is never bigger than 0.01 per day, thus ensuring that latently infected cells have a relatively long life span. As a consequence, homeostatic proliferation only occurs in our model at a low rate of less than one division per cell per 100 days ($\rho < 0.01$), if at all.

Estimation of the relative reservoir size r_L poses a particular challenge, since studies reporting both the size of the latent reservoir and the number of actively infected cells are scarce, especially in non-treated patients. To our knowledge, only Chun *et al.* (1997) report these kind of data, and only for the chronic, asymptomatic phase of infection. From their results we directly estimated the relative size of the reservoir during chronic infection for the 7 patients included in their study. In addition, we developed an indirect method to estimate the relative reservoir size using studies that report HIV DNA levels before and during antiretroviral treatment (Ibáñez *et al.*, 1999; Andreoni *et al.*, 2000; Ngo-Giang-Huong *et al.*, 2001; Koelsch *et al.*, 2008; Chomont *et al.*, 2009). Using our direct and indirect methods, we arrive at estimates for the relative reservoir size that vary between 0.06 and 3.1 (Figure 2.2, see also Methods and Supplementary Table 1 for full data per patient per study). In other words, our estimates vary between a setting in which the number of latently infected cells is approximately 20 times less than the number of actively infected cells and a setting in which there are 3 times as many latently infected cells as actively infected cells.

The presence of a reservoir can severely delay within-host evolutionary dynamics.

Using the modified quasispecies model, we determined the influence of the reservoir on within-host evolutionary dynamics. HIV infections are generally established by a single viral genotype (Keele *et al.*, 2008; Abrahams *et al.*, 2009; Tully *et al.*, 2016), and therefore the model was initialised with a single founder strain, with a further 15 strains generated through mutation giving a maximum of 16 strains. Importantly, we assume that the within-host dynamics are completely determined by the initial conditions, thus ignoring potential superinfections. We study the model both for the within-host selection case and the scenario in which within-host evolution is neutral.

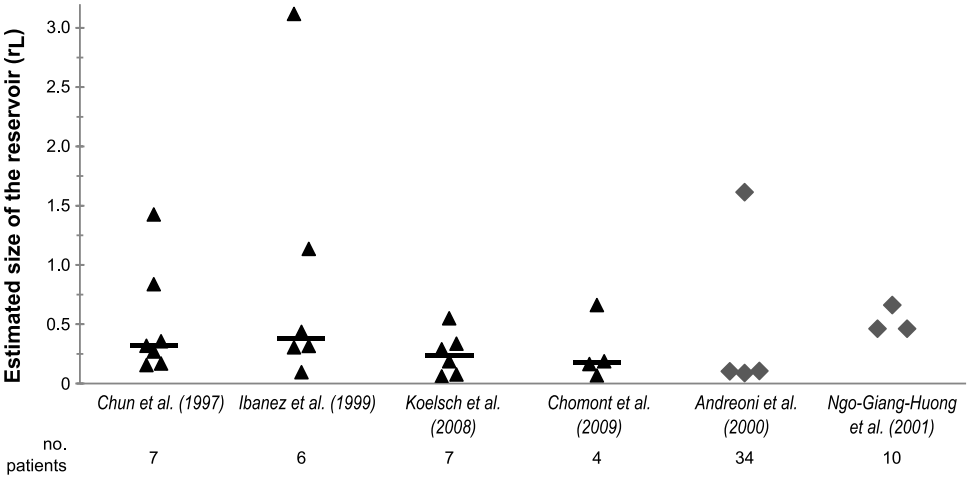

Figure 2.2. Estimated relative reservoir size r_L during chronic infection. Estimates were made using either a direct method based on the number of active and latent infected CD4+ T cells (data from Chun *et al.* (1997)), or an indirect method using HIV DNA levels pre- and post-treatment (data from Ibáñez *et al.* (1999); Andreoni *et al.* (2000); Ngo-Giang-Huong *et al.* (2001); Koelsch *et al.* (2008); Chomont *et al.* (2009)). For the left four studies, triangles represent single patients and the bar indicates the median. Two studies did not report data on individual patients, but on patient groups only. In these cases, the group mean (Andreoni *et al.*, 2000) or median (Ngo-Giang-Huong *et al.*, 2001) was used to estimate r_L for each group.

A comparison of model dynamics in the absence and presence of a reservoir is given in Figure 2.3, where $r_L = 0.5$ and $a = 0.01$ per day when the reservoir is present. First, consider the within-host selection scenario. We initiated the infection with strain 9, which has intermediate within-host fitness. In the absence of a reservoir (Figure 2.3a), as expected, strains with higher replication rates quickly increase in frequency in the viral population, until the population is dominated by the strain with the highest fitness. A similar process takes place if a latent reservoir is included in the model, where parameters are chosen such that there is no homeostatic proliferation of latently infected cells (*i.e.*, the inflow and outflow from the reservoir are equal) (Figure 2.3b). However, when comparing the timescales we see that in the presence of a reservoir the founder strain persists at high frequency for longer and it takes more time for the system to approach equilibrium. Using the time it takes for the founder strain to drop to 10% frequency as our benchmark, the dynamics are delayed by approximately 1.5 years when the reservoir is included in the model. This large effect can be understood by recognising that although viral lineages only rarely enter and exit the reservoir, once in the reservoir they remain

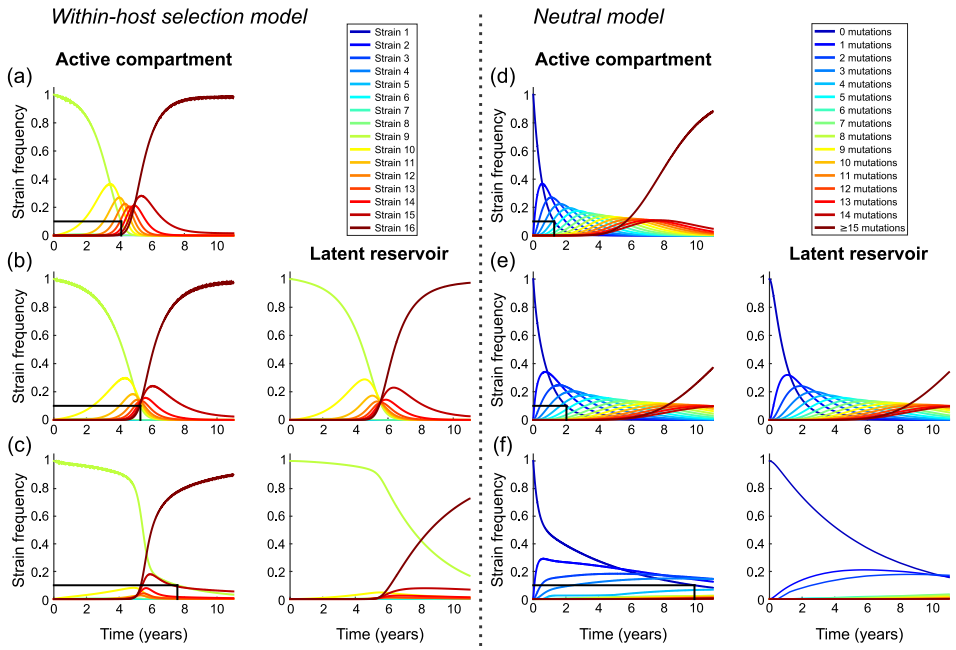

Figure 2.3. Within-host dynamics for the within-host selection model (panels a-c) and the within-host neutral model (panels d-f). (a,d) in the absence of a reservoir ($k = a = 0$), (b,e) in the presence of a reservoir, but without homeostatic proliferation in the reservoir ($r_L = 0.5$, $k = 5 \times 10^{-3}$, $a = 0.01$ per day, $\rho = 0$ per day), and (c,f) in the presence of a reservoir, with a low level of homeostatic proliferation ($r_L = 0.5$, $k = 5 \times 10^{-4}$, $a = 0.01$ per day, $\rho = 9 \times 10^{-3}$ per day). The black line indicates the time at which the frequency of the initial strain has declined to 10%. The presence of a latent reservoir delays the within-host dynamics, and this delay becomes even more profound if there is a low level of homeostatic proliferation in the reservoir. The number of strains is $n = 16$. In the within-host selection model, strains have linearly increasing replication rates between $\gamma_1 = 1.0$ and $\gamma_{16} = 1.05$ and the infection is initiated with strain 9. In the within-host neutral model, all strains have equal within-host fitness and strains are characterised by the number of neutral mutations they carry compared to the founder strain. In this case the last strain (carrying ≥ 15 mutations) is absorbing, *i.e.*, there are no mutations out of this bin. All other parameter values are as stated in Table 2.1.

there for a long period of time (with a mean generation time in the reservoir of $1/a$ days). Assuming a viral generation time of 1 day in the active compartment, and no homeostatic proliferation, the overall mean generation time will approach $(1 - k) + k/a$ days as infection progresses (Kelly, 1996). Note that because of our assumption of no homeostatic proliferation in the reservoir, we set the inflow (kL/r)

equal to the outflow (a), *i.e.*, we assume that the relative reservoir size $r_L = k/a$. Hence, in the absence of homeostatic proliferation the mean generation time will be approximately equal to $1 + rL$ (for $k \ll 1$), and therefore we should expect the cycling of virus through the latent reservoir to drastically delay the within-host evolutionary dynamics, if this reservoir is sufficiently big relative to the number of actively infected cells.

Next, we break the balance between the influx into and the efflux from the reservoir by assuming that the outflow rate exceeds the inflow rate, by setting $k = 5 \times 10^{-4}$. Under these conditions, we implicitly assume that a low level of homeostatic proliferation takes place in the reservoir, at a rate $\rho = 9 \times 10^{-3}$ per day. We find that the evolutionary dynamics are even further delayed (Figure 2.3c). In particular, there is a prolonged period of time at the start of the infection in which the founder strain dominates the population and all other strains remain at very low frequency. Again, the presence of the reservoir increases the mean generation time of the virus, although this mean generation time can no longer easily be calculated due to propagation of lineages within the reservoir through homeostatic proliferation. However, we here also observe a second way in which the reservoir affects the evolutionary dynamics. At the start of the infection, the viral population in both the active compartment and the latent reservoir consists of the founder strain. No mutations take place in the reservoir, so any mutational variation in the reservoir originates from inflow from the active compartment. Homeostatic proliferation sustains the strains already present in the reservoir, and so the reservoir functions as a memory of ancestral strains (*i.e.*, the strains that entered the reservoir earlier in infection), making them disproportionately represented in the reservoir compared to the active compartment. Strains present in the reservoir will constantly be fed back into the active compartment via activation of latently infected cells, effectively providing these strains with a fitness advantage and reducing the rate at which other, "new", strains grow in frequency in the active compartment. This memory function of the reservoir is illustrated by the reservoir dynamics (Figure 2.3c, right panel), which clearly lag behind those of the active compartment. Although the reservoir also functions as an archive of the initial founder strain to some extent in the absence of homeostatic proliferation (Figure 2.3b), the memory effect is much stronger if latently infected cells do proliferate at low rates (Figure 2.3c), since then both the initial strain and strains that later enter the reservoir are actively sustained within the reservoir.

In conclusion, we find two distinct mechanisms by which the latent reservoir affects the within-host evolutionary dynamics: (i) cycling through the reservoir causes a direct delay of the evolutionary dynamics because even when entry is rare, viral lineages spend a considerable amount of time in the reservoir where no mutations occur, and (ii) the reservoir can provide an archive of ancestral viral strains since

they are at a higher frequency in the reservoir than in the active compartment. Homeostatic proliferation of latently infected cells greatly enhances the effect of this second mechanism.

Similar results are found when within-host evolution is neutral (Figure 2.3d–f). We find that the presence of a reservoir can delay the rate at which neutral mutations accumulate (compare Figure 2.3d and 2.3e), and that this delay increases further if latently infected cells proliferate at a low rate (Figure 2.3f). The most profound differences between the within-host selection model and the within-host neutral model are seen in the presence of homeostatic proliferation in the reservoir (Figure 2.3c and 2.3f). Because of the relatively fast rate at which we assume neutral mutations accumulate ($\mu = 5\times10^{-3}$ to gain an extra neutral mutation in the within-host neutral model, compared to $\mu = 5\times10^{-5}$ to mutate into the next strain in the within-host selection model), in the within-host neutral model we do not observe a long delay during which the founder strain dominates. However, as in the selection model, the reservoir dynamics lag behind those in the active compartment and as a result strains carrying fewer neutral mutations dominate the population for much longer than in the absence of homeostatic proliferation.

To further investigate the effect of the relative reservoir size, r_L, the activation rate, a, and the homeostatic proliferation rate, ρ, on within-host dynamics, we calculated the delay in the evolutionary dynamics caused by the inclusion of a reservoir for different values of these parameters (Figure 2.4). Specifically, we consider the time after infection at which the frequency of the initial strain has declined to 10%, and calculate the delay as the difference between this time and the case without a latent reservoir. This metric of delay in time till decline of the initial strain was chosen to measure both the delaying and the archiving effect of the reservoir (which most profoundly affects the initial strain), with the 10% cut-off chosen arbitrarily. First, we consider a balanced case in which for every parameter combination the inflow parameter k is tuned such that reservoir inflow and outflow are equal (*i.e.*, $k = a \cdot r_L$), meaning there is no homeostatic proliferation in the reservoir. We find that the delay caused by including the reservoir increases with both the activation rate of latent cells and the relative size of the reservoir (Figure 2.4a). The result for the relative reservoir size can easily be understood from the intuitive argument presented above: as the relative reservoir size increases, the mean generation time of viral lineages, which is approximately equal to $1 + r_L$ if $k \ll 1$, will increase as well. The effect of the activation rate is a bit more subtle. As the activation rate increases, the outflow of cells from the reservoir (*i.e.*, $a \cdot r_L$) rises, thus increasing the influence the reservoir has on the active compartment. However, if the outflow rate increases in the absence of homeostatic proliferation, the influx probability k also needs to increase to maintain the constant relative reservoir size, and an increased influx from the active compartment into the reservoir will reduce the memory effect

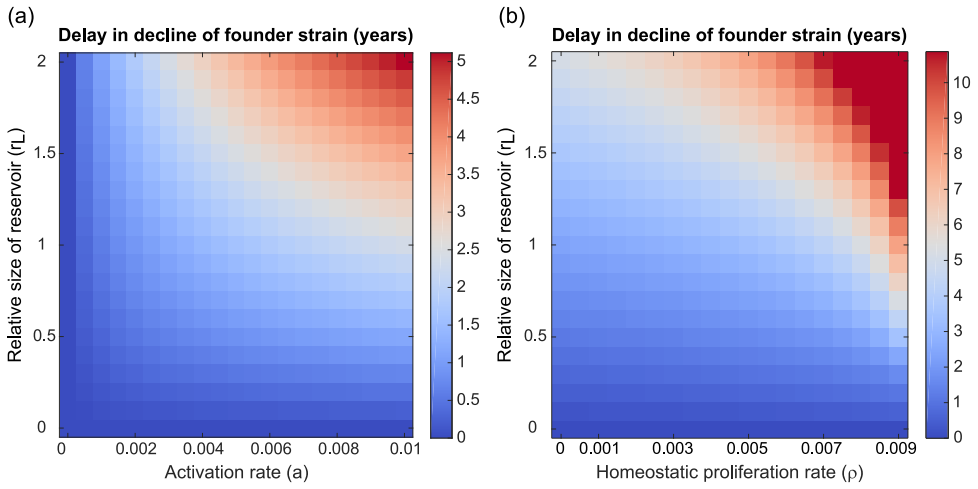

Figure 2.4. Delay in decline of the founder strain for varying reservoir parameter values in the within-host selection model. Persistence of the founder strain is defined as the time it takes for the founder strain to decline to a frequency $< 10\%$ in the within-host population, and the delay in decline was calculated as the difference in persistence between the settings of interest and a control case in which the reservoir was absent. (a) Varying the activation rate a and the relative reservoir size r_L in the absence of homeostatic proliferation ($\rho = 0$, $k = r_L \cdot a$), and (b) varying the homeostatic proliferation rate ρ and the relative reservoir size r_L for fixed activation rate ($a = 0.01$ per day). The homeostatic proliferation rate was varied by tuning the proportion of newly infected cells that enter the reservoir, k. The delay of the within-host dynamics increases with the relative size of the reservoir, and with the activation and homeostatic proliferation rate of latently infected cells. Note that the scales in panel (a) and (b) are different: the delays found in the presence homeostatic proliferation can be much larger than if latently infected cells do not proliferate. Results are shown for strains with increasing replication rates ($\gamma_1 = 1.0 - \gamma_{16} = 1.05$), with the infection founded by strain 9. Similar results were found for the within-host neutral case (Supporting Figure S2.1).

of the reservoir. For the within-host selection model, we find here that the increase in effect of the reservoir on the active compartment outweighs the reduction in memory function caused by the effect of the active compartment on the reservoir, and the highest evolutionary delays occur when the activation rate of latently infected cells is large. The balance between these two effects is however clearly illustrated in the within-host neutral model, where we find that the within-host evolutionary dynamics are most delayed for high relative reservoir sizes but intermediate values of the activation rate a (Supporting Figure S2.1a).

Next, we fix the activation rate ($a = 0.01$ per day) and study the effect of

changing the relative reservoir size, r_L, and the probability that newly infected cells become latent, k, thus implicitly varying the homeostatic proliferation rate ρ (remember $\rho = a - \frac{k}{r_L}$). As observed above, we find that a low level of homeostatic proliferation in the reservoir increases the observed delay of the evolutionary dynamics (Figure 2.3b) since the homeostatic proliferation augments the memory function of the reservoir. Similar effects of the relative reservoir size r_L and homeostatic proliferation rate ρ on the within-host dynamics were found for the within-host neutral model (Supporting Figure S2.1b).

So far, we have considered a relatively small fitness difference of 5% between the slowest and fastest replicating strains, representing, for example, mutations towards the population consensus that generally have a small effect and which take a long time to sweep through a within-host population (Zanini *et al.*, 2015). However, some mutations can have much larger within-host benefits and sweep through quickly. In line with these observations, in our model we find that mutations that confer a large within-host fitness benefit rapidly sweep through both the active compartment and the reservoir (Supporting Figure S2.2). The presence of a reservoir has very little effect on the speed of these dynamics even if homeostatic proliferation in the reservoir occurs.

In conclusion, we have shown that the presence of a latent reservoir can drastically delay within-host evolutionary dynamics. This effect depends on the fitness effect of mutations: for neutral or small-effect mutations substantial delays are expected, but not if mutations have a moderate or large effect on within-host fitness. The delay of within-host evolutionary dynamics increases with the relative size of the reservoir, and the activation rate and homeostatic proliferation rate of latently infected cells. Our model thus predicts a negative correlation between the relative reservoir size and the within-host evolutionary rate.

2.2.2. Between-host dynamics

Model

Next, we consider how the impact of the reservoir on within-host dynamics influences the evolution of virulence at the between-host level. To describe this between-host level, we follow Lythgoe *et al.* (2013) and use a standard demographic susceptible-infected (SI) model with several types of infected individuals (see Diekmann and Heesterbeek (2000)). For a full description of the model, see the Methods. In short, we define a type-j infected individual as someone initially infected by strain j, and track $I_j(t)$, the total number of type-j infected individuals in the population over time. New susceptible individuals are added to the population at rate B individuals per year, while all individuals have a natural mortality rate ν per year. Furthermore, we assume that all type-j infected individuals die at time T_j (years) after infection,

which represents disease induced mortality. A full overview of the model parameters is given in Table 2.1.

The within-host model is nested in this between-host framework via strain-specific infectivity profiles $\beta_{ij}(\tau)$ (Lythgoe *et al.*, 2013; Mideo *et al.*, 2008). These profiles describe the rate at which type-j infected individuals transmit strain i virus at time τ after infection. The strain specific infectivity profile is the product of the frequency of strain i in the host, $x_{ij}(\tau)$, which we solve from the within-host model, and a predefined total infectivity profile, $\alpha_j(\tau)$, which is only dependent on the infecting strain, j. Individuals initially infected with a highly virulent strain (high set-point viral load) have a short chronic infection period but high overall infectivity during this chronic phase, whereas individuals initially infected with a low virulent strain (low set-point viral load) have a long chronic infection period with a low overall infectivity (Supporting Figure S2.3a), and consequently moderately virulent strains have the highest transmission potential (Fraser *et al.*, 2007; Lythgoe *et al.*, 2013; Blanquart *et al.*, 2016), where this is defined as the average number of secondary infections caused by an individual infected by strain j during their entire infectious period in an otherwise totally susceptible population. Duration and infectivity of the acute and late phases of infection are assumed to be the same for all infections.

Since viral load has been shown to correlate with the replicative capacity of the virus as measured *in vitro*, albeit weakly (Kouyos *et al.*, 2011; Quinones-Mateu *et al.*, 2000; Prince *et al.*, 2012), and remains approximately constant during chronic infection, in the within-host selection scenario we assume that the set-point viral load of a type-j infected individual is determined by the replication rate γ_j of the initial infecting strain. Specifically, we assume that high values of j represent strains with a large replicative capacity and consequently highly virulent infections, whereas low values of j represent strains with a small replicative capacity and therefore less virulent infections (see cartoon in chapter 1: Figure 1.3b). To form a baseline expectation of the results of between-host selection, we also investigate a within-host neutral scenario in which all strains are assumed to have the same within-host replicative rate, but where we continue to assume that high values of j represent very virulent strains and low values of j represent less virulent strains. Thus, even though in this scenario mutations are neutral at the within-host level, they are not neutral at the between-host level and intermediate stains within a high transmission potential are expected to be selected.

Epidemiological dynamics and evolution of virulence

We again consider a case with $n = 16$ viral strains, and in all simulations a population of $N = 10\,000$ individuals was initialised with one individual infected with a moderately virulent strain (strain 7). The nested model was numerically solved to

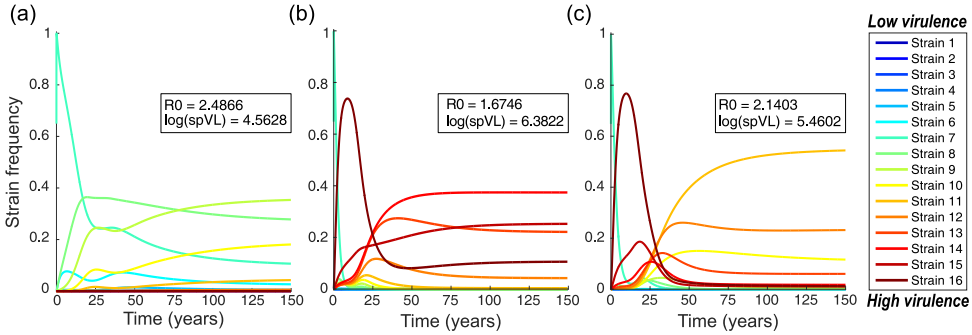

Figure 2.5. Dynamics of the between-host model. The relative prevalence of infections initiated by different viral strains, $I_j(t)$, is shown. The insets show the basic reproduction number R_0 and average set-point viral load (spVL) at the end of the numerical integration. Panels (a) and (b) show baseline expectations for the case without a latent reservoir, comparing a scenario in which within-host evolution is neutral to the within-host selection model. Panel (c) illustrates the effect of adding a latent reservoir. (a) No selection within-host with no reservoir. All strains have equal within-host fitness ($\gamma_1 = \gamma_{16} = 1.0$), but do differ in spVL and associated virulence and duration of the infection. Moderately virulent strains are selected, which have optimal transmission potential. (b) Within-host selection model with no reservoir; strains have linearly increasing within-host replication rates (between $\gamma_1 = 1.0$ and $\gamma_{16} = 1.05$) and increasing virulence. We clearly see the effects of short-sighted evolution: more virulent strains dominate the population, even though this reduces the population level fitness (R_0) of the infection. (c) Within-host selection model with a reservoir; strains have increasing fitness and there is a relatively large reservoir ($r_L = 0.5$) with a low level of homeostatic proliferation ($a = 0.01$ per day, $k = 5 \times 10^{-4}$, $\rho = 9 \times 10^{-3}$ per day, settings as in Figure 2.3c). The presence of a latent reservoir delays within-host dynamics, resulting in the dominance of less virulent strains at the population level, and hence reduces the effects of short-sighted within-host evolution.

find the epidemiological and evolutionary dynamics. Example dynamics are shown in Figure 2.5. Equilibrium population sizes vary between $N = 1150$ individuals (infection with high virulence) and $N = 2150$ individuals (moderately virulent infection). In the absence of a reservoir, and where all strains have the same within-host fitness, as expected the strain with maximum transmission potential and moderate virulence is selected (*e.g.*, strain 9 in our 16-strain scenario; Figure 2.5a). The basic reproduction number, R_0, of the viral population, which is defined as the average number of new infections a single infected individual would cause in a fully susceptible population over the course of its infection, is optimal and the average set-point viral load is close to the value observed in populations of untreated individuals: $\log(\text{spVL}) = 4.5$ (Fraser *et al.*, 2007). However, if strains have different within-host fitnesses, rapidly replicating high virulence strains quickly dominate within hosts

and are transmitted to the next host. Consequently, in the absence of a reservoir within hosts, new infections are dominated by highly virulent strains and we observe an associated drop in the basic reproduction number R_0 and increase in the average set-point viral load in the host population (Figure 2.5b). Thus, these results illustrate how short-sighted within-host selection for high replicative capacity dominates the evolutionary process at the between-host level (*c.f.*, Lythgoe *et al.* (2013)).

In contrast, when a latent reservoir is included in the model we see the dominance of intermediately virulent strains at the population level, even when there is selection for more virulent strains within individuals (Figure 2.5c). Although the basic reproduction number and the average set-point viral load are not optimal in this population, the effect of the reservoir dynamics on evolution at the population level is substantial: the mere presence of a latent reservoir causes a drop of 1.0 log in the average set-point viral load. Hence, in this example the latent reservoir has a major effect on the evolution of HIV at the population level and could to some extent explain why the virus has not evolved to be highly virulent.

This result can be understood in terms of the timescales of within-host evolution on the one hand, and transmission and duration of the infection on the other hand. The total duration of a type-j infection, T_j, sets a time limit on when within-host evolution and transmission to susceptibles can occur. In the presence of a reservoir the initial strain dominates the within-host viral population for a larger proportion of this infectious period than when the reservoir is absent (Supporting Figure S2.3), thus increasing the probability that the infecting strain, or strains with a similar virulence, are transmitted, which in turn enables the between-host adaptation of the virus.

As with the within-host dynamics, model outcomes depend strongly on the choice of parameters, particularly the relative reservoir size, the activation rate of latently infected cells, and the degree of homeostatic proliferation of latently infected cells (Supporting Figure S2.4). Importantly, the results of this analysis are very similar to the within-host results shown in Figure 2.4. The larger the within-host delay of the evolutionary dynamics, the higher the R_0 and the lower the average spVL in the population-level model. This is an intuitive result, since delay of the within-host evolutionary dynamics results in a longer period of time in which the founder strain can be transmitted, thus providing the virus with a mechanism to "escape" the effects of short-sighted within-host evolution.

Because of the strong dependence of our model results on the relative reservoir size r_L, we revisited the simplifying assumption that this relative reservoir size remains constant over the entire course of an infection. We based this assumption on *in vivo* observations showing that the reservoir fills up quickly at the start of infection (Chun *et al.*, 1998a; Whitney *et al.*, 2014). To check that our model parameters

are consistent with these observations, we developed a simplified population dynamical version of our model that describes the number of actively and latently infected cells during the acute, chronic and late phases of the infection (Supporting Text 2.6.1). Even though the probability of reservoir entry, k, and the activation rate of latently infected cells, a, are assumed to be low, we find that the size of the reservoir quickly increases after initial infection and can stabilise early in the chronic phase (Supporting Figure S2.5). The results of this population dynamical model also illustrate that we should expect the relative reservoir size to be much smaller during the acute and late phases of infection because the viral load, and hence the number of actively infected cells, will typically be much higher during these phases than during the chronic phase, due to the absence or failure of immune responses mounted by the host. To examine the effect of smaller relative reservoir sizes during the acute and late phases of infection, we repeated our analyses under the conservative assumption that the latent reservoir only impacts the evolution of the active compartment during chronic infection, while the within-host evolution during the acute and late phases of infection is only determined by the dynamics of the active compartment. The results were almost identical to those of the original model (Supporting Figures S2.3d and S2.6), indicating that our conclusions do not depend on the simplifying assumption of a constant relative reservoir size throughout the entire course of infection. This is because, even in the absence of a reservoir, little evolutionary change happens during the first three months (*i.e.*, the acute phase) of the infection (Figure 2.3), and similarly little evolution takes place in the final nine months, or the late phase, of most infections (Supporting Figure S2.3).

2.3. Discussion

We have investigated how the presence of a latent reservoir affects the evolutionary dynamics of HIV within individuals and at the population level. Surprisingly, we find that the latent reservoir can cause a significant delay to the within-host evolutionary process. Furthermore, if within-host evolution is sufficiently delayed the virus can evolve intermediate levels of virulence which optimise transmission at the population level. This is in contrast to the situation in which a within-host reservoir is absent and where high virulence strains are expected to dominate. Hence, the delay in within-host evolution can prevent the short-sighted evolution of very high levels of virulence.

It is important to note that these between-host effects only occur if the latent reservoir is relatively large compared to the active compartment. In the lower ranges of our estimates for the relative reservoir size (*e.g.*, $r_L \approx 0.1$), almost no effect of the reservoir on within-host evolutionary dynamics was found. For these conditions, the

preferential transmission of strains similar to the ancestral virus, stored in long-lived memory cells, might provide an alternative explanation to the observed population level adaptation of virulence (Fraser *et al.*, 2014). This is not an unreasonable hypothesis: ancestral strains are, by definition, transmissible, and during the course of a single infection there will not be selection to maintain transmissibility per se. There is now a growing body of indirect evidence that ancestral virus might be preferentially transmitted, including work on individual transmission pairs (Redd *et al.*, 2012; Deymier *et al.*, 2015), a large cohort study (Carlson *et al.*, 2014), and phylogenetic studies (Pybus and Rambaut, 2009; Alizon and Fraser, 2013; Vrancken *et al.*, 2014).

Our model can be extended to investigate the population level effects of preferential transmission of ancestral virus. As a case study, we incorporated this mechanism into our model by assuming that, during the course of an infection, the virus acquires additional mutations that lower its relative transmissibility per transmission event compared to strains carrying fewer of these mutations, but which are neutral at the within-host level and do not affect virulence (Supporting Text 2.6.2). We then find that inclusion of preferential transmission of ancestral virus can result in the dominance of strains with intermediate virulence that maximise the population level reproduction number, R_0, of the infection, even for cases where high virulence strains dominate in the absence of preferential transmission (Supporting Figure S2.7). As might be expected, however, the effect of this preferential transmission depends on the strength of the preference and the rate at which transmissibility-lowering mutations are acquired, and we only find population level adaptation of the virus if preferential transmission is sufficiently strong (Supporting Figure S2.8). Although this model provides a proof of concept that preferential transmission of ancestral virus can lead to population level adaptation of the virulence, more biologically realistic models should be developed to further study this mechanism.

Because both our within-host and between-host results are very sensitive to the relative size of the reservoir compared to the number of infected actively replicating cells, our model produces testable predictions for the effect of the relative reservoir size on the within-host evolutionary dynamics of the virus. The larger the reservoir compared to the active compartment, the more delayed within-host evolutionary dynamics are expected to be, ranging from almost no delay in individuals with a small relative reservoir size (lower bounds of our r_L estimates) to a delay of multiple years in individuals in whom the reservoir is large relative to the number of actively infected cells (higher bounds of our r_L estimates). In particular, this might explain the low rates of evolution in natural controllers of HIV infection who maintain very low plasma HIV RNA levels, and in whom we therefore speculate that the relative size of the reservoir compared to the active compartment is large. In these patients there is growing evidence for low levels of ongoing viral replication (Sedaghat *et al.*,

2009; Mens *et al.*, 2010; Hatano *et al.*, 2013) and the evolutionary rate has been estimated to be 3–4 times lower than in non-controllers (Mens *et al.*, 2010). Furthermore, in another study a negative correlation between set-point viral load and evolutionary rate has been described (Lemey *et al.*, 2007), a trend that we would predict if a high set point viral load is indicative of a small relative reservoir size. Although these data support the hypothesis that a relatively large latent reservoir delays within-host evolutionary dynamics, caution is needed in interpreting these and other results since confounding factors, such as APOBEC induced mutations, also affect both set-point viral load and rates of evolution (Cuevas *et al.*, 2015).

Quantifying the number of latently infected cells containing viable provirus in HIV patients is a major challenge. Empirical estimates of the size of the latent reservoir within patients on ART can vary 2 logs in magnitude depending on the experimental method used (Eriksson *et al.*, 2013). Viral outgrowth assays tend to underestimate the reservoir size, while PCR based methods tend to lead to an overestimation (Ho *et al.*, 2013). We have hoped to avoid some of these biases by estimating a relative reservoir size compared to the number of actively infected cells, which should be relatively insensitive to errors in estimates of the absolute number of infected active and latent cells, as long as both are biased in the same way. Using both direct and indirect methods we found that the relative size of the latent reservoir can vary enormously among patients, ranging from 0.06 to 3.1 latently infected cells per infected active cell. At this moment it is unclear to what extent this variation is caused by differences in the experimental methods used or is true variation between the patients themselves. Other studies have suggested that the relative size of the reservoir is much smaller than we have estimated here because most viral DNA in the reservoir is not viable (*e.g.*, Immonen *et al.* (2015)). However, recent evidence suggests that the same is true of viral DNA in actively replicating cells (Cuevas *et al.*, 2015), leading us to conclude that our estimates of the relative reservoir size are probably in the right ball park. Furthermore, although at first sight our estimates for the relative reservoir size might appear high, it is important to recognise that they represent a "snapshot" of viral dynamics. Although many active CD4+ T cells are infected over the course of an HIV infection, the total number of actively infected cells at any given point is small (Chun *et al.*, 1997). Thus, the ratio between the numbers of latently and actively infected cells at any given time point might be larger than intuitively expected.

As well as relative reservoir size, the rate at which the reservoir is replenished and depleted, and hence the (assumed) homeostatic proliferation rate in the reservoir, is another important determinant of within-host dynamics. There is a growing body of evidence suggesting that latent reservoirs are maintained by homeostatic proliferation in patients on antiretroviral therapy. Modelling studies have suggested that homeostatic proliferation must occur to maintain stable reservoir sizes under

therapy (Kim and Perelson, 2006; Rong and Perelson, 2009), and in support of this Chomont *et al.* (2009) found direct evidence of ongoing homeostatic proliferation in a subset of infected memory CD4+ T cells. More recent studies of HIV DNA integration sites at single-cell level (Maldarelli *et al.*, 2014; Wagner *et al.*, 2014) found that multiple cells carry identical proviral sequences at the same integration site, suggesting that up to 40% of cells in the latent reservoir have arisen from clonal expansion (Maldarelli *et al.*, 2014). We should however be careful in interpreting these results, since the clonally expanded proviruses were not tested for replication competency. In a different study Cohn *et al.* (2015) found that although the majority of integrated proviruses resided in clonally expanded T cells, all of the 75 proviruses found in these clones were defective. However, since in our model we only assume a very low level of proliferation of latently infected cells, if at all, these results do not directly contradict our assumptions.

We find that the within-host evolutionary dynamics of HIV can be severely delayed by the presence of a latent reservoir if mutations are neutral within-host or have a small within-host fitness effect. Some mutations might however confer a larger within-host fitness benefit, as has been suggested for some immune escape mutations (Ganusov *et al.*, 2011; Herbeck *et al.*, 2011; Maldarelli *et al.*, 2013), although other studies have found that immune escape might be relatively slow, especially during the chronic phase of infection (Ganusov *et al.*, 2011; Asquith *et al.*, 2006; Roberts *et al.*, 2015). For mutations that have a large effect on within-host fitness, we predict that the presence of the reservoir will have very little effect on within-host evolutionary dynamics because the fittest variant will quickly sweep the active compartment and the reservoir. However, since recombination happens very frequently during HIV replication (Zanini *et al.*, 2015; Jetzt *et al.*, 2000; Schlub *et al.*, 2010) we still expect to see the predicted effect of the latent reservoir when considering neutral mutations or mutations with small within-host fitness effects.

When modelling the evolution of virulence at the population level, we have confined ourselves to considering viral factors, and not host factors or host-virus interactions, which are likely to be mediated through the host immune response. The high heritability of HIV set-point viral load (Fraser *et al.*, 2014) suggests that viral factors are important determinants of virulence, although as yet we do not know what these factors are, and this is the subject of ongoing research. Since the human population is very heterogeneous (*e.g.*, with regard to immune responses) and this might impact epidemiological and evolutionary dynamics (van Dorp *et al.*, 2014), an important next step will be to determine how the incorporation of host heterogeneity affects our conclusions.

Because of the problems they pose to eradication of viral infection, latent HIV reservoirs have mainly been studied in the context of antiretroviral treatment (Chun and Fauci, 2012; Eisele and Siliciano, 2012). Here, however, we have investigated

how reservoir dynamics influence the evolutionary dynamics of HIV in untreated individuals with ongoing active viral replication. Overall, our models have shown that latently infected cells can have a major impact on the evolution of the virus. The latent reservoir plays a role in the determination of the within-host evolutionary rate and the outcome of population level evolution of virulence. Therefore, latently infected cells should be considered if we want to understand the evolutionary dynamics of HIV at the within- and between-host levels.

2.4. Methods

We developed a multilevel mathematical model that nests the within-host evolutionary dynamics of HIV in a between-host epidemiological model of HIV using a time-since-infection framework. At the between-host level, we follow Lythgoe *et al.* (2013) and use a standard multitype epidemic model (Diekmann and Heesterbeek, 2000). At the within-host level, we use two coupled quasi-species equations (Eigen, 1971) to describe the frequency distribution of different viral strains in actively infected cells and the latent reservoir. We model strain frequencies at the within-host level, rather than the total number of virions (or infected cells) of each strain, since tractable mathematical models of HIV infection that can reproduce the observed ranges of profiles of infection among patients (such as differences in spVL and duration of infection) do not currently exist (Lythgoe *et al.*, 2016). In our between-host model, we therefore use known associations between spVL, transmissibility and duration of infection to characterise the overall infectivity profile, $\alpha_j(\tau)$, of a host initially infected by strain j at time τ after infection. Using our within-host model, we separately model the frequency of strains i within a host infected by strain j, $x_{ij}(\tau)$, assuming an infinite population size, and then couple the between-host and within-host levels via the strain specific infectivity profile $\beta_{ij}(\tau)$, which is a combination of $x_{ij}(\tau)$ and $\alpha_j(\tau)$ and describes the infectivity of strain i in a host originally infected with strain j at time τ after infection (Lythgoe *et al.*, 2013; Mideo *et al.*, 2008). All models were implemented in `Matlab`, version R2013a.

2.4.1. Within-host model

Within a host we consider two compartments: an active compartment and a latent reservoir. The active compartment describes the infection of active CD4+ T cells. In this compartment, viral replication (*i.e.*, new infections) and mutation take place. A small fraction, k, of the newly infected cells enter the reservoir compartment as long-lived latently infected cells. These cells are reactivated at a rate a per day. An overview of the model structure is shown in Figure 2.1.

Consider n different viral strains that can differ in their replication rate, γ_i ($i = 1, 2, \ldots, n$). Let x_i be the frequency of strain i in the active compartment, and y_i its frequency in the latent reservoir. Mutations are described by a mutation matrix $M = (m_{ij})$, where m_{ij} is the probability that strain j mutates into strain i during replication. The dynamics of the system are described by the following differential equations:

$$\begin{cases} \frac{\mathrm{d}x_i}{\mathrm{d}t} = (1-k)\sum_{j=1}^{n} m_{ij}\gamma_j x_j + a r_L y_i - x_i\left((1-k)\sum_{j=1}^{n}\gamma_j x_j + a r_L \sum_{j=1}^{n} y_j\right) \\ \frac{\mathrm{d}y_i}{\mathrm{d}t} = \frac{k}{r_L}\sum_{j=1}^{n} m_{ij}\gamma_j x_j - a y_i - y_i\left(\frac{k}{r_L}\sum_{j=1}^{n}\gamma_j x_j - a\sum_{j=1}^{n} y_j\right), \end{cases} \tag{2.1}$$

or in matrix-vector notation

$$\begin{cases} \frac{\mathrm{d}\mathbf{x}}{\mathrm{d}t} = (1-k)Q\mathbf{x} + a r_L \mathbf{y} - \mathbf{x}\left((1-k)\overline{\gamma} + a r_L\right) \\ \frac{\mathrm{d}\mathbf{y}}{\mathrm{d}t} = \frac{k}{r_L}Q\mathbf{x} - a\mathbf{y} - \mathbf{y}\left(\frac{k}{r_L}\overline{\gamma} - a\right), \end{cases} \tag{2.2}$$

where $\mathbf{x} = (x_1, x_2, \ldots, x_n)^T$, $\mathbf{y} = (y_1, y_2, \ldots, y_n)^T$, $Q = (q_{ij}) = (m_{ij}\gamma_j)$ is the replication-mutation matrix and $\overline{\gamma} = \sum_{j=1}^{n}\gamma_j x_j$ is the total replication rate of the virus. The last term in all of these equations represents a chemostat-assumption, which assures that the frequencies x_j and y_j add up to one at all times (Eigen, 1971). This chemostat-assumption is equivalent to assuming that the death rate of cells within a given compartment is the same for all strains.

Note that Eq 2.1 introduces an additional parameter, the relative reservoir size r_L. Since we describe strain frequencies, rather than absolute numbers of infected cells, this parameter is needed to account for a potential difference in size between the two connected compartments. Let A be the total number of infected active CD4+ T cells, and L the total number of latently infected memory CD4+ T cells. Then, the number of memory CD4+ T cells latently infected with strain i is given by $y_i L$. Since these cells are reactivated at a rate a per day, the total rate of re-entry of strain i into the active compartment is $a y_i L$ cells per day. The contribution of these reactivated cells to the change in frequency of strain i in the active compartment is given by

$$\Delta x_i(a) = \frac{a y_i L}{A} \tag{2.3}$$

since the size of the active compartment is A cells. A similar argument can be made to describe the contribution of newly latently infected cells to the strain distribution in the reservoir, which is given by

$$\Delta y_i = \frac{k\sum_{j=1}^{n} m_{ij}\gamma_j x_j A}{L} = \frac{A}{L}\,k\sum_{j=1}^{n} m_{ij}\gamma_j x_j. \tag{2.4}$$

In both cases we see that if the reservoir and the active compartment are of unequal

size, this size difference has to be accounted for. Hence, we define

$$r_L = \frac{L}{A} \tag{2.5}$$

as the relative size of the reservoir. The use of this parameter r_L is also illustrated in Figure 2.1.

Note that our model implicitly includes the possibility of homeostatic proliferation of latently infected cells. Viral load stays approximately constant during chronic infection, and therefore we can expect the number of actively infected cells (*i.e.*, the absolute size of the active compartment) to be relatively constant as well, as is also predicted by models of within-host infection dynamics (see Alizon and Magnus (2012) and Perelson and Ribeiro (2013) for recent reviews). In the model, we make the additional assumption that the relative size of the reservoir compared to the active compartment remains constant during chronic infection. This means that the absolute size of the reservoir must also remain the same (see Eq 2.5). Using the notation of Eq 2.5, let A and L be the absolute size of the active compartment and the reservoir, respectively. Since $\sum_{j=1}^{n} \gamma_j x_j \approx 1$ (see Table 2.1 for parameter values) the total entry rate of cells entering the reservoir is approximately $k \cdot A$, while the total outflow rate of cells leaving the reservoir is $a \cdot L$. To maintain a constant reservoir size in the absence of homeostatic proliferation these entry and outflow rates must be equal, *i.e.*, $k = a \cdot \frac{L}{A} = a \cdot r_L$. If however the outflow is greater than the inflow (*i.e.*, $a > \frac{k}{r_L}$), then homeostatic proliferation of latently infected cells is implicitly assumed to take place so as to maintain the reservoir size, at a rate

$$\rho = a - \frac{k}{r_L}. \tag{2.6}$$

Since new HIV infections are generally established by a single viral genotype (Keele *et al.*, 2008; Abrahams *et al.*, 2009; Tully *et al.*, 2016), we assume that all within-host processes are started with only a single strain present at time $\tau = 0$. It has been shown that the reservoir of latently infected cells is established very quickly, as early as 10 days after infection (Chun *et al.*, 1998a; Whitney *et al.*, 2014). We incorporate this into our model by assuming that the initial strain is immediately present in both the active compartment and the latent reservoir. From these initial conditions, Eq 2.2 is numerically integrated to calculate $x_{ij}(\tau)$ and $y_{ij}(\tau)$, the frequency of strain i in the active compartment and the reservoir at time τ after infection in an individual originally infected with strain j at time $\tau = 0$. Note that a constraint of using the time-since-infection framework is the assumption that no superinfection takes place. Numerical integration was done with Matlab's built-in differential equation solver `ode45`, using default settings.

Then, following Lythgoe *et al.* (2013) we define the strain specific infectivity profile

$$\beta_{ij}(t) = \alpha_j(t)x_{ij}(t). \tag{2.7}$$

Here, $\alpha_j(t)$ is a predefined overall infectivity profile of infections established by strain j. We assume that the infectivity profile $\alpha_j(t)$ consists of three stages: acute infection, a chronic phase and a late phase. The durations of the acute and late phases are assumed to be equal for all infections, as is the infectivity during these phases. The duration and infectivity of the chronic phase, however, are assumed to be functions of spVL: infections with higher spVLs have shorter chronic phases, and higher infectivities during this chronic phase, than infections with lower spVLs (illustrated in Supporting Figure S2.3, see Lythgoe *et al.* (2013); Fraser *et al.* (2007); Blanchard *et al.* (2016) for details and parameter estimates). Because the duration of the chronic phase depends on the spVL, the total duration of the infection, T_j, will also be shorter for more virulent strains (*i.e.*, those with a higher spVL) (Lythgoe *et al.*, 2013; Fraser *et al.*, 2007). Viral load is relatively stable during chronic infection, even though a large amount of within-host evolution takes place during this period. We therefore assume that the spVL in turn is determined by the infecting strain. Since spVL correlates with replicative capacity of the virus (Kouyos *et al.*, 2011; Quinones-Mateu *et al.*, 2000; Prince *et al.*, 2012), we furthermore assume that strains with higher replication rates result in infections with higher spVLs (Lythgoe *et al.*, 2013).

2.4.2. Between-host model

Following Lythgoe *et al.* (2013), we use the strain specific infectivity profiles described by Eq 2.7 to nest the within-host dynamics into a multitype epidemiological model to describe the between-host dynamics (Diekmann and Heesterbeek, 2000). Here we will provide a short description of the model, see Lythgoe *et al.* (2013) and Diekmann and Heesterbeek (2000) for the full derivation.

We use a susceptible-infected model with demography. Let $S(t)$ and $I(t)$ be the number of susceptible and infected individuals at time t, respectively, and let $N(t) = S(t) + I(t)$ be the total number of individuals in the population. Let $I_j(t)$ be the number of type-j infected individuals, *i.e.*, individuals initially infected with strain j. Then, $I(t) = \sum_{j=1}^{n} I_j$. Assume that all individuals die at a natural death rate ν, and furthermore that type-j infected individuals die at time T_j after initial infection if they have not succumbed to natural mortality. Let B be the rate at which new susceptible individuals enter the population. Lastly, let $H_i(t)$ denote the incidence of type-i infections, *i.e.*, the rate at which new type-i infections occur. Assuming random mixing of the population, the epidemiological dynamics are then

described by

$$H_i(t) = \frac{S(t)}{N(t)} \sum_{j=1}^{n} \int_0^{T_j} \beta_{ij}(\tau) H_j(t-\tau) \mathrm{e}^{-\nu\tau} d\tau, \tag{2.8}$$

$$S(t) = N(t) - \sum_{i=1}^{n} \int_0^{T_j} H_i(t-\tau) \mathrm{e}^{-\nu\tau} d\tau, \tag{2.9}$$

$$\frac{dN(t)}{dt} = B - \nu N(t) - \sum_{i=1}^{n} H_i(t-T_i) \mathrm{e}^{-\nu\tau}, \tag{2.10}$$

$$I_i(t) = \int_0^{T_i} H_i(t-\tau) \mathrm{e}^{-\nu\tau} d\tau. \tag{2.11}$$

These equations were numerically integrated using Matlab, using Matlab's function `trapz` to numerically solve the integrals and the forward Euler method to solve the differential equations (timestep $dt = 0.01$ year).

The next-generation matrix $K = (k_{ij}) = (\int_0^{T_j} \beta_{ij}(\tau) \mathrm{e}^{-\nu\tau} d\tau)$ can easily be calculated. This next-generation matrix can be used to quickly find the equilibrium of the model without numerically solving Eqs 2.8–2.11. Namely, at equilibrium the basic reproduction number R_0 of the infection is equal to the dominant eigenvalue of the next-generation matrix K, while the corresponding eigenvector (normalised to have components summing up to one) gives the relative incidence $(\overline{H}_i^*)$ (Lythgoe *et al.*, 2013; Diekmann and Heesterbeek, 2000). R_0 represents the average number of new infections one infected individual would cause in a fully susceptible population during its lifetime. At equilibrium, however, the number of infected individuals is constant over time and hence the number of new cases arising from a single infection should be equal to one. Therefore, at equilibrium

$$\frac{S^*}{N^*} = \frac{1}{R_0}, \tag{2.12}$$

where the star denotes equilibrium values. Setting Eqs 2.8–2.11 to equilibrium and using Eq 2.12 we can now directly derive

$$I_i^* = \frac{B(R_0 - 1)\overline{H}_i^* (1 - \mathrm{e}^{-\nu T_i})}{\nu(R_0 - \sum_{j=1}^{n} \overline{H}_i^* \mathrm{e}^{-\nu T_i})}, \tag{2.13}$$

and similar expressions for H_i^*, S^* and N^* (see Lythgoe *et al.* (2013)). Since R_0 and $(\overline{H}_i^*)$ can be found from the next-generation matrix K, all equilibrium values can thus be directly calculated from the next-generation matrix.

2.4.3. Estimation of the relative reservoir size during chronic infection

To estimate the relative reservoir size rL, two data sources were used: (i) a direct report on the number of active and latent CD4+ T cells with integrated HIV-1 DNA in several chronic phase patients (Chun *et al.*, 1997), and (ii) several studies reporting HIV-1 DNA levels pre- and during anti-retroviral treatment in patients starting treatment during chronic phase (Ibáñez *et al.*, 1999; Andreoni *et al.*, 2000; Ngo-Giang-Huong *et al.*, 2001; Koelsch *et al.*, 2008; Chomont *et al.*, 2009).

Chun *et al.* (1997) report the concentration of cells with integrated HIV-1 DNA and the percentage of total cells that are latent. Then, the relative reservoir size can be directly calculated as

$$r_L = \frac{[\mathrm{HIV_{DNA}}]_l(1-P_a)}{[\mathrm{HIV_{DNA}}]_a P_a}. \tag{2.14}$$

Here, P_a denotes the percentage of CD4+ T cells that is activated (HLA DR+), and $[\mathrm{HIV_{DNA}}]_a$ and $[\mathrm{HIV_{DNA}}]_l$ are the concentrations of HIV-DNA positive active and latent cells (per 10^6 active/latent cells), respectively.

For the second set of studies, note that if treatment is effective, all HIV DNA measured during treatment can be assumed to be integrated in long-lived memory CD4+ cells (Chomont *et al.*, 2009). If we furthermore assume that reservoir size does not decrease drastically with treatment (which is in agreement with the very long half-lives found for the reservoir (Siliciano *et al.*, 2003)), the HIV DNA levels during treatment represent the size of the reservoir before treatment was initiated. Pre-treatment HIV DNA levels, however, represent the size of the total infected population (*i.e.*, actively and latently infected cells). Using these proxies we can calculate the relative reservoir size as

$$r_L = \frac{[\mathrm{HIV_{DNA}}]_t}{[\mathrm{HIV_{DNA}}]_n - [\mathrm{HIV_{DNA}}]_t}, \tag{2.15}$$

where $[\mathrm{HIV_{DNA}}]_t$ and $[\mathrm{HIV_{DNA}}]_n$ denote the HIV DNA-level during treatment and pre-treatment (naive), respectively.

Note that we do not incorporate the fraction of defective integrated proviruses into our indirect method. Approximately 88% of integrated proviruses in resting CD4+ T cells in patients on ART are completely replication incompetent because of genetic defects (Ho *et al.*, 2013). However, since most of these mutations are induced pre-integration (either due to reverse transcriptase infidelity or host cell APOBEC activity), we should expect to find defective integrated proviruses in activated CD4+ T cells as well. Indeed, it was recently shown that a substantial proportion of HIV DNA sequences isolated from peripheral blood mononuclear cells from treatment-naïve patients contain premature stop codons (Cuevas *et al.*, 2015). If mutations

in the HIV sequence happen at equal rate during infection of activated and resting CD4+ T cells, and if resting CD4+ cells infected with defective virus live the same amount of time and proliferate at the same rate as those latently infected with non-defective virus (an assumption that has however recently been challenged, see Cohn *et al.* (2015)), the fraction of cells infected with replication competent proviruses should be similar in both compartments. Hence, the ratio of replication competent HIV DNA levels does not change and our estimate for the relative reservoir size is unaffected.

Acknowledgements

We thank Rob J. de Boer for valuable discussions and comments while performing this work. We furthermore thank Gabriel E. Leventhal and Katherine Atkins for their constructive comments, which helped to improve this manuscript.

2.5. Supporting Figures

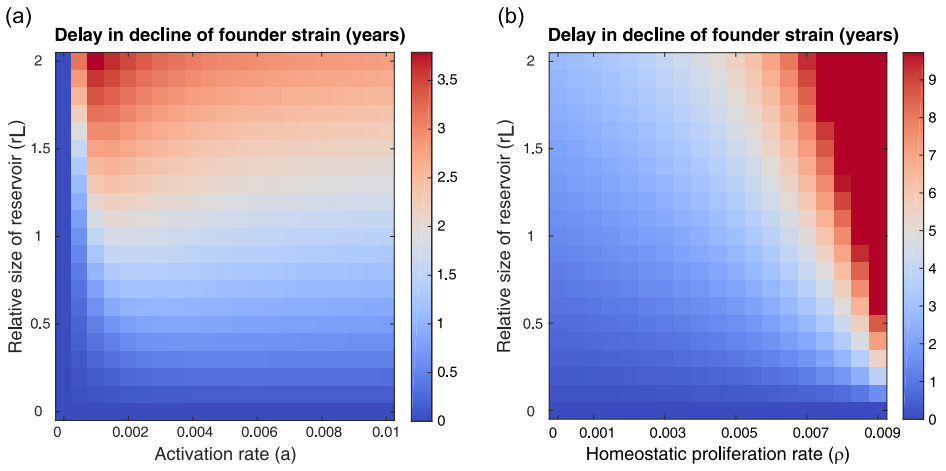

Supporting Figure S2.1. Delay in decline of the founder strain for varying reservoir parameter values in the within-host neutral model. Persistence of the founder strain is defined as the time it takes for the founder strain to decline to a frequency $< 10\%$ in the within-host population, and the delay in decline was calculated as the difference in persistence between the settings of interest and a control case in which the reservoir was absent. All strains have equal within-host replication rates, and parameter settings were as described in Table 2.1. (a) Varying the activation rate a and the relative reservoir size r_L in the absence of homeostatic proliferation ($\rho = 0$, $k = r_L \cdot a$), and (b) varying the homeostatic proliferation rate ρ and the relative reservoir size r_L for fixed activation rate ($a = 0.01$ per day). The homeostatic proliferation rate was varied by tuning the proportion of newly infected cells that enter the reservoir, k. The delay of the within-host dynamics increases with the relative size of the reservoir, and with the activation and homeostatic proliferation rate of latently infected cells. Note that the scales in panel (a) and (b) are different: the delays found in the presence homeostatic proliferation can be much larger than if latently infected cells do not proliferate. In general, these results resemble the results found for the within-host selection model (Figure 2.4): the delay of the within-host dynamics increases with the relative size of the reservoir, and with the activation and homeostatic proliferation rate of latently infected cells. For large reservoir sizes ($r_L > 1$) in the absence of homeostatic proliferation, however, we find that the delay is maximised for smaller values of the activation rate a. This is due to the no-homeostatic proliferation assumption, which dictates that for smaller activation rates a the probability of cells entering the reservoir is also smaller (remember $k = r_L \cdot a$), thus reducing the effect of within-host replication and mutation on the strain distribution in the reservoir.

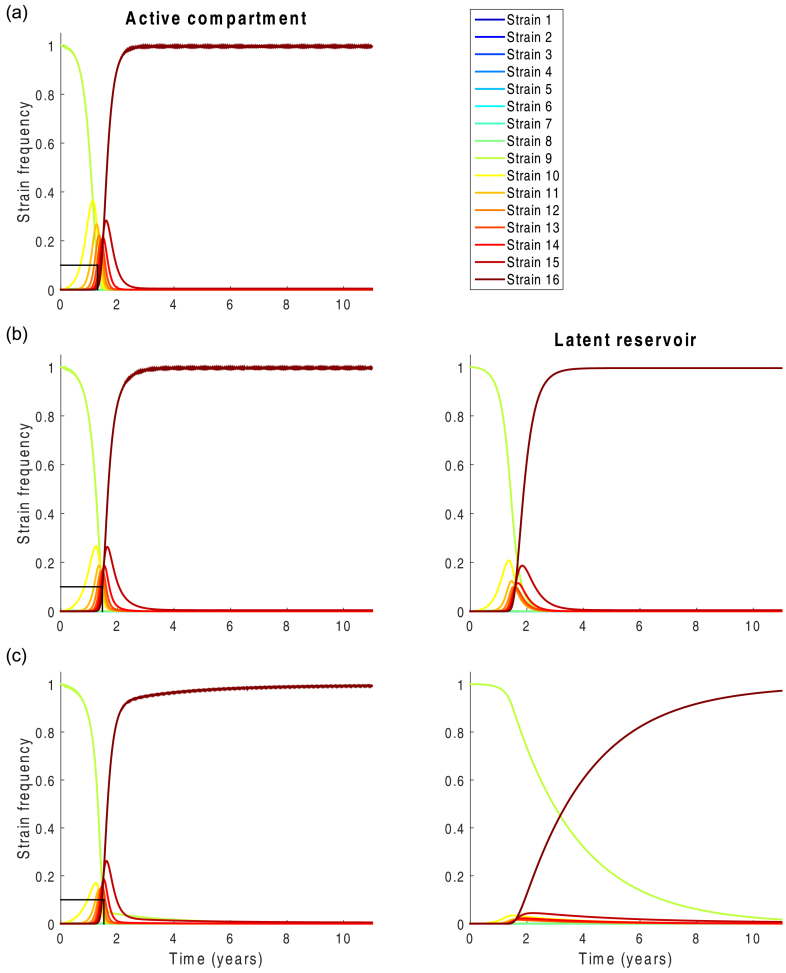

Supporting Figure S2.2. Within-host evolutionary dynamics if within-host fitness differences are large, (a) in the absence of a reservoir ($k = a = 0$), (b) in the presence of a reservoir, but without homeostatic proliferation in the reservoir ($r_L = 0.5$, $k = 5 \times 10^{-3}$, $a = 0.01$ per day, $\rho = 0$ per day), and (c) in the presence of a reservoir, with a low level of homeostatic proliferation ($r_L = 0.5$, $k = 5 \times 10^{-4}$, $a = 0.01$ per day, $\rho = 9 \times 10^{-3}$ per day). Strains have linearly increasing replication rates between $\gamma_1 = 1.0$ and $\gamma_{16} = 1.2$ and the infection is initiated with strain 9. All other parameter values are as stated in Table 2.1. Both in the absence and the presence of a reservoir the fittest strain (strain 16) rapidly sweeps the active compartment and the reservoir if present. The latent reservoir hence has little effect on the within-host evolutionary dynamics (compare these dynamics to the case with small within-host fitness differences, Figure 2.3).

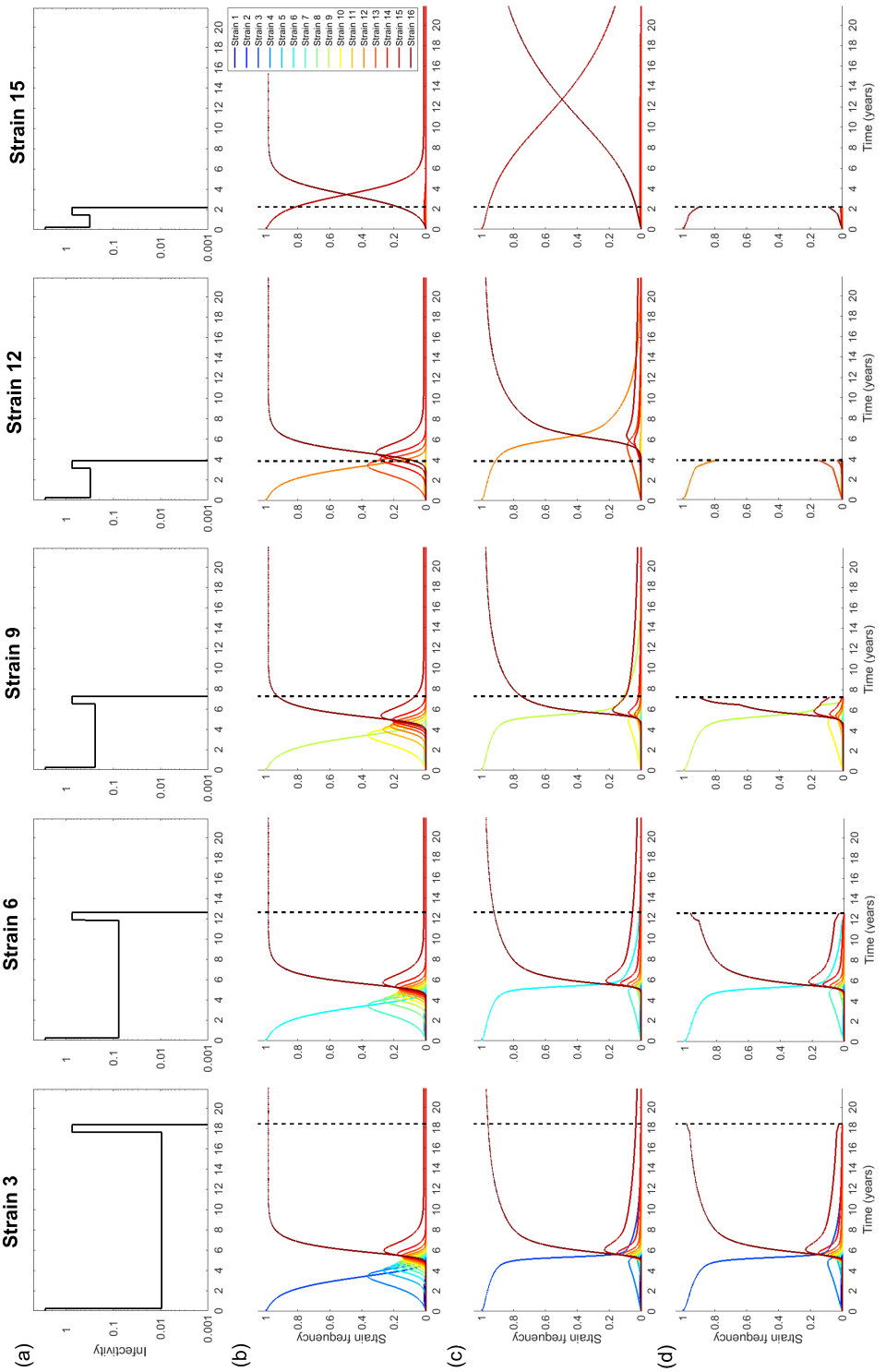
(a)
(b)
(c)
(d)
Strain 3
Strain 6
Strain 9
Strain 12
Strain 15
Infectivity
Strain frequency
Time (years)
Strain 1
Strain 2
Strain 3
Strain 4
Strain 5
Strain 6
Strain 7
Strain 8
Strain 9
Strain 10
Strain 11
Strain 12
Strain 13
Strain 14
Strain 15
Strain 16

Supporting Figure S2.3. Predefined infectivity profiles $\alpha_j(\tau)$, and within-host evolutionary dynamics without and with a reservoir for infections initiated by strains differing in within-host fitness. Strains differ in set-point viral load, with $\log(\text{spVL})$ linearly increasing from $\log(\text{spVL}) = 2$ for infections initiated by strain 1 to $\log(\text{spVL}) = 7$ for infections initiated by strain 16. For panels (b-d) strains were furthermore assumed to have linearly increasing within-host replication rates between $\gamma_1 = 1.0$ and $\gamma_{16} = 1.05$. Plots were made for strains varying from low (strain 3) to high (strain 15) set-point viral load. (a) Predefined infectivity profiles $\alpha_j(\tau)$, which describe the duration of the infection, as well as the infectivity during the acute, chronic and late phase of the infection (Lythgoe *et al.*, 2013). Infectivity and duration of the acute and late phase are the same for all infections, but the duration and infectivity of the chronic phase depend on the set-point viral load of the infection, which is determined by the strain that initiated the infection. In the within-host selection model the spVL depends in turn on the within-host fitness of the initial strain. (b) Within-host evolutionary dynamics in the absence of a latent reservoir ($k = a = 0$). Vertical lines indicate the maximal duration of the infection, T_j. (c) Within-host evolutionary dynamics in the presence of a latent reservoir, with a low level of homeostatic proliferation in this reservoir ($r_L = 0.5$, $k = 5 \times 10^{-4}$, $a = 0.01$ per day, $\rho = 9 \times 10^{-3}$ per day). All other parameter values are as stated in Table 2.1. Especially for the strains with high within-host replication rate and hence high virulence, we see that the addition of a reservoir delays the within-host dynamics to such an extent that for most of the duration of the infection, the initial strain dominates the within-host viral population at high frequency. (d) Within-host evolutionary dynamics under the conservative assumption that the active compartment is unaffected by the reservoir during the acute and late phases of infection. Parameter values were set as in panel (c), except the reservoir is assumed to fill up instantaneously at the end, rather than at the beginning, of the acute phase of infection. The activation rate a was set to 0 during the acute and the late stage of infection meaning that the reservoir could not influence the dynamics in the active compartment. Note that since the dynamics of this conservative model differ for each phase of the infection, no dynamics can be shown for this model after the end of the infection, T_j. The results for the conservative model are very similar to the results of the original model (panel (c)), showing that the results are insensitive to the simplifying assumption of a constant relative reservoir size for the entire duration of the infection.

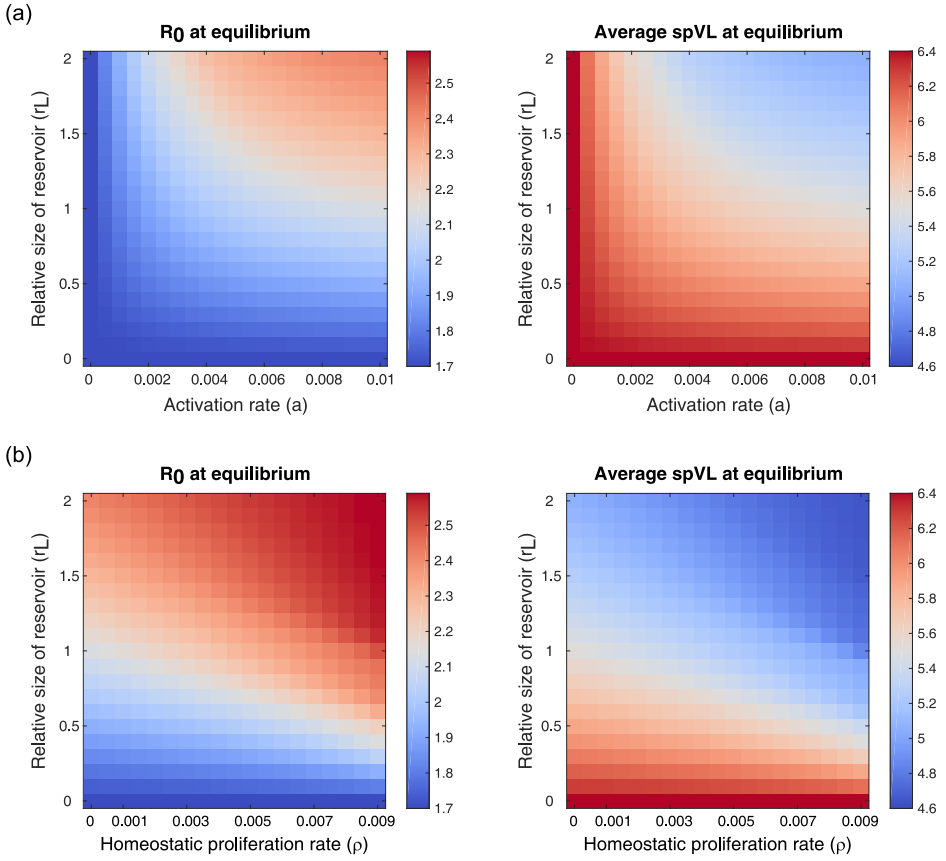

Supporting Figure S2.4. Basic reproduction number R_0 and average set-point viral load predicted by the between-host model for varying reservoir parameter values. (a) Varying the activation rate a and the relative reservoir size r_L in the absence of homeostatic proliferation ($\rho = 0$, $k = r_L \cdot a$), and (b) varying the homeostatic proliferation rate ρ and the relative reservoir size r_L for fixed activation rate ($a = 0.01$ per day). Homeostatic proliferation rate was varied by tuning the proportion of newly infected cells that enter the reservoir, k. Note the resemblance to Figure 2.4. High population level fitness of the virus (*i.e.*, high R_0 and intermediate set-point viral loads) is found precisely when the within-host dynamics are delayed.

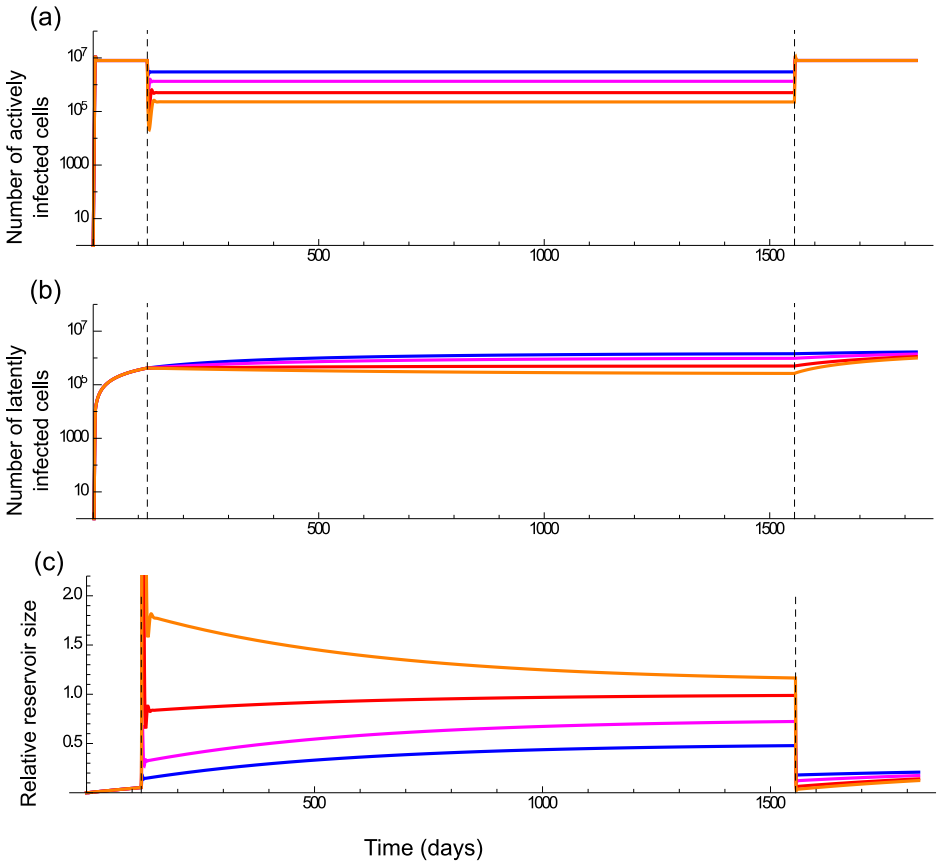

Supporting Figure S2.5. Dynamics of the number of actively and latently infected cells, and the relative reservoir size during the acute, chronic and late phase of infection. A simplified population dynamical version of our model was developed to investigate the initial filling up of the reservoir, and the relative reservoir size at the different phases of infection (Supporting Text 2.6.1). This population dynamical model was numerically solved starting from a single actively infected cell, no latently infected cells and a susceptible cell population at equilibrium ($W = \frac{\sigma}{d}$, see Supporting Text 2.6.1), to find (a) the number of actively infected cells X, (b) the number of latently infected cells Y, and (c) the relative reservoir size r_L. The infection is assumed to last for 5 years (1825 days), with the acute phase lasting 3 months (*i.e.*, $\tau \leq 120$ days) and the late phase lasting 9 months (*i.e.*, $\tau \leq 1555$ days). Results are shown for a case with a low level of homeostatic proliferation in the reservoir, corresponding to the parameters in Figures 2.3c and 2.5 ($a = 0.01$ per day, $k = 5 \times 10^{-4}$, $\rho = 9 \times 10^{-3}$ per day). We set the entry rate of new susceptible cells $\sigma = 107$ cells per day. Susceptible cells die at a rate $d = 0.5$ per day (Lythgoe and Fraser, 2012), the basic death rate of actively infected cells $\delta_X = 1$ (Perelson *et al.*, 1996), latently infected cells die at a rate $\delta_Y = 0.001$ per day (Alizon and Magnus, 2012; de Boer and Perelson, 1998), and the per capita infectivity of infected cells, $\beta = 2.5 \times 10^{-7}$ such that the within-host $R_0 = \frac{\beta\sigma}{d\delta_X} = 5$ newly infected cells per actively infected cell per day (Ribeiro *et al.*, 2010). During the chronic phase of infection the death rate of actively infected cells is increased by δ_{CTL} to simulate killing by the host's immune system, and results are shown for $\delta_{CTL} = 1$ (blue line), $\delta_{CTL} = 2$ (magenta line), $\delta_{CTL} = 3$ (red line), and $\delta_{CTL} = 3.5$ (orange line). Note that results for $\delta_{CTL} \geq 4$ cannot be obtained because that would reduce the within-host R_0 of the infection below 1. Both the number of actively and latently infected cells increases quickly during the acute phase of the infection. When the number of actively infected cells drops at the acute-chronic transition, the relative reservoir size suddenly increases and can quickly stabilise (*e.g.*, red line, $\delta_{CTL} = 3$). This result does however depend on the strength of the immune response (Supporting Text 2.6.1). For all choices of the parameter value of δ_{CTL}, the relative reservoir size is small during the acute and late phases of the infection due to the high number of actively infected cells during these phases.

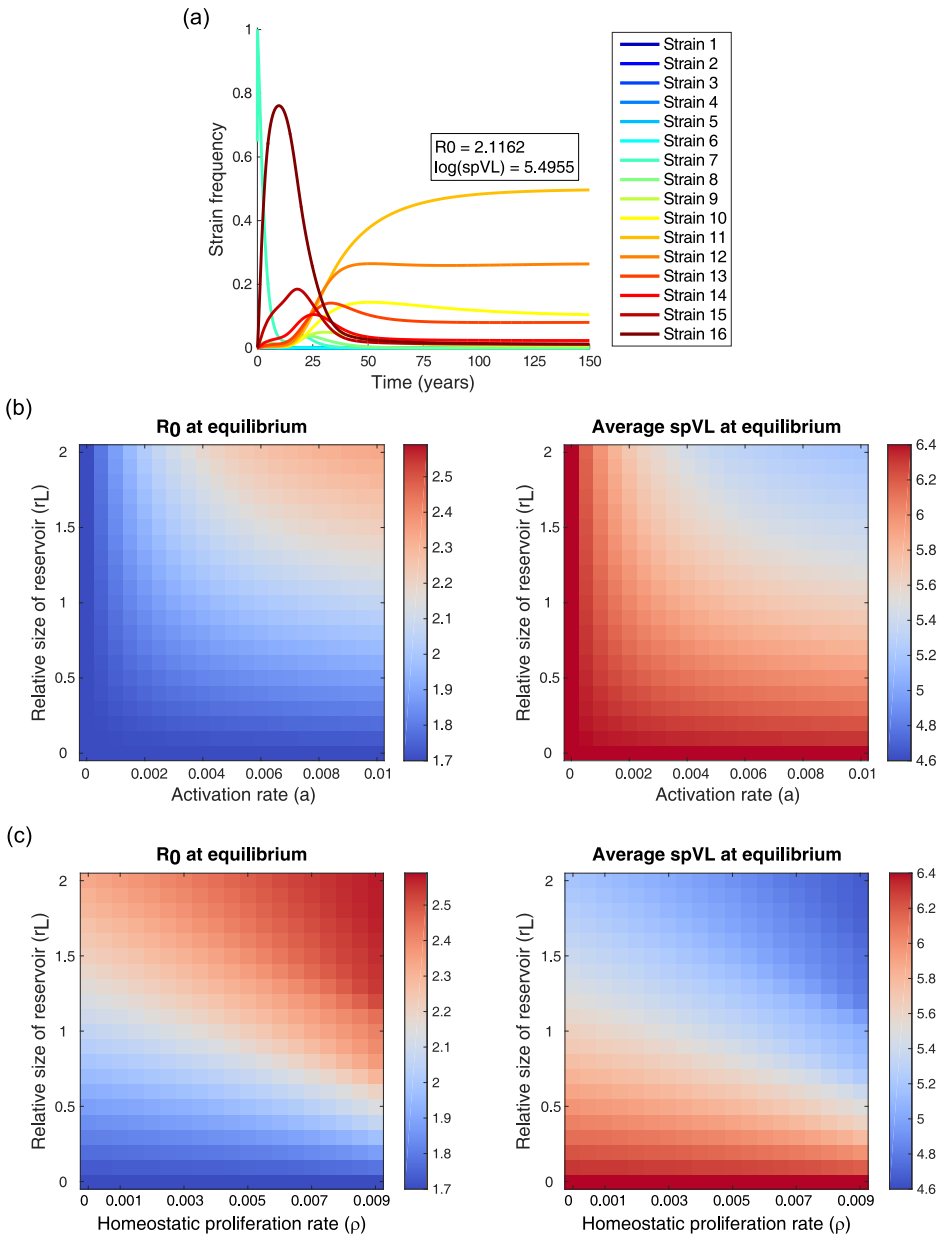

Supporting Figure S2.6. Between-host results under the conservative assumption that the latent reservoir influences the evolutionary dynamics during the chronic phase only. To investigate the impact of our assumption that the relative reservoir size is constant over the entire duration of the infection, we repeated the analyses of Figure 2.5 (panel (a)) and Supporting Figure S2.4 (panels (b) and (c)), but now assuming that the evolutionary dynamics are only influenced by the reservoir during the chronic phase of infection, while the active compartment is unaffected by the reservoir during the acute and late phases of infection. The reservoir is assumed to fill up instantaneously at the end, rather than at the beginning, of the acute phase of infection. The activation rate a was furthermore set to 0 during the acute and late phases of infection, ensuring that the reservoir could not influence the dynamics in the active compartment during these phases of the infection. Both the between-host dynamics (panel (a)) as well as the predicted basic reproduction number R_0 and the average set-point viral load in the population at equilibrium for varying parameter values (panels (b) and (c)) are very similar to the results found for our original model.

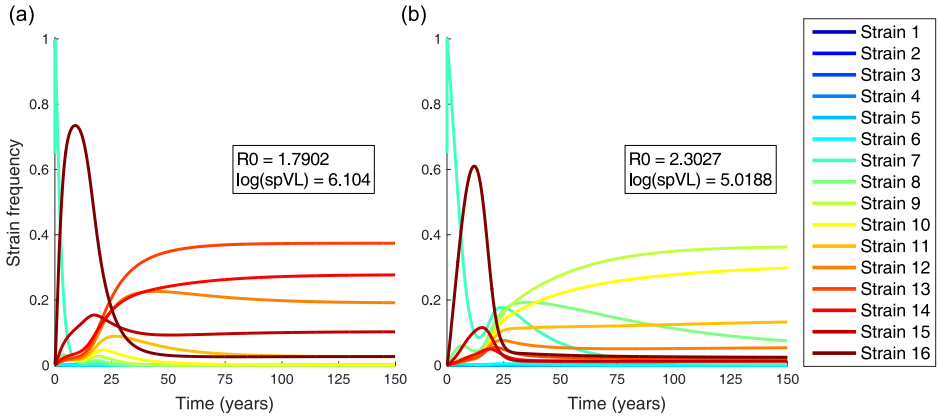

Supporting Figure S2.7. Epidemiological dynamics when preferential transmission of ancestral virus is included. Relative prevalence of the different strains in the population for the case where the relative reservoir size $r_L = 0.1$ and there is a low level of homeostatic proliferation in the reservoir ($a = 0.01$ per day, $k = 10^{-4}$, $\rho = 9 \times 10^{-3}$ per day). (a) If ancestral virus is not preferentially transmitted, the population is dominated by strains with high virulence, and consequently the basic reproduction number of the infection, R_0, is relatively low. (b) If viral strains accumulate transmissibility-lowering mutations over time and hence ancestral virus is preferentially transmitted, viral strains with lower virulence are selected at the population level and the R_0 of the infection is high. The transmissibility-lowering mutations are assumed to be neutral at the within-host level and independent of mutations affecting within-host fitness and/or virulence. Transmissibility-lowering mutations are acquired with probability $\mu_{\theta+} = 5 \times 10^{-3}$ and reverted with probability $\mu_{\theta-} = 5 \times 10^{-5}$ during within-host replication, and each mutation decreases the relative transmissibility of a strain by $\theta_{\text{step}} = 0.25$. Note that the absolute transmissibility of the virus (*i.e.*, the infectiousness of an infected individual) is still assumed to stay constant during the chronic stage of the infection.

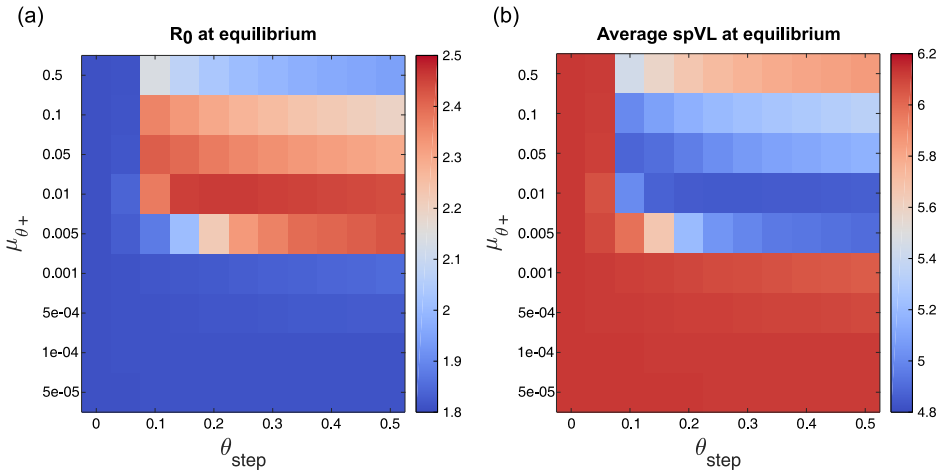

Supporting Figure S2.8. Effect of preferential transmission of ancestral virus on between-host viral evolution for varying parameter settings. The basic reproduction number R_0 and the average set-point viral load at equilibrium are plotted for different values of the effect on relative transmissibility of a single transmissibility-lowering mutation (θ_{step}) and the rate at which strains acquire transmissibility-lowering mutations ($\mu_{\theta+}$). Plots were made for a case with relatively small reservoir size ($r_L = 0.1$) and a low level of homeostatic proliferation in the reservoir ($a = 0.01$ per day, $k = 1 \times 10^{-4}$, $\rho = 9 \times 10^{-3}$ per day). All other parameters as in Figure 2.5. If both θ_{step} and $\mu_{\theta+}$ are sufficiently large viral strains of intermediate virulence are selected and the virus has high population level fitness (R_0). Furthermore, the highest population level fitness is reached if θ_{step} and $\mu_{\theta+}$ are well-balanced: if transmissibility-lowering mutations accumulate faster (higher $\mu_{\theta+}$) then a smaller effect per mutation (lower θ_{step}) will cause a similar decline of transmissibility in time (and hence in non-founder strains) as if $\mu_{\theta+}$ is smaller and θ_{step} is larger. If the decline in transmissibility is very fast (either because θ_{step} or $\mu_{\theta+}$ is very large), the frequency of viruses with high transmissibility (that are similar to the founder virus) will drop too quickly to contribute significantly to transmission events, even though they have a high transmission advantage.

2.6. Supporting Texts

2.6.1. A population dynamical model of actively and latently infected cell dynamics during different stages of the infection

In the main text, we consider a system of coupled quasispecies equations to model the changing strain frequencies during the course of infection in the active compartment and the reservoir. In doing this, we make the assumption that the relative reservoir size, $r_L = \frac{A}{L}$ (where L is the number of latently infected cells and A the number of actively infected cells) stays constant over the entire course of the infection. One of the requirements for this assumption is that the reservoir fills up quickly at the start of an infection, as is also observed *in vivo*. Here we present a simplified dynamical version of our model, in the absence of evolution, to test the validity of this assumption.

Let W be the number of susceptible cells, X the number of infected cells in the active compartment, and Y the number of latently infected cells in the reservoir. The equations for the population dynamical version of our model are then given by

$$\frac{\mathrm{d}W}{\mathrm{d}t} = \sigma - dW - \beta WX, \tag{S2.1}$$

$$\frac{\mathrm{d}X}{\mathrm{d}t} = (1-k)\beta WX - \delta(t)X + aY, \tag{S2.2}$$

$$\frac{\mathrm{d}Y}{\mathrm{d}t} = k\beta WX + \rho Y - \delta_Y Y - aY. \tag{S2.3}$$

Here, σ is the rate at which susceptible cells enter the system, d is the death rate of susceptible cells, β is the per capita infectivity of infected cells, k is the probability that a newly infected cell becomes latently infected, $\delta(t)$ is the death rate of actively infected cells, a is the activation rate of latently infected cells, ρ is the proliferation rate of latently infected cells, and δ_Y is the death rate of latently infected cells.

As in our between-host model, we model an infection with three stages: an initial acute phase, a chronic phase and a late phase. For consistency with our between-host model and previous observations (Fraser *et al.*, 2007), we assume that the acute phase of infection lasts 3 months and the late phase of infection lasts 9 months. We model the transition from the acute phase to the chronic phase of infection and the associated drop in viral load by assuming that after three months the death rate of actively infected cells is increased due to killing by the host's immune system, and similarly describe the transition from the chronic phase to the late phase of infection and the associated rise in viral load by the subsequent loss

of these immune responses. *I.e.*,

$$\delta(t) = \begin{cases} \delta_X & \text{if } \tau \leq 120 \text{ days or } \tau \geq (T - 270) \text{ days,} \\ \delta_X + \delta_{\text{CTL}} & \text{if } 120 \leq \tau \leq (T - 270) \text{ days,} \end{cases} \tag{S2.4}$$

where τ is the time since infection and T is the maximal duration of the infection (ignoring natural host mortality). We set $\delta_X = 1$ per day (Lythgoe *et al.*, 2016) and vary δ_{CTL}. We assume $\sigma = 10^7$ cells per day (Lythgoe and Fraser, 2012), $d = 0.5$ per day (Lythgoe and Fraser, 2012), and $\delta_Y = 0.001$ per day (Alizon and Magnus, 2012; Schlub *et al.*, 2010). We also assume that the within-host R_0 of the virus is 5 (de Boer and Perelson, 1998), giving us $\beta = (R_0 d \delta_X)/\sigma = 2.5 \times 10^{-7}$ per actively infected cell per day. For the parameters k, a, and ρ we assumed a low level of homeostatic proliferation of latently infected cells ($k = 5 \times 10^{-4}$, $a = 0.01$ per day, $\rho = 9 \times 10^{-3}$ per day; these are the parameters used in Figures 2.3c and 2.5c of the main text).

In Supporting Figure S2.5 we show the results of numerically solving Eqs S2.1–S2.3, starting with a single actively infected cell, no latently infected cells, σ/d susceptible cells, and for varying strengths of the immune response, δ_{CTL}. Both the number of actively and latently infected cells quickly increases at the start of the infection. However, since the number of actively infected cells is high the relative reservoir size during the acute phase of infection is low. As the number of actively infected cells drops due the increased effectiveness of the immune response in the chronic phase, the relative reservoir size goes up and can quickly reach equilibrium (*e.g.*, red line in Supporting Figure S2.5c), although this takes longer the lower the strength of the immune response. If the strength of the immune response is very big the reservoir seems to be "overfilled" and we see an overshoot in the relative reservoir size before it gradually falls to reach equilibrium levels (orange line in Supporting Figure S2.5c). During the late phase of infection, the number of actively infected cells very rapidly increases due to the failure of the host's immune system. As expected, this again causes a drop in the relative reservoir size, to a value similar to the value during the acute phase of the infection.

This dynamical model (Eqs S2.1–S2.3) provides a proof of concept for our assumption of early filling of the reservoir during the acute phase of infection (even if the probability that infected cells enter the reservoir is very small, as we have assumed in this example) and constant r_L during chronic infection. However, it also shows that the assumption of constant r_L during the entire course of infection is more problematical. We therefore repeated our analyses with the assumption that the reservoir has no impact on the evolutionary dynamics of the active compartment during early and late stage infection (Supporting Figures S2.3d and S2.6) and found that the effect is negligible.

We note that the results presented here are sensitive to the strength of the immune response and associated changes in viral load, and more elaborate models should be developed to more accurately describe the dynamics of actively and latently infected cells during the initial and late phases of an infection. This is however beyond the scope of this article.

2.6.2. Modelling preferential transmission of ancestral virus

It has been argued that upon transmission of HIV, ancestral virus might be preferentially transmitted. We adjusted the within-host and between-host model to incorporate this possibility. We assume that during the within-host evolutionary process the virus acquires certain mutations that lower its transmissibility relative to the other viral strains present in the host, up to a certain maximum number of mutations m. The overall transmissibility of a host is not affected by these mutations. In addition, these mutations are assumed to be neutral at the within-host level, and are not linked to the mutations that increase the replication rate and/or virulence.

Let $x_j^k(\tau)$ and $y_j^k(\tau)$ be the frequency of strain j carrying k of these transmissibility-lowering mutations in the active compartment and the reservoir, respectively. Define the vectors

$$\mathbf{x} = (x_1^0, x_1^1, \dots, x_1^m, x_2^0, x_2^1, \dots, x_n^m), \tag{S2.5}$$

$$\mathbf{y} = (y_1^0, y_1^1, \dots, y_1^m, y_2^0, y_2^1, \dots, y_n^m). \tag{S2.6}$$

Let $\mu_{\theta+}$ be the rate at which transmissibility-lowering mutations occur during replication, and let these mutations be reverted at rate $\mu_{\theta-}$. The within-host system is then again described by Eq 2.2, however now with

$$Q = \begin{pmatrix} \tilde{q}_{11}J & \cdots & \tilde{q}_{1n}J \\ \vdots & \ddots & \vdots \\ \tilde{q}_{n1}J & \cdots & \tilde{q}_{nn}J \end{pmatrix}, \tag{S2.7}$$

where $\tilde{q}_{ij} = m_{ij}\gamma_j$ is the entry in the original replication-mutation matrix and

$$J = \begin{pmatrix} (1-\mu_{\theta+}) & \mu_{\theta-} & 0 & \cdots & 0 & 0 \\ \mu_{\theta+} & (1-\mu_{\theta+}-\mu_{\theta-}) & \mu_{\theta-} & \cdots & 0 & 0 \\ \vdots & \vdots & \vdots & \ddots & \vdots & \vdots \\ 0 & 0 & 0 & \cdots & \mu_{\theta+} & (1-\mu_{\theta-}) \end{pmatrix} \tag{S2.8}$$

represents the acquisition of transmissibility-lowering mutations within a strain. The initial infecting strain is assumed to carry none of the transmissibility-lowering mutations, such that for a type-j infection at $\tau = 0$, $x_j^0(0) = y_j^0(0) = 1$ and all other vector entries are zero. Using these initial conditions, the within-host equations can

again be numerically integrated to calculate the frequencies of strain i carrying k transmissibility-lowering mutations in the active compartment and the reservoir, $x_{ij}^k(\tau)$ and $y_{ij}^k(\tau)$, for an infection established by strain j at time $\tau = 0$.

Next, we again define the strain specific infectivity profile $\beta_{ij}(t)$. The relative contribution of strains to the infectivity now depends both on their frequency and the number of transmissibility-lowering mutations they carry. Let θ_k represent the relative transmissibility of a strain with k transmissibility-lowering mutations compared to a strain without these mutations (*i.e.*, $\theta_0 = 1$). Then, we can define

$$\beta_{ij}(\tau) = \alpha_j(\tau)\frac{\sum_{k=0}^{m}\theta_k x_{ij}^k(\tau)}{\sum_{i=1}^{n}\sum_{k=0}^{m}\theta_k x_{ij}^k(\tau)}. \tag{S2.9}$$

Here, the denominator ensures that the total infectivity does not reduce over time. Only the relative transmissibility of strains carrying a certain number of transmissibility-lowering mutations is affected. Relative transmissibility is assumed to decrease linearly with the number of transmissibility-lowering mutations, up to a certain minimum θ_{min}. *I.e.*,

$$\theta_k = \max(\theta_{\text{min}}, 1 - k\theta_{\text{step}}), \tag{S2.10}$$

where θ_{step} is the slope of the decrease. The strain specific infectivity profiles as described by Eq S2.9 were used to directly implement the preferential transmission mechanism in the between-host model described by Eqs 2.8–2.11 (main text).

Supplementary Table 1. Estimates of the relative reservoir size r_L.

DIRECT ESTIMATES							
Chun et al., Nature, 1997							P_a = 0.4
Donor	**Active CD4 T cells with integrated HIV DNA (per 10^6 cells)**			**Resting CD4 T cells with integrated HIV DNA (per 10^6 cells)**			**Estimated r_L**
4	387			92			0.36
5	101			96			1.43
6	257			29			0.17
8	172			96			0.84
9	598			62			0.16
10	345			62			0.27
12	80			17			0.32
Median	***257***			***62***			***0.32***
INDIRECT ESTIMATES							
Ibáñez et al., AIDS, 1999.							
Subject	**$CD4^+$ T cell count pre-ART (cell/ml)**	**Integrated HIV-1 DNA copies pre-ART (per 10^6 PBMCs)**	**Integrated HIV-1 DNA copies pre-ART (~per ml)**	**$CD4^+$ T cell count during ART (cell/ml)**	**Integrated HIV-1 DNA copies during ART (per 10^6 PBMCs)**	**Integrated HIV-1 DNA copies during ART (~per ml)**	**Estimated r_L**
1	1147	113	0.130	1128	87	0.098	3.1
2	471	198	0.093	748	30	0.022	0.32
3	607	73	0.044	928	173	0.161	-*
4	660	1000	0.660	1012	198	0.200	0.44
5	616	233	0.144	1016	33	0.034	0.30
6	439	280	0.123	935	960	0.898	-*
7	300	467	0.140	560	133	0.074	1.14
8	919	453	0.416	1212	30	0.036	0.10
9	435	53	0.023	807	87	0.070	-*
10	660	198	0.131	940	327	0.307	-*
Median	***611.5***	***215.5***	***0.130***	***937.5***	***110***	***0.086***	***0.38***

Koelsch et al., JID, 2008.

Subject	HIV DNA level pre-ART (per µg DNA)	HIV DNA level during ART (per µg DNA)	Estimated r_L
C1	100	125.9	-*
C2	35.5	12.6	0.55
C3	398.1	89.1	0.29
C4	446.7	25.1	0.06
C5	398.1	63.1	0.19
C6	708.0	177.8	0.34
C7	251.2	17.8	0.08
Median	***398.11***	***63.10***	***0.24***

Chomont et al., Nat Med, 2009.

Subject	Integrated HIV DNA pre-ART (per 10^6 $CD4^+$ T cells)	Integrated HIV DNA during ART (per 10^6 $CD4^+$ T cells)	Estimated r_L
A	19952	1259	0.07
D	3981	562	0.16
K	2511	1000	0.66
L	7943	1259	0.19
Median	***5962***	***1129***	***0.18***

Andreoni et al., AIDS, 2000.

Group†	$CD4^+$ count pre-ART (cell/ml)	HIV-DNA copies pre-ART (per 10^6 CD4+ T cells)	HIV-DNA copies pre-ART (per ml)	$CD4^+$ count during ART (cell/ml)	HIV-DNA copies during ART (per 10^6 CD4+ T cells)	HIV-DNA copies during ART (per ml)	Estimated r_L
1	756	288	0.218	1040	17	0.018	0.09
2	737	676	0.498	920	50	0.046	0.10
3	394	2570	1.012	600	161	0.096	0.11
4	70	6761	0.473	300	974	0.292	1.61

Ngo-Giang-Huong et al., AIDS, 2001.

	HIV DNA copies pre-ART (per 10^6 PBMCs)	HIV DNA copies during ART (per 10^6 PBMCs)	Estimated r_L
1st Q	794	316	0.66
median	3548	1144	0.46
3rd Q	7943	2512	0.46

* r_L could not be calculated because $[HIV_{DNA}]_t > [HIV_{DNA}]_n$; † Groups defined based on CD4 count (high/low) and viral load (high/low), see Andreoni et al.

3

Repeated outbreaks drive the evolution of communication between bacteriophages

Hilje M. Doekes, Glenn A. Mulder, Rutger Hermsen

Manuscript under review
Preprint available at bioRxiv, DOI: 10.1101/2020.04.29.068247

Abstract

Communication based on small signalling molecules is widespread among bacteria. Recently, such communication was also described in bacteriophages. Upon infection of a host cell, temperate phages of the *Bacillus subtilis*-infecting SPbeta group induce the secretion of a phage-encoded signalling peptide, which is used to inform the lysis-lysogeny decision in subsequent infections: the phages produce new virions and lyse their host cell when the signal concentration is low, but favour a latent infection strategy, lysogenising the host cell, when the signal concentration is high. Here, we present a mathematical model to study the ecological and evolutionary dynamics of such viral communication. We show that a communication strategy in which phages use the lytic cycle early in an outbreak (when susceptible host cells are abundant) but switch to the lysogenic cycle later (when susceptible cells become scarce) is favoured over a bet-hedging strategy in which cells are lysogenised with constant probability. However, such phage communication can evolve only if phage-bacteria populations are regularly perturbed away from their equilibrium state, so that acute outbreaks of phage infections in pools of susceptible cells continue to occur. Our model then predicts the selection of phages that switch infection strategy when half of the available susceptible cells have been infected.

3.1. Introduction

For several decades now, it has been recognised that communication between individuals is not limited to multi-cellular organisms, but is also common among microbes. The best-known example of microbial communication is bacterial *quorum sensing*, a process in which bacteria secrete signalling molecules to infer the local cell density and consequently coordinate the expression of certain genes (Nealson *et al.*, 1970; Miller and Bassler, 2001). A wide variety of bacterial behaviours have been found to be under quorum-sensing control (Miller and Bassler, 2001; Hense and Schuster, 2015), including bioluminescence (Nealson *et al.*, 1970), virulence (Antunes *et al.*, 2010), cooperative public good production (Diggle *et al.*, 2007; Darch *et al.*, 2012), and antimicrobial toxin production (Cornforth and Foster, 2013; Kleerebezem and Quadri, 2001). Remarkably, it has recently been discovered that even some bacterial viruses (bacteriophages, or phages for short) use signalling molecules to communicate (Erez *et al.*, 2017). Here, we use a mathematical model to explore the dynamics of this viral small-molecule communication system. We study under what conditions communication between phages evolves, and predict which communication strategies are then selected.

Bacteriophages of the *Bacillus*-infecting SPbeta group encode a small signalling peptide named arbitrium, which is secreted when the phages infect bacteria (Erez *et al.*, 2017). These phages are *temperate* viruses, meaning that each time a phage infects a bacterium, it makes a life-cycle decision: to enter either (i) the *lytic* cycle, inducing an active infection in which tens to thousands of new phage particles are produced and released through host-cell lysis, or (ii) the *lysogenic* cycle, inducing a latent infection in which the phage DNA is integrated in the host cell's genome (or episomally maintained) and the phage remains dormant until it is reactivated. This lysis-lysogeny decision is informed by the arbitrium produced in nearby previous infections: extracellular arbitrium is taken up by cells and inhibits the phage's lysogeny-inhibition factors, thus increasing the propenstiy towards lysogeny of subsequent infections (Erez *et al.*, 2017). Hence, peptide communication is used to promote lysogeny when many infections have occurred. Similar arbitrium-like systems have now been found in a range of different phages (Stokar-Avihail *et al.*, 2019). Notably, these phages each use a slightly different signalling peptide, and do not seem to respond to the signals of other phages (Erez *et al.*, 2017; Stokar-Avihail *et al.*, 2019).

The discovery of phage-encoded signalling peptides raises the question of how this viral communication system evolved. While the arbitrium system has not yet been studied theoretically, previous work has considered the evolution of lysogeny and of other phage-phage interactions. Early modelling work found that lysogeny can evolve as a survival mechanism for phages to overcome periods in which the

density of susceptible cells is too low to sustain a lytic infection (Stewart and Levin, 1984; Maslov and Sneppen, 2015). In line with these model predictions, a combination of modelling and experimental work showed that selection pressures on phage virulence change over the course of an epidemic, favouring a virulent phage strain early on when the density of susceptible cells is high, but a less virulent (*i.e.*, lysogenic) phage strain later in the epidemic when susceptible cells have become scarce (Berngruber *et al.*, 2013; Gandon, 2016). Other modelling work has shown that if phages, lysogenised cells, and susceptible cells coexist for long periods of time, the susceptible cell density becomes low because of phage exploitation, and less and less virulent phages are selected (Mittler, 1996; Wahl *et al.*, 2019).

Erez *et al.* (2017) propose that the arbitrium system may have evolved to allow phages to cope with the changing environment during an epidemic, allowing the phages to exploit available susceptible bacteria through the lytic cycle when few infections have so far taken place and hence the concentration of arbitrium is low, while entering the lysogenic cycle when many infections have taken place and the arbitrium concentration has hence increased. This explanation resembles results for other forms of phage-phage interaction previously found in *Escherichia coli*-infecting phages (Abedon, 2017, 2019). In the obligately lytic T-even phages, both the length of the latent period of an infection and the subsequent burst size increase if additional phages adsorb to the cell while it is infected – a process called *lysis inhibition* (Hershey, 1946; Doermann, 1948; Abedon, 2019). In the temperate phage λ, the propensity towards lysogeny increases with the number of co-infecting virions, called the multiplicity of infection (MOI) (Kourilsky, 1973). In both cases, modelling work has shown that the effect of the number of phage adsorptions on an infection can be selected as a phage adaptation to host-cell density, as it allows phages to switch from a virulent infection strategy (*i.e.*, a short latent period or a low lysogeny propensity) when the phage:host-cell ratio is low to a less virulent strategy (*i.e.*, a longer latent period or higher lysogeny propensity) when the phage:host-cell ratio is high (Abedon, 1989, 1990; Sinha *et al.*, 2017).

Here, we present a mathematical model to test if similar arguments can explain the evolution of small-molecule communication between viruses, and to explore the ecological and evolutionary dynamics of temperate phage populations that use such communication systems. We show that arbitrium communication can indeed evolve and that communicating phages consistently outcompete phages with non-communicating bet-hedging strategies. We however find that communication evolves under certain conditions only, namely if the phages regularly cause new outbreaks in substantial pools of susceptible host cells. Moreover, when communication evolves under such conditions, we predict that a communication strategy is selected in which phages use arbitrium to switch from a fully lytic to a fully lysogenic strategy when approximately half of all susceptible cells have been infected.

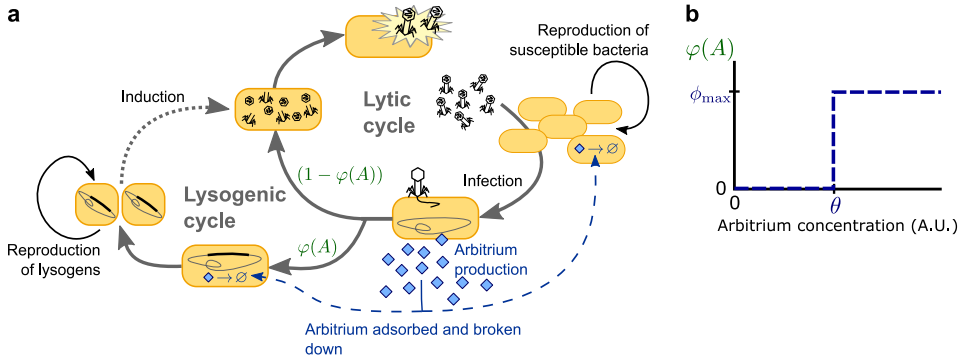

Figure 3.1. Model overview. (a) Free phages infect susceptible bacteria, at which point a fixed amount of arbitrium is produced. This arbitrium is taken up and degraded by susceptible cells and lysogens. Upon infection, a cell enters the lysogenic cycle with propensity $\varphi(A)$, or the lytic cycle with propensity $(1-\varphi(A))$; the lysogeny propensity $\varphi(A)$ depends on the current arbitrium concentration. The lytic cycle leads to immediate lysis of the host cell and release of a burst of new virions. In the lysogenic cycle, the phage remains dormant in the lysogen population, which grows logistically with the same rate as the susceptible cell population. Lysogens are spontaneously induced at a low rate, at which point they re-enter the lytic cycle. (b) In communicating phages, the lysogeny propensity $\varphi(A)$ is modelled by a step-function characterised by two phage characteristics: θ, the arbitrium concentration above which the phage increases its lysogeny propensity, and $\phi_{\max}$, the lysogeny propensity of the phage at high arbitrium concentration.

3.2. Methods

3.2.1. Model

Following earlier modelling work (*e.g.*, Stewart and Levin (1984); Berngruber *et al.* (2013); Sinha *et al.* (2017); Wahl *et al.* (2019)), we use ordinary differential equations to describe a well-mixed system consisting of susceptible bacteria, lysogenically infected bacteria (also called lysogens), free phages, and an arbitrium-like signalling peptide (Figure 3.1a). For simplicity, we consider phages that do not affect the growth of lysogenised host cells; susceptible bacteria and lysogens hence both grow logistically with the same growth rate r and carrying capacity K. Lysogens are spontaneously induced at a low rate α, after which they lyse and release a burst of B free phages per lysing cell. Free phage particles decay at a rate δ and adsorb to bacteria at a rate a. Adsorptions to lysogens result in the decay of the infecting

phage, thus describing the well-known effect of superinfection immunity (Hutchison and Sinsheimer, 1971; Susskind *et al.*, 1974; McAllister and Barrett, 1977; Kliem and Dreiseikelmann, 1989; Bondy-Denomy *et al.*, 2016), while adsorptions to susceptible bacteria result in infections with success probability b. We consider the lytic cycle to be fast compared to both bacterial growth and the lysogenic cycle (*c.f.*, Stewart and Levin (1984); Berngruber *et al.* (2013); Sinha *et al.* (2017); Wahl *et al.* (2019)), so that a lytic infection can be modelled as immediate lysis releasing a burst of B free phages. Since the genes encoding arbitrium production are among the first genes to be expressed when a phage infects a host cell (Erez *et al.*, 2017; Stokar-Avihail *et al.*, 2019), each infection leads to an immediate increase of the arbitrium concentration A by an increment c. The lysis-lysogeny decision is affected by the current arbitrium concentration: a fraction $\varphi(A)$ of the infections results in the production of a lysogen, while the remaining fraction $(1-\varphi(A))$ results in a lytic infection. Arbitrium does not decay spontaneously in the model (since it is a small peptide, spontaneous extracellular degradation is considered to be negligible), but it is taken up by bacteria at a rate u (*e.g.*, through general bacterial peptide importers such as OPP (Erez *et al.*, 2017)), and then degraded intracellularly.

Consider competing phage variants i that differ in their (arbitrium-dependent) lysogeny propensity $\varphi_i(A)$. The population densities of susceptible bacteria S, phage particles P_i and corresponding lysogens L_i, and the concentration of arbitrium A can then be described by:

$$\frac{\mathrm{d}S}{\mathrm{d}t} = \underbrace{rS(1-N/K)}_{\text{logistic growth}} - \underbrace{baS\sum_i P_i}_{\text{infection}}, \tag{3.1}$$

$$\frac{\mathrm{d}L_i}{\mathrm{d}t} = \underbrace{rL_i(1-N/K)}_{\text{logistic growth}} + \underbrace{\varphi_i(A)baSP_i}_{\text{lysogenic infection}} - \underbrace{\alpha L_i}_{\text{induction}}, \tag{3.2}$$

$$\frac{\mathrm{d}P_i}{\mathrm{d}t} = \underbrace{B\alpha L_i}_{\text{burst from induction}} + \underbrace{B(1-\varphi_i(A))baSP_i}_{\text{burst from lytic infection}} - \underbrace{\delta P_i}_{\text{phage decay}} - \underbrace{aNP_i}_{\text{adsorption}}, \tag{3.3}$$

$$\frac{\mathrm{d}A}{\mathrm{d}t} = \underbrace{cbaS\sum_i P_i}_{\text{production upon infection}} - \underbrace{uNA}_{\text{adsorption and degradation}}, \tag{3.4}$$

where $N = S + \sum_i L_i$ is the total density of bacteria.

We study two scenarios for the lysis-lysogeny decision: (i) the arbitrium concentration does not affect the lysis-lysogeny decision; each phage variant has a constant lysogeny propensity ϕ_i, and (ii) the arbitrium concentration does affect the lysis-lysogeny decision; each phage variant causes lytic infection when the arbitrium concentration is low, but switches to some lysogeny propensity $\phi_{\max_i}$ when

the arbitrium concentration exceeds the phage's response threshold θ_i (Figure 3.1b). Though omitted from Eq 3.1–3.4 for readability, mutations between phage variants were included in the model (Supplementary Text 3.6.1). Under scenario (ii), mutations in $\phi_{\max}$ and θ are implemented as independent processes.

3.2.2. Parameters

In total, the model (Eq 3.1–3.4) has 9 parameters. As far as we are aware, none of these have been estimated for phages of the SPBeta group, but many have been measured for other phages, most of which infect *E. coli* (Little *et al.*, 1999; de Paepe and Taddei, 2006; Wang, 2006; Shao and Wang, 2008; Zong *et al.*, 2010; Berngruber *et al.*, 2013). We first nondimensionalised the equations, which reduced the number of parameters to 5, and then derived estimates for these parameters using data from other phages (Supplementary Text 3.6.1.4). To account for the uncertainty in these estimates, we analysed the model for a broad range of parameter values (Supplementary Table S3.1) to confirm that the results hold in general.

Numerical integration and analysis were performed in Matlab R2017b, using the built-in ODE-solver `ode45`. Scripts are available from the corresponding author upon request.

3.3. Results

Evolution of the lysis-lysogeny decision and arbitrium communication requires perturbations away from equilibrium

A common approach to analysing ODE-models such as Eq 3.1–3.4 is to characterise the model's equilibrium states (*c.f.*, Stewart and Levin (1984); Wahl *et al.* (2019); Cortes *et al.* (2019)). Such an analysis is provided in Supplementary Text 3.6.2. However, we will here argue that to understand the evolution of arbitrium communication, and the lysis-lysogeny decision in general, considering the equilibrium states is insufficient.

Firstly, the function of the arbitrium system is to allow phages to respond to changes in the density of susceptible cells and phages as reflected in the arbitrium concentration. But when the population approaches an equilibrium state, the densities of susceptible cells and phages become constant, and so does the arbitrium concentration. Equilibrium conditions hence defeat the purpose of small-molecule communication such as the arbitrium system. Evolution of small-molecule communication must be driven by dynamical ecological processes, and hence can only be studied in populations that are regularly perturbed away from their ecological

steady state.

Secondly, under equilibrium conditions natural selection can act on the lysis-lysogeny decision only if infections still take place, and hence lysis-lysogeny decisions are still taken. We argue that this is unlikely. If the phage population is viable (*i.e.*, if the parameter values are such that the phages proliferate when introduced into a fully susceptible host population), the model converges to one of two qualitatively different equilibria, depending on parameter conditions (Supplementary Text 3.6.2): either (i) susceptible host cells, lysogens and free phages all coexist, or (ii) all susceptible host cells have been infected so that only lysogens and free phages remain. The evolution of a constant lysogeny propensity in a host-phage population with a stable equilibrium of type (i) was recently addressed by Wahl *et al.*, who show that under these conditions selection always favours phage variants with high lysogeny propensity (*i.e.*, $\phi = 1$) (Wahl *et al.*, 2019). However, only a narrow sliver of parameter conditions permits a stable equilibrium of type (i) (Sinha *et al.*, 2017; Cortes *et al.*, 2019), and when we estimated reasonable parameter conditions based on a variety of well-studied phages, we found that they typically lead to a stable equilibrium of type (ii) (Supplementary Text 3.6.2, parameter estimates based on Little *et al.* (1999); de Paepe and Taddei (2006); Wang (2006); Shao and Wang (2008); Zong *et al.* (2010); Berngruber *et al.* (2013)). This is because phage infections tend to be highly effective: their large burst size and consequent high infectivity cause temperate phages to completely deplete susceptible host cell populations, replacing them with lysogens that are immune to superinfection (Bossi *et al.*, 2003; Gama *et al.*, 2013). In that case, after a short epidemic no more infections take place, and competition between different phage variants ceases (see Figure 3.2a for example dynamics). Hence there is no long term selection on the lysis-lysogeny decision, and studying its evolution in this state is pointless.

We therefore consider a scenario in which the system of Eq 3.1–3.4 is regularly perturbed away from equilibrium. To do so, we expose the phage population to a serial-passaging regime (*c.f.*, Bull *et al.* (1993, 2004); Bollback and Huelsenbeck (2007); Betts *et al.* (2013); Broniewski *et al.* (2020)). We initialise the model with a susceptible bacterial population at carrying capacity ($S = K$) and a small density of phages, numerically integrate Eq 3.1–3.4 for a time T, then transfer a fraction of the phage population to a new population of susceptible bacteria at carrying capacity, and repeat this cycle to bring about a long series of epidemics. The phage population is diluted when it is transferred but the relative frequency of the different phage variants is kept constant, thus ensuring that the phage variants that were highly prevalent in the phage population at the end of an episode remain at a high relative frequency at the start of the new episode.

In the absence of arbitrium communication, bet-hedging phages are selected with low constant lysogeny propensity

To form a baseline expectation of the evolution of the lysis-lysogeny decision under the serial-passaging regime, we first considered a population of phage variants that do not engage in arbitrium communication, but do differ in their constant lysogeny propensity ϕ_i. Under typical parameter conditions (Supplementary Table S3.1), each passaging episode starts with an epidemic in which the susceptible cell population is depleted, followed by a period in which the bacterial population is made up of lysogens only (Figure 3.2a, dynamics shown for a passaging episode length $T = 12\,\text{h}$). The composition of the phage and lysogen populations initially changes over subsequent passaging episodes (Figure 3.2a), but eventually an evolutionarily steady state is reached in which one phage variant dominates the phage population ($\phi = 0.04$; Figure 3.2b), confirming that the lysis-lysogeny decision is indeed under selection.

The distribution of phage variants at evolutionarily steady state depends on the time between passages, T (Figure 3.2c). If this time is short ($T \leq 5\,\text{h}$), the phage variant with $\phi = 0$ dominates at evolutionarily steady state. This is an intuitive result: under these conditions phages are mostly exposed to environments with a high density of susceptible cells, in which a lytic strategy is favourable. Surprisingly, however, if the time between passages is sufficiently long ($T > 5\,\text{h}$), the viral quasi-species at evolutionarily steady state always centres around the same phage variant, independent of T ($\phi = 0.04$; Figure 3.2c). This result can be explained by considering the dynamics within a passaging episode (see Figure 3.2a): Once the susceptible cell population has collapsed, free phages no longer cause new infections and are hence "dead ends". New phage particles are then formed by reactivation of lysogens only, so that the distribution of variants among the free phages comes to reflect the relative variant frequencies in the lysogen population. Hence, when the time between passages is sufficiently long, the phage type that is most frequent in the sample that is eventually passaged is the one that is most frequent in the population of lysogens (Supplementary Figure S3.1). Under default parameter conditions, these are the phages with a low lysogeny propensity of $\phi = 0.04$.

To examine how these results depend on the model parameters, we determined which phage variant was most abundant at evolutionarily steady state for 500 randomly chosen parameter sets (see Supplementary Table S3.1 for parameter ranges), always using a long time between passages ($T = 24\,\text{h}$). The selected ϕ-values for all parameter settings lie between $\phi = 0$ and $\phi = 0.12$ (y-axis of Figure 3.2d). We can hence conclude that selection favours phages with low but usually non-zero lysogeny propensities. These phages employ a bet-hedging strategy: throughout the epidemic they "invest" a small part of their infection events in the production of lysogens, such that they are maximally represented in the eventual lysogen population.

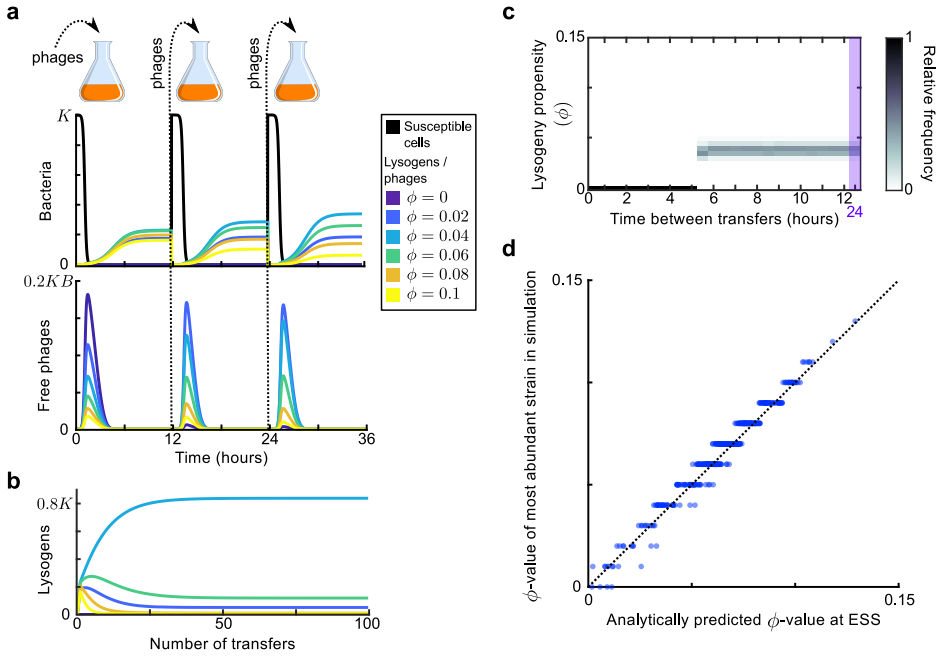

Figure 3.2. Results in the absence of phage communication. (a) Short-term model dynamics under default parameter conditions (Supplementary Table S3.1) and a passaging episode duration of $T = 12$ hours. The model was initialised with a susceptible bacterial population at carrying capacity ($S = K$) and a low frequency of phages ($\sum_i P_i = 10^{-5}KB$), and upon passaging the phages were diluted 100-fold. Dynamics within a single passaging episode are further illustrated in Supplementary Figure S3.1. (b) Long-term model dynamics for default parameter settings and $T = 12$ h. Over many passages, a single phage variant ($\phi = 0.04$) is selected. (c) Distribution of phage variants at evolutionarily steady state as a function of the time between passages, T. A total number of 101 phage variants was included, with lysogeny propensities varying between $\phi_1 = 0$ and $\phi_{101} = 0.5$. When the interval between passages is short, the susceptible cells are not depleted during the rounds of infection and a fully lytic strategy ($\phi = 0$) is selected. For larger values of T, however, a bet-hedging strategy with small but non-zero ϕ-value is selected ($\phi \approx 0.04$). (d) Parameter sweep results. The model was run with 500 sets of randomly sampled parameters, and for each run the most abundant ϕ-value in the population at evolutionarily steady state was plotted against the analytically predicted evolutionarily stable strategy (ESS; see Supplementary Text 3.6.3, 3.6.4 and Box 3.1). The dotted line is the identity line. The analytically derived ESS is a good predictor of the simulation outcome.

To better understand how the lysogeny propensity ϕ that is selected depends on parameter values, we derived an analytical approximation for the evolutionarily stable strategy (ESS) under the serial-passaging regime (Supplementary Text 3.6.3, 3.6.4). Because the phage dynamics during an epidemic affect the dynamics of the susceptible cells and *vice versa*, phage fitness is frequency dependent and the ESS is not found by a simple optimisation procedure, but by identifying the particular ϕ-value, denoted ϕ^*, that maximises phage fitness given that this strategy ϕ^* itself shapes the dynamics of the epidemic (Box 3.1). We find that the ESS can be approximated by the surprisingly simple expression

$$\phi^* = \frac{1 - (bB)^{-1}}{-\log\left(\frac{P_0}{BK}\right)}, \tag{3.5}$$

where P_0 is the density of phages at the start of a passaging episode. Since $P_0/(BK) \ll 1$, the logarithm in the denominator of Eq 3.5 is negative. This approximation corresponds well with the results of the parameter sweep (Figure 3.2d), indicating that it indeed captures the most important factors shaping the evolution of the lysogeny propensity ϕ.

Eq 3.5 shows that the ESS depends on the initial phage density in a passaging episode, P_0, relative to the burst size B and maximal host-cell density K, and the effective burst size bB, which represents the expected number of progeny phages per phage that adsorbs to a susceptible bacterium. The ESS ϕ^* decreases with the dilution factor of the phages upon passage (*i.e.*, with lower P_0). On the other hand, ϕ^* increases with the effective burst size bB (note that $(bB)^{-1}$ decreases when (bB) increases). Both effects can be intuitively understood by considering how these factors affect the duration of the epidemic, T_E. If the phage density is low at the start of a passaging episode or if the phages have a small effective burst size, it takes a while before the phage population has grown sufficiently to cause the susceptible population to collapse. Since a lytic strategy is favoured early in the epidemic, when the susceptible cell density is still high, a longer epidemic favours phages with lower values of ϕ (see the red line in the figure in Box 3.1). On the other hand, if the initial phage density is high or if the phages have a high effective burst size, the susceptible cell population collapses quickly, phages have a much shorter window of opportunity for lysogen production, and hence phages with higher ϕ-values are favoured.

Box 3.1: Lysogeny propensity of the evolutionarily stable strategy (ESS)

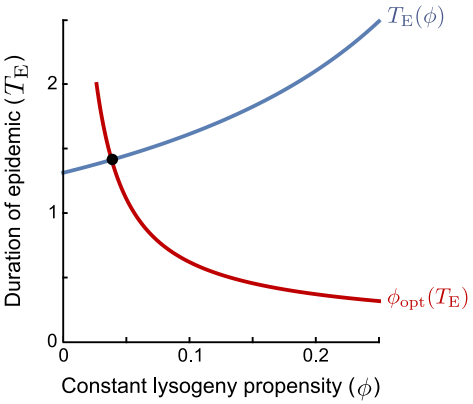

An evolutionarily stable strategy (ESS) is a strategy that cannot be invaded by any other strategy. In the context of the lysogeny propensity ϕ, it is the value ϕ^* such that a population currently dominated by a phage with $\phi = \phi^*$ cannot be invaded by any phage variant with a different ϕ-value. A phage variant with $\phi = \phi_i$ invading in a resident population with the same $\phi = \phi_i$ always grows exactly like the resident. If this is the best possible invader, any other phage variant must perform worse than the resident and cannot invade. Hence, the ESS is the *optimal response to itself*. However, we still have to define what it means to be the "best possible invader" under the serial-passaging regime. Note that if the time between passages is sufficiently long, phages are selected on their ability to produce lysogens during the active epidemic (see Main Text). The optimal invader is hence the phage variant that, when introduced at a very low frequency, produces the most lysogens *per capita* between time $t = 0$ and the time that the susceptible cell population collapses, T_E. The ϕ-value of the optimal invader depends on T_E (red line in plot): if the epidemic phase is short, lysogens have to be produced quickly and a high ϕ-value is optimal, while if the epidemic lasts longer, phages can profit more from lytic replication and a lower ϕ-value is optimal. In turn, however, the duration of the epidemic T_E depends on the lysogeny propensity ϕ of the resident phage population (blue line in plot): phages with a lower value of ϕ replicate more rapidly and hence cause an earlier collapse of the susceptible population. The ESS is the value ϕ^* that is optimal given the collapse time $T_E(\phi^*)$ that results when ϕ^* itself is the resident strategy. Graphically, this value can be identified as the intersection of $T_E(\phi)$ and $\phi_{opt}(T_E)$ (the red and blue lines).

If arbitrium communication is included, communicating phages are selected that switch from a fully lytic to a fully lysogenic strategy

Next, we included the possibility of arbitrium communication and let phage variants be characterised by two properties: their arbitrium response threshold, θ_i, and their lysogeny propensity when the arbitrium concentration exceeds their response threshold, $\phi_{\max_i}$ (see Figure 3.1b). We then again considered the dynamics of our model under serial passaging of the phage population.

In Figure 3.3a, example dynamics are shown for three competing phage variants, all with $\phi_{\max} = 1$ but with different response thresholds θ_i. The arbitrium concentration increases over the course of the epidemic, and the phage variants switch from lytic infection to lysogen production at different times because of their different response thresholds.

Note that the maximum arbitrium concentration obtained during a passaging episode is approximately $A = cK$ (Figure 3.3a). This is because during the epidemic the dynamics of the susceptible cell density are mostly determined by infection events and not so much by the (slower) bacterial growth. Since the arbitrium concentration increases by an increment c every time a susceptible cell is infected, the infection of all initial susceptible cells will result in an arbitrium concentration of $A = cK$ (assuming that the degradation of arbitrium is also slow and can be ignored during the growth phase of the epidemic). The arbitrium concentration during the early epidemic then is a direct reflection of the fraction of susceptible cells that have so far been infected.

To study the evolution of arbitrium communication, we again considered the distribution of phage variants at evolutionary steady state for varying values of the time between passages, T. Similar to the results shown in Figure 3.2c, we find two regimes (Figure 3.3b): if the time between passages is short ($T < 5$ hours, illustrated by $T = 2$ h in Figure 3.3b)), selection favours phage variants that only cause lytic infections ($\phi_{\max} = 0$); if the time between passages is sufficiently long ($T \geq 5$ h, illustrated by $T = 12$ h in Figure 3.3b) the phage population is dominated by variants with $\phi_{\max} = 1$ and $\theta \approx 0.65cK$. Hence, if the time between passages is sufficiently long, phage variants are selected that switch from a completely lytic to a completely lysogenic strategy when the arbitrium concentration exceeds a certain threshold.

In the simulations of Figure 3.3b, phage variants could have emerged that use the bet-hedging strategy found in the absence of communication (in phage variants with $\theta = 0$, the lysogeny propensity is always $\phi_{\max}$, independently of the arbitrium concentration), but this did not happen. This suggests that any bet-hedging phage variants were outcompeted by variants that do use arbitrium communication.

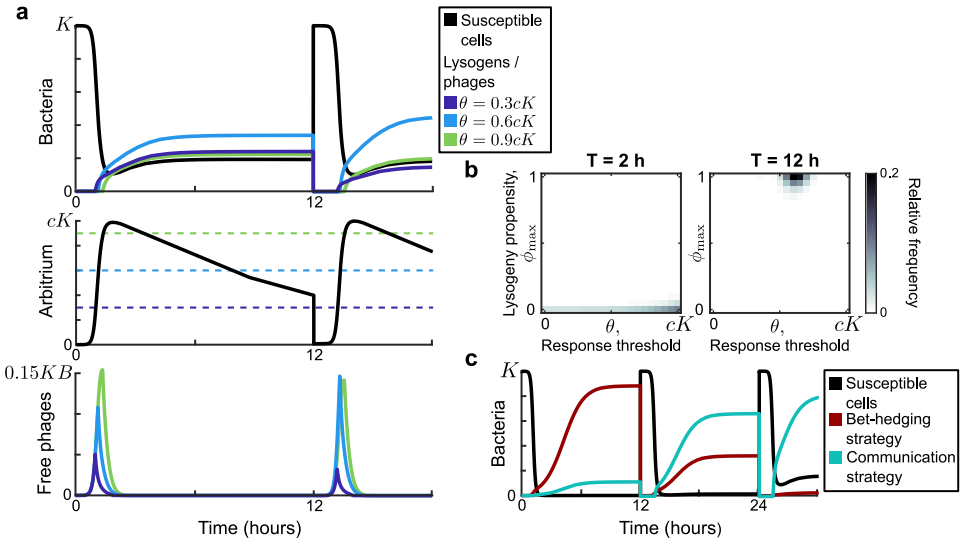

Figure 3.3. Model dynamics if phage communication is included in the model. (a) Short-term dynamics for default parameter conditions (Supplementary Table S3.1) and the same serial-passaging regime as in Figure 3.2. This example shows the competition between three phage variants, all with $\phi_{\max} = 1$ but with varying response thresholds θ. (b) Distribution of phage variants at evolutionary steady state for varying passaging episode durations T. In total 441 phage variants were included in this analysis, covering all combinations of $\phi_{\max}$ between 0 and 1 and θ between 0 and cK with step sizes 0.05 and $0.05cK$, respectively. When the interval between passages is very short, again a fully lytic strategy ($\phi_{\max} = 0$) is selected. For longer times between passages, however, we consistently see that a strategy with $\phi_{\max} = 1$ and $\theta \approx 0.65cK$ dominates the population. The results shown for $T = 2$ h are representative for values of $T \leq 4$ h, while the results shown for $T = 12$ h represent results obtained for $T \geq 5$ h (see Supplementary Figure S3.2 for distributions for a large range of T-values). (c) Rapid invasion by "optimally" communicating phages into a population of phages with the "optimal" bet-hedging strategy. The bet-hedging phages have $\phi = 0.04$ (see Figure 3.2c), while the communicating phages are characterised by $\phi_{\max} = 1$ and $\theta = 0.66cK$ (see panel c). The communicating phage is initialised at a frequency of 1% of the bet-hedging phage.

To confirm this observation, we simulated a competition experiment between the bet-hedging phage variant that was selected in the absence of communication and the communicating variant selected when arbitrium dynamics were included (Figure 3.3c). The communicating phage quickly invades on a population of bet-hedging phages and takes over the population, confirming that communication is indeed favoured over bet-hedging.

Evolved phages switch from the lytic to the lysogenic life-cycle when approximately half of the susceptible cells have been infected

To study how the evolution of phage communication depends on phage and bacterial characteristics, 500 simulations were performed with randomly sampled sets of parameter values (Supplementary Table S3.1), using a long time between serial passages ($T = 24$ h). For each simulation, we determined which phage variant was most prevalent at evolutionary steady state. Although we varied the parameter values over several orders of magnitude, the most prevalent phage variant had a lysogeny propensity of $\phi_{\max} = 1$ and a response threshold of $\theta = 0.5cK$ or $\theta = 0.6cK$ in almost all simulations (Figure 3.4a). Hence, over a broad range of parameter values, phages are selected that use the arbitrium system to switch from a fully lytic to a fully lysogenic strategy (*i.e.*, $\phi_{\max} = 1$). This suggests that over the course of an epidemic, there is an initial phase during which the lytic strategy is a "better" choice (*i.e.*, produces the most progeny on the long run), while later in the epidemic the production of lysogens is favoured and residual lytic infections that would results from a lysogeny propensity $\varphi < 1$ are selected against.

To better understand the intriguing consistency in θ-values found in the parameter sweep, we used a similar approach as before to analytically derive an approximation for the response threshold θ^* of the evolutionarily stable strategy (Supplementary Text 3.6.5). Again, we find a surprisingly simple expression for the ESS:

$$\theta^* = \frac{cK}{2 - (bB)^{-1}}. \tag{3.6}$$

Note that the expression in Eq 3.6 again depends on the effective burst size bB, which is an indicator of the phage's infectivity. The evolutionarily stable response threshold θ^* declines as the effective burst size increases, converging to a value of $\theta^* = \frac{1}{2}cK$ for highly infective phages (Figure 3.4b, green line). The same result was found for simulations of the competition between phage variants with different θ-values under different effective burst sizes (Figure 3.4b, blue dots). Eq 3.6 hence provides a good prediction for the response threshold value that is selected over evolutionary time, especially for phages with high effective burst size (Figure 3.4b).

The result in Eq 3.6 can be further understood biologically. Remember that the arbitrium concentration during the epidemic varies between $A = 0$ and $A = cK$, and is a reflection of the fraction of susceptible cells that have so far been infected. It makes sense that the evolutionarily stable response threshold causes phages to switch infection strategy somewhere in the middle of the epidemic: if a phage variant switches to the lysogenic strategy too early, its free phage population does not expand enough to compete with phages that switch later, but if it switches too late, the susceptible-cell density has decreased to such a degree that the phage has missed the window of opportunity for lysogen production. The ESS results

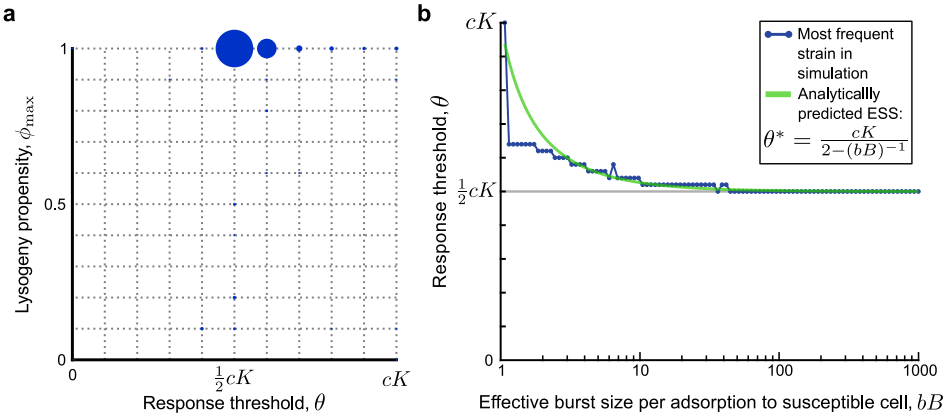

Figure 3.4. Parameter dependance of the selected values of ϕ_{max} and θ. (a) Parameter sweep results. 500 simulations were run with randomly sampled parameters (Supplementary Table S3.1). In each simulation, 121 phage variants were included, covering all combinations of $\phi_{max} = 0$ to $\phi_{max} = 1$ and $\theta = 0$ to $\theta = cK$ with step sizes 0.1 and $0.1cK$, respectively. The size of the circles corresponds to the number of simulations that yielded that particular phage variant as most abundant at evolutionary steady state. (b) Analytically predicted θ-value as a function of the effective burst size per adsorption to a susceptible cell, bB), and most abundant phage variant found in a simulation with varying bB but otherwise default parameter values, $T = 24$ h, $\phi_{max} = 1$ and $\theta = 0, 0.02cK, \ldots, cK$. The range on the x-axis is equal to the range sampled in the parameter sweep. The analytically derived evolutionarily stable θ^* is a good prediction for the response threshold selected in the simulations, especially for phages with high effective burst size.

from a balance between the fast production of phage progeny during the initial lytic cycles and the eventual production of sufficient lysogens. For phages with a high effective burst size, this balance occurs around the time that half of the available susceptible cells have been infected. Phages with lower effective burst size are however predicted to switch later, because these phages need to invest a larger portion of the available susceptible cells in the production of free phages to produce a sufficient pool of phages that can later form lysogens. Note, however, that the range of biologically reasonable effective burst sizes includes many high values (range of x-axis in Figure 3.4b, Supplementary Table S3.1), *i.e.*, many real-life phages have high infectivity. Hence, for natural phages in general, we predict that if they evolve an arbitrium-like communication system, communication will be used to switch from causing mostly lytic to mostly lysogenic infections when in an outbreak approximately half of the pool of susceptible bacteria has been infected.

3.4. Discussion

We have presented a mathematical model of a population of phages that use an arbitrium-like communication system, and used this model to explore the evolution of the lysis-lysogeny decision and arbitrium communication under a serial-passaging regime. When arbitrium communication was excluded from the model, we found that bet-hedging phages with relatively low lysogeny propensity were selected. But when arbitrium communication was allowed to evolve these bet-hedging phages were outcompeted by communicating phages. These communicating phages switch from a lytic strategy early in the epidemic to a fully lysogenic strategy when approximately half of the available susceptible cells have been infected.

The serial-passaging set-up of the model is crucial for the evolution of the lysis-lysogeny decision and arbitrium communication. This has two main reasons. Firstly, it ensures that the phages are regularly exposed to susceptible cells, thus maintaining selection pressure on the lysis-lysogeny decision. Because of their high infectivity (see Methods section and de Paepe and Taddei (2006); Wang (2006)), most temperate phage outbreaks will completely deplete pools of susceptible bacteria, resulting in a bacterial population consisting of lysogens only in which the phage no longer replicates through infection (Bossi *et al.*, 2003; Gama *et al.*, 2013). The bet-hedging strategy we found in the absence of phage communication is a mechanism to deal with these (self-inflicted) periods of low susceptible cell availability, consistent with earlier studies (Maslov and Sneppen, 2015; Sinha *et al.*, 2017). Secondly, the serial-passaging set-up imposes a dynamic of repeated epidemics in which a small number of phages is introduced into a relatively large pool of susceptible cells. Such dynamics are necessary for the arbitrium system to function: the arbitrium concentration provides a reliable cue for a phage's lysis-lysogeny decision only if it is low at the beginning of an epidemic and subsequently builds up to reflect the fraction of cells that have so far been infected.

Based on these considerations, we can stipulate which environments promote the evolution of small-molecule communication such as the arbitrium system. One major factor that can ensure a regular exposure to susceptible cells (the first requirement) is spatial structure. If phages mostly infect bacteria that are physically close to them, a global susceptible population can be maintained even though susceptible bacteria may be depleted in local environments (Kerr *et al.*, 2006). Indeed, spatial structure has been shown to greatly influence phage evolution, for instance by promoting the selection of less virulent strains that deplete their local host populations more slowly (Kerr *et al.*, 2006; Heilmann *et al.*, 2010; Berngruber *et al.*, 2015). For small-molecule communication to evolve, however, the phages would also have to undergo repeated, possibly localised, outbreak dynamics (the second requirement). Such dynamics could occur in structured meta-populations of isolated bacterial pop-

ulations, between which the phages spread at a limited rate. Alternatively, phages might encounter large pools of newly susceptible bacteria if they escape superinfection immunity through mutation (Zinder, 1958; Bailone and Devoret, 1978; Scott *et al.*, 1978). This scenario does however require the arbitrium concentration to be low when the mutation occurs, so that the signal again provides information about the number of susceptible cells available. This could happen either if the arbitrium produced during previous epidemics has been degraded once the mutation occurs, or if the mutation co-occurs with a second mutation that changes the phage's signal specificity. This second argument might in part explain the large diversity of phage signalling peptides observed (Erez *et al.*, 2017; Stokar-Avihail *et al.*, 2019).

The model presented in this paper allows us to put hypotheses about the arbitrium system to the test. For instance, it has been suggested that the arbitrium system would benefit from the production of arbitrium by lysogens, because phages thereby would be warned about the presence of neighbouring lysogens (which are immune to superinfection) (Hynes and Moineau, 2017). Above we have argued, however, that under repeated epidemics, such as caused by serial passaging, selection on the lysis-lysogeny decision and arbitrium signalling is limited to the relatively short window of time in which all (locally) present susceptible cells become infected: afterwards no new infections occur and arbitrium therefore has no effect. During this short time window, the density of lysogens is still low, and any arbitrium produced by lysogens contributes little to the information already conveyed by arbitrium produced during infection events. Hence, our model predicts that, under repeated epidemics that completely deplete (local) pools of susceptible cells, the effects of arbitrium production by lysogens are likely very minimal.

Intriguingly, our model predicts that phages using small-molecule communication to coordinate their lysis-lysogeny decision would be selected to switch from a lytic to a lysogenic strategy once approximately half of the available susceptible bacteria have been lytically infected. This prediction warrants experimental testing. However, it also raises the question of how the phages would "know" at what bacterial density the susceptible population has been halved. For the arbitrium signal to carry information about the density of remaining susceptible cells, the initial concentration of susceptible bacteria has to be similar from outbreak to outbreak. While this was imposed in the serial-passaging regime used here, it is much less obvious that such a requirement would be met in natural environments. This limitation, however, is not unique to phage communication. For instance, it also complicates bacterial quorum sensing: as previously described, the concentration of a signalling molecule is often not determined by the local cell density only, but also depends on environmental properties (Platt and Fuqua, 2010; Popat *et al.*, 2015).

Next to the arbitrium system, several other examples of temperate phages affected by small signalling molecules have recently been described. For instance,

the *Vibrio cholerae*-infecting phage VP882 "eavesdrops" on a quorum sensing signal produced by its host bacteria, favouring lytic over lysogenic infections when the host density is high (Silpe and Bassler, 2019), while in coliphages λ and T4 and several phages infecting *Enterococcus faecalis*, the induction of prophages, *i.e.*, the lysogeny-lysis decision, is affected by bacterial quorum sensing signals (Ghosh *et al.*, 2009; Rossmann *et al.*, 2015; Laganenka *et al.*, 2019). Mathematical and computational modelling can help to better understand the ecology and evolution of these fascinating regulation mechanisms as well.

Acknowledgments

We thank Rob J. de Boer for valuable discussions and comments on the manuscript.

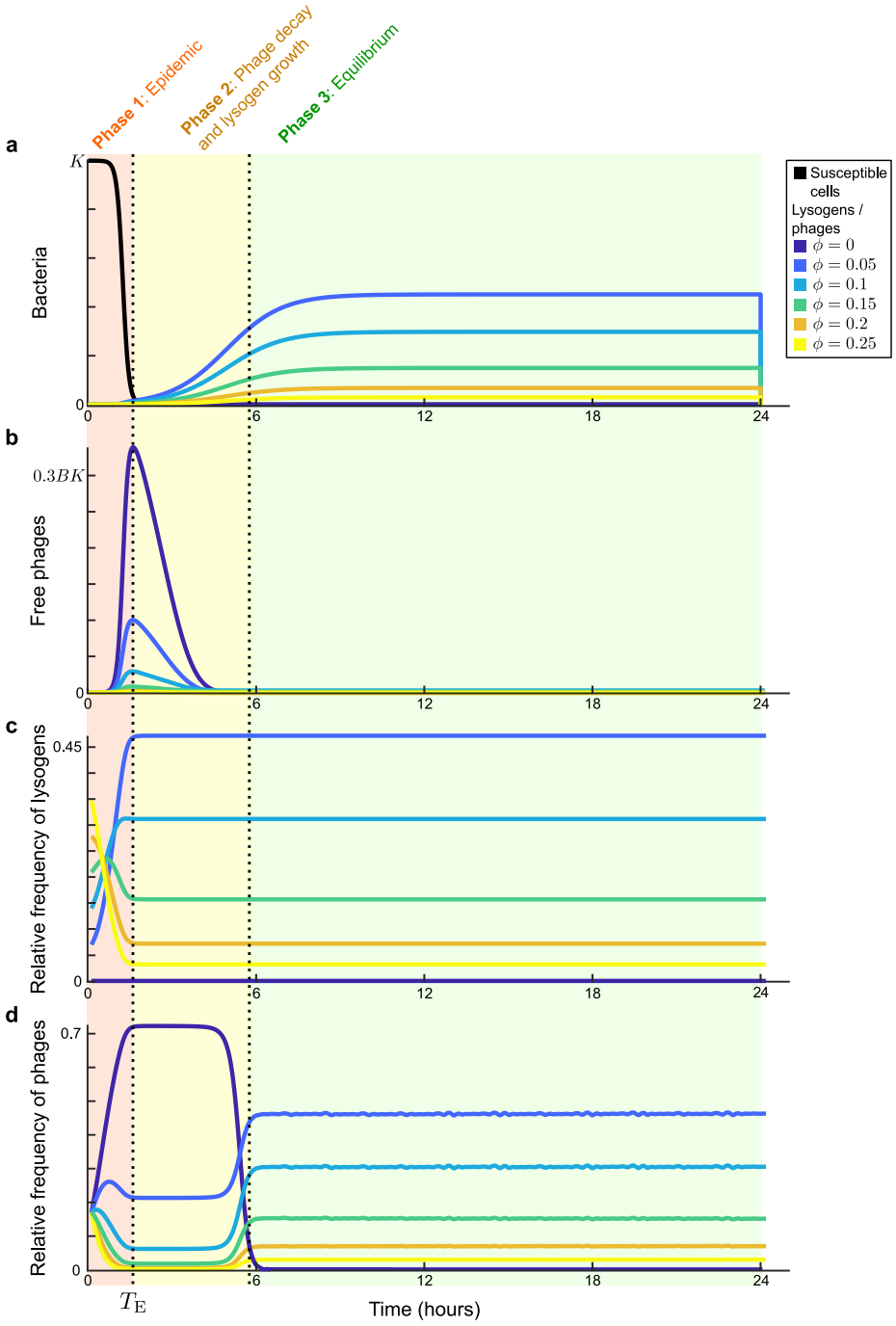

Supplementary Figure S3.1.

3.5. Supplementary Figures

(LEFT) **Supplementary Figure S3.1**

Model dynamics during a single passaging episode for default parameter values and constant lysogeny propensities (no communication). Absolute frequencies of susceptible cells and lysogens (panel a) and phages (panel b) are plotted as a function of time, as well as the relative frequency of the different phage variants in the lysogen population (panel c) and the free phage population (panel d). The dynamics can be divided into three distinct phases: (1) Epidemic: Susceptible cells are still present ($S > 0$) but are being depleted by infection. Phage and lysogen densities increase depending on their lysogeny propensity ϕ_i. The relative frequencies in the lysogen population are established. (2) Transition phase: Infections no longer take place because the susceptible cell population has been depleted ($S \approx 0$). The lysogen population grows until it reaches its carrying capacity. Free phage densities decline because of natural decay and adsorption to lysogens. The influx of free phages by reactivation of lysogens differs per phage variant because the density of their corresponding lysogens differs, and the relative frequencies in the free phage pool change to reflect this. (3) Equilibrium phase: The total lysogen population is at carrying capacity, and the relative frequencies of the phage variants in the (eventually passaged) free phage pool reflect the relative frequencies of phage variants in the lysogen population.

(NEXT PAGE) **Supplementary Figure S3.2**

Most abundant phage variant at evolutionary steady state for different lengths of the time interval between passages T. Default parameter settings (Supplementary Table S3.1). In each run, 441 variants were included: all combinations of $\phi_{\max} = 0, 0.05, \ldots, 1$ and $\theta = 0, 0.05cK, \ldots, cK$. Simulations were run for 1000 passaging episodes to reach evolutionary steady state, after which the phage variant distribution was plotted. For $T < 4\,\mathrm{h}$ phages with a fully lytic strategy ($\phi_{\max} = 0$) are selected, while for $T \geq 5\,\mathrm{h}$ phages are selected that switch from a fully lytic strategy at low arbitrium concentration to a fully lysogenic strategy ($\phi_{\max} = 1$) at high arbitrium concentration.

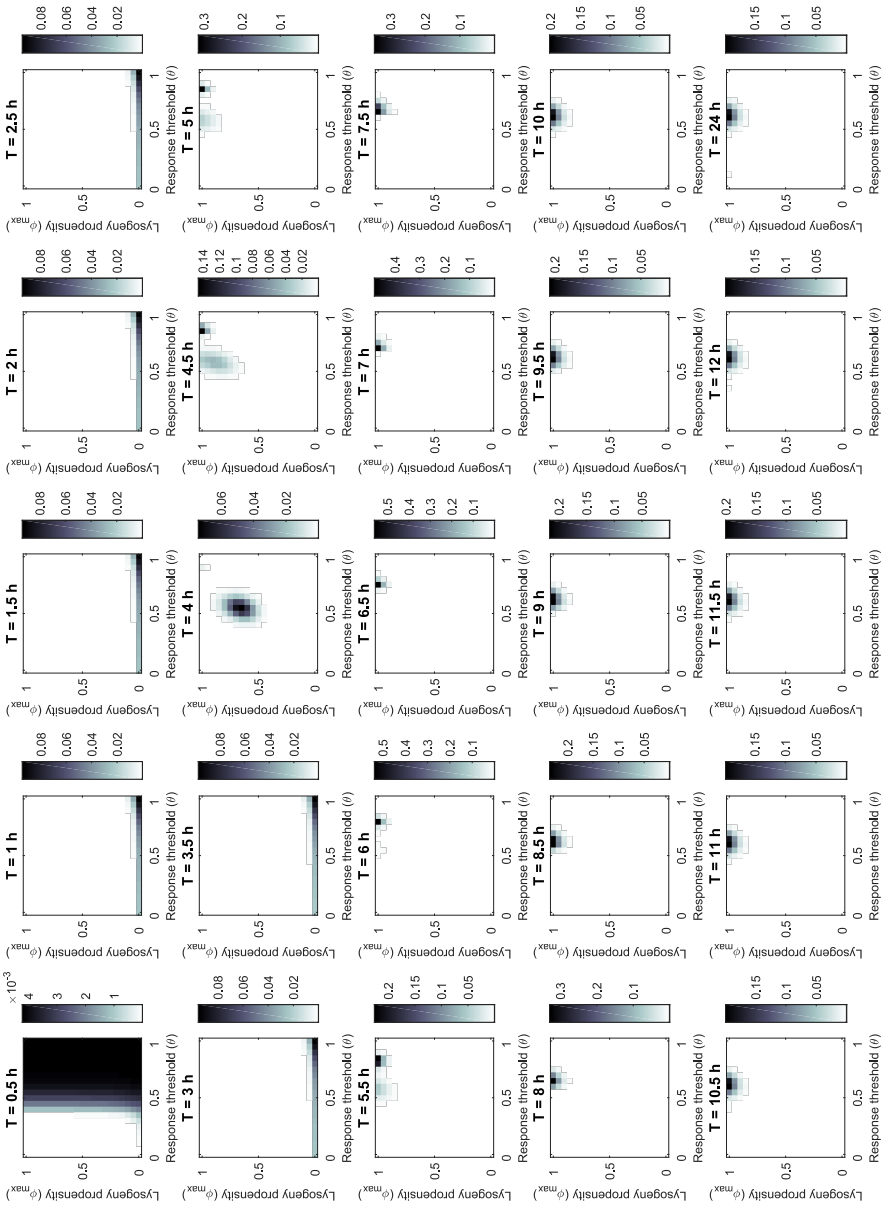

Supplementary Figure S3.2.

3.6. Supplementary Text

3.6.1. Model equations and Parameters

3.6.1.1. Full model equations, including mutations

For readability, the model equations in the main text (Eq 3.1–3.4) did not include mutations between phage variants. Here, we present the full model equations, including mutations. We assume that mutations happen when new phage particles (and hence new copies of the phage's genetic material) are formed prior to lysis of the host cell. Infection with a parent phage of variant j results in progeny phages of variant i with probability μ_{ij}, where μ_{ii} is the probability that offspring of a parent phage of type-i has no mutations. The full model reads:

$$\frac{\mathrm{d}S}{\mathrm{d}t} = rS(1 - N/K) - baSP, \tag{S3.1}$$

$$\frac{\mathrm{d}L_i}{\mathrm{d}t} = rL_i(1 - N/K) + \varphi_i(A)baSP_i - \alpha L_i, \tag{S3.2}$$

$$\frac{\mathrm{d}P_i}{\mathrm{d}t} = B\sum_j \mu_{ij}\left(\alpha L_j + [1 - \varphi_j(A)]baSP_j\right) - \delta P_i - aNP_i, \tag{S3.3}$$

$$\frac{\mathrm{d}A}{\mathrm{d}t} = cbaSP - uNA, \tag{S3.4}$$

with

$$\varphi_i(A) = \phi_i \tag{S3.5}$$

if arbitrium communication is excluded from the model, and

$$\varphi_i(A) = \begin{cases} 0 & \text{if } A \leq \theta_i, \\ \phi_{\max_i} & \text{if } A > \theta_i \end{cases} \tag{S3.6}$$

if arbitrium communication is included (see Figure 3.1b).

In the first part of the manuscript, where we exclude arbitrium communication from the model, phage variants are characterised by their constant lysogeny propensity ϕ_i (Eq S3.5). Mutations between phage variants were implemented in a hill-climbing fashion, *i.e.*, $\mu_{ij} = \mu > 0$ if ϕ_j is one step higher or lower than ϕ_i, and $\mu_{ij} = 0$ $(i \neq j)$ otherwise. Throughout this study, a value of $\mu = 5 \cdot 10^{-4}$ was used. Varying μ affects the width of the quasispecies found, but not the actual outcome of the simulations.

In the second part of the manuscript, where we include the possibility of arbitrium communication, phage variants are characterised by two properties (Eq S3.6):

their arbitrium threshold θ_i and the lysogeny propensity obtained when the arbitrium concentration exceeds this threshold, $\phi_{\max_i}$. Mutations in the values of $\phi_{\max}$ and θ were implemented as independent processes, both happening in a hill-climbing fashion as explained above.

3.6.1.2. Phage variants included in simulations

In the simulations of the restricted model (arbitrium communication excluded) shown in Figure 3.2c, a range of phage variants was included with $\phi_1 = 0$, $\phi_2 = 0.005$, ..., $\phi_{100} = 0.495$, $\phi_{101} = 0.5$. In the simulations presented in Figure 3.2d, a range of phage variants was included of $\phi_1 = 0$, $\phi_2 = 0.01$, ..., $\phi_{100} = 0.99$, $\phi_{101} = 1.0$.

In the simulations of the full model (arbitrium communication included) shown in Figure 3.3b, 441 phage variants were included, representing all possible combinations of $\phi_{\max} = 0, 0.05, \ldots, 1$ and $\theta = 0, 0.05cK, \ldots, cK$. In the simulations of Figure 3.4a, 121 phage variants were included representing all possible combinations of $\phi_{\max} = 0, 0.1, \ldots, 1$ and $\theta = 0, 0.1cK, \ldots, cK$. In the simulations of Figure 3.4b, all phage variants had $\phi_{\max} = 1$, but they varied in $\theta = 0, 0.02cK, \ldots, cK$.

3.6.1.3. Parameter reduction

In total, the model of Eq S3.1-S3.6 has 9 parameters (ignoring mutation probabilities). This number can, however, be reduced by non-dimensionalising the equations. We introduce the dimensionless variables

$$\hat{t} = rt, \qquad \hat{S} = \frac{S}{K}, \qquad \hat{L}_i = \frac{L_i}{K}, \qquad \hat{P}_i = \frac{P_i}{KB}, \qquad \hat{A} = \frac{A}{cK}, \qquad \hat{\theta}_i = \frac{\theta_i}{cK},$$

and define $\hat{P} = \sum_i \hat{P}_i$, $\hat{L} = \sum_i \hat{L}_i$, and $\hat{N} = \hat{S} + \hat{L}$. Let furthermore

$$\hat{B} = bB, \qquad \hat{a} = \frac{aK}{r}, \qquad \hat{\alpha} = \frac{\alpha}{r}, \qquad \hat{\delta} = \frac{\delta}{r}, \qquad \hat{u} = \frac{uK}{r}.$$

Using these new variables and parameters, the equations reduce to:

$$\frac{\mathrm{d}\hat{S}}{\mathrm{d}\hat{t}} = \hat{S}(1 - \hat{N}) - \hat{B}\hat{a}\hat{S}\hat{P}, \tag{S3.7}$$

$$\frac{\mathrm{d}\hat{L}_i}{\mathrm{d}\hat{t}} = \hat{L}_i(1 - \hat{N}) + \hat{\varphi}_i(\hat{A})\hat{B}\hat{a}\hat{S}\hat{P}_i - \hat{\alpha}\hat{L}_i, \tag{S3.8}$$

$$\frac{\mathrm{d}\hat{P}_i}{\mathrm{d}\hat{t}} = \sum_j \mu_{ij}\left(\hat{\alpha}\hat{L}_j + [1 - \hat{\varphi}_j(\hat{A})]\hat{B}\hat{a}\hat{S}\hat{P}_j\right) - \hat{\delta}\hat{P}_i - \hat{a}\hat{N}\hat{P}_i, \tag{S3.9}$$

$$\frac{\mathrm{d}\hat{A}}{\mathrm{d}\hat{t}} = \hat{B}\hat{a}\hat{S}\hat{P} - \hat{u}\hat{N}\hat{A}, \tag{S3.10}$$

with

$$\hat{\varphi}_i(\hat{A}) = \phi_i \tag{S3.11}$$

if arbitrium communication is excluded from the model, and

$$\varphi_i(A) = \begin{cases} 0 & \text{if } A \leq \hat{\theta}_i, \\ \phi_{\max_i} & \text{if } A > \hat{\theta}_i \end{cases} \tag{S3.12}$$

if arbitrium communication is included (see Figure 3.1b).

Five dimensionless parameters are left in Eq S3.7–S3.12: the effective burst size per adsorption of a phage to a susceptible cell, $\hat{B}$, and the scaled rates $\hat{a}$, $\hat{\alpha}$, $\hat{\delta}$, and $\hat{u}$. These non-dimensionalised equations are used throughout the rest of this supplementary text, unless stated otherwise, dropping the hats for convenience.

3.6.1.4. Parameter values

As far as we are aware, no estimates exist for the parameters characterising phages of the SPbeta group. However, many parameters have been measured for a variety of phages infecting *Escherichia coli* (Little *et al.*, 1999; de Paepe and Taddei, 2006; Wang, 2006; Shao and Wang, 2008; Zong *et al.*, 2010; Berngruber *et al.*, 2013). Based on these measurements, we derived reasonable ranges for the model parameters, and chose default parameter values (Table S3.1). To study how our results depend on the model parameter values, parameter sweeps were performed, consisting of 500 simulations with parameter values randomly sampled from the broad parameter ranges (Table S3.1). To ensure that low values of the parameters were well-represented, parameter values were sampled log-uniformly.

A small default value of the effective burst size was chosen to enhance the clarity of Fig 3.2a and Fig 3.3a,c; with a small effective burst size, the epidemic takes some time and competition between phage variants can be visualised more clearly. But much larger effective burst sizes were appropriately included in the parameter sweeps.

3.6.2. Equilibrium analysis

In this section, we find the dynamical equilibria existing in the model, and derive parameter conditions for their stability. This analysis provides us with a baseline expectation of the densities of phages, lysogens, and susceptible cells that the model converges to after sufficient time.

Equilibria of the model are found by equating Eq S3.7–S3.10 to zero and solving for the model variables. By the definition of equilibrium, the arbitrium concentration

Supplementary Table S3.1. Model parameters

Parameter	Description	Default value	Parameter sweep range	References
$\hat{B} = bB$	Effective burst size	2	$1 - 10^3$	de Paepe and Taddei (2006); Wang (2006); Berngruber *et al.* (2013)
$\hat{a} = \frac{aK}{r}$	Scaled adsorption rate of phages to cells	10	$1 - 100$	de Paepe and Taddei (2006); Shao and Wang (2008)
$\hat{\delta} = \frac{\delta}{r}$	Scaled decay rate of phage particles	0.01	$10^{-3} - 0.1$	de Paepe and Taddei (2006)
$\hat{\alpha} = \frac{\alpha}{r}$	Scaled spontaneous phage induction rate	10^{-3}	$10^{-4} - 10^{-2}$	Little *et al.* (1999); Zong *et al.* (2010)
$\hat{u} = \frac{uK}{r}$	Scaled rate of arbitrium uptake and degradation by cells	0.1	$10^{-3} - 1$	-
D	Dilution factor of phages at serial passages	0.01	$10^{-3} - 0.1$	-

at equilibrium is constant:

$$\bar{A} = \begin{cases} \dfrac{Ba\bar{S}\bar{P}}{u\bar{N}} & \text{if } \bar{N} > 0, \\ \bar{A} = 0 & \text{if } \bar{N} = 0, \end{cases} \tag{S3.13}$$

where the bar indicates equilibrium values. Because the equilibrium arbitrium concentration is constant, at equilibrium the different phage variants are characterised by their lysogeny propensity $\varphi_i(\bar{A})$ only, irrespective of whether arbitrium communication is included in the model or not. Hence, expressions for the model equilibria are the same in the absence and presence of arbitrium communication. Below, we derive these expressions, and determine under what conditions the different model equilibria are stable.

In the model, four qualitatively different types of equilibria can occur.

Firstly, there is a trivial equilibrium at $\bar{S} = 0$, and $\bar{L}_i = 0$, $\bar{P}_i = 0$ for all phage variants i. This equilibrium is unstable as long as the bacterial logistic growth rate $r > 0$.

Secondly, there is an equilibrium in which the susceptible population is at car-

rying capacity and the infection is absent: $\bar{S} = 1$, and $\bar{L}_i = 0$, $\bar{P}_i = 0$ for all phage variants i. This equilibrium is stable if no phage-lysogen pairs P_i-L_i can invade on the susceptible population. To derive stability conditions, we approximate the dynamics of P_i and L_i in the vicinity of the equilibrium by the linearised equations

$$\begin{pmatrix} \frac{\mathrm{d}L_i}{\mathrm{d}t} \\ \frac{\mathrm{d}P_i}{\mathrm{d}t} \end{pmatrix} \approx \begin{pmatrix} -\alpha & \bar{\phi}_i B a \\ \alpha & (1-\bar{\phi}_i)Ba - \delta - a \end{pmatrix} \begin{pmatrix} L_i \\ P_i \end{pmatrix} =: J \begin{pmatrix} L_i \\ P_i \end{pmatrix}, \tag{S3.14}$$

where $\bar{\phi}_i = \varphi_i(0)$ is the lysogeny propensity of phage type i at the equilibrium. No phage-lysogen pair can invade (*i.e.*, the equilibrium is stable) precisely if the real parts of both eigenvalues of the Jacobian matrix J are negative for all i. The eigenvalues of the Jacobian matrix J are given by

$$\lambda_{+/-} = \frac{\Gamma \pm \sqrt{\Delta}}{2}, \text{ with } \Gamma = a\left(B(1-\bar{\phi}_i) - 1\right) - \delta - \alpha \text{ and } \Delta = \Gamma^2 + 4\alpha\left(a(B-1) - \delta\right).$$

The real parts of $\lambda_{+/-}$ are both negative precisely if $\Delta < \Gamma^2$ and $\Gamma < 0$. From $\Gamma < 0$, we find

$$a(B(1-\bar{\phi}_i) - 1) < \delta + \alpha, \tag{S3.15}$$

while $\Delta < \Gamma^2$ yields

$$a(B-1) < \delta. \tag{S3.16}$$

Since all parameters are non-negative and $0 \leq \bar{\phi}_i \leq 1$, condition S3.16 is more stringent than condition S3.15. Note also that condition S3.16 does not depend on the lysogeny propensity of the invading phages, $\bar{\phi}$. Hence, the equilibrium $\bar{S} = 1$, $\bar{L}_i = 0$, and $\bar{P}_i = 0$ for all phage variants i is stable exactly if condition S3.16 is satisfied. This condition makes sense: phages cannot spread in a susceptible cell population at carrying capacity if their infection rate $Ba\bar{S}$ is smaller than the decay rate of phage particles $\delta + a\bar{S}$.

Thirdly, there is a class of equilibria in which $\bar{S} = 0$, and $\bar{L}_i > 0$, $\bar{P}_i > 0$ for some i. In these equilibria, the total densities of lysogens $\bar{L}$ and of free phages $\bar{P}$ are given by

$$\bar{L} = 1 - \alpha, \qquad \bar{P} = \frac{\alpha \bar{L}}{\delta + a\bar{L}} = \frac{\alpha(1-\alpha)}{\delta + a(1-\alpha)}. \tag{S3.17}$$

In the absence of susceptible cells at equilibrium, no infections can take place and hence all phage variants behave identically (since phages vary only in $\varphi_i(A)$, which occurs exclusively in the infection terms). This is reflected in the equations for the different lysogen variants, which for $\bar{S} = 0$ and $\bar{L} = 1 - \alpha$ (Eq S3.17) reduce to

$$\frac{\mathrm{d}L_i}{\mathrm{d}t} = L_i(1 - \bar{L}) - \alpha L_i = 0.$$

Hence, any combination of $\bar{L}_i$ values with $\sum_i \bar{L}_i = \bar{L} = 1 - \alpha$ and corresponding $\bar{P}_i$-values,

$$\bar{P}_i = \frac{\alpha \sum_j \mu_{ij} \bar{L}_j}{\delta + a(1-\alpha)}, \tag{S3.18}$$

is an equilibrium. Analogous to the reasoning above, such an equilibrium is stable if the susceptible cells cannot invade the phage-lysogen population at equilibrium. The linearised equation for the dynamics of S near the equilibrium of Eq S3.17 reads

$$\frac{\mathrm{d}S}{\mathrm{d}t} \approx S(1-\bar{L}) - BaS\bar{P} = S\left(\alpha - \frac{Ba\alpha(1-\alpha)}{\delta + a(1-\alpha)}\right). \tag{S3.19}$$

The right-hand side of this equation is negative (*i.e.*, susceptible cells cannot invade) precisely if $\delta + a(1-\alpha) < Ba(1-\alpha)$, or summarised

$$\delta < a(B-1)(1-\alpha). \tag{S3.20}$$

(Note that to arrive at condition (S3.20) we assume $\delta + a(1-\alpha) > 0$. This assumption is justified because the spontaneous induction rate of lysogens α is small, and hence $1 - \alpha > 0$ (see Table S3.1).)

Lastly, there can be an equilibrium in which the susceptible cells, lysogens and phages all coexist. Expressions for $\bar{S}$, $\bar{P}_i$ and $\bar{L}_i$ at this equilibrium are bulky and not directly insightful. This type of equilibrium was however extensively analysed in recent work by Wahl *et al.* (2019) for phages with a constant lysogeny propensity (*i.e.*, the restricted model where arbitrium communication is excluded). Remember that in an equilibrium state, phage variants are characterised by their lysogeny propensity $\varphi_i(\bar{A})$ only (*i.e.*, differences in response threshold θ are relevant only if they are reflected in differences in $\varphi_i(\bar{A})$; phage variants i and j with $\theta_i \neq \theta_j$ but $\varphi_i(\bar{A}) = \varphi_j(\bar{A})$ can for all practical purposes be considered the same), and hence the results found by Wahl *et al.* can be extended to the model analysed here. Phage variants with different lysogeny propensity $\varphi_i(\bar{A})$ can be seen as consumers that compete for a single resource, namely susceptible cells to infect. As long as $\bar{S} > 0$, we hence expect competitive exclusion, and the phage population at equilibrium will be dominated by phages with a single lysogeny propensity value $\bar{\phi} \equiv \varphi(\bar{A})$ (when mutations are ignored, these phages will be the only ones present; otherwise we find a quasispecies). Furthermore, Wahl *et al.* show that if susceptible host cells coexist with a resident lysogen-phage population with some lysogeny propensity $\bar{\phi}_\mathrm{r}$, a phage-lysogen pair of a variant with higher lysogeny propensity $\bar{\phi}_\mathrm{i} > \bar{\phi}_\mathrm{r}$ can always invade on this equilibrium. Hence, in this equilibrium, the dominant phage will be the one with the highest equilibrium lysogeny propensity, $\bar{\phi} = 1$.

As has been demonstrated previously (Stewart and Levin, 1984; Wahl *et al.*, 2019), the "coexistence equilibrium" is stable only if phages and lysogens can invade on a susceptible population at carrying capacity (*i.e.*, condition S3.16 is violated),

and susceptible cells can invade on the phage-lysogen population in equilibrium (*i.e.*, condition S3.20 is violated). Hence, susceptible cells, lysogens and phages all coexist precisely if

$$(1-\alpha)(B-1)a < \delta < (B-1)a. \tag{S3.21}$$

If the effective burst size $B > 1$ (a necessary condition for the phage to be viable), this can be rewritten as

$$(1-\alpha) < \frac{\delta}{(B-1)a} < 1. \tag{S3.22}$$

Because the spontaneous induction rate of lysogens, α, is small ($\alpha < 0.01$, see Table S3.1), condition S3.22 is very specific. Susceptible cells, lysogens and phages coexist only if the exponential growth rate of a lytic phage spreading in a susceptible population at carrying capacity, $(B-1)a - \delta$, is positive but very small, *i.e.*, if the epidemic is viable but only barely so. In reality, however, most phage epidemics are characterised by a high infectivity, mainly because of a large burst size (de Paepe and Taddei, 2006). Therefore, condition S3.22 is rarely satisfied, and for most phages we should instead expect to converge to equilibria of the third type ($\bar{S} = 0, \bar{L} > 0, \bar{P} > 0$).

This observation has consequences for the selection pressures on phage variants over the course of a typical epidemic. As soon as the pool of susceptible host cells is depleted, competition between the different phage variants vanishes and the relative frequency of the variants freezes (see Supplementary Figure S3.1 for an illustration). Under these conditions, no infections take place and hence there is no selection on the lysis-lysogeny decision. We conclude that the evolution of the lysis-lysogeny decision of typical phages requires regular perturbations away from equilibrium conditions.

3.6.3. Derivation of the Evolutionarily Stable Strategy (ESS) under the serial-passaging regime: General approach

In the main text, we present simulation results of the evolution of the lysis-lysogeny decision of phages exposed to a serial-passaging regime, both when arbitrium communication is excluded from the model (Figure 3.2), and when it is included (Figures 3.3–3.4). These simulations show that, after many passaging episodes, a single variant dominates the phage population (accompanied by its quasispecies, see Figure 3.2 and Figure 3.3). We therefore assume that, within the parameter range of interest, a pure Evolutionary Stable Strategy (ESS) exists. In this section, we derive analytical expressions for the ESS. In this section, we first provide a definition of the ESS under a serial-passaging regime, and give a general description of how this ESS can be found. Then, we apply this general approach to derive the ESS of phages that differ in a constant lysogeny propensity, ϕ (absence of arbitrium communication, section 3.6.4), and the ESS of communicating phages that differ in their response threshold θ (section 3.6.5).

Consider a population of phages under a serial-passaging regime with long time T between passages. At the start of each passaging episode, a fraction D of the phages is taken from the end of the previous episode, and is added to a "fresh" population of susceptible bacteria at carrying capacity. This procedure is repeated over many episodes. Within each episode, the dynamics of the susceptible bacteria, lysogens, phages, and arbitrium are described by Eq S3.7–S3.12.

An **evolutionarily stable strategy (ESS)** is defined as a strategy that cannot be invaded by any other strategy that is initially rare. To find the ESS, we therefore consider a scenario where an invader phage variant attempts to invade a resident phage variant. Below, we specify what it means for a phage variant to be able to invade in a resident phage population under the imposed serial-passaging regime.

Envision a resident population consisting of an isogenic phage population that has gone through many passaging episodes. Over time, the dynamics within these episodes have converged to a repeatable trajectory characterised by $P_r(t)$, the resident phage density over time, $S(t)$, the density of susceptible bacteria over time, and $L_r(t)$, the density of lysogens over time. At the start of one episode, now suddenly introduce a second phage with its own (possibly different) strategy. Crucially, the initial density of this invading phage $P_i(0)$ is infinitesimally small. Consequently, during the first passaging episode the dynamics of the resident phage and the bacteria ($P_r(t)$, $S(t)$, and $L_r(t)$) are not affected by the invader. The invader is able to invade precisely if at the end of the first episode its frequency has increased relative to that of the resident, *i.e.*, if $P_i(T)/P_r(T) > P_i(0)/P_r(0)$.

Note that the relative frequency of an invader with exactly the same strategy as the resident does not change during an episode. Suppose that such an invader is the best-performing invader under the environment set up by the resident; then this implies that no invader can increase in frequency over a passaging episode, and therefore the resident strategy must be an ESS. In other words, in a resident phage population consisting of the ESS only, the ESS itself is the optimal strategy for an invading phage variant, *i.e., the ESS is the optimal response to itself.*

What does it take to be the best-performing invader? To answer this question, we consider the dynamics within a single passaging episode in more detail.

If the time between passages T is long, and the parameter conditions are such that the system converges to an equilibrium with $S = 0, P > 0, L > 0$ (typical parameter values, see sections 3.6.1.4 and 3.6.2), the dynamics within an episode can be divided in three distinct phases (Supplementary Figure S3.1):

1. **Epidemic phase.** A substantial population of susceptible bacteria ($S > 0$) supports an ongoing epidemic. Free phages and lysogens are formed through infection of susceptible bacteria.

2. **Transition phase.** The population of susceptible cells has collapsed ($S \approx 0$). The lysogen population expands to fill up the space left behind by lysed cells. Free phages particles can no longer infect susceptible cells, and disappear through decay and adsorption to lysogens.

3. **Equilibrium phase.** The composition of the population is well-characterised by an equilibrium of "type 3" (see Eq S3.17). There is a small but consistent population of free phages that originates from lysogens through spontaneous induction. The distribution of phage variants in the free phage population is a direct representation of the relative frequency of the variants in the lysogen population (Eq S3.18).

Let T_E be the time at which the susceptible population collapses, *i.e.*, the end of the epidemic phase. If the time between passages T is sufficiently larger than T_E, the passage takes place during the equilibrium phase. The relative frequency of phage variants in the transferred sample then directly reflects the relative frequency of the corresponding lysogens. Since lysogens are only differentially formed through infection dynamics (and not through lysogen replication, which happens at the same rate for all lysogen variants), the relative frequency of the different lysogens is established during the epidemic phase and does not change afterwards. The performance of an invading phage can hence be measured by its lysogen production between $t = 0$ and $t = T_E$.

The dynamics of $S(t)$, and consequently T_E, are determined by the resident phage: highly virulent resident phages (that cause many lytic infections, for instance because of a low ϕ-value) deplete the susceptible cell population faster than less virulent residents. The optimal invader under a certain resident is the phage variant that produces the most lysogens during the limited window of opportunity that it is offered by the environment set up by the resident. Since the ESS is the optimal response to itself, it is the strategy that, as an invader, produces the most lysogens during an epidemic phase set up by itself. We will use this reasoning to identify the ESS.

3.6.4. Evolutionarily stable lysogeny propensity of non-communicating phages

Consider the restricted model in which arbitrium communication is excluded and phages are characterised by a fixed lysogeny propensity ϕ. To find the ESS under this scenario, we take the following steps:

1. Derive how the duration of the epidemic, T_E, depends on the ϕ-value of a resident phage population.

2. Find the optimal ϕ given a fixed value of T_{E}, *i.e.*, the ϕ-value that yields a maximal lysogen density at time T_{E}.

3. Combine 1. and 2. to find the ESS: the ϕ-value ϕ^* that maximises its lysogen density at time $T_{\mathrm{E}}(\phi^*)$, the duration of the epidemic as dictated by its own ϕ-value, ϕ^*.

3.6.4.1. Simplifying assumptions

To make the model analytically tractable, we make the following simplifying assumptions (based on the typical infection dynamics, see Figure 3.2a):

1. Bacterial growth, decay of free phages and induction of lysogens are considered to be much slower than the phage infection dynamics. We hence ignore these processes when describing the epidemic phase.

2. The epidemic ends when all susceptible cells have been infected. In other words, we solve T_{E} from $\int_{t=0}^{T_{\mathrm{E}}} BaSP_{\mathrm{r}}\mathrm{d}t = 1$ (where this 1 represents the carrying capacity in the non-dimensionalised units).

3. The density of lysogens during the epidemic is small, hence $N \approx S$.

4. The susceptible population remains relatively constant for some time, after which it rapidly collapses. We approximate these dynamics with a block function, setting $S = 1$ for $t \leq T_{\mathrm{E}}$, and $S = 0$ for $t > T_{\mathrm{E}}$.

Under these assumptions the dynamics of the resident phage population for the period $0 \leq t \leq T_{\mathrm{E}}$ are described by:

$$\frac{\mathrm{d}P_{\mathrm{r}}}{\mathrm{d}t} = (Ba(1-\phi_{\mathrm{r}})S - aS)\,P_{\mathrm{r}} = (B(1-\phi_{\mathrm{r}}) - 1)\,aP_{\mathrm{r}}, \tag{S3.23}$$

with solution

$$P_{\mathrm{r}}(t) = P_{\mathrm{r},0}\mathrm{e}^{(B(1-\phi_{\mathrm{r}})-1)at} = P_{\mathrm{r},0}\mathrm{e}^{(\eta-\phi_{\mathrm{r}})Bat}, \tag{S3.24}$$

where $P_{\mathrm{r},0} \equiv P_{\mathrm{r}}(0)$ is the initial density of resident phages and we have introduced $\eta := 1 - B^{-1}$. Note that the description of the infection dynamics in Eq S3.23 is meaningful only if early in the epidemic the phage population indeed grows exponentially, *i.e.*, if $\phi_{\mathrm{r}} < \eta$. For default parameter settings, this upper bound on ϕ_{r} is well above the ϕ-values that are typically selected ($\phi \approx 0.04$ (Figure 3.2c), while $\eta = 0.5$ (Table S3.1)), indicating that this assumption is reasonable.

3.6.4.2. Duration of the epidemic T_{E} given a resident phage

First, we derive how the duration of the epidemic, T_{E}, depends on the lysogeny propensity of a resident phage variant ϕ_{r}. To find $T_{\mathrm{E}}(\phi_{\mathrm{r}})$, we substitute Eq S3.24

into assumption 2:

$$\int_{t=0}^{T_\mathrm{E}} BaSP_\mathrm{r}(t)\,\mathrm{d}t = \int_{t=0}^{T_\mathrm{E}} BaP_{\mathrm{r},0}\mathrm{e}^{(\eta-\phi_\mathrm{r})Bat}\,\mathrm{d}t = \frac{P_{\mathrm{r},0}}{(\eta-\phi_\mathrm{r})}\left(\mathrm{e}^{(\eta-\phi_\mathrm{r})BaT_\mathrm{E}}-1\right),$$

and then equate this integral to 1 to find

$$T_\mathrm{E}(\phi_\mathrm{r}) = \frac{1}{Ba(\eta-\phi_\mathrm{r})}\log\left(\frac{\eta-\phi_\mathrm{r}}{P_{\mathrm{r},0}}+1\right). \tag{S3.25}$$

Note that the density of the resident phage at time T_E is now given by

$$P_\mathrm{r}(T_\mathrm{E}) = P_{\mathrm{r},0}\mathrm{e}^{(\eta-\phi_\mathrm{r})BaT_\mathrm{E}} = P_{\mathrm{r},0}+\eta-\phi_\mathrm{r}. \tag{S3.26}$$

Therefore, the expression for T_E (Eq S3.25) can also be read as:

$$T_\mathrm{E}(\phi_\mathrm{r}) = \frac{1}{Ba(\eta-\phi_\mathrm{r})}\log\left(\frac{P_\mathrm{r}(T_\mathrm{E})}{P_{\mathrm{r},0}}\right). \tag{S3.27}$$

Eq S3.27 will prove useful later for the derivation of the ESS.

3.6.4.3. Optimal invader strategy ϕ_i given a fixed duration of the epidemic

Next, we ask what invader lysogen propensity $\phi_{\mathrm{i,opt}}$ maximises the invader's lysogen production, $L_\mathrm{i}(T_\mathrm{E})$, if the duration of the epidemic T_E is fixed. For $0 \le t \le T_\mathrm{E}$, the dynamics of $L_i(t)$ are described by

$$\frac{\mathrm{d}L_\mathrm{i}}{\mathrm{d}t} = \phi_\mathrm{i}BaP_\mathrm{i}. \tag{S3.28}$$

Since $P_\mathrm{i}(t) = P_{\mathrm{i},0}\mathrm{e}^{(\eta-\phi_\mathrm{i})Bat}$ (see Eq S3.24) and $L_\mathrm{i}(0) = 0$, we can now solve

$$L_\mathrm{i}(t) = P_{\mathrm{i},0}\frac{\phi_\mathrm{i}}{\eta-\phi_\mathrm{i}}\left(\mathrm{e}^{(\eta-\phi_\mathrm{i})Bat}-1\right). \tag{S3.29}$$

To find the ϕ_i-value that maximises $L_\mathrm{i}(T_\mathrm{E})$, we take the derivative of Eq S3.29 with respect to ϕ_i:

$$\frac{\partial L_\mathrm{i}(T_\mathrm{E})}{\partial\phi_\mathrm{i}} = P_{\mathrm{i},0}\left(\frac{\eta(\mathrm{e}^{(\eta-\phi_\mathrm{i})BaT_\mathrm{E}}-1)}{(\eta-\phi_\mathrm{i})^2} - \frac{\phi_\mathrm{i}BaT_\mathrm{E}\mathrm{e}^{(\eta-\phi_\mathrm{i})BaT_\mathrm{E}}}{\eta-\phi_\mathrm{i}}\right). \tag{S3.30}$$

To find $\phi_{\mathrm{i,opt}}$, we should hence solve

$$\frac{P_{\mathrm{i},0}}{\eta-\phi_\mathrm{i}}\left(\frac{\eta(\mathrm{e}^{(\eta-\phi_\mathrm{i})BaT_\mathrm{E}}-1)}{\eta-\phi_\mathrm{i}} - \phi_\mathrm{i}BaT_\mathrm{E}\mathrm{e}^{(\eta-\phi_\mathrm{i})BaT_\mathrm{E}}\right) = 0. \tag{S3.31}$$

Unfortunately, Eq S3.31 cannot be solved analytically. We can however simplify Eq S3.31 by noting that for sufficiently small ϕ_i, $(\eta-\phi_\mathrm{i})$ is of order $0.1-1$, while T_E

is typically of order 1, and Ba is of order $10-1000$ (Table S3.1). Hence, $e^{(\eta-\phi_i)BaT_E}$ is typically $\gg 1$, and Eq S3.31 can be approximated by

$$\frac{P_{i,0}e^{(\eta-\phi_i)BaT_E}}{\eta-\phi_i}\left(\frac{\eta}{\eta-\phi_i}-Ba\phi_iT_E\right)=0. \tag{S3.32}$$

From Eq S3.32 we find

$$\begin{aligned}&\frac{\eta}{\eta-\phi_i}=Ba\phi_iT_E\\ \Leftrightarrow\ &BaT_E\phi^2-\eta BaT_E\phi_i+\eta=0\\ \Leftrightarrow\ &\phi_{i,opt}(T_E)=\tfrac{1}{2}\eta\pm\tfrac{1}{2}\sqrt{\eta^2-\tfrac{4\eta}{BaT_E}}.\end{aligned} \tag{S3.33}$$

3.6.4.4. The ESS

Eq S3.25 and its alternative formulation Eq S3.27 describe how the duration of the epidemic T_E depends on the lysogeny propensity ϕ_r of the current resident, while Eq S3.33 gives the value $\phi_{i,opt}$ that maximises the lysogen production of an invader during an epidemic of a fixed duration T_E. The ESS is now given by the value ϕ^* that is "optimal" as defined by Eq S3.33, when it itself is the resident and hence dictates $T_E(\phi^*)$. Combining Eq S3.33 and Eq S3.27 we find

$$\begin{aligned}&\phi^*=\tfrac{1}{2}\eta\pm\tfrac{1}{2}\sqrt{\eta^2-4\frac{\eta(\eta-\phi^*)}{\log(P_r(T_E)/P_{r,0})}}\\ \Leftrightarrow\ &(\phi^*-\tfrac{1}{2}\eta)^2=\tfrac{1}{4}\eta^2-\frac{\eta(\eta-\phi^*)}{\log(P_r(T_E)/P_{r,0})}\\ \Leftrightarrow\ &(\phi^*)^2-\phi^*\left(\eta+\frac{\eta}{\log(P(T_E)/P_0)}\right)+\frac{\eta^2}{\log(P_r(T_E)/P_{r,0})}=0,\end{aligned}$$

from which we can solve:

$$\phi_{+/-}=\tfrac{1}{2}\eta(1+\frac{1}{\log(P_r(T_E)/P_{r,0})})\pm\tfrac{1}{2}\eta(1-\frac{1}{\log(P_r(T_E)/P_{r,0})}). \tag{S3.34}$$

Of these two solutions, $\phi_+=\eta$ is an asymptote at which our approximation no longer holds (remember that we previously demanded that $\phi_r<\eta$ to ensure initial spread of the infection). Hence, ϕ^* should be given by ϕ_-:

$$\phi^*=\frac{\eta}{\log(P_r(T_E)/P_{r,0})}. \tag{S3.35}$$

Although Eq S3.35 seems to provide an elegant equation for the ESS, it still depends on $P_r(T_E)$ and $P_{r,0}$. If the interval between passages is sufficiently long, the

phage density at the end of a passaging cycle will be given by Eq S3.17 and hence

$$P_{\mathrm{r},0} = D\frac{\alpha(1-\alpha)}{\delta + a(1-\alpha)}, \tag{S3.36}$$

where D is the dilution factor of phages upon passaging. While the value of $P_{\mathrm{r},0}$ does not depend on the lysogeny propensity ϕ_{r}, $P_{\mathrm{r}}(T_{\mathrm{E}})$ does (see Eq S3.26). Substituting $P_{\mathrm{r}}(T_{\mathrm{E}}) = P_{\mathrm{r},0} + \eta - \phi^*$ yields

$$\phi^* = \frac{\eta}{\log(1 + \frac{\eta - \phi^*}{P_{\mathrm{r},0}})}. \tag{S3.37}$$

This equation cannot be solved analytically. However, we can make a reasonable approximation of Eq S3.37 by considering the differences in orders of magnitude of the terms within the logarithm. As argued above, $(\eta - \phi^*)$ is generally of order $0.1 - 1$, while typical values of $P_{\mathrm{r},0}$ are several orders of magnitude smaller ($P_{\mathrm{r},0} \approx 10^{-5}$). Therefore, we can approximate the logarithm in Eq S3.37 by

$$\log(1 + \tfrac{\eta - \phi^*}{P_{\mathrm{r},0}}) \approx \log\left(\frac{1}{P_{\mathrm{r},0}}\right) = -\log(P_{\mathrm{r},0}).$$

Using this approximation, we find

$$\phi^* = \frac{\eta}{-\log(P_{\mathrm{r},0})}, \tag{S3.38}$$

which is also presented in the main text (Eq 3.5). Eq S3.38 and S3.36 were used to find the analytical predictions shown in Figure 3.2d.

3.6.5. Evolutionarily stable response threshold of communicating phages

Next, consider a population of phages that do engage in arbitrium communication, again under a serial-passaging regime with sufficiently long time between the passages. Below, we use an approach similar to section 3.6.4, but more general, to derive the evolutionarily stable arbitrium response threshold, θ^*. We take the following steps:

1. Describe the dynamics of an invading phage and its corresponding lysogens in an environment dictated by a resident phage.
2. Find the optimal invader response threshold under a fixed resident response threshold, *i.e.*, find the θ-value that maximises the invader's lysogen production at time T_{E} when the dynamics of susceptible cells (and hence T_{E}) are determined by a fixed resident phage.

3. Determine the ESS, θ^*, as the optimal response to itself: the optimal invader response threshold (as found in step 2) if that same response threshold is the resident strategy.

We found that the results below are best understood in terms of the non-scaled model; in particular the (non-scaled) burst size of the phages turns out to be an important parameter. Therefore, the derivations below are presented for the dimensionalised equations Eq S3.1–S3.6.

3.6.5.1. Simplifying assumptions

To make the model tractable, we again make a few simplifying assumptions:

1. As in section 3.6.4, we assume that there is a separation of time scales between the infection dynamics of the phages and the reproduction of the bacteria, spontaneous phage decay and lysogen induction. Hence, when describing the epidemic phase we ignore these other processes.

2. Additionally, we assume that there also is a separation of time scales between the production of arbitrium through infections (first term in Eq S3.4) and its uptake and degradation by cells (second term in Eq S3.4). We ignore the uptake and degradation of arbitrium during the early epidemic, such that the increasing arbitrium concentration reflects the decrease of the susceptible cell density because of infections.

3. We assume that communicating phages switch from a completely lytic strategy ($\varphi(A) = 0$) to a completely lysogenic strategy ($\varphi(A) = 1$) once the arbitrium concentration exceeds the phages' response threshold. This is in line with observations from simulations, where we find that phage variants with $\phi_{\max} = 1$ dominate the population for a wide range of parameter values (Figure 3.4a).

The assumptions above are less strict then the assumptions made in section 3.6.4. In particular, we no longer assume that the density of susceptible cells, $S(t)$, remains constant for the duration of the epidemic $0 \leq t \leq T_{\mathrm{E}}$. Rather, for the derivations below it suffices to assume that $S(t)$ is a declining function which is completely determined by the resident phage, and that $S(t)$ is sufficiently close to 0 after the epidemic, *i.e.*, for times $t > T_{\mathrm{E}}$ (where T_{E} still depends on the characteristics of the resident phage).

It will be useful to refer to the *time* when the resident and invader switch to lysogeny as τ_{r} and τ_{i}, respectively. Given particular dynamics of the susceptible cell density and the arbitrium concentration dictated by a resident phage population, there is a direct relation between τ_{i} and θ_{i} (the arbitrium response threshold of the

invader). Keep in mind, however, that this relation changes if the resident phage is changed.

3.6.5.2. Dynamics of the invading phage and its corresponding lysogens

First, we describe how the dynamics of an invading phage variant depend on the resident phage population. Remember that we consider an invader phage variant that starts off at infinitesimally small density, and attempts to invade an isogenic resident phage population that has already converged to a repeatable trajectory of $P_\mathrm{r}(t)$, $L_\mathrm{r}(t)$, $S(t)$, and $A(t)$ per passaging episode. Under these conditions, the dynamics of $S(t)$, $N(t) = S(t) + L_\mathrm{r}(t)$ and $A(t)$ over the first passaging episode do not depend on the switch time τ_i of the invader, but only on the switch time of the resident phage, τ_r. Based on the assumptions formulated above, the ODEs for the density of the invading phage and its corresponding lysogens can be written as

$$\frac{\mathrm{d}P_\mathrm{i}(t|\tau_\mathrm{i},\tau_\mathrm{r})}{\mathrm{d}t} = \begin{cases} BbaS(t|\tau_\mathrm{r})P_\mathrm{i}(t|\tau_\mathrm{i},\tau_\mathrm{r}) - aN(t|\tau_\mathrm{r})P_\mathrm{i}(t|\tau_\mathrm{i},\tau_\mathrm{r}), & (t < \tau_\mathrm{i}) \\ -aN(t|\tau_\mathrm{r})P_\mathrm{i}(t|\tau_\mathrm{i},\tau_\mathrm{r}), & (t \geq \tau_\mathrm{i}) \end{cases} \tag{S3.39}$$

$$\frac{\mathrm{d}L_\mathrm{i}(t|\tau_\mathrm{i},\tau_\mathrm{r})}{\mathrm{d}t} = \begin{cases} 0, & (t < \tau_\mathrm{i}) \\ baS(t|\tau_\mathrm{r})P_\mathrm{i}(t|\tau_\mathrm{i},\tau_\mathrm{r}), & (t \geq \tau_\mathrm{i}) \end{cases} \tag{S3.40}$$

where vertical lines are used to indicate which phage charactistics the trajectories of variables depend upon. Eq S3.39–S3.40 capture the switch from a completely lytic infection strategy (for $t \leq \tau_\mathrm{i}$), in which new phage particles are produced through infection but no lysogens are formed, to a completely lysogenic strategy (for $t > \tau_\mathrm{i}$), in which no new phage particles are produced but all infections result in the production of lysogens (see assumption 3). Remember that we here use the dimensionalised equations, so B is the burst size, a the rate of adsorption of phages to bacterial cells (irrespective of whether they are susceptible or lysogen), and b the probability that adsorption to a susceptible cell leads to an infection.

The solution to Eq S3.39 can be written as

$$P_\mathrm{i}(t|\tau_\mathrm{i},\tau_\mathrm{r}) = P_{\mathrm{i},0} \times \begin{cases} \exp\left(Bba\int_0^t S(t'|\tau_\mathrm{r})dt' - a\int_0^t N(t'|\tau_\mathrm{r})dt'\right), & (t < \tau_\mathrm{i}) \\ \exp\left(Bba\int_0^{\tau_\mathrm{i}} S(t'|\tau_\mathrm{r})dt' - a\int_0^t N(t'|\tau_\mathrm{r})dt'\right), & (t \geq \tau_\mathrm{i}) \end{cases} \tag{S3.41}$$

as is easily verified by differentiating this solution with respect to t.

As before, the performance of the invading phage variant is determined by its lysogen production during the epidemic phase, *i.e.*, between $t = 0$ and $t = T_\mathrm{E}$. At any time t, the density of invader lysogens is

$$L_\mathrm{i}(t|\tau_\mathrm{i},\tau_\mathrm{r}) = \begin{cases} 0, & (t < \tau_\mathrm{i}) \\ \int_{\tau_\mathrm{i}}^t baS(t'|\tau_\mathrm{r})P_\mathrm{i}(t|\tau_\mathrm{i},\tau_\mathrm{r})dt'. & (t \geq \tau_\mathrm{i}) \end{cases} \tag{S3.42}$$

Invading phage variants are selected on their lysogen density at the end of the epidemic, $L_\mathrm{i}(T_\mathrm{E}|\tau_\mathrm{i},\tau_\mathrm{r})$. Once the epidemic phase has ended ($t \geq T_\mathrm{E}$), no new phage particles or lysogens are formed through infection. Hence, any reasonable switching time must obey $\tau_\mathrm{i} < T_\mathrm{E}$. Furthermore, since $S(t) \approx 0$ for any time $t \geq T_\mathrm{E}$,

$$L_\mathrm{i}(T_\mathrm{E}|\tau_\mathrm{i},\tau_\mathrm{r}) = \int_{\tau_\mathrm{i}}^{T_\mathrm{E}} baS(t'|\tau_\mathrm{r})P_\mathrm{i}(t'|\tau_\mathrm{i},\tau_\mathrm{r})dt' = \int_{\tau_\mathrm{i}}^{\infty} baS(t'|\tau_\mathrm{r})P_\mathrm{i}(t'|\tau_\mathrm{i},\tau_\mathrm{r})dt' \quad \text{(S3.43)}$$

which we will denote $\Lambda_\mathrm{i}(\tau_\mathrm{i},\tau_\mathrm{r})$.

3.6.5.3. Optimal invader strategy τ_i given some resident phage

The optimal invader strategy τ_i given $S(t|\tau_\mathrm{r})$ and $N(t|\tau_\mathrm{r})$ is the one that maximises $\Lambda_\mathrm{i}(\tau_\mathrm{i},\tau_\mathrm{r})$. To find this optimal strategy, we differentiate Eq S3.43 with respect to τ_i:

$$\frac{\partial\Lambda_\mathrm{i}(\tau_\mathrm{i},\tau_\mathrm{r})}{\partial\tau_\mathrm{i}} = -baS(\tau_\mathrm{i}|\tau_\mathrm{r})P_\mathrm{i}(\tau_\mathrm{i}|\tau_\mathrm{i},\tau_\mathrm{r}) + \int_{\tau_\mathrm{i}}^{\infty} baS(t'|\tau_\mathrm{r})\frac{\partial P_\mathrm{i}(t'|\tau_\mathrm{i},\tau_\mathrm{r})}{\partial\tau_\mathrm{i}}dt'. \quad \text{(S3.44)}$$

The derivative in the integrand can be calculated from Eq S3.41 (noting that, inside the integral, $t' \geq \tau_\mathrm{i}$):

$$\begin{aligned}\frac{\partial P_\mathrm{i}(t|\tau_\mathrm{i},\tau_\mathrm{r})}{\partial\tau_\mathrm{i}} &= \frac{\partial}{\partial\tau_\mathrm{i}}\left(Bba\int_0^{\tau_\mathrm{i}} S(t'|\tau_\mathrm{r})dt'\right)P_{\mathrm{i},0}\exp\left(Bba\int_0^{\tau_\mathrm{i}} S(t'|\tau_\mathrm{r})dt' - a\int_0^{t} N(t'|\tau_\mathrm{r})dt'\right)\\ &= BbaS(\tau_\mathrm{i}|\tau_\mathrm{r})P_\mathrm{i}(t|\tau_\mathrm{i},\tau_\mathrm{r}). \quad \text{(S3.45)}\end{aligned}$$

Inserting the last expression into Eq S3.44 yields

$$\begin{aligned}\frac{\partial\Lambda_\mathrm{i}(\tau_\mathrm{i},\tau_\mathrm{r})}{\partial\tau_\mathrm{i}} &= -baS(\tau_\mathrm{i}|\tau_\mathrm{r})P_\mathrm{i}(\tau_\mathrm{i}|\tau_\mathrm{i},\tau_\mathrm{r}) + Bb^2a^2S(\tau_\mathrm{i}|\tau_\mathrm{r})\int_{\tau_\mathrm{i}}^{\infty} S(t'|\tau_\mathrm{r})P_\mathrm{i}(t'|\tau_\mathrm{i},\tau_\mathrm{r})dt'\\ &= -baS(\tau_\mathrm{i}|\tau_\mathrm{r})P_\mathrm{i}(\tau_\mathrm{i}|\tau_\mathrm{i},\tau_\mathrm{r}) + BbaS(\tau_\mathrm{i}|\tau_\mathrm{r})\Lambda_\mathrm{i}(\tau_\mathrm{i},\tau_\mathrm{r}). \quad \text{(S3.46)}\end{aligned}$$

The terms in Eq S3.46 have a clear interpretation. By taking the derivative of $\Lambda_\mathrm{i}(\tau_\mathrm{i},\tau_\mathrm{r})$ to τ_i, we are implicitly comparing one possible invading phage variant (phage 1) that switches at time $t = \tau_\mathrm{i}$ to a second invading phage variant (phage 2) that switches ever so slightly later, at $t = \tau_\mathrm{i} + \mathrm{d}\tau$. Eq S3.46 says that the lysogen density of these two variants at the end of the epidemic will differ because of two effects: On the one hand (first term) phage 2 will have a *lower* lysogen density than phage 1 because it does not produce lysogens in the time interval from τ_i to $\tau_\mathrm{i} + \mathrm{d}\tau$. The damage is $-baS(\tau_\mathrm{i}|\tau_\mathrm{r})P_\mathrm{i}(\tau_\mathrm{i}|\tau_\mathrm{i},\tau_\mathrm{r})\mathrm{d}\tau$ lysogens per volume. On the other hand, phage 2 will have a higher *higher* lysogen density because it produces additional free phages in the time interval from τ to $\tau + \mathrm{d}\tau$, which results in additional lysogens in the rest of the epidemic. As a result, throughout the rest of the epidemic the second phage has $(1 + BbaS(\tau_\mathrm{i}|\tau_\mathrm{r})\mathrm{d}\tau)$ times as many phages as the first phage variant,

and therefore produces an additional number of $BbaS(\tau_i|\tau_r)L_i(\tau_i,\tau_r)d\tau$ lysogens per volume.

The optimal invading phage variant given a resident phage is the variant with the value of $\tau_{i,opt}(\tau_r)$ for which the two terms in Eq S3.46 cancel precisely:

$$P_i(\tau_{i,opt}(\tau_r)|\tau_{i,opt}(\tau_r),\tau_r) = B\Lambda_i(\tau_{i,opt}(\tau_r),\tau_r). \tag{S3.47}$$

That is, the optimal invader switches precisely when its phage density is equal to its total eventual lysogen production multiplied by the burst size B.

We may rewrite Eq S3.47 as

$$BE_i(\tau_{i,opt}(\tau_r)|\tau_r) = 1, \tag{S3.48}$$

where $E_i(\tau_i|\tau_r) \equiv \Lambda_i(\tau_i,\tau_r)/P_i(\tau_i|\tau_i,\tau_r)$ is the number of lysogens eventually produced per phage of the invader phage variant present at time τ_i. $E_i(\tau_i|\tau_r)$ can be interpreted as a kind of "exchange rate", expressing the value of a single phage at time τ_i in the currency of lysogens. This suggests another way of phrasing the results above, where we compared two phage variants of which phage 2 switched slightly later than phage 1: During the time interval from $\tau_{i,1}$ to $\tau_{i,2} = \tau_{i,1} + d\tau$, both competing invading phage variants infect $baS(\tau_{i,1})P_i(\tau_{i,1}|\tau_{i,1},\tau_r)d\tau$ susceptible bacteria per volume. Phage 1 directly converts these infected bacteria into lysogens. Phage 2 instead converts each of them into B additional phages. Whether this is a good idea depends precisely on whether increasing the phage density by B phages per volume will, during the rest of the epidemic, result in an increased lysogen density of more than 1 lysogen per volume. That is, phage 2 is the better invader precisely if $BE_i(\tau_i|\tau_r) > 1$, while phage 1 is the better invader if $BE_i(\tau_i|\tau_r) < 1$. Again we see that the optimal invader must obey Eq S3.47 and S3.48.

3.6.5.4. The ESS

To find the ESS, we ask what phage variant is the optimal response to itself, *i.e.*, what phage variant satisfies

$$\tau_{i,opt}(\tau^*) = \tau^*. \tag{S3.49}$$

In other words, the ESS must obey a special case of Eq S3.47 and S3.48:

$$P_i(\tau^*|\tau^*,\tau^*) = B\Lambda_i(\tau^*,\tau^*) \qquad \text{or} \qquad BE_i(\tau^*|\tau^*) = 1. \tag{S3.50}$$

Importantly, in this case the resident and invader behave identically, so that the exchange rate of the resident must be the same as that of the invader. That is,

$$E_i(\tau^*|\tau^*) = E_r(\tau^*|\tau^*) = \Lambda_r(\tau^*)/P_r(\tau^*|\tau^*), \tag{S3.51}$$

where $\Lambda_r(\tau_r)$ is the total density of lysogens eventually produced by a resident with switching time τ_r. Combined with Eq S3.50 this results in:

$$B\Lambda_r(\tau^*)/P_r(\tau^*|\tau^*) = 1. \tag{S3.52}$$

Hence, the ESS is the strategy that, when it is the only phage variant present, switches from the lytic to the lysogenic cycle precisely when the density of free phage particles it has is equal to the burst size times the density of lysogens it will still produce in the remainder of the active epidemic (see explanation in the previous section).

So far, we have expressed the results for the ESS as a switching time τ^*. In reality, however, the communicating phages switch when a certain threshold arbitrium concentration θ^* is reached. As a last step, we therefore have to relate the terms in Eq S3.52 to the arbitrium concentration. Under our simplifying assumptions, the arbitrium dynamics between time $t = 0$ and $t = \tau_\mathrm{r}$ are described by

$$\frac{\mathrm{d}A(t|\tau_\mathrm{r})}{\mathrm{d}t} = cbaS(t|\tau_\mathrm{r})P_\mathrm{r}(t|\tau_\mathrm{r}), \tag{S3.53}$$

where c is increase in arbitrium concentration per infection. The total arbitrium concentration at time t is hence given by

$$A(t|\tau_\mathrm{r}) = \int_0^t cbaS(t'|\tau_\mathrm{r})P_\mathrm{r}(t'|\tau_\mathrm{r})dt', \tag{S3.54}$$

which can be written as $A(t|\tau_\mathrm{r}) = cI_\mathrm{r}(t|\tau_\mathrm{r})$, where

$$I_\mathrm{r}(t|\tau_\mathrm{r}) = \int_0^t baS(t'|\tau_\mathrm{r})P_\mathrm{r}(t'|\tau_\mathrm{r})dt' \tag{S3.55}$$

is the infection density: the number of infections that has occurred per volume at time t.

To express the ESS in terms of the arbitrium concentration, we first show that $P_\mathrm{r}(\tau^*|\tau^*)$ is approximately proportional to $I_\mathrm{r}(\tau^*|\tau^*)$. In general, the resident phage density obeys an equation equivalent to Eq S3.39 (even though this equation was originally written down for the invading phage). For the time period $t < \tau_\mathrm{r}$, the solution of this equation can be expressed as

$$\begin{aligned} P_\mathrm{r}(t|\tau_\mathrm{r}) &= P_{\mathrm{r},0} + \int_0^t (Bb-1)aS(t'|\tau_\mathrm{r})P_\mathrm{r}(t'|\tau_\mathrm{r})dt' \\ &= P_{\mathrm{r},0} + (B-b^{-1})I_\mathrm{r}(t|\tau_\mathrm{r}) \end{aligned} \tag{S3.56}$$

Provided that the initial phage density $P_{\mathrm{r},0}$ is negligible compared to the phage density at time τ^*, we find that

$$P_\mathrm{r}(\tau^*|\tau^*) \approx (B-b^{-1})I_\mathrm{r}(\tau^*|\tau^*). \tag{S3.57}$$

Next, we use that the epidemic will eventually consume (almost) all susceptible bacteria. (Note that this is equivalent with our earlier assumption that $S(t) \approx 0$ for

$t > T_{\mathrm{E}}$.) Hence, we must have that

$$\Lambda_{\mathrm{r}}(\tau^*) \approx S(0) - I_{\mathrm{r}}(\tau^*|\tau^*). \tag{S3.58}$$

If we insert Eq S3.57 and S3.58 into Eq S3.47 and solve for $I_{\mathrm{r}}(\tau^*|\tau^*)$, we arrive at

$$I_{\mathrm{r}}(\tau^*|\tau^*) = \frac{S(0)}{2 - (bB)^{-1}}. \tag{S3.59}$$

That is, the ESS switches when the infection density obeys Eq S3.59. This implies that the ESS should have the threshold

$$\theta^* = cI_{\mathrm{r}}(\tau^*|\tau^*) = \frac{cK}{2 - (bB)^{-1}}, \tag{S3.60}$$

where we have substituted $S(0) = K$, the carrying capacity of the bacteria. Eq S3.60 is also presented in the main text (Eq 3.6). This equation was used to provide the analytical estimates shown in Figure 3.4b.

4

Toxin production spontaneously becomes regulated by local cell density in evolving bacterial populations

Hilje M. Doekes, Rob J. de Boer, Rutger Hermsen

PLoS Computational Biology 15(8): e1007333 (2019)

Abstract

The production of anticompetitor toxins is widespread among bacteria. Because production of such toxins is costly, it is typically regulated. In particular, many toxins are produced only when the local cell density is high. It is unclear which selection pressures shaped the evolution of density-dependent regulation of toxin production. Here, we study the evolution of toxin production, resistance and the response to a cell-density cue in a model of an evolving bacterial population with spatial structure. We present results for two growth regimes: (i) an undisturbed, fixed habitat in which only small fluctuations of cell density occur, and (ii) a serial-transfer regime with large fluctuations in cell density. We find that density-dependent toxin production can evolve under both regimes. However, the selection pressures driving the evolution of regulation differ. In the fixed habitat, regulation evolves because it allows cells to produce toxin only when opportunities for reproduction are highly limited (because of a high local cell density), and the effective fitness costs of toxin production are hence low. Under serial transfers, regulation evolves because it allows cells to switch from a fast-growing non-toxic phenotype when colonising a new habitat, to a slower-growing competitive toxic phenotype when the cell density increases. Colonies of such regulating cells rapidly expand into unoccupied space because their edges consist of fast-growing, non-toxin-producing cells, but are also combative because cells at the interfaces with competing colonies do produce toxin. Because under the two growth regimes different types of regulation evolve, our results underscore the importance of growth conditions in the evolution of social behaviour in bacteria.

Author Summary

Bacteria live in microbial communities, in which they compete with many other microbes for nutrients and space. In this competitive environment, almost all known bacterial strains produce toxins that impair or kill other bacteria. This chemical warfare is thought to be one of the major factors shaping microbial diversity. Many toxins are produced only if the local density of bacteria is high. To achieve this, bacteria respond to cell-density cues: signalling molecules or other indicators of the presence of other cells. Here, we use a computational model to study the evolution of density-based regulation of toxin production in bacterial populations. We show that such regulation can arise under various growth conditions, and analyse the selection pressures driving its evolution. In particular, we find that if bacteria regularly need to colonise a new habitat, density-based regulation allows them to express a fast-growing, non-toxic phenotype when expanding into uncolonised territory, and a slower-growing, toxin-producing phenotype when competing with other strains. Colonies of regulating cells show a typical structure, with cells of the fast-growing, sensitive phenotype at their expanding edges, and toxin-producing cells in the colony interior and at interfaces between colonies.

4.1. Introduction

Many bacteria produce antimicrobial toxins that impede the growth of competing bacteria or even kill them (Klaenhammer, 1988; Riley and Wertz, 2002a; Gonzalez and Mavridou, 2019). A wide variety of such toxins has been discovered, ranging from narrow-range bacteriocins to broad-range antimicrobials that may even affect eukaryotic cells (Cornforth and Foster, 2013; García-Bayona and Comstock, 2018). Because producing and secreting toxins is metabolically costly, toxin producing strains have a reduced growth rate compared to non-producers (Chao and Levin, 1981; Kerr *et al.*, 2002; Riley and Wertz, 2002b). Toxin production is therefore an example of spiteful behaviour: it is costly to the actor and harmful to the recipient (Gardner *et al.*, 2004; Nadell *et al.*, 2009).

Over the years, the questions how and under what conditions such spiteful production of anticompetitor toxins can evolve have inspired many experimental and theoretical studies (Chao and Levin, 1981; Kerr *et al.*, 2002; Durrett and Levin, 1997; Gardner *et al.*, 2004; Kirkup and Riley, 2004; Narisawa *et al.*, 2008; Bucci *et al.*, 2011). These studies showed that the spatial scale over which interactions between bacteria take place is a key determinant of the evolutionary stability of toxin production. Modelling work predicted that toxin production is evolutionarily unstable in homogeneous, well-mixed environments with global interactions (*e.g.*, a shaken flask), while stable coexistence between a toxin-producing strain (or killer, K) and sensitive strain (S) can arise in spatially structured environments where interactions are local (*e.g.*, agar plates) (Durrett and Levin, 1997; Kerr *et al.*, 2002). Under well-mixed conditions, the K strain is fully outcompeted by resistant (R) cells (which for instance arise from K cells through mutational loss of toxin production but not resistance), because R cells avoid the metabolic costs for toxin production but equally benefit from the killing of S cells by the K strain. In spatially structured environments, however, killing and competition are local processes and hence K cells preferentially benefit from the killing effect of their toxin compared to non-producing cells. The population dynamics then follow local cycles of non-transitive "rock-paper-scissors" interactions: The K strain invades patches of S cells; these K cells are subsequently outcompeted by the R strain; and these R cells are in turn outcompeted by the faster-growing S strain (Kerr *et al.*, 2002). These local KRS-dynamics cause the emergence of wave-like spatial patterns, in which all three strains (K, R, and S) coexist (Durrett and Levin, 1997; Reichenbach *et al.*, 2007; Szolnoki *et al.*, 2014). These theoretical predictions were confirmed *in vitro* in populations of colicin-producing, -sensitive and -resistant *Escherichia coli* cells growing in flasks or on plates (Chao and Levin, 1981; Kerr *et al.*, 2002), and *in vivo* in enteric bacterial populations in a mouse model (Kirkup and Riley, 2004). Coexistence of a toxin-producing, -resistant, and -sensitive strain was also found in

the more complex environment of a growing biofilm *in vitro* (Narisawa *et al.*, 2008), and *in silico* modelling showed that the structure of the biofilm strongly affects the evolution of toxin production (Bucci *et al.*, 2011).

In all studies described above, genes for toxin production and resistance were constitutively expressed. Like many metabolically costly traits, however, toxin production is often tightly regulated (Cornforth and Foster, 2013; LeRoux *et al.*, 2015; Gonzalez and Mavridou, 2019). In particular, the expression of many anticompetitor toxins is regulated by cell-density cues: small diffusible molecules that are excreted by bacterial cells, such that their extra-cellular concentration reflects the local density of bacteria (see Cornforth and Foster (2013); Kleerebezem and Quadri (2001); Jimenez and Federle (2014) for reviews). Responding to a density cue allows bacteria to express costly genes only when the local cell density is high.

The high prevalence of toxin regulation by density cues raises the question of how such regulation evolved. A common explanation for the regulation of social behaviours by cell-density cues is that the benefits of the regulated social behaviour outweigh the costs only if a sufficient number of cells (the *quorum*) display the behaviour at the same time; the regulation is then also called *quorum sensing* (QS) (Nealson *et al.*, 1970; Miller and Bassler, 2001). This is for instance the case for the cooperative production of some public goods, like the siderophores of the common pathogen *Pseudomonas aeruginosa* (Diggle *et al.*, 2007; Darch *et al.*, 2012). For such costly public-good production, both theoretical and experimental work has shown that production of, and response to, a quorum sensing signal can be beneficial, as it allows cells to produce the public good only if the cell density is high and the benefit of coordinated public-good production is hence substantial (Brookfield, 1998; Brown and Johnstone, 2001; Nadell *et al.*, 2008; Czárán and Hoekstra, 2009; Darch *et al.*, 2012; Drescher *et al.*, 2014).

Whereas the evolution of density-dependent regulation is quite well-understood in the context of cooperative public goods, its evolution in relation to spiteful toxin production is less well-studied. In a single modelling study, Czárán and Hoekstra (2007) considered whether the evolution of density-dependent toxin production could be explained by similar reasoning as described above for public goods (Czárán and Hoekstra, 2007). A key feature of their model is that the toxin was assumed to be effective only if the local density of toxin producing cells exceeded a threshold density, which required toxin producers to cooperate. Furthermore, the model allowed gain and loss mutations of QS signal production, the hypothesis being that a genotype-specific cue that is produced by killer cells only might evolve to inform the killer cells about the local killer cell density. The study found, however, that QS regulation of toxin production was evolutionarily unstable to resistant "cheater" cells that produce the QS signal (and hence induce killer cells to produce toxin) but not the costly toxin (Czárán and Hoekstra, 2007). Hence, considering anticompeti-

tor toxin as a type of public good that is cooperatively produced has so far been unsuccessful in explaining density regulation of toxin production, and it remains unclear what selection pressures drive the evolution of toxin regulation by density cues.

Here, we therefore explore different explanations for the evolution of density-dependent toxin production. We use a computational model of evolving, spatially structured bacterial populations that deliberately differs from previous studies. In particular, we do not impose that a minimal quorum of toxin-producing cells is required in order to affect sensitive cells, but instead assume that the effect of toxin increases linearly with its concentration. Also, we focus on cases where toxin production is regulated by density cues that are produced by all cells (including cells that are sensitive to the toxin). For instance, production of the antimicrobial pyocyanin by *P. aeruginosa* increases in the presence of peptidoglycan fragments, a general indicator of the local density of gram-positive bacteria (Korgaonkar and Whiteley (2011), see Discussion for more examples). In such cases, the cue indicates the total cell density rather than the density of killer cells. We obtain results for two growth regimes: (i) a long-term local competition regime, in which the population evolves in a fixed, densely populated habitat, and (ii) a serial-transfer regime in which small, random subsets of the population repeatedly colonise new habitats, and show that density-dependent regulation of toxin production can evolve under both regimes. By characterising the selection pressures shaping the evolution of regulation, we explain how density-dependent toxin production can evolve under various growth regimes.

4.2. Model

We developed a spatially explicit individual-based model of a population of bacteria in which production of anticompetitor toxin, resistance to the toxin, and response to a cell-density cue can evolve. Here, a general overview of the model is given; details of the implementation and analysis are provided in the Methods section.

4.2.1. Bacteria and their genotypes

The bacteria in our model live on a square lattice (Figure 4.1). The model bacteria have several evolvable characteristics, which constitute their "genotype" (Figure 4.1A). Firstly, they carry a toxin production "gene" and a resistance "gene", each with three possible alleles: inactive ("Off"), constitutively expressed ("On"), or expressed in response to the density cue ("Regulated", or "Reg"). We refer to a cell's toxin production and resistance genotype using a bracket notation: *e.g.*, bac-

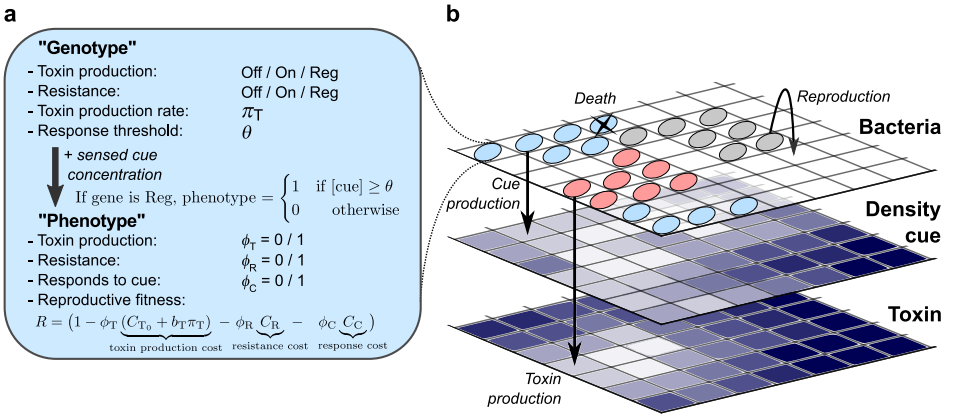

Figure 4.1. Illustration of the model. (a) The model bacteria's "genotype" consists of a toxin production "gene", a resistance "gene", a toxin production rate π_T and a response threshold θ. Bacteria regulating their toxin production and/or resistance only express these genes if the local concentration of the density cue exceeds the cell's response threshold. Expression of the toxin, resistance, and response to the cue come at a fitness cost. (b) The model consists of three coupled 2D lattices, which hold the bacteria, the density cue concentration and the toxin concentration. Bacteria locally compete for unoccupied space to reproduce. All cells have a natural death rate. For cells that are not resistant the death rate increases linearly with the local toxin concentration. All bacteria produce the cue, while the toxin is produced only by bacteria that express their toxin gene. The toxin and density cue diffuse and are degraded at fixed rates.

teria with genotype "(Reg, On)" regulate their toxin production but constitutively express resistance. Secondly, bacteria that express their toxin gene may differ in their toxin production rate π_T. Lastly, each bacterium has a response threshold value θ, which is the cue concentration above which it expresses its regulated genes, if it has any.

4.2.2. Concentration profiles of cell-density cue and toxin

The concentrations of the cell-density cue and the toxin are modelled with partial differential equations describing their local production, degradation, and diffusion. The cue molecule is produced by all cells, while the toxin is only produced by cells expressing the toxin production gene. We consider the dynamics of the cue and toxin to be much faster than the population dynamics of the bacteria, so that the concentration profiles of the cue and toxin at any given time are determined

by the current spatial distribution of bacteria (Picioreanu *et al.*, 2000; Xavier and Foster, 2007; Nadell *et al.*, 2008; Bucci *et al.*, 2011). We choose arbitrary units of concentration such that the concentration of the density cue varies between 0 and 1 and the toxin concentration varies between 0 and $\max(\pi_T)$, the largest toxin production rate in the bacterial population (see Methods).

4.2.3. Dynamics of bacteria

Time in the model progresses in discrete steps. At the beginning of each time step, each bacterium senses the local cue concentration, which together with the cell's genotype determines the cell's "phenotype" (Figure 4.1a). The phenotype is given by three variables: toxin production ϕ_T, resistance ϕ_R, and cue response ϕ_C, which take the value 0 (Not expressed) or 1 (Expressed). If the cell has a regulated gene, the corresponding phenotype value is set to 1 if the cue concentration exceeds the cell's response threshold value θ, and to 0 otherwise. Variable ϕ_C indicates whether the cell expresses a regulatory response system; it is 1 if the cell has at least one Reg gene, and 0 otherwise.

Note that a regulating cell's phenotype adapts to the local cue concentration at each simulation time step. An exception to this instantaneous adaptation is made in cells that regulate both their toxin production and resistance (genotype (Reg, Reg)): inspired by the *com*-regulon of *Streptococci* which displays a delay in the expression of the bacteriocins CbpD and LytA relative to the immunity factor ComM (Claverys and Håvarstein, 2007; Berg *et al.*, 2012; Slager *et al.*, 2019), a delay of τ_{delay} time steps is implemented between the expression of resistance and the expression of toxin. This delay prevents cells from killing neighbouring cells that have exactly the same genotype but coincidentally experience a slightly lower cue concentration and therefore do not (yet) express resistance.

Reproduction and cell death depend on a cell's phenotype. The death rate of sensitive bacteria increases linearly with the local toxin concentration (similar to Durrett and Levin (1997); Kerr *et al.* (2002); Bucci *et al.* (2011)). Importantly, this means that no minimal density (quorum) of toxin producers is required for the toxin to have an effect on sensitive cells (in constrast to Czárán and Hoekstra (2007)). Rather, each toxin producing cell proportionally adds to the killing rate of sensitive cells in the local neighbourhood.

The bacteria locally compete for a growth-limiting resource. To incorporate such local competition, at most one bacterium is allowed to occupy each lattice site. Bacteria surrounding an empty site compete for reproduction based on their respective reproduction rates (which depend on their phenotypes, as described below). When a cell reproduces, the daughter cell inherits the parent's genotype, except that with small probability mutations are introduced.

4.2.4. Fitness costs

Toxin production and resistance are metabolically expensive (Chao and Levin, 1981; Kerr *et al.*, 2002; Riley and Wertz, 2002b). Being able to respond to the density cue requires the production of receptors and a signal transduction pathway, and therefore likely also bears a metabolic cost. We incorporate these metabolic costs by reducing the reproduction rate of cells expressing these phenotypes. The costs for resistance and the ability to respond to the cue are constant, while the cost for toxin production increases linearly with the cell's toxin production rate π_T. Note that cells that regulate a gene always pay a cost for being able to respond to the cue, but in return may avoid the costs of toxin production and resistance when the density cue concentration is below their response threshold θ.

4.3. Results

4.3.1. Evolution of toxin regulation in a fixed, densely populated habitat

We first considered a bacterial population growing in a fixed habitat without external perturbations, by running the model on an undisturbed simulation lattice. Because we aimed to investigate the evolutionary potential of the production of anticompetitor toxin and its density-dependent regulation in general, rather than to model a specific strain of bacteria, we explored possible evolutionary outcomes of the model by performing a parameter sweep over the six defining parameters of our model: the spatial range of the density cue L_{cue}, the spatial range of the toxin L_{tox}, R_0^{-1} of the bacteria (where R_0 is the maximal expected number of daughter cells produced per bacterial life time), the scaled toxin production cost $\hat{b}_T$, the resistance cost C_R, and the cue response cost C_C (see Supporting Text 4.8.1 for the derivation of these parameters). We performed 2000 simulations with random parameter settings uniformly sampled from broad parameter ranges (see Methods, Table 4.1). For each simulation, we then calculated the mean abundance of each genotype and each phenotype after an evolutionary steady state was reached. Based on this evolved population composition, the simulations were classified into four categories (Supporting Figure S4.1).

In 1737 of the 2000 runs, the sensitive genotype (Off, Off) fixed in the population, indicating that most parameter conditions were unfavourable to the evolution of toxin production. In 228 simulations, at least one toxin producing genotype, sensitive genotype, and resistant genotype were found, hence yielding a KRS-system. Most of these evolved KRS-systems consisted of non-regulating killers (genotype (On, On)), non-regulating resistant cells (genotype (Off, On)), and sensitive cells

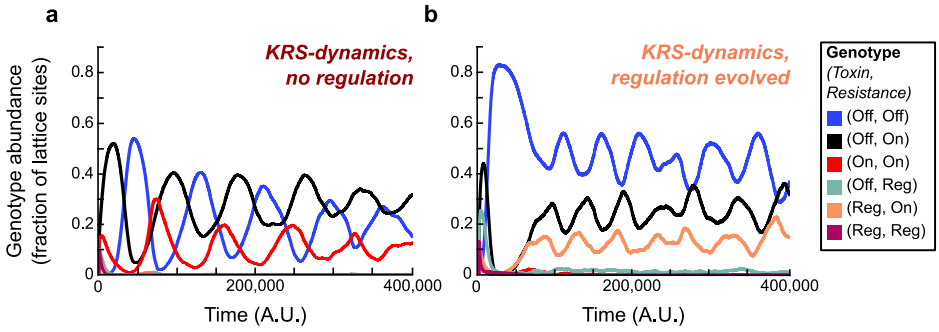

Figure 4.2. Types of KRS-systems that evolved in a fixed, densely populated habitat. Simulations were initialised with bacteria with random genotypes, and then run until evolutionary steady state was reached. Out of the 2000 simulations in the parameter sweep, 228 resulted in a KRS-system. (a) In 206 runs killer cells (genotype (On, On)), resistant cells (genotype (Off, On)) and sensitive cells (genotype (Off, Off)) coexisted, but no regulation evolved. (b) In 22 runs regulation did evolve, and in most of these (17 runs) coexistence was found between cells that regulate their toxin production but constitutively expresses resistance (genotype (Reg, On)), non-regulating resistant cells (genotype (Off, On)), and sensitive cells (genotype (Off, Off)). Parameter values for the example runs shown here are: (a) $L_{\text{cue}} = 3.7$, $L_{\text{tox}} = 16.5$, $R_0^{-1} = 0.1$, $\hat{b}_{\text{T}} = 0.045$, $C_{\text{R}} = 0.12$, and $C_{\text{C}} = 0.07$; (b) $L_{\text{cue}} = 6$, $L_{\text{tox}} = 6$, $R_0^{-1} = 0.125$, $\hat{b}_{\text{T}} = 0.32$, $C_{\text{R}} = 0.1$, and $C_{\text{C}} = 0.02$.

(genotype (Off, Off)) (Figure 4.2a), reproducing the KRS-dynamics observed in earlier studies (Kerr *et al.*, 2002; Durrett and Levin, 1997; Reichenbach *et al.*, 2007; Szolnoki *et al.*, 2014). In 22 of the 228 simulations yielding KRS-dynamics, however, at least one regulating genotype was selected. In a clear majority of these (17 runs), a single regulating genotype was found: cells that regulate their toxin production, but constitutively express resistance (genotype (Reg, On)). These regulating cells coexisted with sensitive cells (genotype (Off, Off)) and resistant cells (genotype (Off, On)) (Figure 4.2b). Lastly, 35 simulations did not result in fixation of sensitives or a KRS-system and were classified as "other". In none of these simulations regulation evolved, and they were therefore not further considered.

Regulation of toxin production can evolve when regulation costs are low, the density cue is short-ranged, and toxin production is costly

To determine which parameter combinations favour the evolution of regulation, we compared the parameter sets that resulted in KRS-dynamics without regulation ($n = 206$) to those that resulted in KRS-dynamics with regulation ($n = 22$) (Fig-

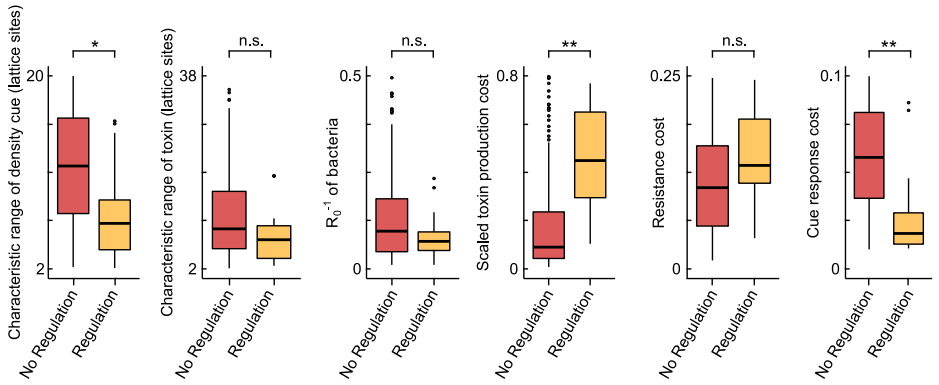

Figure 4.3. Parameter conditions for the evolution of regulation. The distribution of parameter values for simulations that yielded KRS-dynamics without regulation ($n = 206$) and those that yielded KRS-dynamics with regulation ($n = 22$). In simulations that resulted in the evolution of regulation, the spatial range of the cue and the response costs were lower, while the toxin production costs were higher. Results of 2-sided t-tests with Bonferroni-correction for multiple testing: $**$: $p < 10^{-6}$, $*$: $p < 10^{-3}$, n.s.: not significant.

ure 4.3). Unsurprisingly, in simulations in which regulation evolved, the cost of regulation was typically much lower. Regulation also evolved more readily when toxin production was costly and when the spatial range of the cell-density cue was limited. These conditions seem reasonable: the potential benefits of regulation are largest when it controls a costly behaviour, and a short-ranged cue contains more information about the current local environment than a longer-ranged cue. Since competition in the model occurs over short spatial ranges, responding to a short-ranged cue allows bacteria to quickly adapt to changes in their immediate competition environment.

Cells that regulate their toxin production occupy the killer niche in KRS-dynamics.

To better understand how density-dependent toxin regulation evolved in our model, we studied the example run of Figure 4.2b in more detail. The evolving population displayed KRS-dynamics, with regulating killer cells (genotype (Reg, On)) invading patches of sensitive cells (genotype (Off, Off)), constitutively resistant cells (genotype (Off, On)) invading patches of regulating killer cells, and sensitive cells invading patches of resistant cells (Figure 4.4a, Supporting Movie S4.1). The (Reg, On)-cells

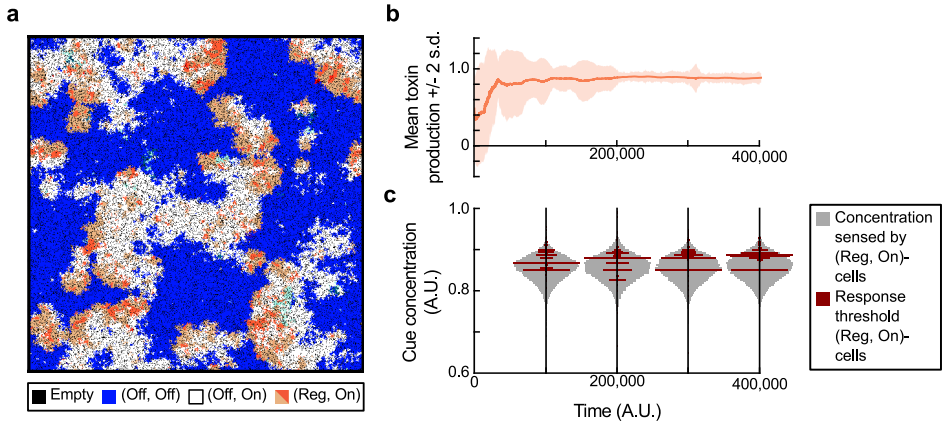

Figure 4.4. Model dynamics of a run in which density-dependent toxin regulation evolved. (a) Snapshot of the simulation lattice. KRS-dynamics emerge with sensitive cells (genotype (Off, Off), blue), resistant cells (genotype (Off, On), white) and regulating killer cells (genotype (Reg, On), orange). The latter switch between two phenotypes: toxin producing (dark orange) and resistant (light orange). See also Supporting Movie S4.1. (b) Toxin production rate in the (Reg, On)-cells over time. Cells were initialised with a toxin production rate sampled at random between 0 and 1. Over time, a mean value of $\pi_T \approx 0.8$ is selected. (c) Distribution of response threshold values in (Reg, On)-cells over time, plotted against a background distribution of the cue concentration sensed by these (Reg, On)-cells. Response threshold values around $\theta = 0.875$ are selected. The selected response threshold values tend to be higher than the median cue concentration sensed by regulating cells, indicating that at any time only a minority of cells produces toxin.

hence acted as the killer in these KRS-dynamics, replacing the constitutive killers (genotype (On, On)) found in non-regulating KRS-systems.

When the evolved (Reg, On)-cells express their toxin gene they produce a considerable amount of toxin ($\pi_T \approx 0.8$, Figure 4.4b), but due to regulation they do so only when they sense a high cue concentration. This regulation is governed by the evolved response threshold θ, the cue concentration above which regulated genes are expressed. To interpret the observed response threshold values, we compared them to the distribution of cue concentrations that (Reg, On)-cells sense (Figure 4.4c). Most response threshold values were greater than the median cue concentration observed, indicating that evolved (Reg, On)-cells are more often in their inactive resistant state than in their active toxin-producing state.

To make sure that we do not base our conclusions on contingencies in a particular

example run, we performed ten replicate runs with the same parameter settings, and found that the results were highly reproducible (Supporting Figure S4.2).

Regulation decreases the effective fitness cost of toxin production.

What selection pressures drive the observed evolution of density-dependent toxin regulation? In the cyclic KRS-system, two main factors determine the success of toxin-producing cells: their competitive advantage over sensitive cells and their disadvantage to resistant cells. To quantify the effect of regulation on these competitive (dis)advantages, we performed controlled invasion experiments comparing the invasion dynamics of the evolved (Reg, On)-cells to non-regulating (On, On)-cells evolved under the same parameter conditions but in a simulation where regulation was disabled (Supporting Figure S4.3). First, we directly competed the regulating (Reg, On)-strain with the (On, On)-strain, and found that the regulating killer strain invades and eventually fully displaces the constitutive killer strain, as expected. Next, we calculated the speed at which both killer strains invade a sensitive population, and the speed at which they are invaded by a resistant strain (Supporting Figure S4.3). Surprisingly, compared to the (On, On)-strain, the (Reg, On)-strain both invaded a sensitive population faster **and** was invaded more slowly by the resistant strain (Supporting Figure S4.3). Cells that regulate their toxin production hence have an advantage over non-regulating killer cells both in their invasion of new patches of sensitives, and in their competition with resistant cells.

The difference in the invasion speed into sensitive patches is explained by a difference in mean toxin production: the evolved (Reg, On)-cells on average produce more toxin per cell (mean long-term toxin production rate: 0.20) than the (On, On)-cells that evolved under the same conditions if regulation was excluded (mean long-term toxin production rate: 0.13). Naively, a higher mean toxin production rate should result in higher fitness costs. However, the increased competitiveness against resistant cells and the results of the direct competition between the two killer strains suggest that the regulating cells actually have a higher effective reproductive fitness than the constitutive killers. Here, the information conferred by the density cue comes into play. Remember that the metabolic costs of toxin production lead to a reduction in the producing cell's reproduction rate. However, because reproduction can only occur if empty lattice sites are available, the *effective* fitness costs of a reduction in reproduction rate also depend on the cell's environment and social neighbourhood. If several lattice sites in the cell's neighbourhood are unoccupied, the local competition for reproduction is a major determinant of the cell's fitness and the effective fitness costs resulting from the metabolic costs of toxin production are high. On the other hand, if no neighbouring lattice sites are vacant, the cell has no opportunity to reproduce and the effective fitness costs vanish. By exploiting the cue, the evolved (Reg, On)-cells produce toxin only when none or at most

one of their neighbouring sites is empty, and never do so when more than two neighbouring lattice sites are empty (Supporting Figure S4.4). At the wavefront where the (Reg, On)-cells compete with sensitive (Off, Off)-cells, the produced toxin frees up lattice sites by killing sensitive cells, causing a drop in the density cue concentration, which leads to the expression of the faster-reproducing, non-toxic phenotype in the (Reg, On)-cells benefitting from these available sites (which either produced the toxin themselves or profit from toxin production by closely related neighbouring (Reg, On)-cells). Regulation thus allows cells to produce toxin when reproduction opportunities are scarce and the effective fitness costs of production are hence low, and to exhibit a faster-replicating resistant phenotype when more space is available and hence competition for rapid reproduction is stronger.

Regulation works only if the density cue is sufficiently reliable and phenotypic adaptation is sufficiently fast

The evolved regulation mechanism described above requires that the cue concentration conveys detailed information about the environment. The evolved system might therefore be vulnerable to disturbances in the cue, *e.g.*, caused by stochasticity in production of the cue molecule, its diffusion and degradation, or in the response pathway. To test this hypothesis, we performed simulations in which at each time step independent Gaussian noise was added to the cue concentration at each lattice site. Regulation still evolved in 4 out of 5 replicate runs if a moderate noise level was used (standard deviation of noise was $\sigma_{\text{noise}} = 0.025$, which is comparable to the change in local cue concentration experienced if one of the eight direct neighbouring cells is removed). At an increased noise level ($\sigma_{\text{noise}} = 0.05$), however, only 2 out of 5 replicate runs showed evolution of regulation, and at an even higher noise level ($\sigma_{\text{noise}} = 0.1$) regulation evolved once in 5 replicate runs. Hence, regulation is effective only if the cue concentration is a sufficiently precise predictor of the current local density.

In the model, when the cue concentration changes, regulating cells adjust their phenotype instantaneously. In reality, such a phenotypic switch takes time (Monod, 1949; Rolfe *et al.*, 2012). To investigate how such a lag affects our results, we introduced a lag time between sensing a change and altering the phenotype. Regulation still evolved when a relatively short lag times of 5 simulation time steps was used, which is equivalent to 50% of the minimal doubling time of the bacteria (Supporting Figure S4.5). When the lag time was longer, regulation no longer evolved, indicating that the evolved regulation mechanism requires cells to be able to adjust their phenotype relatively fast. This result seems intuitive: a regulation mechanism that relies on cells reverting to a fast-growing, non-toxin-producing phenotype when locally empty sites are detected can only be effective if this reversion happens faster than the recolonisation of these empty sites.

4.3.2. Evolution of toxin regulation under a serial-transfer regime

So far, we have considered model bacteria living in a fixed, undisturbed habitat. Natural growth conditions, however, tend to vary substantially over space and time, and such variations in growth conditions may cause large fluctuations in cell density. To examine how externally induced density fluctuations affect the evolution of density-dependent toxin regulation, we simulated serial transfers: a procedure, well-known from experimental evolution studies, in which a small sample of the population is regularly transferred to fresh medium (Lenski *et al.*, 1991; Rainey and Travisano, 1998; Velicer and Yu, 2003; Kawecki *et al.*, 2012; Inglis *et al.*, 2016). The population dynamics were simulated as before, except that periodically the simulation was paused, a random sample of cells was taken from the population, and these founder cells were randomly placed on a new simulation lattice ("fresh medium"). These serial transfers were continued for many cycles to allow the system to approach evolutionary steady state.

Regulation evolves more frequently under serial transfers than in a fixed habitat.

To explore the model's behaviour under the serial-transfer regime, we simulated serial transfers for the same 2000 parameter conditions used in the fixed-habitat parameter sweep. The evolutionary outcome of simulations was again classified based on genotype and phenotype abundances at evolutionary steady state (Supporting Figure S4.6). Now, 1894 out of the 2000 parameter combinations resulted in the fixation of sensitives, an even larger fraction than in the fixed-habitat case. This makes sense: if cells regularly have to colonise a new, unpopulated environment, selection is expected to favour the fast-replicating sensitive genotype. Toxin production and resistance did evolve in 86 simulations, which were hence classified as "KRS". The 20 remaining simulations of the parameter sweep were classified as "other", and were further disregarded.

Out of the 86 simulations that yielded a KRS-system, regulation evolved in a majority of 68 cases (Supporting Figure S4.6). Hence, regulation evolved more readily under the serial-transfer regime than in the fixed habitat (in which only 22 parameter combinations out of 206 simulations yielding KRS-dynamics resulted in the evolution of regulation). Compared to the simulations that yielded a KRS-system without regulation ($n = 18$), the simulations in which regulation did evolve ($n = 68$) had relatively high toxin production and resistance costs, and low response costs (Supporting Figure S4.6), consistent with the observations in the fixed habitat (*c.f.*, Figure 4.3).

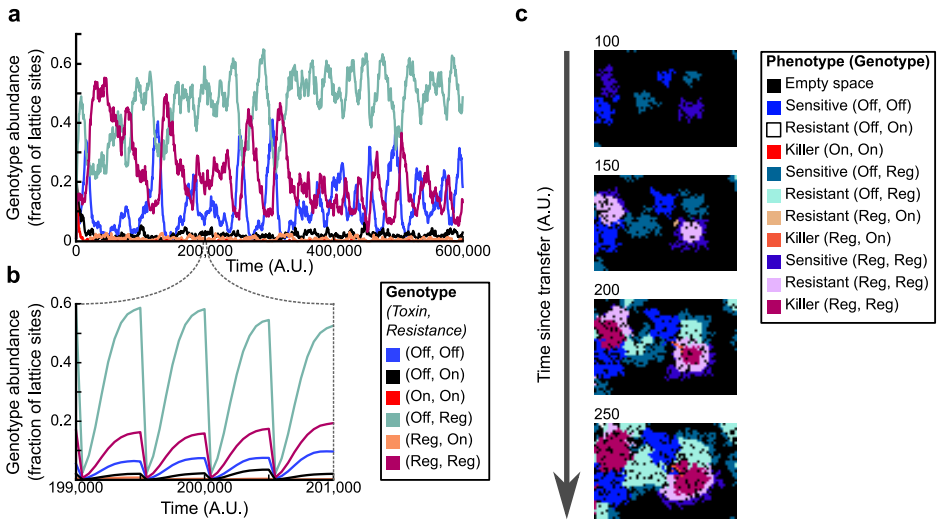

Figure 4.5. Model dynamics under a serial-transfer regime. The simulation was initialised with cells with random genotypes. Every 500 time steps, a random sample of 1000 cells from the current population was transferred to a new, empty lattice ("fresh medium"). (a, b) Abundance of genotypes over time on long (panel a) and short (panel b) time scales. Since the number of cells varies greatly within each transfer cycle, in panel A only the genotype abundances observed at the end of each cycle are plotted. The evolved population mainly consists of three genotypes: sensitives (genotype (Off, Off)), regulating resistants (genotype (Off, Reg)), and regulating killers, that also regulate their resistance (genotype (Reg, Reg)). (c) Snapshots of a small part of the simulation lattice showing colony growth between two transfers. Early on, (Off, Off)-, (Off, Reg)- and (Reg, Reg)-cells all express the sensitive phenotype. As the size of the colonies increases, the phenotype of cells in the interior of (Off, Reg)- and (Reg, Reg)-colonies switches to resistant, and in the case of (Reg, Reg)-cells after τ_{delay} time steps to toxin producing. Cells on colony edges remain sensitive, allowing the colony to grow rapidly. See also Supporting Movie S4.2. Parameter values: $L_{\text{cue}} = 6$, $L_{\text{tox}} = 6$, $R_0^{-1} = 0.125$, $\hat{b}_{\text{T}} = 0.072$, $C_{\text{R}} = 0.1$, and $C_{\text{C}} = 0.02$.

Under serial transfers, bacteria are selected for fast colony expansion.

In 62 of the 68 simulations in which regulation evolved, two types of regulating cells were found: (i) (Reg, Reg)-cells that regulate both their toxin production and their resistance, and (ii) (Off, Reg)-cells, that regulate their resistance and do not produce toxin. These cells coexisted with (Off, Off)- and sometimes (Off, On)-cells. A typical example of such dynamics is shown in Figure 4.5 and Supporting Movie S4.2, and we next consider this example in more detail.

At low cell density, cells with the three dominant genotypes ((Off, Off), (Off, Reg) and (Reg, Reg)) all express a sensitive phenotype. Cells with a sensitive phenotype have low fitness costs and hence a high replication rate. The genotypes (Off, Off), (Off, Reg) and (Reg, Reg) dominated in all ten replicate simulations performed (Supporting Figure S4.7), indicating that serial transfers robustly select for genotypes capable of growing at a high rate when cell density is low.

Shortly after each transfer into a new, empty, simulation lattice, founder cells of the three evolved genotypes indeed form colonies with a sensitive phenotype (Figure 4.5c, first panel; Supporting Movie S4.2 and Supporting Movie S4.3). As the colonies grow, the cue concentration within colonies increases. This causes cells in the interior of (Off, Reg)- and (Reg, Reg)-colonies to switch phenotype and become resistant (Figure 4.5c, second and third panel; Supporting Movie S4.2 and Supporting Movie S4.3). After the delay τ_{delay} between expression of resistance and toxin production, the (Reg, Reg)-cells furthermore switch to a toxin producing phenotype (Figure 4.5c, third and fourth panel; Supporting Movie S4.2 and Supporting Movie S4.3). As a consequence, a ring of non-producing resistant (Reg, Reg)-cells forms that acts as a buffer between the outer layers of sensitives cells and the toxin producing cells in the colony interior. While the phenotype of cells in the interior switches to resistant or toxin producing, the cells at the colony edge retain a sensitive phenotype. From a functional perspective, this again seems reasonable: colonies grow at their edges, and expressing a sensitive phenotype at the colony edge maximises the rate at which a colony expands into unoccupied space. Since cell density is per definition low at the edge of a colony, regulation based on the density cue allows toxin producing and resistant cells to express the fast-replicating sensitive phenotype exactly there where the colony is growing.

Regulation allows cells to adjust their phenotype to changing growth conditions.

Regulating cells can maintain a sensitive phenotype at the edge of growing colonies if their response threshold θ is larger than the cue concentration at the edge. Approximating the shape of a colony by a circle, we analytically calculated that the cue concentration at the edge of a colony is ≤ 0.49 (Supporting Text 4.8.2). This analytical approximation corresponds well to measurements from single-colony simulations (Figure 4.6a). Although there is some variation between response threshold values of (Reg, Reg)-cells in the replicate runs, all values were well above this lower bound (Figure 4.6b), showing that the evolved (Reg, Reg)-cells indeed exploit the density cue to form fast-expanding colonies.

Next to the lower bound, the evolved response threshold values are bounded from above by the cue concentrations that cells perceive at the end of a transfer cycle, *i.e.*, when the population approaches carrying capacity (Figure 4.6b). The

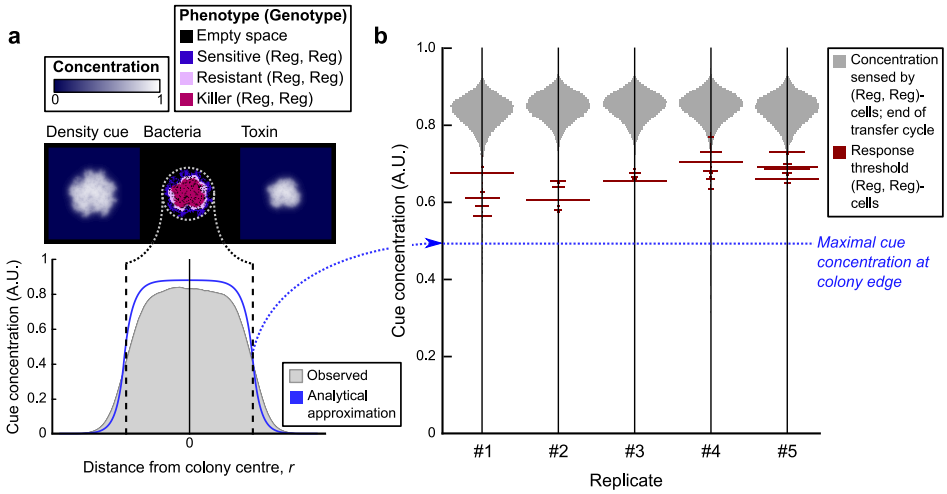

Figure 4.6. Density cue concentration profile of expanding colonies and the evolved response threshold values of (Reg, Reg)-cells. (a) Colonies were grown from a single (Reg, Reg)-cell to characterise the radial density cue concentration profile of an expanding colony. Measured values from the simulations correspond well to the analytical approximation (see Supporting Text 4.8.2). (b) Distribution of the evolved response threshold values in (Reg, Reg)-cells at the end of the simulation (time $= 600,000$), plotted against the background of the cue concentration sensed by these cells at the end of a transfer cycle (*i.e.* when the population approaches carrying capacity) for five replicate simulations. The evolved response threshold values vary somewhat between replicates, but are always lower than the cue concentration at local carrying capacity (grey distributions) and higher than the maximum of the cue concentration at the edge of a growing colony. Hence, cells on the colony edge never express their toxin production and resistance genes, while cells in the colony interior and at the interface between colonies (where local cell density is close to carrying capacity) are resistant and do produce toxin.

evolved (Reg, Reg)-cells hence do produce toxin (and consequently pay fitness costs) when the local cell density is high, suggesting that these cells have been selected to exhibit their competitive phenotype (*i.e.*, toxin production) when the population locally approaches carrying capacity. Importantly, such high cell densities not only occur in the interior of expanding colonies, but also at interfaces between colonies where cells of two colonies (with potentially different genotypes) compete. At the interfaces between colonies, (Reg, Reg)-cells hence express their toxin producing phenotype (Supporting Movie S4.3). The evolved regulating cells adjust their phenotype to varying growth conditions, exhibiting a sensitive phenotype when repli-

cating into unoccupied space, and expressing toxin production and resistance when in competition with other cells.

Over many transfer cycles, the (Reg, Reg)-, (Off, Reg)- and (Off, Off)-cells show KRS-dynamics.

So far, we have focused on explaining the evolution of cells that regulate both their toxin production and resistance. However, a large fraction of the evolved populations is made up of cells that do not produce toxin and regulate their resistance only (Figure 4.5a and Supporting Figure S4.7). These (Off, Reg)-cells had response threshold values very similar to those of (Reg, Reg)-cells (Supporting Figure S4.7), and hence express the same fast-growing sensitive phenotype at the edges of growing colonies, but exhibit a resistant phenotype at the colony interior and where colonies interact (Figure 4.5c, Supporting Movie S4.2 and Supporting Movie S4.3).

While the toxin-producing phenotype of (Reg, Reg)-cells provides an advantage when competing with a colony of sensitive (Off, Off)-cells, it confers a disadvantage when competing with a colony of (Off, Reg)-cells. Similarly, the competitive resistant phenotype of (Off, Reg)-cells yields a competitive advantage against (Reg, Reg)-cells, but a disadvantage against (Off, Off)-cells. Hence, within the evolved regulating genotypes we again found cyclic dominance (see Supporting Movie S4.3), and this is reflected in the long term population dynamics (Figure 4.5a): the number of (Off, Off)-cells, (Off, Reg)-cells and (Reg, Reg)-cells oscillated in a K-R-S order. These KRS oscillations now occur on the time scale of many transfer cycles.

The evolution of regulation under serial transfers is highly robust to variations in the transfer regime, cue concentration and phenotype expression timing.

Because serial transfers have such a profound impact on the evolution of regulation, we examined how the evolutionary outcome depends on the frequency of transfers and the number of founder cells used to seed the next population (Supporting Figure S4.8). The evolution of regulation depends on the balance between selection for fast colony growth in sparsely populated environments, and selection for competitive phenotypes in dense environments. When transfers were very frequent, or the number of founder cells was very small, cells were continuously selected for fast growth and the sensitive (Off, Off)-genotype fixed in the population. On the other hand, when transfers were very infrequent or the number of founder cells was very large, we recovered the results found in the absence of serial transfers. In between, however, regulation was found in a wide parameter range: regulating genotypes still evolved when the time between transfers was increased 5-fold compared to the example parameter set of Figure 4.5, or the number of founder cells was increased by an order of magnitude (Supporting Figure S4.8).

Regulation also readily evolved when we relaxed the assumption that the time between subsequent transfers is fixed and instead transferred the population with a fixed probability per time step (that is, as a Poisson process, producing an exponential waiting-time distribution) (Supporting Figure S4.9). Results of these simulations were similar to the results obtained with fixed cycle lengths, indicating that the evolution of regulation is robust against variation in transfer timing.

Furthermore, the evolution of regulation was also robust to variation in the time delay τ_{delay} between expression of resistance and toxin production in (Reg, Reg)-cells, with (Reg, Reg)-cells evolving even when $\tau_{\text{delay}} = 0$ and the ring of non-producing resistant cells in colonies disappears (Supporting Figure S4.10). Regulation also readily evolved when significant lag times (up to 3 bacterial doubling times) were implemented between the first instance that cells sense a change in cue concentration and the moment these cells change their phenotype accordingly (Supporting Figure S4.11).

Lastly, the regulatory mechanism that evolved under serial transfers is highly robust to noise in the cue concentration. Even when large Gaussian noise ($\sigma_{\text{noise}} = 0.1$, on cue concentrations varying between 0 and 0.85) was added to the cue concentration at each lattice site at each time step, regulation still evolved (Supporting Figure S4.12). The regulation mechanism that evolved under the serial-transfer regime is hence more robust to noise in the cue concentration than the mechanism that evolved in a fixed habitat.

4.3.3. Spatial structure is crucial for the evolution of toxin production and regulation

So far, we have considered a spatially structured population in which reproduction and competition occur locally. This implementation was chosen because previous work has shown that constitutive toxin production is not evolutionarily stable in well-mixed environments (Durrett and Levin, 1997; Kerr *et al.*, 2002) (see Introduction). We therefore did not expect toxin production to evolve in our model in the absence of spatial structure, even if regulation was allowed.

To test this, we repeated all runs of our parameter sweep (both in a fixed habitat and under serial transfers) but now randomised the positions of the bacteria at each time step. We then classified the evolutionary outcome of these simulations in the same way as we analysed the spatially structured simulations (see Supporting Figure S4.1). As expected, the sensitive genotype (Off, Off) fixed in all 4000 simulation runs. Particularly, even under parameter conditions that did yield (regulating) toxin producing cells in the spatially structured simulations, toxin production did not evolve under well-mixed conditions. This result underscores the crucial importance of spatial structure for the evolution of toxin production, regulated or not.

4.4. Discussion

Using a simulation model, we have shown that the production of anticompetitor toxins can become regulated by a cell-density cue in evolving populations under two different growth regimes: in a fixed habitat, and in serial-transfer cycles. Under both regimes, regulation of toxin production evolves because it allows cells to adjust their investment in toxin production to changes in the local competition and growth opportunities. However, the selection pressures driving the evolution of toxin production at high density, and the resulting types of regulation that evolve, differ between the growth regimes.

In the fixed habitat, regulating killer cells evolved that produce toxin only at very high local cell densities (Figure 4.4). We showed that these cells use the density cue to produce toxin only if reproduction opportunities are very scarce and the effective fitness costs of toxin production are therefore low (Supporting Figure S4.4). This type of regulation relies on the fact that, in the model, cells that cannot reproduce due to a lack of empty neighbouring lattice sites can nevertheless produce toxin, at very low or even zero fitness cost. This phenomenon could occur in reality if at low cell density reproduction and toxin production are limited by the same resource(s) (*e.g.*, the availability of carbon or nitrogen substrates), while at high cell density reproduction is limited by a different resource that does not limit toxin production (*e.g.*, crowding or a lack of substrate not required for toxin production). Interestingly, such conditions have previously been found to stabilise cooperative secretions of swarming-promoting biosurfactants in *P. aeruginosa* (Xavier *et al.*, 2011). Production and secretion of these carbon-rich biosurfactants is regulated by nutrient availability, such that they are only produced when growth is limited by another nutrient than carbon (in this case, the nitrogen source) and the fitness costs of biosurfactant secretion are hence low, a mechanism called *metabolic prudence* by Xavier *et al.* (2011). Our model hence predicts that such *metabolic prudence* could also promote the evolution of density-dependent toxin regulation in long-term local competition environments by reducing the effective fitness costs of toxin production.

Under the serial transfer regime, we find that the evolution of regulation is dictated by two selection pressures: (i) selection for fast reproduction at the edge of expanding colonies, and (ii) selection for the expression of competitive phenotypes (toxin producing and/or resistant) at the interface between colonies (Figure 4.5-4.6). The dynamics of single cells founding expanding colonies leads to competition between these clonal colonies, and bacteria are selected for the colony structure that they produce (see Supporting Movie S4.3). After a serial transfer, those colonies that express a sensitive phenotype at their edges expand more rapidly into the newly available empty (or "resource-rich") space. Regulation allows cells to recognise the expanding edges of their colonies, because the local cell density at colony edges is

low, and to thus express a sensitive phenotype at these edges.

The selection for fast colony expansion explains why cells are selected to express a sensitive phenotype at the edge of expanding colonies, but does not explain why expression of resistance and/or toxin production at high cell density is favoured. As long as a colony clonally expands without interacting with other colonies, the production of toxins does not confer any benefit. However, since the colony expands at its edges and the spatial range of the toxin is limited, the observed production of toxin in the interior of the colony also does not hamper the fast expansion of the colony. As soon as the expanding colony meets another colony, the situation changes: toxin production then yields a potential benefit in the competition with cells of the other colony (which might be sensitive to the toxin). Regulating cells cannot distinguish between the interior of a single colony or the interface between two colonies, because at both sites the local cell density is high. Responding to high cell density however allows the cells to express their competitive phenotype (toxin production or resistance) when in direct competition with cells of another colony (thus performing "competition sensing" *c.f.*, Cornforth and Foster (2013)), while expression of the competitive phenotype in the interior of the colony does not slow down the colony's expansion.

The marked differences between results obtained in the fixed habitat and under serial transfers show that the evolutionary dynamics in the model strongly depend on the growth regime. This is not just true for the model presented here. For instance, in experimentally grown colonies of toxin-producing, resistant, and sensitive *E. coli* strains it was found that populations under range expansion do not always show the coexistence patterns found in a stationary environment (Weber *et al.*, 2014). In experimental evolution, it has also long been known that the experimental regime can pose strong selection pressures on evolving populations (Atwood *et al.*, 1951; Levin *et al.*, 2000). Because results obtained in one growth condition often do not generalise to other conditions, it is important to consider multiple regimes in theoretical and experimental evolutionary studies.

The differences between the evolution of regulation in the two growth regimes also warrant the question which results provide the more likely explanation for the observed density-dependent regulation of toxin production in nature. In our model, regulation evolved more frequently in the serial transfer regime than in the fixed habitat (Supporting Figure S4.6). The regulation that evolved under serial transfers was also more robust to a lag between the change in cue concentration and the switch in phenotype (Supporting Figures S4.5 and S4.11), and to noise in the cue concentration (Supporting Figure S4.12). Lastly, the limitation of toxin production to instances where the effective fitness cost is very low (similar to *metabolic prudence*, *c.f.*, Xavier *et al.* (2011)) which we found in the fixed habitat, can only explain the evolution of density-dependent toxin regulation if specific conditions on the resources

limiting reproduction and toxin production are met (see discussion above). The use of the density cue to recognise the edge of an expanding colony after a serial transfer, however, can favour the evolution of density-dependent toxin regulation as long as bacterial replication is limited by a resource that is present at higher concentration on the edge of a colony than in its interior. This seems to be a fairly general condition. Although "metabolic prudence" might contribute to the evolution of regulation for some toxins, we consider selection for the ability to switch between a fast-growing phenotype when colonising a new environment and a competitive phenotype when competing with other bacteria as the biologically more feasible and general candidate to explain evolution of density-dependent toxin regulation.

A similar switch between a fast-growing phenotype when colonising an environment and slower-growing social phenotypes when cell density is high was recently found in a model of quorum-sensing (QS) regulated cooperative public good production in growing biofilms (Schluter *et al.*, 2016). In this model, cells that regulated the production of costly public good through QS were found to outcompete constitutive producer cells, because the regulating cells exhibited a fast-growing, non-producer phenotype during the early stages of biofilm growth, and only switched to public good production when cell density increased. Regulation hence allowed colonies to expand rapidly when cell density was low, and to express a cooperative phenotype when cell density was high. Although this selection for fast colonisation is indeed reminiscent of our results, the selection pressures underlying the social behaviour (public good secretion or toxin production) differ substantially. In the case of public good secretion, Schluter *et al.* show that the QS signal acts as a measure of local relatedness, allowing cells to delay the secretion of public good until they are surrounded by clone mates and the benefit of public good production is high. In the case of toxin production, however, relatedness is a double-edged sword. While toxin production is promoted by high relatedness between toxin producers and those benefitting from the killing, this benefit only arises when non-related sensitive cells are present in the local neighbourhood (Queller, 1994; Gardner and West, 2004). In the model presented here, the benefits of the toxin production at high cell density are not explained by high local relatedness, but rather by the presence of (unrelated) sensitive competitors.

A key feature of the density cue considered in this study is that it is produced by all bacteria. The choice of such a "total-density" cue was inspired by many natural examples. For instance, expression of the bacteriocin mutacin in the dental bacterium *Streptococcus mutans* is regulated by autoinducer-2 (AI-2) (Qi *et al.*, 2004; Merritt *et al.*, 2005), a general quorum sensing molecule that is produced by many species of bacteria as a metabolic byproduct (Hense and Schuster, 2015; Whiteley *et al.*, 2017). AI-2 is also involved in the regulation of bacteriocin production in the insect pathogen *Photorhabdus luminescens* (Krin *et al.*, 2006). Additionally,

in *P. aeruginosa* the production of the broad-spectrum antimicrobial pyocyanin is enhanced by the presence of peptidoglycan fragments, which indicates high local density of gram-positive bacteria (Korgaonkar and Whiteley, 2011).

In addition to the examples of regulation by total-density cues provided above, a wide variety of density-dependent toxin regulation mechanisms exists. Instead of using a density cue as an indicator for the presence of competitor cells, some bacteria more directly sense the presence of competitors, for instance through cell damage caused by these competitors, and respond with toxin production (Be'er *et al.*, 2009; Mavridou *et al.*, 2018). Other toxins promote their own production; examples include several colicins (Mavridou *et al.*, 2018; Pugsley, 1983; Ghazaryan *et al.*, 2014) and the lantibiotics, a large class of bacteriocins produced by Gram-positive bacteria including nisin and subtilin (Kleerebezem and Quadri, 2001; Alkhatib *et al.*, 2012). For these bacteriocins, a modelling study showed that during invasion events, cells that regulate their bacteriocin based on cell density outcompete cells that constitutively express bacteriocin, if the cost of bacteriocin production and the amount of bacteriocin produced are high (Blanchard *et al.*, 2016). Although this study did not consider long-term evolutionary dynamics and did for instance not include resistant, non-toxin-producing strains, its prediction agrees with the conditions that we find for the evolution of regulation (see Figure 4.3 and Supporting Figure S4.6).

Notably, the expression of many other toxins is regulated by quorum sensing molecules that seem to be produced specifically for regulation of the toxin (Cornforth and Foster, 2013; Hibbing *et al.*, 2010; LeRoux *et al.*, 2015). These QS molecules are often produced by toxin producing cells only, and hence act as "killer-specific" cues. A population in which such a killer-specific quorum sensing signal evolves might be prone to social cheating on the signal, *e.g.*, by cells that produce the signal but do not produce the toxin, or by cells that cease their signal production and go "under the radar". Such social signalling cheaters cannot arise for total-density cues, because these are by definition produced by all cells. The evolutionary explanations presented in this work for regulation by total-density cues therefore cannot necessarily be generalised to regulation by killer-specific cues. As far as we are aware, only a single modelling study has been undertaken to examine the co-evolution of toxin production and potentially killer-specific quorum sensing, which found that QS control of toxin production was unstable to social cheating (Czárán and Hoekstra, 2007) (see also the Introduction). In this model, however, cell density was fixed, and only the local population composition (*e.g.*, the fraction of toxin producing bacteria) varied over time. In the model presented here, we have seen that large fluctuations in cell density drastically change the evolution of social behaviours associated with cell density, and might favour the evolution of regulation. Studying the evolution of toxin regulation by killer-specific cues under serial transfers is therefore an interesting and promising direction for future research.

Testing whether or not bacteria employ the types of regulation we identified would require the careful monitoring of the temporal dynamics of toxin production, resistance and cell division in bacterial colonies expanding after serial transfers or growing on a plate at high density, preferably at single-cell level (as *e.g.*, done by Mavridou *et al.* (2018)). Under serial transfers, the model predicts that bacterial colonies should consist of toxin-producing cells at the interior of the colony, and sensitive cells on the edge of the colony. Furthermore, these sensitive cells at the edge should switch to a toxin-producing phenotype when encountering another colony. These predictions can be tested by following toxin production at the single-cell level in growing bacterial colonies of bacteria known to regulate their toxin production with a general cell-density cue. Ahead of such experiments, our modelling work has provided more insight into the mechanisms underlying the evolution of complex regulation systems in microbial populations.

4.5. Methods

The general set-up of the model is discussed in the Model section. Below, we provide details on the implementation and analysis. The model was implemented in C. Code is available from the corresponding author upon request.

4.5.1. Spatially structured individual-based model

We developed a spatially explicit individual-based model of bacteria evolving their production of an anticompetitor toxin, resistance, and response to a cell-density cue. Bacteria in the model are characterised by a genotype of four characteristics: a toxin production gene, a resistance gene, a toxin production rate π_T and a cue response threshold θ (Figure 4.1a). The bacteria live on a square $N \times N$ lattice ($N = 512$ for all simulations in this paper) with periodic boundary conditions. Each lattice site can contain at most one bacterium.

4.5.1.1. Concentration profiles of the cell-density cue and the toxin

The production, degradation and diffusion of the cell-density cue and the toxin are described with partial differential equations. Let $c_k(\mathbf{x}, t)$ be the concentration of secreted product k at location $\mathbf{x}$ at time t, where the index k can be replaced by "cue" or "toxin". Then

$$\frac{\partial c_k(\mathbf{x},t)}{\partial t} = \underbrace{P_k(\mathbf{x},t)}_{\text{production}} - \underbrace{d_k c_k(\mathbf{x},t)}_{\text{degradation}} + \underbrace{D_k \nabla^2 c_k(\mathbf{x},t)}_{\text{diffusion}}, \tag{4.1}$$

where d_k is the degradation rate, D_k the diffusion rate, and $P_k(\mathbf{x}, t)$ the production rate at location $\mathbf{x}$. For simplicity, we assume that the cue molecule is produced by

all bacteria at a fixed rate p_{cue}: $P_{\text{cue}}(\mathbf{x}, t)$ equals p_{cue} if the lattice site at location $\mathbf{x}$ is occupied, and is 0 otherwise (similar to previous implementations of density cue dynamics (Nadell *et al.*, 2008; Schluter *et al.*, 2016)). For the toxin, $P_{\text{tox}}(\mathbf{x}, t)$ equals $\pi_{\text{T}}(\mathbf{x})$, *i.e.*, the toxin production rate of the bacterium at location $\mathbf{x}$, if the lattice site is occupied by a bacterium expressing its toxin production gene, and is 0 otherwise.

Each simulation time step, the quasi-steady-state concentration profile $c_k(\mathbf{x})$ of molecule k is found by equating the right-hand side of Eq 4.1 to zero and solving for c_k. Taking the 2D finite-difference approximation of Eq 4.1 and dropping the index k for brevity, this yields

$$P_{i,j} - dc_{i,j} - 4Dc_{i,j} + D(c_{i-1,j} + c_{i+1,j} + c_{i,j-1} + c_{i,j+1}) = 0, \tag{4.2}$$

for each position (i, j) on the simulation lattice. Here, P is the production matrix containing the production rates of the molecule at each position, d is the degradation rate and D the diffusion rate. Since we consider periodic boundary conditions, all indices in Eq 4.2 should be read modulo N.

Eq 4.2 is a linear system of $N \times N$ equations. To solve it efficiently, we make use of Fourier transformations. Because we assume a square simulation lattice and periodic boundary conditions, $c_{i,j}$ is a discrete periodic function with period N in both indices. Let G be the degradation-diffusion kernel at $(1, 1)$:

$$G := \begin{pmatrix} -4D - d & D & 0 & \cdots & D \\ D & 0 & 0 & \cdots & 0 \\ 0 & 0 & 0 & \cdots & 0 \\ \vdots & \vdots & \vdots & \ddots & \vdots \\ D & 0 & 0 & \cdots & 0 \end{pmatrix}, \tag{4.3}$$

such that $G_{i,j}$ describes the diffusion and degradation effects of the molecule concentration in lattice site (i, j) on the concentration in lattice site $(1, 1)$. The $N \times N$ equations defined by Eq 4.2 can then be rewritten as

$$P + (c *_N G) = 0, \quad \text{or} \quad c *_N G = -P, \tag{4.4}$$

where $c *_N G$ is the circular discrete convolution of matrices c and G. By the circular convolution theorem, $c *_N G$ is equal to the inverse Fourier transform of the element-wise product of the individual Fourier transforms of c and G, *i.e.* we can solve $\mathcal{F}(c)$ from

$$\mathcal{F}(c) \cdot \mathcal{F}(G) = \mathcal{F}(P), \tag{4.5}$$

and then compute the inverse Fourier transform to get the concentration matrix c. Since the degradation and diffusion rates of the molecules are constant over the simulation, so is G. Hence, $\mathcal{F}(G)$ needs to be calculated only once per simulation,

and at each simulation time step we are left with finding the Fourier transform $\mathcal{F}(P)$ of the production matrix, dividing the result element-wise by $\mathcal{F}(G)$, and then using the inverse Fourier transform to find c. Fourier transformations were performed using the `fftw3`-library (Frigo and Johnson, 2005). Since algorithms for Fourier transformations are highly efficient (Frigo and Johnson, 2005), Eq 4.5 allows us to rapidly find the quasi-steady-state concentration profiles even for large simulation lattices.

4.5.1.2. Population dynamics of bacteria

Every time step, the phenotype of bacteria (toxin production ϕ_{T}, resistance ϕ_{R}, and cue response ϕ_{C}) is determined based on their genotype and the current local cue concentration (Figure 4.1a). If a gene is regulated, it is expressed only if the cue concentration exceeds the cell's response threshold θ.

The probability of cell death per time step has a basal value δ and increases linearly with the local toxin concentration $c_{\mathrm{tox}}(\mathbf{x})$, unless the bacterium is resistant:

$$\mathbb{P}(\text{death of cell } j|\mathbf{x}) = \delta + (1 - \phi_{\mathrm{R}_j})\delta_{\mathrm{tox}} c_{\mathrm{tox}}(\mathbf{x}). \tag{4.6}$$

The slope δ_{tox} describes the toxicity of the toxin. When bacteria die, they leave behind an empty lattice site.

Empty sites can be repopulated by reproduction of bacteria on the eight neighbouring lattice sites. For each empty lattice site, the probability that it becomes occupied by reproduction of any of its neighbouring bacteria in the current time step is

$$\mathbb{P}(\text{reproduction}|\mathbf{x}) = 1 - \mathrm{e}^{-\gamma \frac{1}{8} \sum_{i \in \text{neighbours}} R_i}, \tag{4.7}$$

where γ is a scaling factor determining the maximal reproduction rate per time step and R_i is the reproductive fitness of the i-th neighbour (further specified below). If reproduction occurs, neighbour j is selected as the parent with probability

$$\mathbb{P}(\text{reproduction of cell } j|\mathbf{x}) = \frac{R_j}{\sum_{i \in \text{neighbours}} R_i}. \tag{4.8}$$

Eq 4.7 and 4.8 ensure that (i) the overall probability of reproduction increases with the total reproductive fitness of the eight neighbours but never exceeds 1, and (ii) the probability of reproduction of a specific cell is determined by its reproductive fitness relative to its local competitors.

Toxin production, resistance, and the ability to respond to the density cue bear metabolic costs. The metabolic costs of cell j's phenotype are linearly incorporated in its reproductive fitness as

$$R_j = \max\Big[0, \big(1 - \underbrace{\phi_{\mathrm{T}_j}(C_{\mathrm{T}_0} + b_{\mathrm{T}}\pi_{\mathrm{T}_j})}_{\text{toxin production cost}} - \underbrace{\phi_{\mathrm{R}_j} \underbrace{C_{\mathrm{R}}}}_{\text{resistance cost}} - \underbrace{\phi_{\mathrm{C}_j} \underbrace{C_{\mathrm{C}}}}_{\text{response cost}}\big)\Big]. \tag{4.9}$$

The costs for resistance (C_R) and the ability to respond to the cue (C_C) are given by single parameters. The cost for toxin production linearly depends on the cell's toxin production rate π_T, with offset C_{T_0} and slope b_T. Note that we do not include a cost for cue production. Because all cells produce the density cue (at the same rate), such a cost would be the same for all phenotypes, and hence would not influence the competition between cells of different phenotypes.

4.5.1.3. Mutations

When a bacterium reproduces, the daughter cell generally inherits the genotype of its parent. With small probability, however, mutations are introduced. First, mutations can alter the toxin and resistance gene. If a mutation generates a cell that produces toxin while not simultaneously expressing resistance, this cell is considered non-viable and discarded from the simulation. Second, mutations in the response threshold value θ are introduced with a fixed probability μ. If the parent cell has a regulating genotype, the mutated response threshold is generally drawn from a uniform distribution on the interval $[\theta_{\text{parent}} - \sigma_\mu; \theta_{\text{parent}} + \sigma_\mu]$ (if the new threshold value is below 0, it is set to 0). However, to ensure that the genotype space is sufficiently accessible, with probability $p_{\text{largemut}} = 10^{-3}$ the new response threshold is chosen randomly between 0 and 1. Response threshold values of regulating daughter cells with a non-regulating parent are also uniformly sampled from $[0, 1]$. Third, mutations in the toxin production rate π_T are introduced in the same way as response threshold mutations, with the same rate μ, step size σ_μ, and probability of not inheriting the parental value p_{largemut}.

The number of ways a functional sequence can be removed or destroyed by small-scale mutations (substitutions, short indels) usually greatly exceeds the number of mutations that can create such a functional sequence, simply because most sequences do not perform the desired function. For larger scale mutations, gene loss is thought to be the major driver of evolution of many prokaryotic lineages over relatively short evolutionary times (*e.g.*, within genera), occurring several times more frequently than *de novo* gene discovery and gene gain through horizontal gene transfer (Makarova *et al.*, 2006; Puigbò *et al.*, 2014). We therefore consider gain-of-function mutations (Off → On, Off → Reg, and On → Reg) to be less likely than loss-of-function mutations (On → Off, Reg → Off, and Reg → On).

4.5.2. Parameter sweep

4.5.2.1. Parameter reduction and parameter values

Altogether, the model has 18 parameters. Brute-force sampling an 18-dimensional parameter space in an exploratory parameter sweep is computationally infeasible. Fortunately, the parameter space can be reduced by identifying lumped parameters

(Table 4.1, see Supporting Text 4.8.1 for derivations). The 13 parameters remaining after the parameter reduction include the 5 mutation parameters and the delay between expression of resistance and toxin in (Reg, Reg)-cells τ_{delay}. Over many test runs we observed that these parameters only marginally affect the simulation results, as long as mutations happen reasonably frequently. The mutation parameters and τ_{delay} were therefore fixed at default values (Table 4.1). To further reduce the number of parameters included in our parameter sweep, we finally noted that the offset C_{T_0} defines a minimal cost of toxin production and should hence be > 0 to make sure toxin production is never "free", but should also not be too large because else toxin production can never evolve. Because $\hat{b}_{\text{T}}$ is also a measure for the cost of toxin production, we chose to keep $C_{\text{T}_0} = 0.01$ constant, and only vary $\hat{b}_{\text{T}}$ in the parameter sweep along with the five other remaining parameters (Table 4.1).

To capture the different potential evolutionary outcomes for varying bacterial species and environments, we varied our parameters over relatively broad ranges in a parameter sweep (Table 4.1). Since we aimed to investigate regulation by local cell density, the characteristic length scale L_{cue} of the density cue was chosen between 2 and 20 lattice sites. To set reasonable values for the toxin length scale L_{tox}, we noted that in many KRS-models toxin-dependent killing is limited to direct neighbours in space (Durrett and Levin, 1997; Czárán *et al.*, 2002; Kerr *et al.*, 2002; Czárán and Hoekstra, 2007). Experiments show, however, that the inhibition range of toxins is generally much larger, and can span several tens or even hundreds of μm (Chao and Levin, 1981; Mavridou *et al.*, 2018). For colicins, a length scale of 100 - 175 μm has been reported (Weber *et al.*, 2014), which corresponds in size to at least 50 bacteria. We therefore chose the range of L_{tox} twice as broad as the range for L_{cue} (Table 4.1). KRS-systems in general, and regulation of toxin production in particular, evolved more readily for small values of L_{tox} (see Figure 4.3), so an even wider range would not yield more insight into the model.

To determine bounds on δ/γ, note that this lumped parameter is equal to ${R_0}^{-1}$ of the bacteria, where R_0 is the maximal expected number of offspring of a sensitive cell (*i.e.* when it is completely surrounded by empty space). Any population with $R_0 < 1$ is nonviable. Note, furthermore, that for a sensitive population at carrying capacity the cell density is equal to $1 - {R_0}^{-1}$. Since toxin production is most likely to evolve in high-density environments where competition for empty space is strong, the range of δ/γ was chosen such that the density of cells at carrying capacity is at least 50%.

For the three cost parameters, a lower bound of 0.01 was chosen to avoid the occurrence of "free" phenotypes that are not selected for. Metabolic costs for toxin production and resistance have been shown to exist for various toxins, although the extent of these costs may differ between toxins and bacterial species (Chao and Levin, 1981; Dykes and Hastings, 1997; Kerr *et al.*, 2002; Riley and Wertz,

Table 4.1. Model parameters

Varied in parameter sweep		
Parameter	*Description*	*Range*
$L_{\text{cue}} = 2\sqrt{\frac{D_{\text{cue}}}{d_{\text{cue}}}}$	Characteristic length scale of the cell-density cue concentration profile (lattice sites)	$[2, 20]$
$L_{\text{tox}} = 2\sqrt{\frac{D_{\text{tox}}}{d_{\text{tox}}}}$	Characteristic length scale of the toxin concentration profile (lattice sites)	$[2, 38]$
$R_0^{-1} = \frac{\delta}{\gamma}$	$\frac{1}{R_0}$ of the bacteria, where R_0 is the maximal expected number of offspring per bacterial life time (dimensionless)	$[0, 0.5]$
$\hat{b}_{\text{T}} = \frac{\gamma d_{\text{tox}}}{\delta_{\text{tox}}} b_{\text{T}}$	Scaled slope of toxin production cost function (dimensionless)	$[0.01, 0.8]$
C_{R}	Cost of resistance (dimensionless)	$[0.01, 0.25]$
C_{C}	Cost of responding to the density cue (dimensionless)	$[0.01, 0.1]$
Fixed		
Parameter	*Description*	*Value*
C_{T_0}	Offset of toxin production cost function	0.01
τ_{delay}	Delay between expression of resistance and toxin production in (Reg, Reg)-cells	50 time steps
μ_{gain}	Probability of a gain mutation upon reproduction	$5 \cdot 10^{-5}$
μ_{loss}	Probability of a loss mutation upon reproduction	$5 \cdot 10^{-4}$
μ	Probability that a mutation occurs in response threshold θ or toxin production rate π_{T} upon reproduction	$5 \cdot 10^{-4}$
p_{largemut}	Probability that a mutation in θ or π_{T} yields a random value	10^{-3}
σ_μ	Maximum size of a mutation in θ or π_{T} otherwise	0.05

2002b; Weber *et al.*, 2014). To capture these different scenarios, we vary the toxin production cost and resistance cost parameters between the lower bound of 0.01 and relatively high values. For the resistance cost, we go up to a cost of 25% of the reproduction rate, while for the toxin production we set an upper bound on $\hat{b}_{\text{T}}$ such that the reproduction rate of producing cells would be 0 if its production rate $\pi_{\text{T}} = 1$. Since we expect regulation to evolve only if the costs of regulation are

lower than the costs of the regulated behaviours (toxin production and resistance), we consider a narrower range for the cue response cost C_C (Table 4.1).

4.5.2.2. Simulations and analysis

To sample the parameter space, 2000 simulations were performed for random combinations of the six lumped parameters. Parameter values were independently sampled from uniform distributions with a wide, parameter-specific range (Table 4.1). Simulations were initialised with a randomly selected 10% of lattice sites occupied by cells with random genotypes (response threshold values and the toxin production rate values were randomly chosen between 0 and 1), and were run for 400,000 time steps (generally sufficient to reach evolutionary steady state). The mean fraction of cells with each possible geno-/phenotype combination was calculated over the last 50,000 simulation time steps. Based on these genotype and phenotype abundances the simulations were classified using a decision tree with several steps (Supporting Figure S4.1). In the first step, simulations were assessed on the abundance of phenotypes (S: sensitives, R: resistants, or K: killers), and a phenotype was called "fixed" if it was present at $> 98\%$ abundance. Only fixation of sensitives was observed; resistance or toxin production never fixed. If cells of all three possible phenotypes (K, R and S) occurred at appreciable abundance (defined as $> 2\%$ of the population), the simulation was classified as "KRS". Simulations that did not yield fixation of a single phenotype or KRS-dynamics were classified as "other". In the second step, simulations within the KRS-class were called as "potential regulation" if at least one regulating genotype was present at $> 2\%$ abundance. In the final third step, these "potential regulation" cases were only classified as "true regulation" if at least 10% of the cells of the regulating genotype were in the inactive phenotype (regulated gene not expressed), and at least 10% were in the active phenotype. Altogether, this classification assigned all simulations to one of four evolutionary outcomes: (1) Sensitives fix, (2) KRS-dynamics, no regulation evolved, (3) KRS-dynamics, regulation evolved, and (4) other (Supporting Figure S4.1).

4.5.3. Invasion speeds

To understand why the regulating killer cells (genotype (Reg, On)) can outcompete constitutive killer cells (genotype (On, On)) under certain conditions, we compared invasion dynamics of these two killer types. To allow for a fair comparison, we first evolved constitutive killers under conditions that would usually favour regulation by removing the possibility of regulation from the model (Supporting Figure S4.3A, evolved under the same parameter conditions as Figure 4.4). Over three replicate simulations, constitutive killers under these conditions evolved a mean toxin production rate of $\pi_T = 0.13$. Over the ten replicate simulations of evolving (Reg, On)-killers, these cells evolved a mean toxin production rate of $\pi_T = 0.8$ and a

mean response threshold of $\theta = 0.875$ (Supporting Figure S4.2). We therefore constructed two "average evolved killer strains", a constitutive killer with genotype (On, On) and $\pi_T = 0.13$, and a regulating killer with genotype (Reg, On), $\pi_T = 0.8$ and $\theta = 0.875$, and compared the invasion dynamics of these two constructed killer strains.

To characterise the invasion into a sensitive population, a 20-cell-wide strip of one of the two killer strains was placed on a lattice that was otherwise filled with a sensitive population at carrying capacity (Supporting Figure S4.3B). Population dynamics were then simulated and the decline of the number of sensitives over time was followed (Supporting Figure S4.3B). The invasion speed was calculated as

$$v_{\text{inv}_S} = \frac{-\beta_{S \text{ on } t}}{K_S N} \frac{\text{lattice sites}}{\text{time}}, \tag{4.10}$$

where $\beta_{S \text{ on } t}$ is the linear regression coefficient of the number of sensitive cells on time, N is the number of rows of the simulation lattice and $K_S = (1 - \delta/\gamma)$ is the density of sensitive cells at carrying capacity. Similarly, the invasion speed of resistant cells (genotype (Off, On)) into a population of (Reg, On)-cells and (On, On)-cells was measured by placing a 20-cell-wide strip of resistant cells on a lattice otherwise filled with (Reg, On)-cells or (On, On)-cells at carrying capacity and calculating

$$v_{\text{inv}_R} = \frac{\beta_{R \text{ on } t}}{K_R N} \frac{\text{lattice sites}}{\text{time}}, \tag{4.11}$$

where $\beta_{R \text{ on } t}$ is the linear regression coefficient of the number of resistant cells on time and $K_R = (1 - \delta/(\gamma(1 - c_R))$ is the density of sensitive cells at carrying capacity. (The invasion speeds we measure here serve as a tool to quantify the difference between the two killer strains and thus better understand the evolutionary outcome of the simulations. For a more formal analysis of the effect of toxin production and quorum sensing on invasion speeds, see Bewick *et al.* (2017).)

Note that to calculate v_{inv_S} the decline of the number of sensitives is used, while in the calculation of v_{inv_R} the increase in the number of resistant cells is considered. This choice was made because the characteristics of the sensitive strain and the resistant strain are the same in both invasion experiments, while the two killer strains differ. For each invasion experiment, 10 replicate runs were performed.

4.5.4. Serial transfers

Under the serial transfer regime, simulations were again initialised with cells with random genotypes placed at a random 10% of lattice sites. Population dynamics were simulated as before, except that the simulations were periodically paused and a transfer was performed. At each transfer, a random sample of the population at

the end of the growth cycle was taken as founder cells for the new population. These founder cells were then randomly placed on an otherwise empty simulation lattice, and the simulation of the population dynamics was resumed until the next transfer. Unless otherwise noted, transfers were performed every 500 simulation time steps, and each new cycle was seeded with $1,000$ founder cells. Simulations were continued for 800 (parameter sweep) or $1,200$ (example runs) transfer cycles. Evolutionary steady state was generally reached well before the end of the simulation.

4.6. Supporting Videos

S4.1 Video. KRS-dynamics with a regulating killer type.
Dynamics of an example simulation that yielded KRS-dynamics with regulating killers. Parameter settings as in Figure 4.4. The concentration of the density cue (left panel), the spatial distribution of cells (central panel), and the concentration of the toxin (right) are shown. Cells are colour-coded for their genotype and phenotype, see Figure 4.5 for legend. A dynamic steady state is reached in which three genotypes coexist: sensitives (genotype (Off, Off), blue), resistants (genotype (Off, On), white) and cells that regulate their toxin production (genotype (Reg, On), dark orange when toxin production phenotype $\phi_T = 1$, light orange when $\phi_T = 0$). These genotypes follow KRS-dynamics, with the (Reg, On)-cells in the role of killers. Within patches of the (Reg, On) genotype, cells frequently switch between a resistant and toxin producing phenotype.
https://doi.org/10.1371/journal.pcbi.1007333.s003

S4.2 Video. Model dynamics under a serial-transfer regime.
Parameter settings as in Figure 4.5, panels and legend as in Supporting Movie S4.1. Because dynamics under transfers are much faster than in the fixed environment, this video runs 20 times slower than Supporting Movie S4.1. After a transfer, colonies rapidly grow into the empty space. Cells of the three most abundant genotypes, (Off, Off), (Off, Reg) and (Reg, Reg), all initially have a sensitive phenotype. In the interior of growing colonies and wherever colonies meet, the concentration of the density cue increases and regulating cells switch to a resistant and/or toxin producing phenotype.
https://doi.org/10.1371/journal.pcbi.1007333.s004

S4.3 Video. Growth dynamics of and interactions between colonies of the (Off, Off)-, (Off, Reg)- and (Reg, Reg)-cells that evolved under serial transfers.
To better illustrate the colony dynamics under serial transfers, we seeded three colonies at equal distances, each with one of the three genotypes that are found in the evolved population (see Figure 4.5 and Supporting Figure S4.7): (i) the sensitive genotype ((Off, Off)-cells), (ii) the regulating resistant genotype ((Off, Reg)-cells, $\theta = 0.67$), and (iii) the regulating killer genotype ((Reg, Reg)-cells, $\pi_T = 1$, $\theta = 0.67$). Bacteria are coloured based on their genotype and phenotype as in Figure 4.5. Cells in all colonies initially express a sensitive phenotype. As the colonies expand, the concentration of the density cue inside the colonies increases. After some time, regulating cells in the colonies' interior therefore switch to a resistant phenotype and, in the case of (Reg, Reg)-cells, subsequently to a toxin producing phenotype. Where two expanding colonies collide, the local cell density is also high so that regulating cells express their resistant or toxin producing phenotype. At the interfaces between the colonies, KRS-dynamics emerge: the regulating killer colony slowly invades the sensitive colony, the sensitive colony slowly invades the regulating resistant colony, and the regulating resistant colony slowly invades the regulating killer colony.
https://doi.org/10.1371/journal.pcbi.1007333.s005

4.7. Supporting Figures

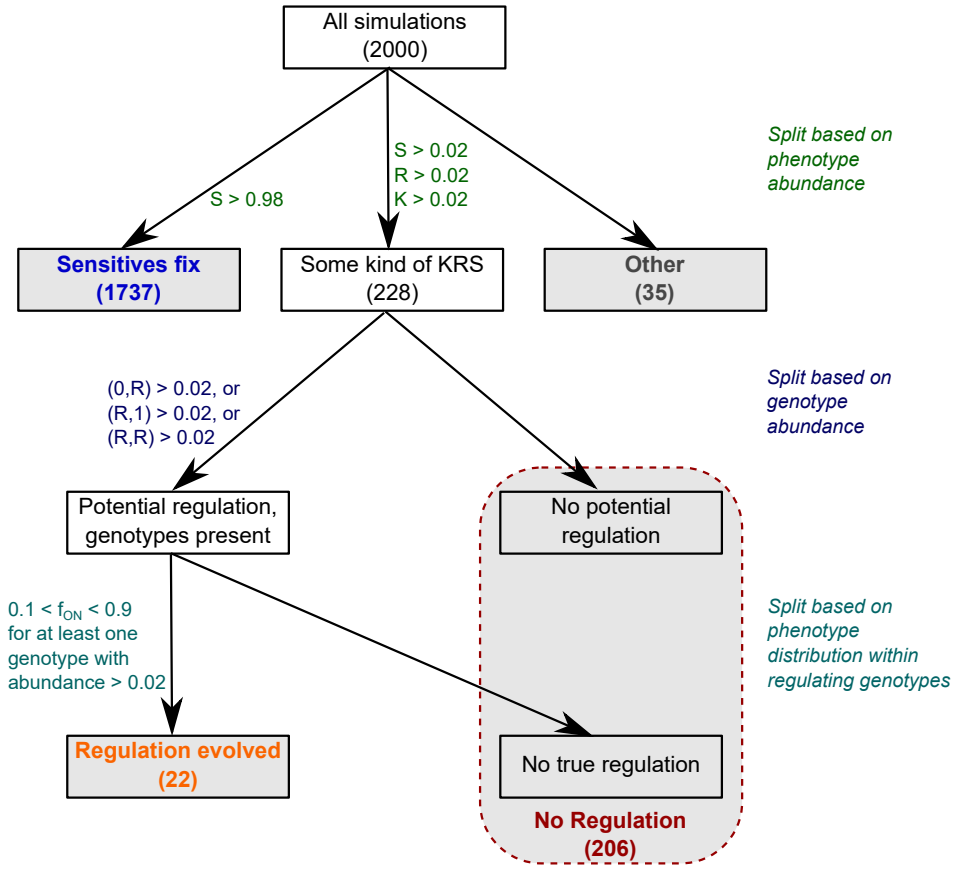

Supporting Figure S4.1. The evolutionary outcome of runs in the parameter sweep was classified based on genotype and phenotype abundance. For 2000 different parameter combinations a simulation was run for 400 000 time steps, and for each simulation the mean abundance of genotypes and phenotypes in the last 50 000 time steps was calculated. Based on these abundance distributions, simulations were classified as showing one of four possible evolutionary outcomes: (i) the sensitive genotype (Off, Off) fixed, (ii) KRS-dynamics arose, no regulation evolved, (iii) KRS-dynamics arose, regulation evolved, and (iv) "other". This classification was performed in several steps: (1) considering the abundance of different phenotypes in the population (sensitive / resistant / toxin producing), (2) asking if any regulating genotype was present at appreciable abundance ($\geq$ 2% of the population), and (3) asking if such a regulating genotype expressed both of its potential phenotypes (both phenotypes expressed by at least 10% of the regulating cells). This final step ensures that cells identified as regulators indeed switch between phenotypes.

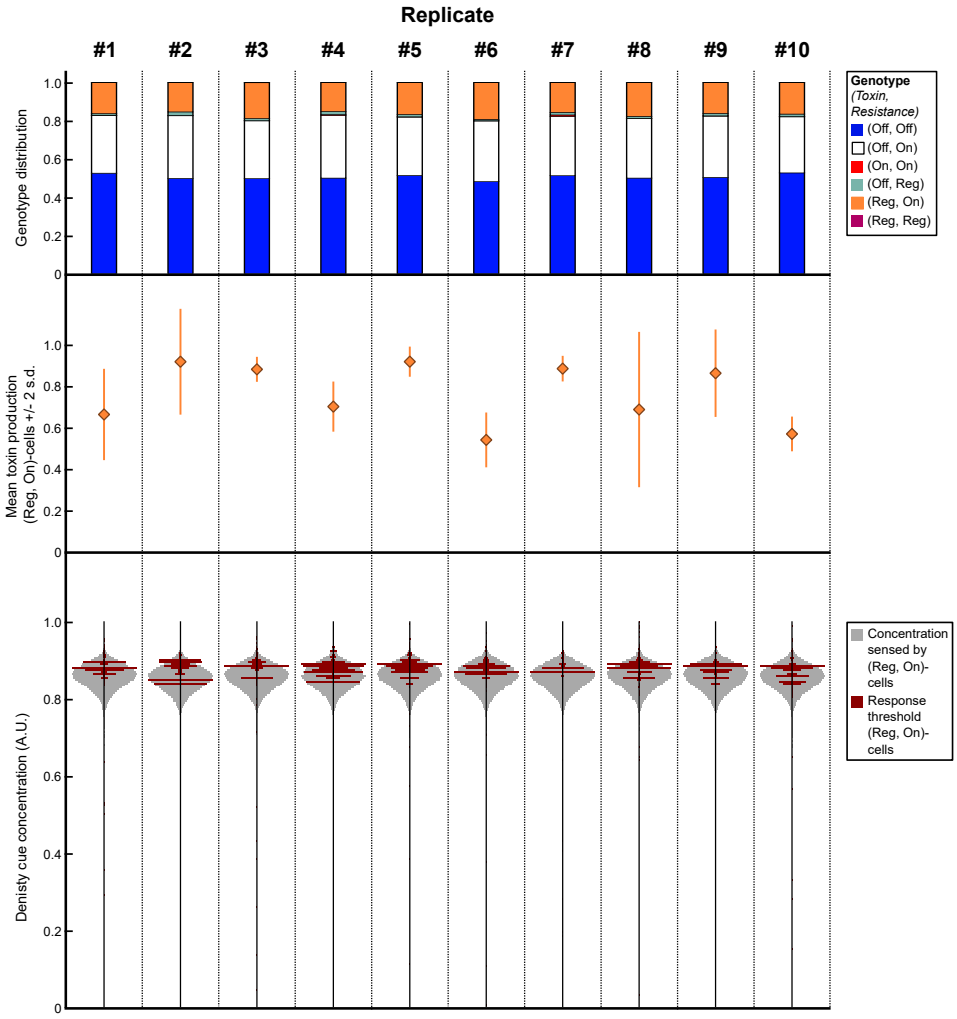

Supporting Figure S4.2. Evolution of regulation in a fixed habitat is highly reproducible. Results of ten independent replicates of the simulation shown in Figure 4.4. Simulations were run for 400 000 time steps, and the genotype distribution was calculated from the mean abundance of genotypes in the last 50 000 simulation time steps. In all runs, a KRS-system evolved with regulating (Reg, On)-killer cells, and the genotype distribution at steady state is very consistent over replicates. The evolved toxin production rate did vary somewhat over replicates, but $0.5 < \pi_T < 1.0$ in all simulations (middle panel). The distribution of response threshold values θ in the (Reg, On)-cells at the end of the simulation is highly consistent over replicates (bottom panel).

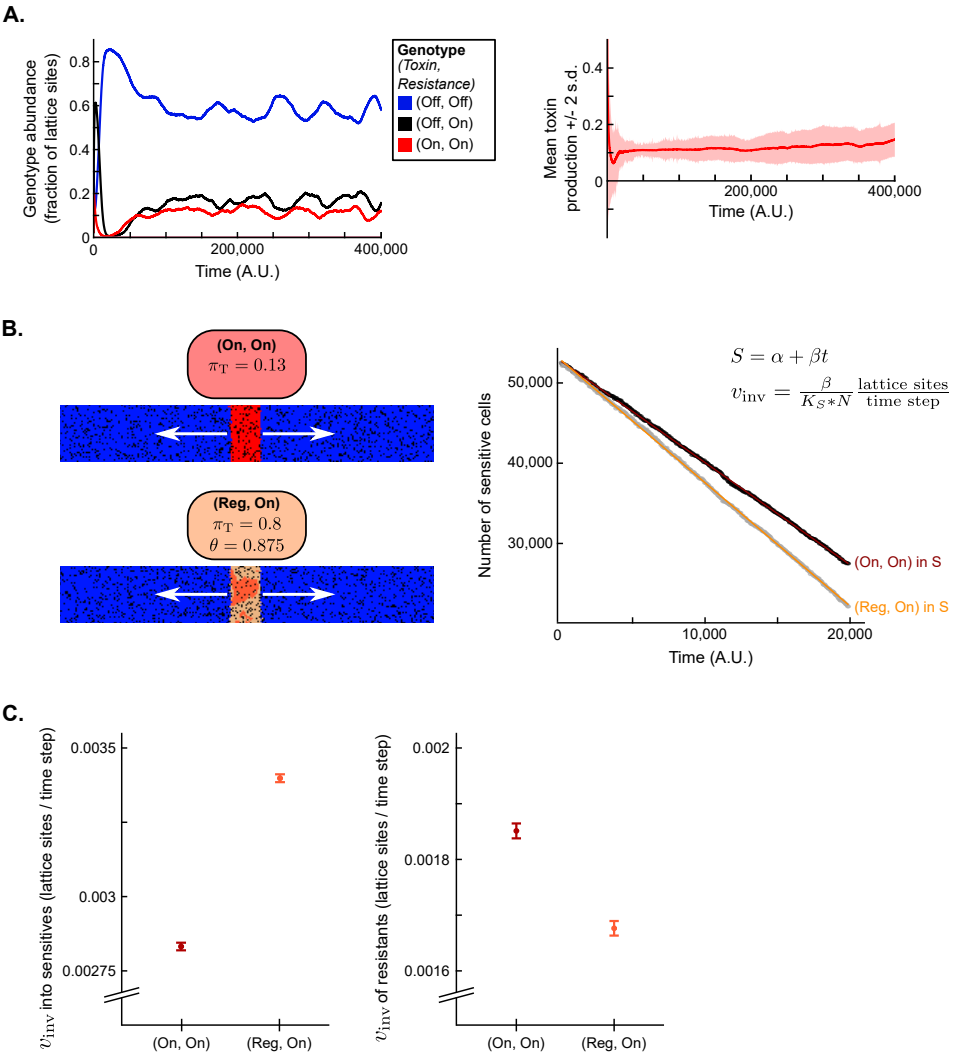

Supporting Figure S4.3. Regulation provides the evolved (Reg, On)-cells with an advantage over constitutive killers both when invading sensitives and in the competition with resistant cells. (A) To allow for a fair comparison with the evolved (Reg, On)-cells, constitutive killer cells (genotype (On, On)) were evolved under the same parameter conditions as Figure 4.4. The example shown here is representative of three replicate runs. (B) Invasion experiments were initialised by placing a 20-cell wide strip of the invading strain in a simulation lattice otherwise filled with the to-be-invaded strain at carrying capacity. The illustration shows the invasion of the (On, On)-strain and the (Reg, On)-strain in a sensitive population; similar experiments were performed for the invasion of a resistant strain in an (On, On)- or (Reg, On)-population. Invasion speed v_{inv} was measured as the decline in the number of sensitives over time, or as the increase of the number of resistant cells over time. (C) Invasion speed of the (Reg, On)-strain into sensitives is higher than the invasion speed of the (On, On)-strain, while invasion speed of the resistant strain is lower in a (Reg, On)-population than in an (On, On)-population. Mean invasion speed ±2 SEM is shown for 10 replicate invasion experiments per combination of invading and invaded strain.

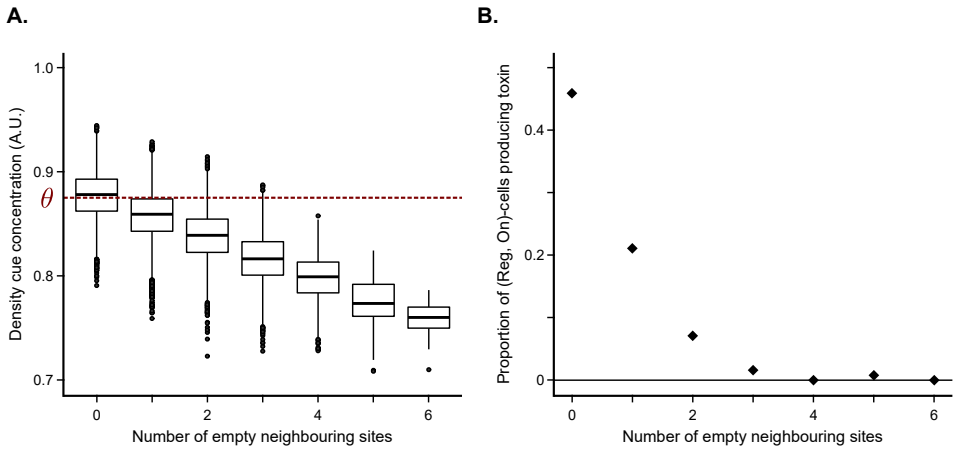

Supporting Figure S4.4. Regulation allows the evolved (Reg, On)-cells to produce toxin only when few of their neighbouring sites are empty. The number of empty neighbouring lattice sites was counted for evolved (Reg, On)-cells at steady state (end of simulation in Figure 4.4). (A) The concentration of the density cue is highest when cells have no empty neighbours, and decreases with the number of empty neighbours. The mean evolved response threshold value ($\theta = 0.875$) is indicated by a dotted line. Of the cells with no empty neighbours, over half sensed a cue concentration $> \theta$, whereas of the cells with 4 or more empty neighbours, none did. (B) The proportion of cells currently producing toxin as a function of their number of empty neighbours. Around 50% of cells without any empty neighbours produce toxin, while (almost) no cells produce toxin when 3 or more of their neighbouring sites are empty.

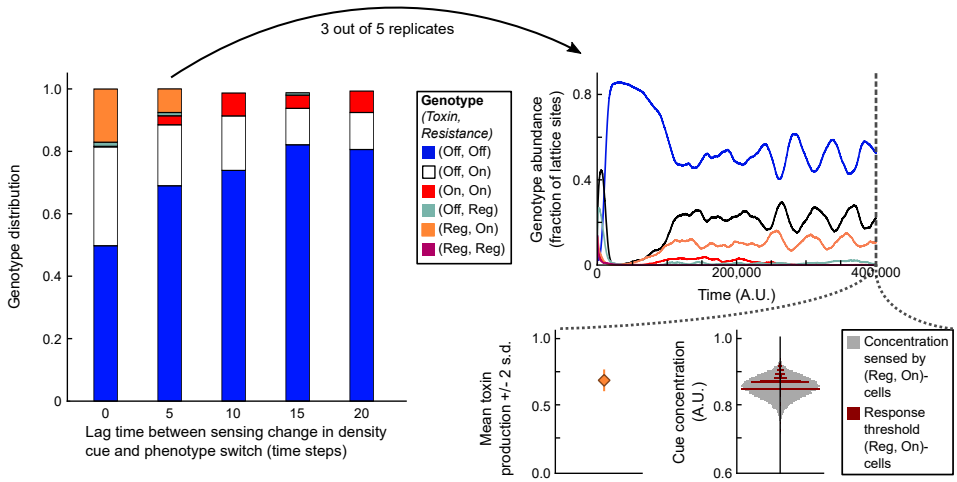

Supporting Figure S4.5. Regulation evolves only if phenotypic adaptation is sufficiently fast. The simulations were repeated for cells that cannot instantaneously adjust their phenotype to the sensed cue concentration, but rather have a lag time between sensing a change in cue concentration and expressing the corresponding phenotype. For each value of this lag time, 5 replicate runs were performed and the genotype distribution was calculated from the mean abundance of genotypes in the last 50 000 simulation time steps (evolutionary steady state). For a relatively short lag (5 time steps, which is equivalent to 50% of the minimal bacterial doubling time), regulation still evolved in 3 out of 5 replicates. For longer lag times ($\geq$ 10 time steps), no regulation was found.

A.

Constant environment		Serial transfers				
		Sensitives fix	KRS, no regulation	KRS, regulation	Other	*Total*
	Sensitives fix	1725	0	3	9	*1737*
	KRS, no regulation	134	12	56	4	*206*
	KRS, regulation	18	0	4	0	*22*
	Other	17	6	5	7	*35*
	Total	*1894*	*18*	*68*	*20*	*2000*

B.

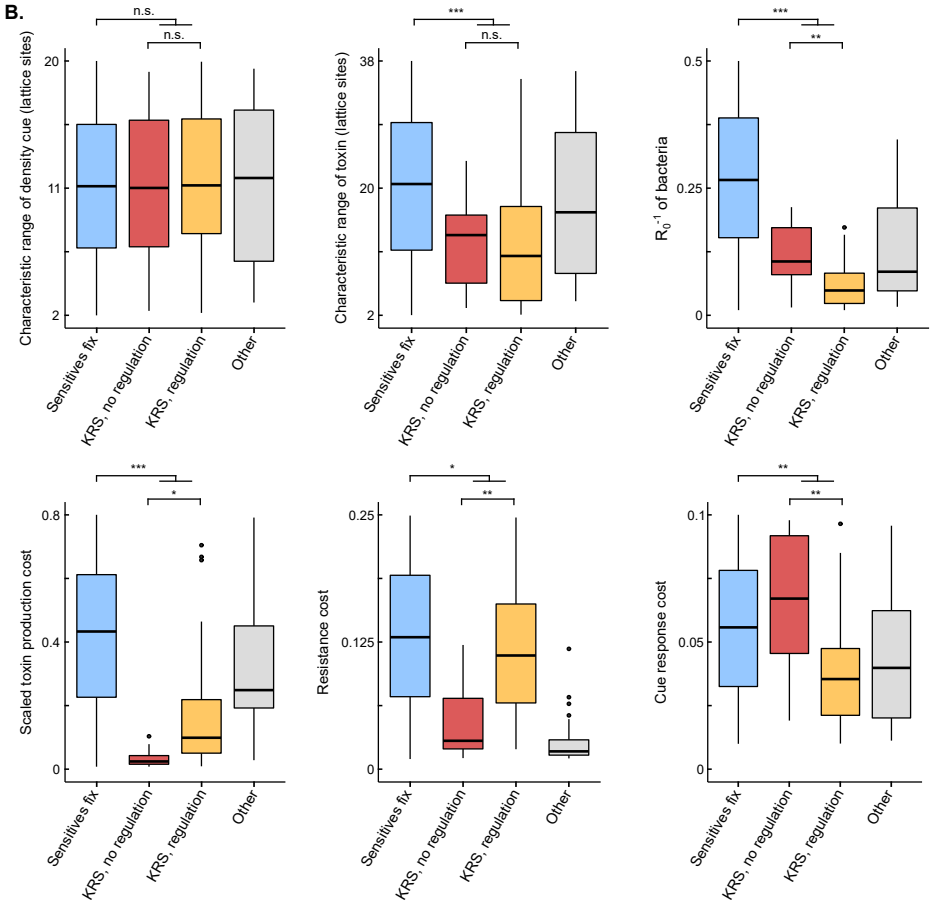

Supporting Figure S4.6. Parameter sweep results under a serial-transfer regime. Simulations were run for the same **2000** parameter settings as used for Supporting Figure S4.1 and Figure 4.3, with the exception that serial transfers were performed once every **500** time steps, reseeding the new population with **1000** founder cells. (A) Table of simulation outcomes, classified as indicated in Supporting Figure S4.1. Parameter conditions in simulations with different outcomes. Significance is shown for 2-sided t-tests with Bonferroni correction for multiple testing: ***: $p < 10^{-10}$, **: $p < 10^{-3}$, *: $p < 0.05$, n.s.: not significant.

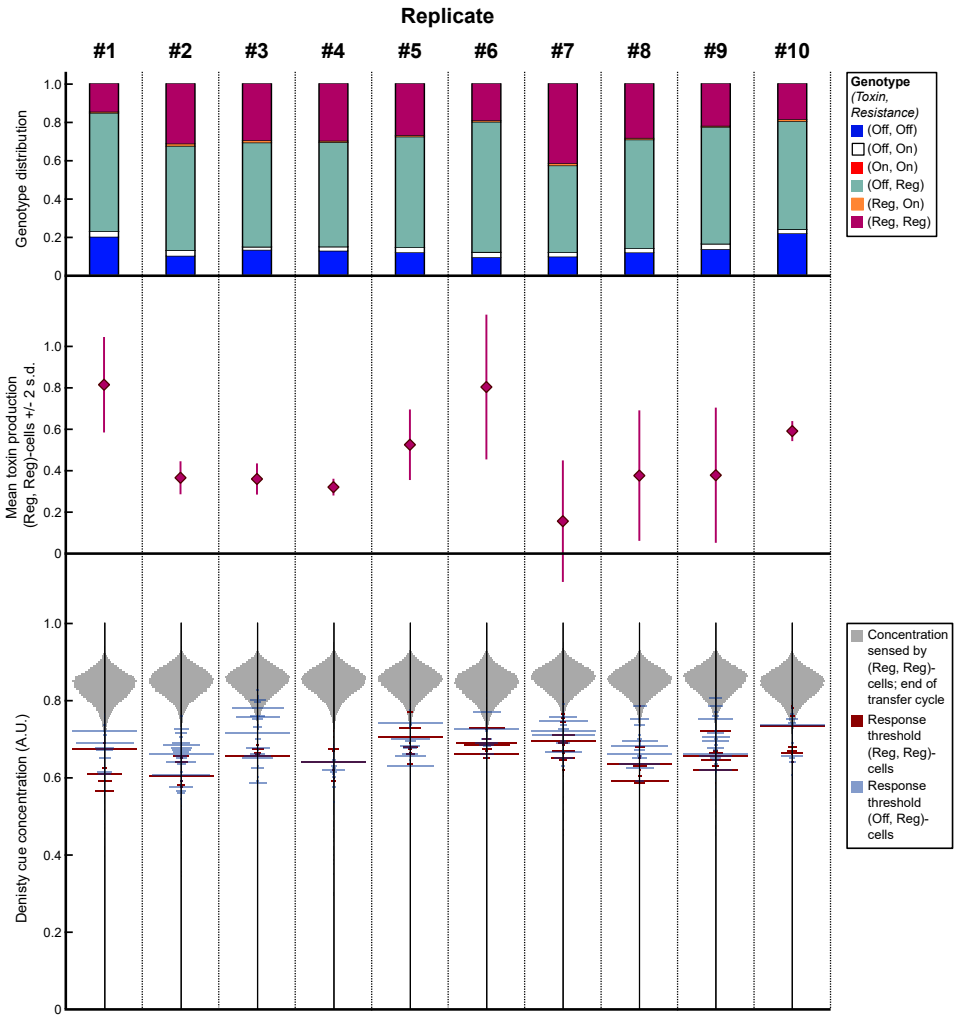

Supporting Figure S4.7. Evolution of regulation under a serial-transfer regime is highly reproducible. Independent replicate runs of the simulation shown in Figure 4.5. The top panel shows the genotype abundance profile, which was calculated as the mean proportion of genotypes in the population over the last 50 000 time steps of the simulation. The middle and bottom panel show the mean evolved toxin production rate of (Reg, Reg)-cells and the distribution of evolved response threshold values in (Reg, Reg)- and (Off, Reg)-cells at the end of the simulation (Time = 600 000). Some quantitative variation exists between replicates, especially in the evolved toxin production rate. However, in all replicates (Off, Off)-, (Off, Reg)- and (Reg, Reg)-cells are selected with similar response threshold values.

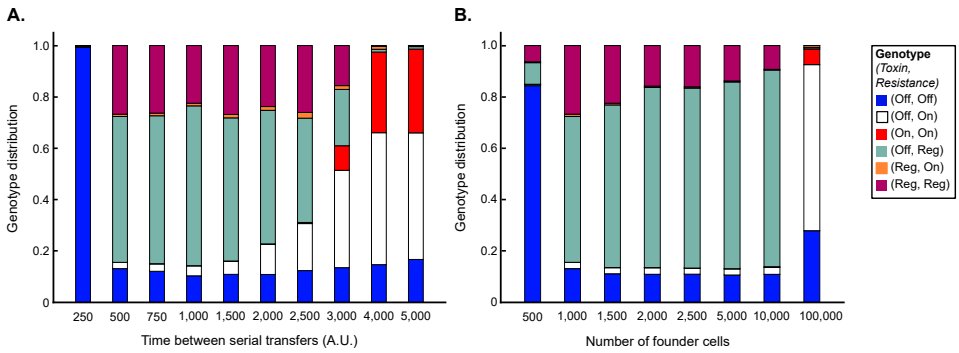

Supporting Figure S4.8. Evolution of regulation under serial transfers is robust to variations in the time between transfers and the number of founder cells. Simulations were performed with parameter conditions as in Figure 4.5, with the exception of the time between transfers or number of founder cells, which were varied. For each parameter setting, five independent replicate runs were performed. The mean proportion of genotypes over the last 50 000 time steps was calculated in the pooled population of all cells in these five replicates. (A) Results of varying the time between transfers. When transfers are very frequent sensitive cells dominate the population, while if transfers are very infrequent non-regulating killer, resistant and sensitive cells are found. However, under a wide range of intermediate transfer intervals regulation readily evolves. (B) Results of varying the number of founder cells. When the population is seeded with very few cells after a transfer, only sensitive cells are selected, while when the number of founder cells is very large a non-regulating KRS-system arises. Again, regulation does evolve for a wide range of intermediate numbers of founder cells.

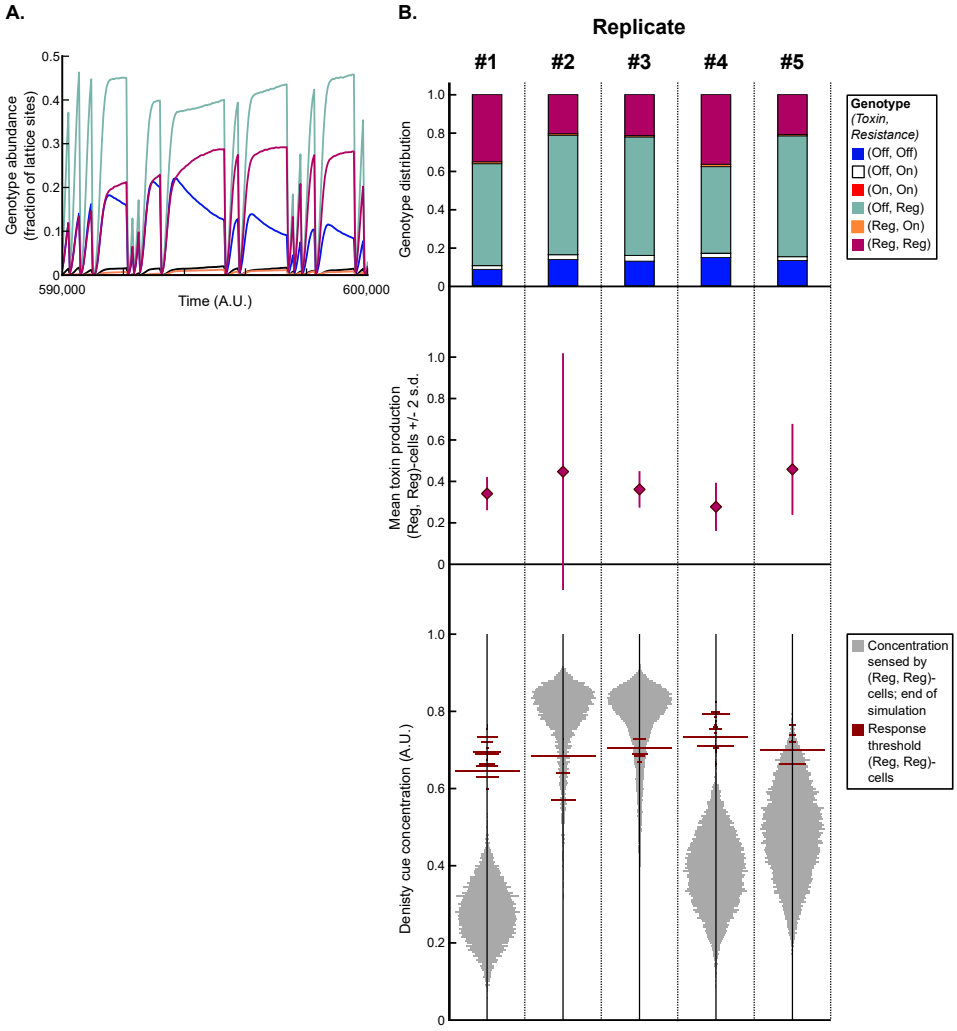

Supporting Figure S4.9. Regulation also evolves if transfers happen stochastically. Instead of a fixed time interval between transfers, the length of each transfer cycle was drawn independently from an geometric distribution with mean $\tau_{\text{transfer}} = 500$. This way, the mean length of a cycle was kept constant, but transfers now happened at a fixed probability per time step. Other settings were the same as in Figure 4.5. (A) Population dynamics over a relatively short time interval, illustrating the irregular transfers. (B) Simulation results for five independent replicate simulations. In all five replicates regulation evolved. The results are very similar to the case with regular transfer (Figure 4.5 and Supporting Figure S4.7).

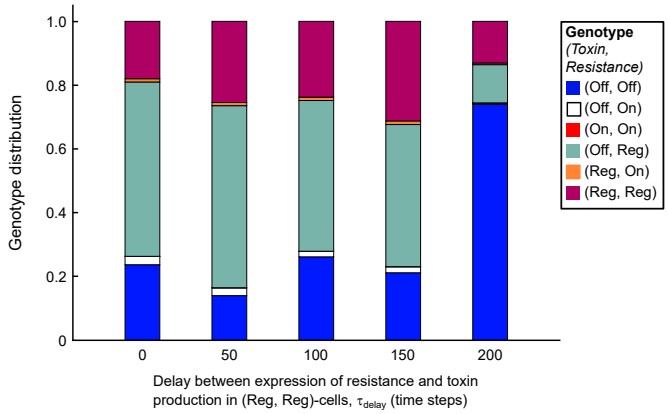

Supporting Figure S4.10. Regulation under serial transfers also evolves when there is no delay between expression of resistance and toxin production. Evolved genotype distribution for varying values of the delay between expression of resistance and toxin production in (Reg, Reg)-cells, τ_{delay} (mean outcome of 5 replicate runs per τ_{delay} value). Regulation of toxin production and resistance (genotype (Reg, Reg)) still evolves when there is no such delay ($\tau_{\text{delay}} = 0$ time steps), and when the delay is up to three times higher than the default value ($\tau_{\text{delay}} = 150$ time steps).

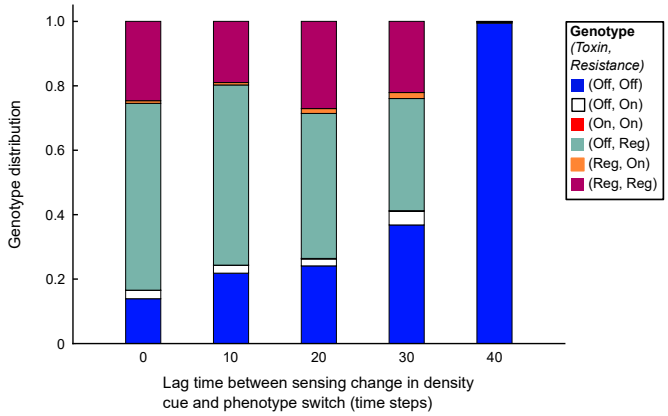

Supporting Figure S4.11. Regulation still evolves under serial transfers when there is substantial lag between the change in cue concentration and the corresponding change in phenotype in regulating cells. A lag time between cue sensing and phenotype adjustment was implemented as in Supporting Figure S4.5, and simulations were run for varying values of this lag (5 replicate simulations per lag time value). Under serial transfers, the evolution of regulation is robust to relatively long lag times: regulation still evolved for lag times up to 30 time steps, or 3 bacterial doubling times.

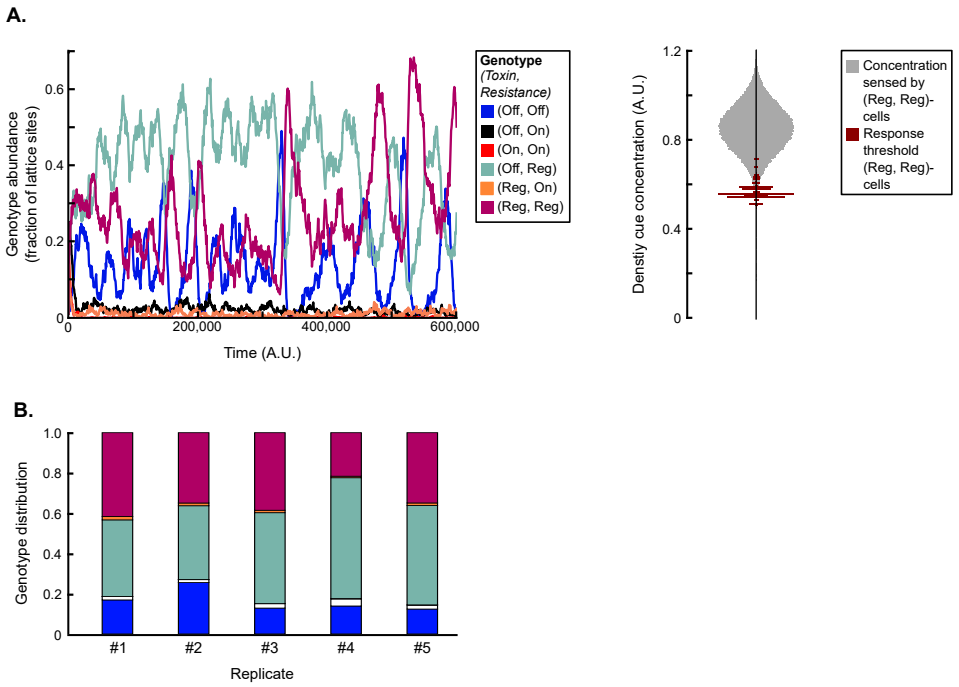

Supporting Figure S4.12. Under serial transfers, regulation is highly robust to noise in the cue concentration. Simulations were run with the same settings as Figure 4.5, but at each time point at each lattice site a Gaussian noise term (mean $\mu_{\text{noise}} = 0$, standard deviation $\sigma_{\text{noise}} = 0.1$) was added to the local concentration of the density cue. (A) Simulation results of a single, representative run. (B) Summarised results of five replicate runs. Regulation evolved in all five replicate runs. The noise term substantially increased the variation in cue concentrations sensed by cells (grey distribution in right panel of A; note the larger range on the y-axis (*c.f.*, Figure 4.6)). The evolved response threshold values are however very similar to the values found in the absence of noise (red distribution in right panel of A, compare to Figure 4.6).

4.8. Supporting Texts

4.8.1. Parameter reduction

To efficiently sample the parameter space in a parameter sweep, the number of parameters was reduced by convenient scaling of the variables. We here consider the cue and toxin concentration profiles and the population dynamics of the bacteria, but do not include mutations and the delay between expression of toxin and resistance, τ_{delay} (See Model and Methods sections).

In the simulations, time progresses in discrete steps, and probabilities for reproduction and death of bacteria are calculated for each time step (Methods, Eq 4.6–4.9). Because we ensure that these probabilities are always small, the simulated discrete-time process approximates a continuous-time Poisson process with (time-dependent) reproduction and death *rates*. This association with a continuous-time process is necessary to allow the time variable to be scaled continuously.

In particular, let Δt be the simulation time step. Then the death rate d_k of cell k is given by

$$d_k \approx \frac{\mathbb{P}(\text{death of cell } k \text{ in simulation time step})}{\Delta t} = \frac{\delta + (1-\phi_{\mathrm{R}_k})\delta_{\text{tox}} c_{\text{tox}}(\mathbf{x}_k)}{\Delta t}. \tag{S4.1}$$

For the reproduction dynamics (Methods, Eq 4.7–4.9), the scaling factor γ is always chosen $\ll 1$, which ensures that the probability of reproduction per time step is small. Then, the probability of reproduction into an empty lattice site is approximately linear in the sum of the reproductive fitnesses R_i of the neighbouring bacteria:

$$\mathbb{P}(\text{reproduction}|\mathbf{x}) \approx \frac{\gamma}{8} \sum_{i \in \text{neighbours}} R_i,$$

and the probability that a specific neighbouring bacterium k reproduces into the empty site is $\frac{1}{8}\gamma R_k$. Since a bacterium can reproduce into any empty neighbouring site, the expected number of offspring of a given cell k in a time step is $f_{\text{empty}}\gamma R_k$, where f_{empty} is the fraction of its eight neighbouring lattice sites that is empty. Conventionally defining a cell's reproduction rate r_k as the rate at which a cell reproduces when surrounded by empty space, we then find

$$r_k \approx \frac{\gamma R_k}{\Delta t} = \frac{\max\left[0, \gamma\left(1 - \phi_{\mathrm{T}_k}(C_{\mathrm{T}_0} + b_{\mathrm{T}}\pi_{\mathrm{T}_k}) - \phi_{\mathrm{R}_k} C_{\mathrm{R}} - \phi_{\mathrm{C}_k} C_{\mathrm{C}}\right)\right]}{\Delta t}. \tag{S4.2}$$

The concentration profiles of the density cue and toxin are found from

$$P_{i,j} - d_{\text{cue}} c_{\text{cue}} + D_{\text{cue}} \nabla^2 c_{\text{cue}} = 0, \tag{S4.3}$$

$$\text{where } P_{i,j} = \begin{cases} p_{\text{cue}} & \text{if there is a cell at position } (i,j), \\ 0 & \text{if not,} \end{cases}$$

and

$$\pi_{T_{i,j}} - d_{\text{tox}} c_{\text{tox}} + D_{\text{tox}} \nabla^2 c_{\text{tox}} = 0, \tag{S4.4}$$

$$\text{where } \pi_{T_{i,j}} = \begin{cases} \pi_T & \text{of the cell at position } (i,j) \text{ if that cell produces toxin,} \\ 0 & \text{otherwise.} \end{cases}$$

Taken together, the simulation dynamics are hence captured by four equations: Eq S4.1 – S4.4.

To reduce the number of parameters in Eq S4.1 – S4.4, we introduce the scaled variables

$$\tau = \frac{\gamma}{\Delta t} t, \quad \hat{c}_{\text{cue}} = \frac{d_{\text{cue}}}{p_{\text{cue}}} c_{\text{cue}}, \quad \hat{c}_{\text{tox}} = \frac{\delta_{\text{tox}}}{\gamma} c_{\text{tox}}, \quad \hat{\pi}_T = \frac{\delta_{\text{tox}}}{\gamma d_{\text{tox}}} \pi_T. \tag{S4.5}$$

In terms of these variables, the equations for the cue and toxin concentration reduce to

$$\hat{P}_{i,j} - \hat{c}_{\text{cue}} + \tfrac{1}{4} L_{\text{cue}}^2 \nabla^2 \hat{c}_{\text{cue}} = 0, \tag{S4.6}$$

$$\text{where } \hat{P}_{i,j} = \begin{cases} 1 & \text{if there is a cell at position } (i,j), \\ 0 & \text{if not,} \end{cases}$$

and

$$\hat{\pi}_{T_{i,j}} - \hat{c}_{\text{tox}} + \tfrac{1}{4} L_{\text{tox}}^2 \nabla^2 \hat{c}_{\text{tox}} = 0, \tag{S4.7}$$

$$\text{where } \hat{\pi}_{T_{i,j}} = \begin{cases} \hat{\pi}_T & \text{of the cell at position}(i,j) \text{ if that cell produces toxin,} \\ 0 & \text{otherwise,} \end{cases}$$

with only one lumped parameter per equation:

$$L_{\text{cue}} = 2\sqrt{\frac{D_{\text{cue}}}{d_{\text{cue}}}}, \qquad L_{\text{tox}} = 2\sqrt{\frac{D_{\text{tox}}}{d_{\text{tox}}}}. \tag{S4.8}$$

The parameters L_{cue} and L_{tox} represent the characteristic length scales of the concentration profiles; they are equal to the mean square displacement of the diffusing cue or toxin molecules before they are degraded.

The death and reproduction rates have the dimension of 1/time. Therefore, after scaling time according to Eq S4.5 the scaled death rate reads

$$\hat{d}_k = \frac{\Delta t}{\gamma} d_k = \frac{\delta}{\gamma} + (1 - \phi_{\mathrm{R}_k})\hat{c}_{\mathrm{tox}}(\mathbf{x}_k), \tag{S4.9}$$

while the reproduction rate reduces to

$$\hat{r}_k = \frac{\Delta t}{\gamma} r_k = \max\left[0, 1 - \phi_{\mathrm{T}_k}(C_{\mathrm{T}_0} + \hat{b}_{\mathrm{T}}\hat{\pi}_{\mathrm{T}_k}) - \phi_{\mathrm{R}_k} C_{\mathrm{R}} - \phi_{\mathrm{C}_k} C_{\mathrm{C}}\right], \tag{S4.10}$$

with lumped parameter

$$\hat{b}_{\mathrm{T}} = \frac{\gamma d_{\mathrm{tox}} b_{\mathrm{T}}}{\delta_{\mathrm{tox}}}.$$

After scaling, seven parameters are left in the description of the system: the characteristic length scales of the concentration profiles L_{cue} and L_{toxt}, the ratio $\frac{\delta}{\gamma}$, which is equal to R_0^{-1} with R_0 the maximum number of expected offspring per bacterial life time, the scaled slope of the toxin production cost function $\hat{b}_{\mathrm{T}}$ and its offset C_{T_0}, the cost of resistance C_{R}, and the cost of responding to the cue C_{C}.

4.8.2. Analytical approximation of the cue concentration in a single growing colony

Here, we present an analytical approximation for the cue concentration profile of a single colony, which we use to derive a theoretical maximum for the cue concentration experienced by cells at the colony edge. Analytical solutions were found using the `DSolve`, `Solve` and `Limit` functions of Wolfram Mathematica 11.0.

Consider a growing, genotypically homogeneous colony of model bacteria. To find the cue concentration profile of this colony, we should solve

$$\frac{\partial c_{\mathrm{cue}}(\mathbf{x}, t)}{\partial t} = P_{\mathrm{cue}}(\mathbf{x}, t) - d_{\mathrm{cue}} c_{\mathrm{cue}}(\mathbf{x}, t) + D_{\mathrm{cue}} \nabla^2 c_{\mathrm{cue}}(\mathbf{x}, t) = 0 \tag{S4.11}$$

for a given production function $P_{\mathrm{cue}}(\mathbf{x}, t)$. We approximate the shape of the growing colony at a given time by a disk of radius ρ, and furthermore assume that the density of bacteria within the disk is equal to the carrying capacity $B^* = 1 - \delta/R$, where R is the reproduction rate of the bacteria and δ their death rate, while there are no bacteria outside of the disk. Let r be the distance from the colony centre. Transforming Eq S4.11 to polar coordinates then yields

$$\frac{\partial c(r, t)}{\partial t} = P(r) - d c(r, t) + D\left(\frac{\partial^2 c(r, t)}{\partial r^2} + \frac{1}{r}\frac{\partial c(r, t)}{\partial r}\right) = 0, \tag{S4.12}$$

dropping the subscripts for convenience. Let p be the cue production rate per bacterium. The production function $P(r)$ is then

$$P(r) = \begin{cases} pB^* & \text{if } 0 \le r \le \rho \\ 0 & \text{if } r > \rho. \end{cases} \tag{S4.13}$$

We proceed by solving Eq S4.12 for two cases: outside the disk of bacteria ($r > \rho$) and inside the disk ($0 \le r \le \rho$). To find the concentration profile outside the disk, we set $P(r) = 0$ and impose the boundary condition $c(\infty) = 0$. The concentration $c(r)$ is then given by

$$c_{\text{out}}(r) = A_1 K_0\Big(\sqrt{\frac{d}{D}}\, r\Big), \tag{S4.14}$$

where $K_n(z)$ is the modified Bessel function of the second kind and A_1 is an arbitrary constant. We ignore any imaginary terms because we are only interested in real solutions. To solve the concentration profile inside the disk, set $P(r) = pB^*$ and remove the boundary condition for $c(\infty)$, because the concentration cannot converge to zero if there is uniform production. Then, the real solution of Eq S4.12 becomes

$$c_{\text{in}}(r) = \frac{pB^*}{d} + A_2 I_0\Big(\sqrt{\frac{d}{D}}\, r\Big), \tag{S4.15}$$

where $I_n(z)$ is the modified Bessel function of the first kind and A_2 is again an arbitrary constant.

At the perimeter of the colony, $r = \rho$, the solutions for the concentration within and outside the disk should be equal, and since the concentration profile should be smooth, so should their derivatives:

$$c_{\text{out}}(\rho) = c_{\text{in}}(\rho); \qquad \left.\frac{\mathrm{d}c_{\text{out}}}{\mathrm{d}r}\right|_{r=\rho} = \left.\frac{\mathrm{d}c_{\text{in}}}{\mathrm{d}r}\right|_{r=\rho}. \tag{S4.16}$$

From Eq S4.16, the constants A_1 and A_2 can be solved to find the solution for the full concentration profile:

$$c(r) = \begin{cases} \frac{pB^*}{d}\Big(1 - \sqrt{\frac{d}{D}}\,\rho\, I_0\Big(\sqrt{\frac{d}{D}}\, r\Big) K_1\Big(\sqrt{\frac{d}{D}}\,\rho\Big)\Big) & \text{if } 0 \le r \le \rho, \\ \frac{pB^*}{\sqrt{dD}}\Big(\rho\, I_1\Big(\sqrt{\frac{d}{D}}\,\rho\Big) K_0\Big(\sqrt{\frac{d}{D}}\, r\Big)\Big) & \text{if } r > \rho. \end{cases} \tag{S4.17}$$

In Figure 4.6 $c(r)$ is plotted for the default parameters used in the simulations. The analytical solution provides a good approximation of the observed concentration profile, although it does slightly overestimate the cue concentration in the colony interior. This overestimation occurs because the local carrying capacity decreases when the phenotype of cells switches from sensitive to resistant and toxin producing, but this effect is not incorporated in the analytical approximation.

In the model, bacteria have the size of 1 lattice site and the dimension of distance is lattice site width. Hence, the concentration of density cue molecule experienced by bacteria at the colony edge is given by $c(\rho - \frac{1}{2})$. Furthermore, as the colony size (i.e. ρ) increases, the cue concentration at the colony edge will also increase. To find the maximal concentration experienced by cells on a colony edge, we should therefore consider $c(\rho - \frac{1}{2})$ for $\rho \to \infty$. For the default model parameter values (see Table 4.1),

$$\lim_{\rho \to \infty} c(\rho - \tfrac{1}{2}) = 0.484. \tag{S4.18}$$

Hence, the cue concentration sensed by bacteria at the colony edge will be < 0.49.

5

Quantifying natural selection at different scales in spatially structured populations

Hilje M. Doekes, Rutger Hermsen

Manuscript in preparation

Abstract

Spatial population structure is a key determinant of many evolutionary processes. Most formal theory quantifying the effect of such structure on natural selection has focussed on populations divided into distinct, non-overlapping groups. Many biological populations, however, are not structured in this way, but rather show (self-)organisation in spatial patterns. Here, a new mathematical framework is presented that quantifies how spatial scales affect natural selection. Combining the Price equation and kernel estimates, we define the Kernel Selection Differential (KSD): a measure of the selection pressure acting on a trait within a given local environment. We then present a spatial decomposition of the global selection differential into a contribution of local selection acting *within* local environments, and a contribution of interlocal selection acting *among* these environments. Varying the size of these local environments allows one to measure how different length scales contribute to selection. The use of this new framework is illustrated in two spatial simulation models of the evolution of traits known to be affected by population structure, altruism and pathogen transmissibility. In both models, the spatial decomposition of selection identifies the relevant length scales for natural selection.

5.1. Introduction

Spatial structure is the rule, rather than the exception, in biological populations, with examples ranging from the large spatial heterogeneity observed in bacterial biofilms (Stacy *et al.*, 2016; Nadell *et al.*, 2016; Yanni *et al.*, 2019) to patterns in vegetation cover (Thiery *et al.*, 1995; Rietkerk *et al.*, 2004). It may arise from heterogeneities in the abiotic environment, such as resource availability, or from self-organisation as a result of ecological interactions between individuals (Lion and van Baalen, 2008).

Because spatial population structure determines with whom organisms interact and compete, it is a key factor shaping evolution. A classical example of this is the evolution of altruism: behaviour that negatively affects an individual's own fitness, but increases the fitness of its interaction partners (Hamilton, 1964; West *et al.*, 2006). It has long been recognised that some form of interaction structure is necessary for such behaviour to evolve, such that the behaviour of altruistic individuals preferentially benefits other altruists (Hamilton, 1964; Wilson, 1975; Lehmann and Keller, 2006; Fletcher and Doebeli, 2009). A natural way for such structure to arise is spatial assortment through local interactions and local reproduction (Nowak and May, 1992; Killingback *et al.*, 1999; Le Galliard *et al.*, 2003; Nadell *et al.*, 2010, 2016; Colizzi and Hogeweg, 2016).

Most general theoretical work on the effect of population structure on evolution so far has focused on populations that are divided in distinct groups, *e.g.*, trait-groups in which selection is compartmentalised for periods of time (Wilson, 1975). Selection is then considered to act at two levels, within and between groups, and the selection pressures at these two levels can be quantified (Price, 1972; Okasha, 2006). However, many biological populations are not subdivided into distinct groups, but are rather structured in space. In such populations, selection pressures could be said to depend on spatial scale, with local selection favouring a certain behaviour (*e.g.*, lower investment in altruism) that not necessarily coincides with the selection pressures at the level of the whole population (Johnson and Boerlijst, 2002; Lion *et al.*, 2011). A formal treatment of selection pressures in such multiscale evolution, however, is currently lacking.

Here, we present a mathematically rigorous way to quantify natural selection at different length scales. A spatial decomposition of selection is derived which splits up global selection into a local component, which describes the average selection within local environments, and an interlocal component, which describes the selection among these environments. To illustrate this framework, we apply it to two models of the evolution of traits known to be affected by spatial structure: altruism and pathogen transmissibility. We show how the spatial decomposition of selection captures the contribution to selection of processes and patterns at different length

scales. This new framework furthermore allows us to identify which spatial scales are relevant to natural selection, rather than *a priori* defining those scales.

5.2. Results

5.2.1. A spatial decomposition of selection

Consider a spatially structured population of individuals that differ in some phenotypic value, ϕ. This could be a quantitative trait value (*e.g.*, an individual's investment in altruistic behaviour) or an indicator variable that is 1 if the individual displays a certain phenotype (*e.g.*, altruism), and 0 if it does not. Exactly 50 years ago, a highly general mathematical description of the evolutionary change in the mean value of ϕ over a given time interval was published by George R. Price (Price, 1970):

$$\underbrace{\Delta\overline{\phi}}_{\text{change in mean value of } \phi} = \underbrace{\mathrm{Cov}(\phi, w)}_{\text{change due to selection}} + \underbrace{\overline{w\Delta\phi}}_{\text{change due to transmission biases}} \tag{5.1}$$

Here, w is the relative fitness of individuals over the time interval, and $\Delta\phi$ captures biases in the transmission of phenotype values from parents to offspring. Importantly, the first term of the Price's equation shows that the effect of selection on the mean phenotype is captured by the covariance between phenotype and fitness; this term is also called the *selection differential*, S.

The selection differential describes the effect of selection at the level of the whole population. In structured populations, however, this may fail to capture the whole story. As an example, consider the hypothetical population in Figure 5.1a. Here, the covariance between phenotype and fitness is positive at a global scale (black line in Figure 5.1b), but negative if the analysis is restricted to individuals within smaller-scale local environments (red lines in Figure 5.1b); an evolutionary Simpson's paradox (Chuang *et al.*, 2009).

To measure selection at these smaller scales, we define local environments through a kernel function (*c.f.*, Tekwa *et al.* (2015)): a probability density function that for any point in space describes how individuals contribute to the local environment around that point. In this paper, we use disk-shaped kernel functions that include an individual in the local environment only if its distance to the environment's midpoint is smaller than a given radius, r. Other reasonable choices for the kernel function include multivariate normal or exponential distributions, such that individuals close to the midpoint are weighted more than individuals further away. For any point in space, the local selection can now be measured as the covariance between phenotype and fitness with individuals weighted by the kernel function centred on this point; we call this the Kernel Selection Differential (KSD; see Methods). Note

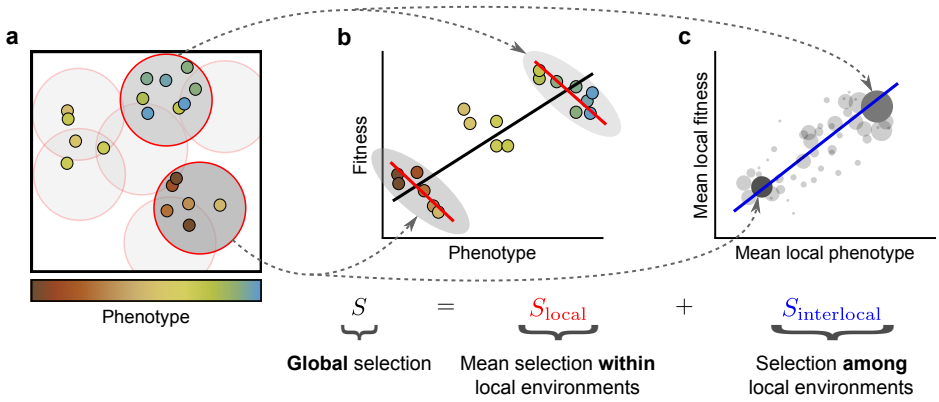

Figure 5.1. Illustration of the spatial decomposition of selection. (a) Spatially structured population of individuals that differ in some phenotypic characteristic. At each point in space, a local environment is defined by a kernel function (see Methods). In this paper, disk-shaped kernel functions are used. (b) Example of global and local selection pointing in different directions. The global covariance between phenotype and fitness is positive (*i.e.*, global selection is positive) while the covariance between phenotype and fitness *within* local environments is negative everywhere (*i.e.*, local selection is negative). This is an example of Simpson's paradox. (c) The negative local selection is counteracted by a positive correlation between the mean phenotype and mean fitness of local environments. Local environments are weighted by their population density and mean fitness (size of points). This correlation measures the selection *among* environments, *i.e.*, the interlocal selection.

that local environments can overlap and that they are not necessarily centred around individuals (Figure 5.1a).

Using this definition of local selection, we can derive a spatial decomposition of the selection differential (see Methods):

$$\begin{aligned} S &= \langle \mathrm{Cov}_{\mathrm{k}}\left(\phi, w \mid \mathbf{m}, r\right)\rangle_{\mathrm{s}} + \mathrm{Cov}_{\mathrm{s}}\left(\{\phi \mid \mathbf{m}, r\}_{\mathrm{k}}, \{w \mid \mathbf{m}, r\}_{\mathrm{k}}\right), \\ &\equiv S_{\mathrm{local}}(r) + S_{\mathrm{interlocal}}(r). \end{aligned} \tag{5.2}$$

Here, $\{\cdot \mid \mathbf{m}, r\}_{\mathrm{k}}$ denotes the "kernel mean" of a characteristic of the individuals present in the local environment defined by midpoint $\mathbf{m}$ and scale r, and $\langle \cdot \rangle_{\mathrm{s}}$ denotes the spatial mean of a quantity defined at each point in space, weighing each point in space by the local population density. The subscripts "k" and "s" in the covariance terms similarly indicate whether the covariance is calculated within a local environment ("kernel covariance") or over space. The first term of the right-hand

side of Eq 5.2 is calculated by sliding the kernel function (in the case of Figure 5.1, a disk) over the space, and averaging the KSD found at each point in space, weighed by the local population density and local mean fitness. It is hence the mean of *local selection*, and represents the selection *within* local environments. The second term of the right-hand side of Eq 5.2, on the other hand, captures the covariance between local mean phenotype and local mean fitness, weighing each local environment by its density (see Figure 5.1c). It can hence be interpreted as the selection *among* environments, which we will call *interlocal selection*.

The measures for local and interlocal selection in Eq 5.2 depend on the size of the local environments that we consider, which is set by the kernel function's scale parameter r (*e.g.*, the radius of the disks in Figure 5.1a). $S_{\text{local}}(r)$ captures the effects of selection mechanisms operating at all length scales below r, while $S_{\text{interlocal}}(r)$ captures the effects of selection mechanisms operating at larger scales, above r. To describe the contribution of a *specific* length scale r to selection, we should ask how the local selection changes if we slightly expand a local environment of that specific scale, *i.e.*, consider the derivative of $S_{\text{local}}(r)$ with respect to r, which we denote by $s(r)$:

$$s(r) \equiv \frac{\mathrm{d}S_{\text{local}}}{\mathrm{d}r} = -\frac{\mathrm{d}S_{\text{interlocal}}}{\mathrm{d}r}. \tag{5.3}$$

Using Eq 5.3, we can rewrite the expression for $S_{\text{local}}(r)$ as

$$S_{\text{local}}(r) = S_{\text{local}}(0) + \int_0^r s(r')\,\mathrm{d}r'. \tag{5.4}$$

From this equation, we see that if the local environments become very large, *i.e.*, $r \to \infty$, then $S_{\text{local}}(r) \to S$ and $S_{\text{interlocal}}(r) \to 0$. This makes sense, large "local" environments should capture the global population dynamics. On the other hand, if two individuals cannot be at the same point in space, for very small scales $r \to 0$, $S_{\text{local}}(r) \to 0$ and $S_{\text{interlocal}} \to S$. This also makes sense, if there is no variation within local environments there cannot be local selection.

To illustrate the use of the spatial selection decomposition (Eq 5.2), we apply it to two models of classical examples of multiscale selection: (i) the evolution of altruism, and (ii) the evolution of pathogen transmissibility.

5.2.2. Example I: Evolution of altruism in self-organising colonies

We model a population of individuals in two dimensional space that reproduce, die, move around slowly and locally compete for resources (Figure 5.2a; Supplementary Text 5.6.1). Individuals are characterised by a continuous trait that represents their investment in altruism. Altruistic behaviour directly reduces an individual's reproduction rate, but benefits all individuals in the local social environment of the

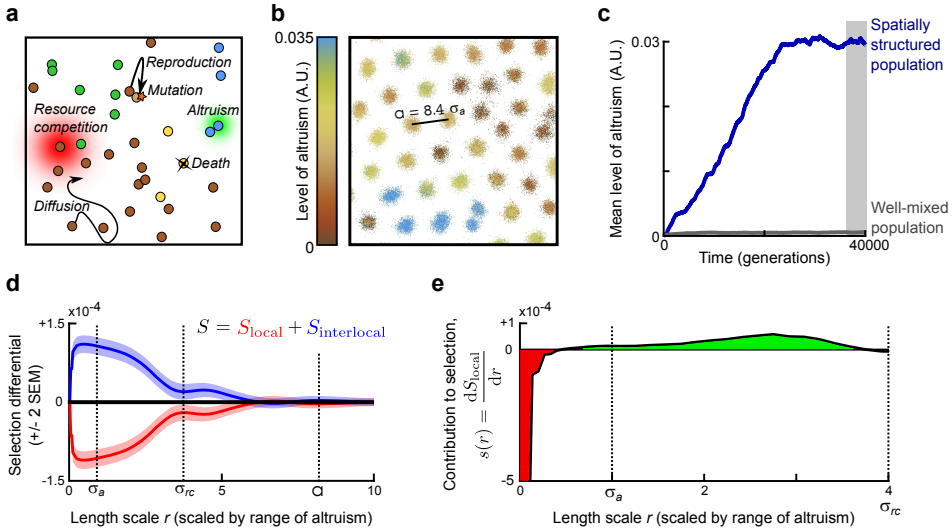

Figure 5.2. Evolution of altruism. (a) Model illustration. (b) Snapshot of part of the simulation plane (see Supplementary Movie S5.1 for dynamics). The hexagonal lattice constant of the emerged colony pattern is $a = 8.4\,\sigma_a$, where σ_a is the range of altruism. (c) Mean level of altruism over time, in a population that is well-mixed (grey) or spatially structured (blue). (d) Spatial decomposition of selection differential S at evolutionary equilibrium for varying length scales of the local environments. Space was scaled such that the range of altruism $\sigma_a = 1$. S_{local} and $S_{interlocal}$ were calculated as averages over 10 000 instances of the simulation plane obtained between Time = 36 000 and 40 000 generations (shaded area in panel c). Dotted vertical lines indicate the range of altruism, σ_a, the range of resource competition, σ_{rc}, and the lattice constant, a. (e) Contribution to selection of different length scales (Eq 5.3). Red areas indicate a negative contribution to selection, green a positive contribution. Dotted vertical lines again indicate the ranges of altruism, σ_a, and resource competition σ_{rc}.

altruistic individual. The effects of altruism and competition are both implemented using normal interaction kernels, such that individuals close to each other benefit more from altruistic action, but also experience stronger competition.

If the scale of altruism, σ_a, is sufficiently smaller than the scale of resource competition, σ_{rc}, the model population shows intriguing self-organisation (Figure 5.2b, Supplementary Movie S5.1): a Turing-like instability results in a hexagonal pattern of distinct colonies that display Darwinian dynamics of their own. In colonies with a high local mean level of altruism, the density of individuals is high because they all benefit from the altruistic behaviour of colony members. Over time, however,

the level of altruism within a colony declines because mutants with lower levels of altruism are selected ("defectors" or "cheaters"). This decline eventually results in the demise of the colony, after which it is replaced by a newly-formed colony that buds from one of the surrounding colonies (see bottom row of Figure 5.2b, Supplementary Movie S5.1). These emergent colony dynamics are studied in depth in a forthcoming paper.

Due to these within- and between-colony dynamics, the mean level of altruism in the population stabilises after a transient (Figure 5.2c). If we perturb the self-organised pattern by mixing the population (*i.e.*, randomly assigning positions to individuals every time step), altruism does not evolve at all (Figure 5.2c). The emergent spatial patterns are hence crucial for the evolution of altruism, a result consistent with previous modelling work (Nowak and May, 1992; Killingback *et al.*, 1999; Le Galliard *et al.*, 2003; Wakano *et al.*, 2009; Uppal and Vural, 2020).

Once the mean level of altruism has stabilised, we would expect the global selection differential to be equal to zero. To average out fluctuations arising from the stochastic dynamics in the finite population, we take the mean of the selection differential over $4\,000$ generations (shaded area in Figure 5.2c), and indeed find that over this period, $S \approx 0$ (black line in Figure 5.2d). However, when we consider the spatial decomposition of selection (Eq 5.2), we see a completely different picture (Figure 5.2d). Even though there is no global directional selection, the mean local selection, as measured by $S_{\text{local}}(r)$, is negative for a significant range of r-values. This negative local selection is however compensated by positive interlocal selection, $S_{\text{interlocal}}(r)$. These results capture and formalise the verbal explanation given above: within local environments individuals with a lower level of altruism are selected because they benefit from the altruistic behaviour of others nearby but pay less costs, but local environments in which the mean level of altruism is low also tend to have a low mean fitness, *i.e.*, selection among local environments favours higher levels of altruism.

Figure 5.2d provides insight in how $S_{\text{local}}(r)$ and $S_{\text{interlocal}}(r)$ depend on the scale of local environment that is considered, r. The effects observed for very small and large r-values represent general properties of the spatial decomposition of selection (see Eq 5.4): for large r, $S_{\text{local}}(r)$ converges to the global selection differential (which is close to zero in Figure 5.2d) and $S_{\text{interlocal}}(r)$ converges to zero, while for small r, $S_{\text{local}}(r)$ declines because the variation in phenotype and fitness within the local environments is reduced. Hence in small environments selection is necessarily weak.

Naively, one might expect that the negative selection on altruism happens within single colonies, balanced by positive selection at large scales. The shortest distance between colonies is given by the hexagonal lattice constant of the emerged colony pattern, $a = 8.4\sigma_{\text{a}}$ (see Figure 5.2b). Indeed, for local environments with radius

$r < \frac{a}{2}$ (such that most disks contain individuals of one colony only), $S_{\text{local}}(r)$ is clearly negative, while $S_{\text{interlocal}}(r)$ is positive (Figure 5.2d). However, when we consider the contribution of varying length scales to selection, we see that only very small length scales of $r < \sigma_a$ contribute negatively to selection, while length scales of $r \gtrapprox \sigma_a$ contribute positively to selection (Figure 5.2e). This indicates that colonies are not homogeneous: already within colonies we observe assortment of individuals with more or less investment in altruistic behaviour, and this assortment contributes positively to the selection on altruism. This is not unreasonable: when individuals are very close together (distance $< \sigma_a$), they experience a similar level of altruism in their neighbourhood. In very small local environments, cheaters hence must have an advantage over altruists. But once local environments become a similar size as the altruism interaction kernel, individuals within the same local environment might experience different levels of altruism, and the local environment hence starts to capture the effect of these smaller-scale heterogeneities.

As a final remark, we note that the length scale for which the differences between S_{local} and $S_{\text{interlocal}}$ vanish does reflect the lattice constant a (Figure 5.2d). This suggests that once most local environments cover more than one colony, the global selection is captured within these local environments.

In conclusion, the spatial decomposition of selection allows us to mathematically show that selection for altruism is negative within local environments, but that this is compensated by positive interlocal selection. It furthermore provides a way to quantify how specific length scales contribute to selection.

5.2.3. Example II: Evolution of pathogen transmissibility in an SI-model

As a second example, we consider the evolution of the transmission rate of an endemic pathogen in a spatially structured population of host individuals. This model is rooted in a long tradition of such epidemiological models (*e.g.*, Rand *et al.* (1995); Haraguchi and Sasaki (2000); Boots and Sasaki (1999); Goodnight *et al.* (2008); Heilmann *et al.* (2010)).

Host individuals in the model live on a 2D square simulation lattice (Figure 5.3). They can be either susceptible to infection, or infected. Susceptible individuals reproduce asexually, in which case the offspring is placed on a neighbouring lattice site. Each lattice point can however hold at most one individual; susceptible individuals therefore locally compete for empty space. Infected individuals do not reproduce, and they die at a rate higher than susceptible individuals. The pathogen is transmitted locally at a rate that depends on the transmissibility of the pathogen. For simplicity each infected individual is considered to carry a single strain of pathogen, with mutations instantaneously changing the transmissibility of all pathogens within

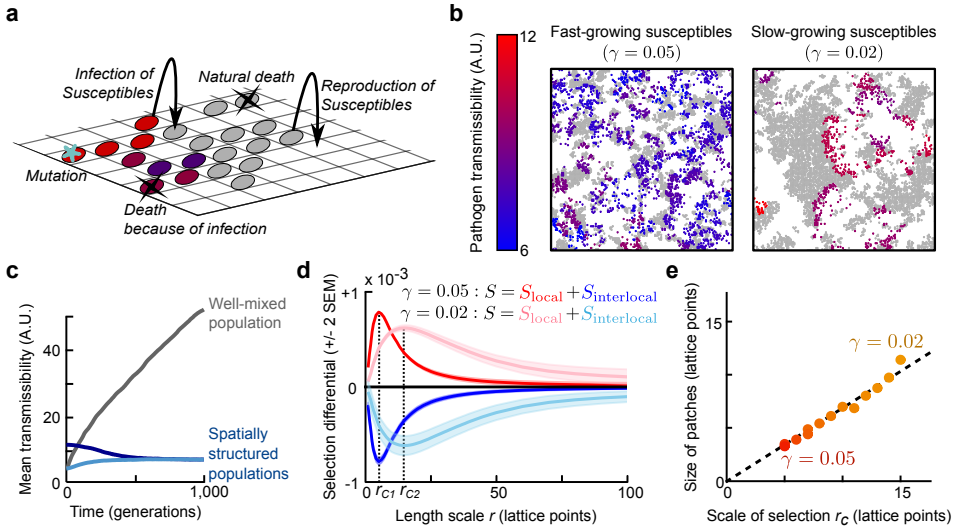

Figure 5.3. Evolution of pathogen transmissibility. (a) Model illustration. (b) Snapshot of part of the simulation lattice for two different values of the reproduction rate of susceptible individuals, γ. Susceptible individuals are plotted in grey, infected individuals are coloured based on the transmissibility of the pathogen they carry. See Supplementary Movies S5.2 and S5.3 for dynamics. (c) Mean transmissibility of the pathogen over time in populations that are well-mixed (grey) or spatially structured, with different initial transmissibility values (blue) (d) Spatial decomposition of selection differential S at evolutionary equilibrium for varying length scales of the local environments. For both values of γ, S_{local} and $S_{\text{interlocal}}$ were calculated as averages over 10 000 instances of the simulation lattice obtained between Time = 9 500 and 10 000 generations. We define the critical scale of selection, r_C, as the length scale at which the contribution to selection switches from positive to negative (*i.e.*, where $s(r) = \frac{dS_{\text{local}}}{dr}$ switches sign). (e) Critical scale of selection, r_C, plotted against size of the emerged patterns for different values of the susceptible reproduction rate γ. Pattern size was determined using the pairwise correlation function (see Supplementary Text 5.6.2).

a single infected individual (*i.e*,, newly arising pathogen variants rapidly sweep the within-host pathogen population). We consider the evolution of pathogen transmissibility.

The population again self-organises into spatial patterns: patches of susceptible individuals are chased through space by the infection (Figure 5.3b, Supplementary Movies S5.2 and S5.3). These patterns strongly influence the evolution of pathogen transmissibility (Figure 5.3c): If pattern formation is prevented by constantly mixing the population, pathogens are selected with ever increasing transmis-

sibility because these pathogens spread faster among the available susceptible hosts. In spatially structured populations, however, the mean transmissibility stabilises after some time (blue lines in Figure 5.3c). This result is explained by the feedback between evolution and the emergent spatial patterns: individuals shape their local environment, and this environment in turn determines the individual's fitness (Savill *et al.*, 1997; Johnson and Boerlijst, 2002; Lion and van Baalen, 2008). In particular, pathogens with very high transmissibility are affected by 'self-shading' (Boots and Sasaki, 1999; Boots and Mealor, 2007): they rapidly deplete the susceptible hosts in their vicinity and are then left with little opportunity to spread, resulting in low pathogen fitness. In contrast, more prudent pathogens shape their environment in such a way that sufficient susceptible hosts remain available to allow continuous spreading of the infection (van Baalen and Sabelis, 1995; Goodnight *et al.*, 2008).

This effect is captured by the spatial decomposition of selection (red and blue line in Figure 5.3d). When the population has reached evolutionary equilibrium, *i.e.*, the gobal mean transmissibility no longer changes and $S \approx 0$, selection within local environments still favours pathogens with high transmissibility ($S_{\text{local}}(r) > 0$ for small r), but this effect is counteracted by negative interlocal selection ($S_{\text{interlocal}}(r) < 0$), which captures the effect that pathogens with high transmissibility more often reside in local environments in which susceptible host availability and hence pathogen spread is limited.

The size of the spatial patterns that emerge in the population depends on several model parameters (Goodnight *et al.*, 2008), including the reproduction rate of the susceptible hosts, with larger patterns emerging for lower reproduction rates (Figure 5.3b). To demonstrate how these larger patterns are reflected in S_{local} and $S_{\text{interlocal}}$, we repeated our analysis with a lower susceptible reproduction rate (right panel in Figure 5.3b, pink and light blue lines in Figure 5.3d). The curves for S_{local} and $S_{\text{interlocal}}$ are stretched towards larger scales, showing that the scales of selection depend on the size of the patterns in the population. This makes sense: selection for pathogen restraint can only be observed if the local environments are large enough to cover multiple patches.

We define the critical scale of selection r_C as the length scale at which the contribution of length scales to selection, $s(r)$, switches sign (Figure 5.3d), such that scales smaller than r_C contribute positively to selection, and scales larger than r_C contribute negatively. By repeating the analysis for a range of susceptible growth rates, we find that this critical scale of selection is proportional to the size of the emergent patterns (Figure 5.3e). Hence, the S_{local}- and $S_{\text{interlocal}}$−curves, and specifically the critical scale of selection r_C, indicate the spatial scale of the population structures that are relevant for natural selection.

In conclusion, this second example illustrated that the spatial decomposition of selection can be used to measure and quantify self-shading. It furthermore allows the identification of the scale(s) of population structures relevant to natural selection.

5.3. Discussion

We have presented a new, multiscale selection framework of evolution in spatially structured populations. This framework consists of a spatial decomposition of selection (Eq 5.2) that quantifies local and interlocal selection for any length scale. Using two example models, we have illustrated how this framework can be used to determine how processes and patterns at varying length scales contribute to selection, and how spatial scales relevant to natural selection can be identified.

The spatial decomposition of selection illustrates how natural selection in local environments might substantially differ from the selection in the global population, even if an average is taken over all local environments. Evolutionary studies based on observations at small local scales can hence provide an incomplete picture of the evolutionary dynamics in the global population, if structures larger than the considered local environments exist that contribute to selection. The framework presented here provides a way to determine whether a local sampling area is representative of the whole population under selection. As the local selection measure $S_{\text{local}}(r)$ converges to the global selection differential S for increasing r, the contribution of specific length scales to selection, $s(r)$, converges to zero. Hence, $s(r)$ indicates if the local environments considered in a study are large enough to capture all evolutionary dynamics. However, a word of caution is in order here: to reliably capture the S_{local}- and $S_{\text{interlocal}}$-curves, and hence measure $s(r)$, observations from many individuals are required (although this depends on the magnitude of the selection differential: if selection is very strong, fewer observations suffice). While such data is easily obtained in simulation studies, it remains to be seen if the multiscale selection framework can also be successfully applied to observational or experimental data.

The examples of multiscale selection studied here, the evolution of altruism and of pathogen transmissibility, were chosen because they are among the best-known examples of a feedback between spatial patterns and eco-evolutionary dynamics (Lion and van Baalen, 2008; Johnson and Boerlijst, 2002), and because this feedback has also been confirmed experimentally. For instance, increased population viscosity facilitates the evolution of altruistic public good production in lab populations of *Pseudomonas aeruginosa* (Diggle *et al.*, 2007; Kümmerli *et al.*, 2009), and several experiments have shown that increased host population viscosity and/or localised pathogen spread select for lower virulence in an insect larval virus (Boots

and Mealor, 2007) and several bacterial viruses (Kerr *et al.*, 2006; Berngruber *et al.*, 2015). The effect of spatial structure on natural selection is however by no means limited to these two examples. The effect of spatial self-organisation on evolutionary dynamics was first described in catalytic hypercycles of self-replicating molecules, which give rise to self-organised rotating spirals that select for higher death rates of the individuals constituting these spirals (Boerlijst and Hogeweg, 1991a,b). The evolution of anticompetitor toxin production in bacteria is also strongly dependant on spatial structure (Chao and Levin, 1981; Durrett and Levin, 1997; Kerr *et al.*, 2002; Bucci *et al.*, 2011; Doekes *et al.*, 2019). Applying the multiscale selection framework to these, and other, examples, might lead to new insights in these systems as well.

The spatial decomposition of selection in Eq 5.2 resembles the decomposition of selection into within- and between-group components for distinct, non-overlapping groups derived by Price (Price, 1972). However, there are several differences. Most importantly, the distinct-groups approach ignores any structure other than the division of individuals into groups, such that all individuals within a group are assumed to experience the same local environmental conditions. In spatially structured populations, this is typically not the case: each individual has a slightly different local environment. Furthermore, the distinct-groups approach requires that distinct and non-overlapping groups are defined. If the spatial structures change over time, such as the patches in the model of pathogen transmissibility, distinct groups cannot be defined and the multiscale approach presented here is more appropriate. If distinct groups can be easily recognised, such as in the altruism model, Price's original approach is feasible (indeed, this approach is used to analyse the altruism model in depth in a forthcoming paper). However, even then the multiscale approach might provide additional insight, showing for instance that even within groups structure exists that is relevant for selection (such as in the altruism model).

While the multiscale decomposition of the selection differential is new and uniquely untangles local and interlocal selection in spatially structured populations, it is not the only, nor the only correct way the selection differential can be decomposed. Next to Price's distinct-groups approach discussed above, the selection differential can also be decomposed in terms that capture the effect of an individual's own character on its fitness, and the effect of its environment (the contextual analysis approach to multilevel selection) (Damuth and Heisler, 1988), or in terms that capture the effect of an individuals behaviour on its own fitness and on the fitness of related interaction partners (the inclusive fitness framework) (Marshall, 2011; Lion *et al.*, 2011; Gardner, 2020). Each decomposition of the selection differential tells a potentially new story about the underlying mechanisms driving evolution. The multiscale selection framework presented here is an addition to the toolbox available to address complex evolutionary questions.

5.4. Methods

Below, we derive Eq 5.2. Full specifications of the simulation models and the computational calculation of the two terms of Eq 5.2 are provided in the Supplementary Text.

Background: Definition of the selection differential S

Consider a population in space that at some time t consists of N individuals that each possess a phenotype ϕ_i. Let W_i be the fitness of individual i, defined as the number of offspring at some later time $t + \Delta t$, including the individual itself if it survived over the time step Δt. The *selection differential* (Eq 5.1, Price (1970))

$$S = \mathrm{Cov}\,(\phi, w)\,, \tag{5.5}$$

where $w_i = W_i/\overline{W}$, is the relative fitness of individual i (we use the common notation $\bar{c}$ to denote the population mean of characteristic c). The analysis presented here focusses on the selection differential only; for a full version of the Price equation with overlapping generations, including transmission and survival bias effects, see *e.g.*, Day and Bonduriansky (2011).

Selection in a local environment: the Kernel Selection Differential (KSD)

Let $K(\mathbf{y}\,|\,r)$ be a normalised centred kernel function with band width r that describes how an individual at position $\mathbf{y}$ contributes to the local environment centred on the origin. For any point in space $\mathbf{m}$, the local density is found as the kernel density estimate:

$$D(\mathbf{m}\,|\,r) \equiv \sum_{i=1}^{N} K(\mathbf{m} - \mathbf{x_i}\,|\,r), \tag{5.6}$$

where $\mathbf{x_i}$ is the position of individual i. Since $K(\mathbf{y}\,|\,r)$ is normalised (*i.e.*, the integral of $K(\mathbf{y}\,|\,r)$ over space is equal to one), it follows that

$$\int_{\mathrm{S}} D(\mathbf{m}\,|\,r)\,\mathrm{d}\mathbf{m} = N, \tag{5.7}$$

where $\int_{\mathrm{S}}$ represents the integral over the entire space. For any characteristic c of individuals, such as phenotype or fitness, we define the *kernel mean* at point $\mathbf{m}$ as

$$\{c\,|\,\mathbf{m}, r\}_{\mathrm{k}} \equiv \frac{\sum_i K(\mathbf{m} - \mathbf{x_i}\,|\,r) c_i}{D(\mathbf{m}\,|\,r)}, \tag{5.8}$$

which is the average of c over all individuals, weighted by their distance to $\mathbf{m}$ according to the kernel function. We will often write $\{c\}_{\mathrm{k}}$ as a shorthand for $\{c\,|\,\mathbf{m}, r\}_{\mathrm{k}}$ to avoid clutter.

Analogous to the selection differential in Price's equation, we can now calculate local selection around point m as the local covariance between phenotype and relative fitness within the environment, which we call the *Kernel Selection Differential (KSD)*:

$$\begin{aligned} S_{\mathrm{k}}(\mathbf{m} \mid r) &\equiv \frac{\{\phi w \mid \mathbf{m}, r\}_{\mathrm{k}} - \{\phi \mid \mathbf{m}, r\}_{\mathrm{k}} \{w \mid \mathbf{m}, r\}_{\mathrm{k}}}{\{w \mid \mathbf{m}, r\}_{\mathrm{k}}} \\ &\equiv \mathrm{Cov}_{\mathrm{k}}\left(\phi, w / \{w\}_{\mathrm{k}} \mid \mathbf{m}, r\right). \end{aligned} \tag{5.9}$$

Decomposing the selection differential into local and interlocal selection

For any function over space $g(\mathbf{m})$, we define the *spatial mean* as

$$\begin{aligned} \langle g(\mathbf{m}) \mid r \rangle_{\mathrm{s}} &\equiv \frac{\int_{\mathrm{S}} D(\mathbf{m} \mid r) g(\mathbf{m}) \, \mathrm{d}\mathbf{m}}{\int_{\mathrm{S}} D(\mathbf{m} \mid r) \, \mathrm{d}\mathbf{m}} \\ &= \frac{1}{N} \int_{\mathrm{S}} D(\mathbf{m} \mid r) g(\mathbf{m}) \, \mathrm{d}\mathbf{m}. \end{aligned} \tag{5.10}$$

For readability, we will often write $\langle g(\mathbf{m}) \rangle_{\mathrm{s}}$ for $\langle g(\mathbf{m}) \mid r \rangle_{\mathrm{s}}$. Note that, with the definitions of Eq 5.8 and 5.10, the spatial mean of the kernel mean is simply the population mean, *i.e.*, $\left\langle \{c\}_{\mathrm{k}} \right\rangle_{\mathrm{s}} = \overline{c}$.

We can now derive

$$\begin{aligned} S = \mathrm{Cov}(\phi, w) &= \overline{\phi w} - \overline{\phi}\,\overline{w} \\ &= \left\langle \{\phi w\}_{\mathrm{k}} \right\rangle_{\mathrm{s}} - \left\langle \{\phi\}_{\mathrm{k}} \right\rangle_{\mathrm{s}} \left\langle \{w\}_{\mathrm{k}} \right\rangle_{\mathrm{s}} \\ &= \left\langle \{\phi w\}_{\mathrm{k}} - \{\phi\}_{\mathrm{k}} \{w\}_{\mathrm{k}} \right\rangle_{\mathrm{s}} + \left\langle \{\phi\}_{\mathrm{k}} \{w\}_{\mathrm{k}} \right\rangle_{\mathrm{s}} - \left\langle \{\phi\}_{\mathrm{k}} \right\rangle_{\mathrm{s}} \left\langle \{w\}_{\mathrm{k}} \right\rangle_{\mathrm{s}} \\ &= \langle \mathrm{Cov}_{\mathrm{k}}(\phi, w \mid \mathbf{m}, r) \rangle_{\mathrm{s}} + \mathrm{Cov}_{\mathrm{s}}\left(\{\phi\}_{\mathrm{k}}, \{w\}_{\mathrm{k}}\right) \\ &\equiv S_{\mathrm{local}}(r) + S_{\mathrm{interlocal}}(r). \end{aligned} \tag{5.11}$$

Hence, S_{local} is the average of the KSD over all possible local environments (*i.e.*, all midpoints in space), where each environment is weighted by its local density and its local mean fitness:

$$S_{\mathrm{local}}(r) = \left\langle \{w\}_{\mathrm{k}} S_{\mathrm{k}}(\mathbf{m} \mid r) \right\rangle_{\mathrm{s}}. \tag{5.12}$$

It hence captures the total effect of selection *within* local environments. On the other hand, $S_{\mathrm{interlocal}}(r)$ is the spatial covariance (defined in terms of spatial means) of the local mean phenotype and local mean fitness. This term captures the selection *among* environments.

Acknowledgements

We thank Reinder Bosman for a preliminary analysis of the SI-model, and Laura van Schijndel for valuable discussions and comments on the manuscript.

5.5. Supplementary Movies

Supplementary Movies are available from
`https://theory.bio.uu.nl/hilje/PhDthesis/Ch5_Movies`.

S5.1 Movie Dynamics of the altruism model. Simulation lattice points are coloured by the mean level of altruism of the individuals in that position, according to the colour scale shown in Figure 5.2b. Empty lattice points are white.

S5.2 Movie Dynamics of the SI-model if reproduction of susceptibles is fast ($\gamma = 0.05$). Empty lattice points are coloured black, susceptible individuals white, and infected individuals are coloured according to the transmissibility of the pathogen they carry (see colour scale in Figure 5.3b). To reduce file size, only $1/16$-th of the simulation lattice is shown (movie shows 256×256 lattice points, simulation lattice is 1024×1024 lattice points).

S5.3 Movie Dynamics of the SI-model if reproduction of susceptibles is slow ($\gamma = 0.02$). Same colour scheme as S5.2 Movie. Again, only $1/16$-th of the simulation lattice is shown (same sizes as in S5.2 Movie).

5.6. Supplementary Text

5.6.1. Individual-based model of the evolution of altruism

As a first example of multiscale selection, we consider the evolution of altruism in a spatially explicit individual-based model. A full analysis of this model will be provided elsewhere.

Model description

We model a population of individuals living in a 2D space with periodic boundary conditions. Each individual can reproduce asexually, die, and move in an undirected fashion. Individuals differ by one continuous phenotype, ϕ, that specifies their level of altruism. By itself, altruistic behaviour is costly: it directly reduces the individual's rate of reproduction. An individual with a highly altruistic phenotype does however improve the living conditions of all individuals in its local neighbourhood (including itself), irrespective of their phenotype. Individuals locally compete for resources: the rate of reproduction of an individual decreases with the density of individuals in its local neighbourhood. Both altruistic interactions and competition are modelled through a 2-dimensional normal interaction kernel function, $J(\mathbf{y} \mid \sigma_{\mathrm{j}})$, which describes the local interaction neighbourhood. The label j can indicate either

competition or altruism; the standard deviation (*i.e.*, scale) of the resource competition neighbourhood, σ_{rc}, may differ from the standard deviation of the altruism neighbourhood, σ_{a}. We denote the total level of altruism experienced by individuals at position $\mathbf{y}$ by

$$\alpha(\mathbf{y} \mid \sigma_{\mathrm{a}}) \equiv \sum_{i=1}^{N} \phi_i J(\mathbf{x_i} - \mathbf{y} \mid \sigma_{\mathrm{a}}). \tag{S5.1}$$

In the simulations, space is discretised into a regular square lattice with lattice constant Δx, and time is discretised into steps Δt. Every time step, the following sequence of events occurs:

1. **Reproduction** Every individual reproduces with probability $\gamma_i \Delta t$. The reproduction rate of an individual is given by

$$\gamma_i = \gamma_0 \max\left[\left(1 - c\,\phi_i + \underbrace{\frac{b_{\max} \cdot \alpha(\mathbf{x_i} \mid \sigma_{\mathrm{a}})}{b_{\max}/b_0 + \alpha(\mathbf{x_i} \mid \sigma_{\mathrm{a}})}}_{\text{benefit from local altruism}}\right) \times \underbrace{\left(1 - \frac{\sum_{j=1}^{N} J(\mathbf{x_j} - \mathbf{x_i} \mid \sigma_{\mathrm{rc}})}{K}\right)}_{\text{competition}},\ 0\right], \tag{S5.2}$$

   where γ_0 is the basal reproduction rate, c the cost of altruism, $\mathbf{x_i}$ the position of the individual, and K is a factor scaling the local carrying capacity. The benefit of altruism is an increasing, saturating function of the locally experienced altruism: it is 0 if the local environment does not contain any altruists, and $b_{\max}$ if $\alpha(\mathbf{x_i} \mid \sigma_{\mathrm{a}}) \to \infty$. When an individual reproduces, a new organism is born and placed at the same lattice point as its parent.

2. **Heritability and mutation** The phenotype ϕ_{child} of the child is copied from its parent, but mutated with probability μ. The effect size of the mutation is drawn from an exponential probability distribution with mean λ; its sign is chosen to be positive or negative with equal probability. If a mutation would result in a negative phenotype, ϕ_{child} is set to zero.

3. **Death** Individuals die with probability $\delta \Delta t$.The death rate δ is independent of phenotype.

4. **Dispersion** All individuals are displaced by adding a random number to both coordinates of their position. These random numbers are independently drawn from a discretised normal distribution with standard deviation $\sigma_{\mathrm{d}} \equiv \sqrt{2 k_{\mathrm{D}} \Delta t}$. This results in movement by diffusion, with diffusion constant k_{D}.

Units and parameters

In the formulation above, we are free to choose the scaling of the phenotype ϕ; this allows one to eliminate one parameter. We choose to set the cost to $c = 1$. We

can eliminate another parameter by choosing suitable units of length; we choose to set $\sigma_a = 1$, so that all lengths become expressed in units of the interaction range of altruism. A last parameter can be eliminated by choosing convenient units of time; we set the death rate $\delta = 1$, such that time is measured in generations.

Other parameter values are shown in Table 5.1. While some parameters were chosen arbitrarily, the following rationale was followed: To resolve the altruistic interactions, the spacing of the lattice needs to be smaller than the range of altruism, $\sigma_a = 1$. We therefore set the size of a lattice point to be $0.1\sigma_a$. Similarly, to ensure that γ_i and δ can indeed be interpreted as rates, the time step should be chosen such that $\gamma_i \Delta t$ and $\delta \Delta t$ are much smaller than 1. We therefore set $\Delta t = 0.08$. Colony formation happens only if the range of competition is significantly larger than the range of altruism (further explored in an upcoming publication). Since the evolution of altruism is favoured under positive genetic assortment (*i.e.*, close proximity of parents and offspring) (Hamilton, 1964), a low diffusion constant was chosen. Lastly, the basal benefit from altruism b_0 was chosen to ensure that the benefit experienced by an isolated individual, $\alpha(\mathbf{x_i}) = \frac{\phi_i}{2\pi}$, is considerably smaller than the cost $c\phi_i = \phi_i$.

Supplementary Table 5.1. Altruism model parameters

Parameter	*Description*	*Value*
σ_a	Range of altruism	1
σ_{rc}	Range of resource competition	4
γ_0	Basal reproduction rate	5
c	Cost of altruism	1
b_0	Basal benefit of altruism	1
b_{max}	Maximal benefit of altruism	5
K	Scaling factor local carrying capacity	40
δ	Death rate	1
k_D	Diffusion constant	0.04
μ	Mutation probability upon reproduction	10^{-3}
λ	Mean of mutation step size	5×10^{-3}
Δx	Simulation lattice constant	0.1
Δt	Simulation time steps	0.08
	Simulation lattice size (lattice points)	1024×1024

5.6.2. SI-model of the evolution of pathogen transmissibility

As a second example, we consider the evolution of pathogen transmissibility in a spatial SI-model. This model is based on a long history of simulation models exploring pathogen evolution (Rand *et al.*, 1995; Haraguchi and Sasaki, 2000; Boots and Sasaki, 1999; Goodnight *et al.*, 2008).

Model description

Consider a population of individuals living on a 2D square lattice. Each lattice point contains at most one individual. Individuals reproduce, die and move randomly (Figure 5.3a). Individuals can be either susceptible to infection with a pathogen, or infected. Infected individuals no longer reproduce, and die at a higher rate than susceptible individuals. The infection spreads locally; the probability that an infected individual transmits the pathogen to a susceptible neighbour depends on the transmissibility of the pathogen that they carry, ϕ. We consider the evolution of this transmissibility.

Time in the model progresses in discrete time steps. Every time step, the following series of events takes place:

1. **Reproduction** Since each lattice point can be occupied by at most one individual, individuals reproduce only if one or more of their neighbouring lattice points is empty. Empty lattice points are repopulated by a susceptible individual with probability $\gamma\, n_S$, where γ is the reproduction rate per susceptible individual, and n_S is the number of susceptible individuals among the eight neighbours (including diagonals) surrounding the empty lattice point.

2. **Infection** For each susceptible individual i, let I_i be the set of infected neighbours among the eight lattice points surrounding the susceptible individual's position. Individual i gets infected with probability

$$P_i = \frac{\sum_{j \in I_i} \phi_j}{h + \sum_{j \in I_i} \phi_j}. \tag{S5.3}$$

   This infection probability is zero when the susceptible individual has no infected neighbours, and approaches 1 if many of the neighbours are infected with highly transmissible pathogens. If an infection takes place, one of the infected neighbours is chosen as the source of this new infection; the probability that a neighbour is chosen is proportional to the transmissibility of its pathogen, ϕ_j. The newly infected individual "inherits" the transmissibility value of the chosen infected neighbour;

3. **Mutation** Since we consider mutation of the pathogen rather than of the host individuals, mutations are not coupled to reproduction events of the hosts.

Instead, each time step the transmissibility of the pathogen within each infected individual is mutated with a small probability μ. This resembles a within-host mutation of the pathogen that (instantly) sweeps the within-host pathogen population. If a mutation occurs, a new transmissibility ϕ_i' is chosen from a uniform distribution $[\phi_i - \lambda; \phi_i + \lambda]$. If $\phi_i' < 0$, it is set to zero.

4. **Death** Susceptible individuals die with probability δ_S. Infected individuals die with probability $\delta_I > \delta_S$.

5. **Dispersion** In a randomly assigned order, each individual moves with probability p_D. If an individual moves, a random neighbouring lattice point is chosen. If the chosen lattice point is empty, the individual moves there; else the individual swaps places with the individual in the chosen lattice point. This procedure approximates movement by random walk, while ensuring that the number of individuals does not change and that the rate of movement per individual does not depend on local population density.

Parameters

An overview of all model parameters and their values is provided in Table 5.2. Reproduction and death probabilities were set to values significantly smaller than 1 per time step, so that these probabilities can be interpreted to good approximation as rates of a Poisson process. To allow spatial patterns to arise, a small value was chosen for the dispersal probability p_D.

Supplementary Table 5.2. SI model parameters

Parameter	*Description*	*Value*
γ	Reproduction rate (per susceptible per time step)	0.05
δ_S	Death rate of susceptible individuals (per time step)	0.05
δ_I	Death rate of infected individuals (per time step)	0.2
h	Scaling factor of infection probability	20
p_D	Dispersal probability (per time step)	0.05
μ	Mutation rate (per time step)	0.005
λ	Maximal mutation step size	0.5
	Simulation lattice size (lattice points)	1024×1024

Scale of emergent spatial patterns

To measure the size of the emergent spatial patterns, we determine the pair correlation function $g(r)$ for all individuals. This function measures the mean density of individuals at distance r from a lattice point, given that this lattice point is occupied by some individual. It thus indicates whether the occupancy of a lattice point correlates with the occupancy of lattice points a distance r away. The function is normalised by the average density of the field. Hence, if $g(r) = 1$, the probability of finding other individuals at distance r from a given focal individual is equal to the probability of finding individuals in any random position; if $g(r) > 1$ the probability of finding other individuals at distance r from a focal individual is larger than one would expect from random sampling of the population.

For patch structures such as the emergent patterns studied here, $g(r)$ can be approximated by an exponential function

$$g(r) = 1 + \exp(a - br). \tag{S5.4}$$

Eq S5.4 was used to fit the observed pair correlation functions using least-squares fitting. The fitted exponent b^{-1} was used as a measure of the size of the patches emerging in the field (Figure 5.3e).

5.6.3. Implementation of calculations of $S_{\text{local}}(r)$ and $S_{\text{interlocal}}(r)$

In the Methods section, we gave a general analytical derivation of the spatial decomposition of the selection differential S in components S_{local} and $S_{\text{interlocal}}$. Below, we describe how these quantities were calculated in practice.

When deriving the spatial decomposition of selection (Methods), we considered a population in continuous space. In the simulations, however, space is discretised. This is easily dealt with by replacing the integral over space in Eq 5.10 with a double summation over the coordinates of the 2D simulation space.

For both models, simulations were performed using periodic boundary conditions (a common choice for these kinds of simulations). Calculating local population densities (Eq 5.6) then requires one to not only take the individuals in the simulation lattice into account, but also their periodic images. The circular convolution theorem provides an efficient way to do this using Discrete Fourier Transforms (DFTs). This is a standard technique from signal processing; we shortly discuss it here for completeness.

For ease of notation we here present derivations for a 1D space, the 2D case follows analogously.

Assume that a sequence $o_0, o_1, \ldots, o_{n-1}$ specifies the occupancy (number of individuals) at discrete positions $j \in \{0, 1, \ldots, n-1\}$ in a simulation field, and let

$N = \sum_{j=0}^{n-1} o_j$ be the total number of individuals. Because we assumed periodic boundary conditions, we should consider this finite field to represent a finite stretch taken from an infinite field that is periodic with period n; that is, the full field, including periodic images, is a sequence $\tilde{o}_j$ with $j \in \mathbb{Z}$ defined by $\tilde{o}_j = o_{(j \bmod n)}$.

On the discretised space, the kernel function is represented by an infinite non-negative sequence k_j with $j \in \mathbb{Z}$, whose sum converges to 1. Because the kernel function is a function of distance, it is symmetric, *i.e.*, $k_{-j} = k_j$. The kernel density d_j for positions $j \in \{0, 1, \ldots, n-1\}$ (*c.f.* Eq 5.6) is now given by

$$d_j = \sum_{m=-\infty}^{\infty} \tilde{o}_m k_{(j-m)}. \tag{S5.5}$$

Eq S5.5 can be rewritten as follows:

$$\begin{aligned} d_j &= \sum_{p=-\infty}^{\infty} \sum_{l=0}^{n-1} \tilde{o}_{l+pn}\, k_{j-l-pn} \\ &= \sum_{l=0}^{n-1} \tilde{o}_l \sum_{p=-\infty}^{\infty} k_{j-l-pn} \\ &= \sum_{l=0}^{n-1} \tilde{o}_l \hat{k}_{(j-l) \bmod n}, \end{aligned} \tag{S5.6}$$

where we introduced the *periodic summation* $\hat{k}_j$ for $j \in \{0, 1, \ldots, n-1\}$ as

$$\hat{k}_j \equiv \sum_{p=-\infty}^{\infty} k_{j-pn}. \tag{S5.7}$$

The sequences $\tilde{o}_j$ and $\hat{k}_j$ are both periodic with period N. Eq S5.6 is the *circular convolution* of these two sequences, which we denote by $\tilde{o} *_N \hat{k}$. By the circular convolution theorem, the DFT of $\tilde{o} *_N \hat{k}$ is equal to the element-wise product of the DFTs of $\tilde{o}$ and $\hat{k}$, *i.e.*,

$$\mathcal{F}(d_j) = \mathcal{F}(\tilde{o} *_N \hat{k}) = \mathcal{F}(\tilde{o}_j) \cdot \mathcal{F}(\hat{k}_j). \tag{S5.8}$$

Using Eq S5.7 and S5.8, we can calculate the local density d_j by

1. calculating the periodic summation $\hat{k}_j$ of k_j;
2. calculating the DFTs of $\hat{k}_j$ and o_j, and calculating their element-wise product;

3. calculating the inverse DFT of this element-wise product, which yields d_j.

Because algorithms for Fourier transformation are highly efficient (Frigo and Johnson, 2005), this proceure allows us to rapidly solve local densities for varying scales r. Fourier transformations were performed using the `fftw3`-library (Frigo and Johnson, 2005).

The kernel mean of a property c of individuals, $\{c \mid j,r\}_\mathrm{k}$ (Eq 5.8), can be calculated in a very similar way. Let $\tilde{c}_j$ be the sequence of the sum of c-values of individuals at position j. In terms of this sequence, we can write

$$\{c \mid j,r\}_\mathrm{k} = \frac{\sum_{l=0}^{n-1} \tilde{c}_j \hat{k}_{(j-l) \bmod n}}{d_j} \tag{S5.9}$$

In other words, the total local kernel value of c, $\{c \mid j,r\}_{\mathrm{k,tot}} \equiv d_j \{c \mid j,r\}_\mathrm{k}$, is given by the circular convolution of the sequences $\tilde{c}$ an $\hat{k}$, and can hence be easily calculated using Fourier transformation as described above. To find the kernel mean, this total local kernel value is divided by the local density, d_j. Note that, for some positions j, the local density might be very small or zero. To avoid numerical problems, division by local density is treated with caution in the calculations of $S_\mathrm{local}(r)$ and $S_\mathrm{interlocal}(r)$ (see below).

By definition, $S_\mathrm{local}(r)$ is the spatial mean of the KSDs, weighted by the local mean fitness $\{w\}_\mathrm{k}$. It is therefore possible to calculate $S_\mathrm{local}(r)$ directly from the kernel selection differential, $S_\mathrm{k}((x,y) \mid r)$:

$$\begin{aligned} S_\mathrm{local}(r) &\equiv \left\langle \{w\}_\mathrm{k} S_\mathrm{k}(j \mid r) \right\rangle_\mathrm{s} \\ &= \frac{1}{N} \sum_j d_j \{w\}_\mathrm{k} S_\mathrm{k}(j \mid r). \end{aligned} \tag{S5.10}$$

However, noting that $\left\langle \{\phi w\}_\mathrm{k} \right\rangle_\mathrm{s} = \overline{\phi w}$ we can also calculate $S_\mathrm{local}(r)$ using Eq 5.12:

$$\begin{aligned} S_\mathrm{local}(r) &= \left\langle \{\phi w\}_\mathrm{k} - \{\phi\}_\mathrm{k} \{w\}_\mathrm{k} \right\rangle_\mathrm{s} \\ &= \overline{\phi w} - \left\langle \{\phi\}_\mathrm{k} \{w\}_\mathrm{k} \right\rangle_\mathrm{s} \\ &= \overline{\phi w} - \frac{1}{N} \sum_j \frac{\{\phi\}_{\mathrm{k,tot}} \{w\}_{\mathrm{k,tot}}}{d_j}, \end{aligned} \tag{S5.11}$$

which is less likely to cause numerical inaccuracies (if the local density $d_j = 0$ for some position j, the corresponding term in the summation is set to zero).

Using the definition of Eq 5.11, the value of $S_\mathrm{interlocal}(r)$ can be calculated directly as the covariance between $\{\phi \mid j,r\}_\mathrm{k}$ and $\{w \mid j,r\}_\mathrm{k}$, in which each position j is

weighted by the local kernel density d_j. However, we can again derive an expression that is numerically more stable:

$$\begin{aligned} S_{\text{interlocal}}(r) &= \left\langle \{\phi\}_{\text{k}} \{w\}_{\text{k}} \right\rangle_{\text{s}} - \overline{\phi}\,\overline{w} \\ &= \left\langle \left(\{\phi\}_{\text{k}} - \overline{\phi} \right) \left(\{w\}_{\text{k}} - \overline{w} \right) \right\rangle_{\text{s}} \\ &= \frac{1}{N} \sum_j \frac{(\{\phi\}_{\text{k,tot}} - d_j \overline{\phi})(\{w\}_{\text{k,tot}} - d_j \overline{w})}{d_j}, \end{aligned} \tag{S5.12}$$

where again the summation term for index j is set to zero if the local density $d_j = 0$. Eq S5.11 and S5.12 were used in the simulations.

6

General Discussion

In this thesis, we have used mathematical and computational models to explore how the evolution of microbes is shaped by processes spanning varying spatial and temporal scales.

In **chapter 2**, we studied the evolution of the human pathogen HIV under the different selection pressures it faces within a single host and when spreading through a host population. We showed that long-lived latent reservoirs, in which the virus does not replicate nor mutate, can markedly affect the evolutionary dynamics at the within-host level. Subsequently, this within-host effect partly explains how the virus may avoid short-sighted evolution at the between-host level (*c.f.*, Levin and Bull (1994); see chapter 1).

Chapter 3 addressed the evolution of peptide-based communication between bacteriophages. We provided a proof of concept that such communication can evolve because it allows phages to adjust their infection strategy to the availability of susceptible host cells, *i.e.*, causing lytic infections early in an outbreak (when susceptible hosts are still abundant), and lysogenic infections later (when susceptible hosts have become scarce). However, we also showed that such communication can only evolve under specific conditions, namely if the phages cause repeated outbreaks in large pools of susceptible host cells.

In **chapter 4**, we considered the evolution of toxin regulation by cell-density cues in bacteria. We found two distinct types of density-dependent regulation that evolved under different growth conditions. Notably, when bacteria were exposed to a serial transfer regime in which they repeatedly had to colonise new environments, they were selected on the spatial structure of the colonies they form. The evolved bacteria used the cell-density cue to express a fast-growing sensitive phenotype when located on the edge of an expanding colony and a slower-growing, toxin-producing phenotype when in a crowded area such as the middle of a colony (see Figure 4.6a).

Lastly, in **chapter 5** a new mathematical framework was presented for the analysis of selection at different spatial scales in spatially structured populations. Using two simple example models, we showed how this framework measures local and interlocal selection for any length scale, and how it identifies the spatial scales that are relevant for selection.

Together, chapters 2–5 span a wide range of microbes and microbial behaviours. Even so, several recurrent themes can be identified. Next to increasing our understanding of the specific systems we studied, our results thus also provide more general insights into the multiscale processes that shape microbial evolution. In this discussion, our results are synthesised by discussing four common themes.

6.1. The evolution of viral latency

Many pathogens possess the ability to cause latent infections, in which they do not exploit their current host cell for reproduction, but rather lay dormant until they are reactivated. Latent strategies are found in a several human pathogens, such as *Mycobacterium tuberculosis* (Esmail *et al.*, 2014), Herpes simplex virus (Kinchington *et al.*, 2012) and of course HIV (Siliciano and Greene, 2011; Castro-Gonzalez *et al.*, 2018). Latent viruses are also highly abundant in microbial communities; it has been estimated that approximately half of all bacteria carries at least one integrated prophage in their genome (Touchon *et al.*, 2016).

In chapter 2 we studied how viral latency affects the multilevel evolution of HIV, and in chapter 3 we investigated under what conditions a communication system can evolve that regulates latency in bacteriophages. Prior to these questions, however, lies the question of how viral latency itself evolved. In bacteriophages, this question has attracted some attention over the years (starting with the seminal paper by Stewart and Levin (1984) and recently reviewed by Gandon (2016)), with a focus on the coliphage λ as a model species. As reviewed in chapter 3, phage λ, and temperate phages in general, are thought to have evolved latency to survive "bad" periods of low host cell availability (Stewart and Levin, 1984; Maslov and Sneppen, 2015). Viral latency hence acts as a persistence mechanism.

Does a similar explanation apply to the presence of latent reservoirs in HIV infections? This is not directly obvious. In fact, it is not even clear to what extent HIV latency is an evolved property of the pathogen. Phage λ encodes several genes that coordinate its lysis-lysogeny decision, latency maintenance, and the eventual reversal to the lytic cycle (Golding *et al.*, 2019). While the exact mechanisms of latency establishment in HIV remain to be elucidated, so far no viral factors strongly controlling this process have been found (Siliciano and Greene, 2011; Romani and Allahbakhshi, 2017). Rather, the main route to HIV latency seems to be the spontaneous reversion of a subset of infected activated CD4+ T cells (the cell type that is most vulnerable to HIV infection) to a resting state, a process that normally ensures the establishment of immunological memory (Siliciano and Greene, 2011). The latent viral reservoirs are then a byproduct of a naturally occurring process in the host organism. However, even if it did not evolve for that purpose HIV latency might still act as a persistence mechanism. In fact, the obstacles we face in finding a cure for HIV show that it does: even if viral growth is completely suppressed by antiretroviral treatment, the latent reservoirs cause HIV to persist for many years.

Next to its role as a persistence mechanism, latency may also shape the evolution of viruses in different ways. In chapter 2, we found that latent reservoirs (i) slow down all evolutionary dynamics because each viral lineage at some point cycles through the reservoir, thus temporarily evading mutation and selection, and (ii)

provide an archive of previously circulating viral strains that are constantly fed back into the active viral population. This second effect enhances the diversity of the viral population, retaining viral variants that otherwise might have been lost due to - potentially short-sighted - selection. Similarly, prophages have also been suggested to act as genetic reservoirs that promote viral diversity and for instance facilitate quick adaptation to resistant bacterial strains (Nadeem and Wahl, 2017).

In summary, latency affects the evolutionary dynamics of viruses in several ways. It serves as a persistence mechanism, allowing the virus to survive periods of poor environmental circumstances that do not support an ongoing active infection. It furthermore provides an archive of viral variants, thus increasing viral diversity. Reactivation of dormant variants may help a viral quasispecies adapt to new selection pressures (whether these arise from transmission to a new host, from the evolution of resistance in the host organisms, of from something else), especially if these new selection pressures are similar to selection pressures experienced by the virus in the past.

6.2. The role of out-of-equilibrium dynamics in evolution

In many introductory theoretical biology courses, one of the first things discussed is how to find the equilibria of biological models (in this case: systems of differential equations) and determine their stability. These are critical skills that allow us to analyse the long-term dynamics of models and help us develop expectations for their behaviour. However, focussing on equilibria might not always tell the full story.

A prime example of this are the results we obtained for the evolution of bacteriophage communication (chapter 3). Firstly, we showed that for most bacteriophages parameter values are such that we should not expect phages and susceptible bacteria to coexist in equilibrium (in well-mixed populations). Since new infections no longer occur once this equilibrium is reached, the lysis-lysogeny decision cannot be under selection in equilibrium. To study the evolution of the lysis-lysogeny decision, repeated or ongoing perturbations away from equilibrium are hence necessary; we include this in our model by imposing a serial-transfer protocol.

Secondly, we argued that regulation by density cues by its very nature does not line up with microbes living in equilibrium conditions. In deterministic models, such as the ODE-model in chapter 3, this is very clear: once the system has converged to equilibrium, the densities of different cell and phage types no longer change over time and a cue conveying information about these densities is useless. In populations with demographic stochasticity, such as the individual-based simulation

model of chapter 4, the information conveyed by a density cue in a population close to equilibrium is however also limited to small fluctuations in local density. While we did find a regulatory mechanism that exploits these small, local density fluctuations to control toxin production (chapter 4), regulation by cell density cues much more readily arose under large, externally induced density fluctuations.The regulation mechanisms that then evolved are highly robust against a range of perturbations (chapter 4).

The serial transfer protocols that we used in chapters 3 and 4 expose the microbes to different selection pressures at different times. Shortly after a transfer, the number of competing microbes is low, resource (*i.e.*, susceptible host cells or empty space to expand into) is abundant, and the microbes are selected for fast exploitation of this resource. As the resource is consumed and the number of microbes increases, selection for fast resource exploitation becomes less important and the microbes are selected for survival in a crowded microbial population. Regulation by arbitrium (chapter 3) or a local cell density cue (chapter 4) allows the microbes to navigate these changing environments, because they can thus adjust their phenotype to the current balance between selection for fast resource exploitation and selection for long-term competitiveness.

It might seem pedantic to so elaborately discuss the importance of culture conditions for evolution. Obviously, culture conditions affect the environment the microbes grow in, and hence influence their evolution. The ways in which they do, however, can be quite surprising. In a recent study, van Dijk *et al.* (2019) showed that virtual microbes can evolve to anticipate the 24h-cycle of a serial transfer protocol. After a transfer, these virtual microbes rapidly deplete the available resources, and then need to survive until the next transfer. While most microbes in these evolved populations indeed survive for 24h, they die *en masse* if no new resource is added for another few hours. Under the balance of selection for fast resource exploitation and long-term persistence, these microbes have evolved to deplete the available resource as fast as possible under the constraint that they still need to survive long enough afterwards to just make it until the next transfer. These results should remind us to never take common protocols for granted, but to always carefully consider how the conditions we expose microbes to (in models or in the lab) might shape their evolution.

6.3. Exploring the diversity of microbial warfare and density-dependent regulation

When studying the evolution of bacterial toxin production and its density-dependent regulation (chapter 4), we chose to model toxins with a relatively small action range (low diffusion constant) that are potentially regulated by a density cue that is produced by all bacteria. These choices were made based on real-life examples of toxin regulation (discussed in chapter 4). However, they are by no means the only reasonable choices. Bacteria display a staggering diversity in mechanisms by which they harm others (recently reviewed by Granato *et al.* (2019)), ranging from the secretion of small toxic molecules to the expression of large speargun-like protein structures that directly deliver toxins to neighbouring cells (the Type-VI secretion system, T6SS (Basler, 2015)). The action spectrum of these mechanisms varies widely: some toxins only affect bacteria of the same genus as the toxin-producing strain, while others harm a broad range of microbes (Riley and Wertz, 2002a). The spatial scales over which these mechanisms act are also very diverse. Diffusible toxins, such as the colicins, act over several tens or hundreds of cell lengths from the place they were produced (Chao and Levin, 1981; Weber *et al.*, 2014). T6SS and contact-dependent inhibition (CDI), on the other hand, require direct cell-cell contact. The spatial scales of these interactions are bound to influence the spatial structure of the populations in which they occur, which in turn will alter the selection pressures on the interactions.

Microbial warfare mechanisms are also regulated in a large variety of ways (Cornforth and Foster, 2013; Gonzalez and Mavridou, 2019). Some toxins are produced in response to highly specific quorum sensing signals that are produced by cells of the same strain only, others in response to very general density cues, such as peptidoglycan fragments (Korgaonkar and Whiteley, 2011) or the widely produced auto-inducer 2 (Qi *et al.*, 2004; Krin *et al.*, 2006). Several toxins are secreted as part of generic stress responses, others in response to cell damage, yet others in response to nutrient limitation (see Cornforth and Foster (2013) for an extensive review).

Where did all this diversity come from? Is it functional? It has been argued that many of these different stimuli are proxies for the same environmental conditions: the presence of competitors ("competition sensing"; *c.f.*, Cornforth and Foster (2013)) or the direct threat of cell damage ("danger sensing"; *c.f.*, LeRoux *et al.* (2015)). If several different cues all convey approximately the same information, diversity in regulatory mechanisms may arise from evolution "using whatever is available". However, it seems unlikely that the information conveyed by all these different cues is equally useful for the regulation of any type of toxin. As an example, consider toxins that, to be effective, require a minimum concentration that can

only be reached if a substantial number of cells produces the toxin (such that toxin production is effectively a cooperative behaviour among killer cells). For producers of these toxins, information about the local density of co-killer cells is crucially important. Hence, a strain-specific quorum sensing signal seems more likely to evolve than regulation by a more generic cue.

Which type of regulation should we expect for which toxins? Models like the one presented in chapter 4 can help to assess the evolutionarily feasibility of different toxin regulation mechanisms under different circumstances. Recent experimental developments now also allow us to look at bacterial communities at the level of single cells, tracking the expression of toxin genes and signalling molecules over time (Mavridou *et al.*, 2018; von Bronk *et al.*, 2019; Bottery *et al.*, 2019; Lories *et al.*, 2020). Combining models with such experiments will allow us to further explore the complexity of bacterial interference competition and competition sensing.

6.4. The many scales of natural selection

Throughout this thesis, we have emphasised that microbial evolution is a multiscale or multilevel process. In chapter 2, we explicitly incorporated two levels in the model of HIV evolution. These levels correspond to different time scales: within-host evolution happens over much shorter time scales than between-host evolution. The serial transfer protocols in chapter 3 and 4 also exposed the microbes to selection pressures that vary over time: on short time-scales fast resource exploitation is favoured, while on longer time-scales other phenotypes (lysogeny or toxin production) are selected to ensure persistence. Furthermore, in the spatially structured populations of chapter 4 bacteria were selected on the spatial structure of the colonies they form. In other words, colony-level selection emerged. Finally, in chapter 5 we developed a formal definition of multiscale evolution in space, defining local and interlocal selection for varying length scales.

How do selection pressures at these different scales (*e.g.*, space and time) relate to each other? I will here argue that they are often different sides of the same coin, but that adopting several perspectives (*e.g.*, a spatial and a temporal view) might lead to additional insights.

As an example, consider the evolution of pathogen transmissibility in the SI-model discussed in chapter 5. In chapter 5, we showed that this is a spatial multiscale evolutionary process: local selection favours higher values of transmissibility, but interlocal selection on transmissibility is negative (see Fig 5.3). The spatial decomposition captures the effects of local self-shading (Boots and Sasaki, 1999): while pathogens with higher transmissibility spread faster than their neighbours within a local environment (and hence have higher fitness), pathogens with high transmissi-

bility rapidly deplete their surroundings of susceptible individuals, such that they are often found in areas with few susceptible individuals (*i.e.*, in patches with high mean transmissibility, pathogen fitness tends to be low). The *spatial decomposition of selection* formally describes these differences between local and interlocal selection, and allows one to determine how each spatial scale contributes to selection. It is however not the only framework in which this system can be analysed.

First, we could consider the system in a *multilevel selection* framework, stating that global selection for pathogen transmissibility is the result of positive selection favouring increased transmissibility at the individual level, and negative selection favouring pathogen restraint at the level of patches. To formalise this argument, we would need to define this higher-level entity ("the patch"), after which we could calculate within-patch and between-patch selection (similar to the within- and between-group selection components in Wilson's trait group model of altruism, see chapter 1). An advantage of this multilevel approach is that it explicitly acknowledges the existence of emergent higher-level entities. This is not well illustrated in the example considered here, because the spatial structures that emerge in the SI-model are highly variable and higher-level entities cannot be easily defined (see Fig 5.3b). In other models of evolution in spatially structured populations, however, clear, distinct higher-level entities can emerge. For instance, in a model of pathogen evolution that includes host resistance (SIR-model), the system self-organises into spiral waves and evolution is shaped by selection pressures at the level of these spiral waves (van Ballegooijen and Boerlijst, 2004). The colony structure in the altruism-model in chapter 5 is another example (see Fig 5.2b). A disadvantage of the multilevel approach, however, is that structures other than the recognised levels, *e.g.*, any spatial structure within the higher-level entities, are ignored (see chapter 5: discussion of the altruism model).

Second, we could consider selection over *different time scales*, rather than different spatial scales (Goodnight *et al.*, 2008). Consider a mutant pathogen with high transmissibility that arises in a population of pathogens with intermediate transmissibility. Over short time scales, this mutant has a high fitness. Because of its fast local reproduction the mutant will however reduce the number of susceptible individuals in its vicinity (self-shading), resulting in a decreasing contribution to new generations of pathogen. Over long time scales, the mutant's fitness is hence low. This approach nicely captures the time it takes for spatial self-structuring to arise and affect pathogen evolution. It however only implicitly captures the reason why the mutant's fitness over long time scales is low, namely, the spatial confinement of interactions and resulting spatial self-structuring.

Last, we could consider the system in an *inclusive fitness* framework (Wild *et al.*, 2009), describing the fitness of a mutant pathogen in terms of how its behaviour impacts its own fitness and the fitness of its relatives. This approach is also able to

capture the effects of self-shading, now stressing that individuals with high transmissibility have a relatively low inclusive fitness because they exhaust the environment of individuals that tend to be related and hence have a high transmissibility too. The inclusive fitness framework highlights the impact of assortment (*i.e.*, individuals mostly affect their relatives). It however only implicitly captures the underlying reason for this assortment: the spatial confinement of interactions and resulting spatial self-structuring.

The discussion above shows that the same process (self-shading by pathogens results in the selection of intermediate levels of pathogen transmissibility) can be approached from different perspectives. Is one perspective better than the others? Each perspective highlights the effects of a particular structure that is present in the simulated population: (i) spatial structure (*multiscale* framework), (ii) hierarchical levels of organisation (*multilevel* framework), (iii) temporal correlation between phenotype of ancestors and the environment of their descendants (*time scale* framework), and (iv) phenotypic assortment (*inclusive fitness* framework; note that in this model inheritance happens at the phenotype level). Each of these frameworks is a tool that may help us to recognise these structures and determine how they affect evolution. Which type of structure provides most insight - and hence which framework is most useful - depends on the system we study and the questions we ask.

6.5. Concluding remarks

Microbes live in complex environments, in which their evolution is shaped by many different selection pressures. Experimental and (meta)genomic studies continue to reveal new ways in which microbes interact with each other and their environment. Modelling these interactions allows us to investigate the feasibility of specific hypotheses, but also more generally lets us explore the structures that emerge from microbial interactions bottom-up. Combined with experiments, models will continue to increase our understanding of microbial evolution as the multiscale process it is.

References

Abedon, S. T. (1989). Selection for bacteriophage latent period length by bacterial density: A theoretical examination. *Microbial Ecology*, 18(2):79–88.

Abedon, S. T. (1990). Selection for lysis inhibition in bacteriophage. *Journal of Theoretical Biology*, 146(4):501–511.

Abedon, S. T. (2017). Commentary: Communication between Viruses Guides Lysis–Lysogeny Decisions. *Frontiers in Microbiology*, 8:983.

Abedon, S. T. (2019). Look who is talking: T-even phage lysis inhibition, the granddaddy of virus-virus intercellular communication research. *Viruses*, 11(10):951.

Abrahams, M.-R., Anderson, J. A., Giorgi, E. E., Seoighe, C., Mlisana, K., Ping, L.-H., Athreya, G. S., Treurnicht, F. K., Keele, B. F., Wood, N., Salazar-Gonzalez, J. F., Bhattacharya, T., Chu, H., Hoffman, I., Galvin, S., Mapanje, C., Kazembe, P., Thebus, R., Fiscus, S., Hide, W., Cohen, M. S., Karim, S. A., Haynes, B. F., Shaw, G. M., Hahn, B. H., Korber, B. T., Swanstrom, R., Williamson, C., CAPRISA Acute Infection Study Team, and Center for HIV-AIDS Vaccine Immunology Consortium (2009). Quantitating the multiplicity of infection with human immunodeficiency virus type 1 subtype C reveals a non-poisson distribution of transmitted variants. *Journal of Virology*, 83(8):3556–3567.

Alizon, S. and Fraser, C. (2013). Within-host and between-host evolutionary rates across the HIV-1 genome. *Retrovirology*, 10(1):49.

Alizon, S., Hurford, A., Mideo, N., and van Baalen, M. (2009). Virulence evolution and the trade-off hypothesis: History, current state of affairs and the future. *Journal of Evolutionary Biology*, 22(2):245–259.

Alizon, S. and Magnus, C. (2012). Modelling the course of an HIV infection: Insights from ecology and evolution. *Viruses*, 4(10):1984–2013.

Alkhatib, Z., Abts, A., Mavaro, A., Schmitt, L., and Smits, S. H. J. (2012). Lantibiotics: How do producers become self-protected? *Journal of Biotechnology*, 159(3):145–154.

Allen, B., Gore, J., and Nowak, M. A. (2013). Spatial dilemmas of diffusible public goods. *eLife*, 2:e01169.

Allison, S. D. (2005). Cheaters, diffusion and nutrients constrain decomposition by microbial enzymes in spatially structured environments. *Ecology Letters*, 8(6):626–635.

Anderson, R. M. and May, R. M. (1982). Coevolution of hosts and parasites. *Parasitology*, 85(2):411–426.

Andreoni, M., Parisi, S. G., Sarmati, L., Nicastri, E., Ercoli, L., Mancino, G., Sotgiu, G., Mannazzu, M., Trevenzoli, M., Tridente, G., Concia, E., and Aceti, A. (2000). Cellular proviral HIV-DNA decline and viral isolation in naïve subjects with <5000 copies/ml of HIV-RNA and >500 x 10^6/l CD4 cells treated with highly active antiretroviral therapy. *AIDS*, 14(1):23–29.

Antunes, L. C. M., Ferreira, R. B. R., Buckner, M. M. C., and Finlay, B. B. (2010). Quorum sensing in bacterial virulence. *Microbiology*, 156(8):2271–2282.

Arrigo, K. R. (2005). Marine microorganisms and global nutrient cycles. *Nature*, 437(7057):349–355.

Asquith, B., Edwards, C. T. T., Lipsitch, M., and McLean, A. R. (2006). Inefficient cytotoxic T lymphocyte-mediated killing of HIV-1-infected cells in vivo. *PLoS Biology*, 4(4):e90.

Atwood, K. C., Schneider, L. K., and Ryan, F. J. (1951). Periodic selection in Escherichia coli. *Proceedings of the National Academy of Sciences*, 37(3):146–155.

Bailone, A. and Devoret, R. (1978). Isolation of ultravirulent mutants of phage Lambda. *Virology*, 84(2):547–550.

Basler, M. (2015). Type VI secretion system: secretion by a contractile nanomachine. *Philosophical Transactions of the Royal Society B: Biological Sciences*, 370(1679):20150021.

Be'er, A., Zhang, H. P., Florin, E.-L., Payne, S. M., Ben-Jacob, E., and Swinney, H. L. (2009). Deadly competition between sibling bacterial colonies. *Proceedings of the National Academy of Sciences*, 106(2):428–433.

Bell, A. S., de Roode, J. C., Sim, D., and Read, A. F. (2006). Within-host competition in genetically diverse malaria infections: parasite virulence and competitive success. *Evolution*, 60(7):1358–1371.

Ben-Ami, F., Regoes, R. R., and Ebert, D. (2008). A quantitative test of the relationship between parasite dose and infection probability across different host-parasite combinations. *Proceedings of the Royal Society B: Biological Sciences*, 275(1636):853–859.

Ben-Ami, F. and Routtu, J. (2013). The expression and evolution of virulence in multiple infections: the role of specificity, relative virulence and relative dose. *BMC Evolutionary Biology*, 13(1):97.

Berg, K. H., Biornstad, T. J., Johnsborg, O., and Havarstein, L. S. (2012). Properties and biological role of Streptococcal fratricins. *Applied and Environmental Microbiology*, 78(10):3515–3522.

Berngruber, T. W., Froissart, R., Choisy, M., and Gandon, S. (2013). Evolution of virulence in emerging epidemics. *PLOS Pathogens*, 9(3):e1003209.

Berngruber, T. W., Lion, S., and Gandon, S. (2015). Spatial structure, transmission modes and the evolution of viral exploitation strategies. *PLOS Pathogens*, 11(4):e1004810.

Betts, A., Vasse, M., Kaltz, O., and Hochberg, M. E. (2013). Back to the future: evolving bacteriophages to increase their effectiveness against the pathogen Pseudomonas aeruginosa PAO1. *Evolutionary Applications*, 6(7):1054–1063.

Bewick, S., Staniczenko, P. P. A., Li, B., Karig, D. K., and Fagan, W. F. (2017). Invasion speeds in microbial systems with toxin production and quorum sensing. *Journal of Theoretical Biology*, 420:290–303.

Blanchard, A. E., Liao, C., and Lu, T. (2016). An ecological understanding of Quorum Sensing-controlled bacteriocin synthesis. *Cellular and Molecular Bioengineering*, 9(3):443–454.

Blanquart, F., Grabowski, M. K., Herbeck, J., Nalugoda, F., Serwadda, D., Eller, M. A., Robb, M. L., Gray, R., Kigozi, G., Laeyendecker, O., Lythgoe, K. A., Nakigozi, G., Quinn, T. C., Reynolds, S. J., Wawer, M. J., and Fraser, C. (2016). A transmission-virulence evolutionary trade-off explains attenuation of HIV-1 in Uganda. *eLife*, 5:e20492.

Boerlijst, M. C. and Hogeweg, P. (1991a). Self-structuring and selection: spiral waves as a substrate for evolution. *Artificial life II*, Proceedings Volume X:255–276.

Boerlijst, M. C. and Hogeweg, P. (1991b). Spiral wave structure in pre-biotic evolution: Hypercycles stable against parasites. *Physica D: Nonlinear Phenomena*, 48(1):17–28.

Bollback, J. P. and Huelsenbeck, J. P. (2007). Clonal interference is alleviated by high mutation rates in large populations. *Molecular Biology and Evolution*, 24(6):1397–1406.

Bondy-Denomy, J., Qian, J., Westra, E. R., Buckling, A., Guttman, D. S., Davidson, A. R., and Maxwell, K. L. (2016). Prophages mediate defense against phage infection through diverse mechanisms. *The ISME Journal*, 10(12):2854–2866.

Boots, M. and Mealor, M. (2007). Local interactions select for lower pathogen infectivity. *Science*, 315(5816):1284–1286.

Boots, M. and Sasaki, A. (1999). 'Small worlds' and the evolution of virulence: infection occurs locally and at a distance. *Proceedings of the Royal Society of London. Series B: Biological Sciences*, 266(1432):1933–1938.

Bossi, L., Fuentes, J. A., Mora, G., and Figueroa-Bossi, N. (2003). Prophage contribution to bacterial population dynamics. *Journal of Bacteriology*, 185(21):6467–6471.

Bottery, M. J., Passaris, I., Dytham, C., Wood, A. J., and van der Woude, M. W. (2019). Spatial organization of expanding bacterial colonies is affected by contact-dependent growth inhibition. *Current Biology*, 29(21):3622–3634.e5.

Bremermann, H. J. and Pickering, J. (1983). A game-theoretical model of parasite virulence. *Journal of Theoretical Biology*, 100(3):411–426.

Broniewski, J. M., Meaden, S., Paterson, S., Buckling, A., and Westra, E. R. (2020). The effect of phage genetic diversity on bacterial resistance evolution. *The ISME Journal*, 14(3):828–836.

Brookfield, J. F. Y. (1998). Quorum Sensing and Group Selection. *Evolution*, 52(5):1263–1269.

Brown, S. P. and Johnstone, R. A. (2001). Cooperation in the dark: signalling and collective action in quorum-sensing bacteria. *Proceedings of the Royal Society of London B: Biological Sciences*, 268(1470):961–965.

Bucci, V., Nadell, C. D., and Xavier, J. B. (2011). The evolution of bacteriocin production in bacterial biofilms. *The American Naturalist*, 178(6):E162–E173.

Bull, J. J., Badgett, M. R., Springman, R., and Molineux, I. J. (2004). Genome properties and the limits of adaptation in bacteriophages. *Evolution*, 58(4):692–701.

Bull, J. J., Cunningham, C. W., Molineux, I. J., Badgett, M. R., and Hillis, D. M. (1993). Experimental molecular evolution of bacteriophage T7. *Evolution*, 47(4):993–1007.

Butaitė, E., Baumgartner, M., Wyder, S., and Kümmerli, R. (2017). Siderophore cheating and cheating resistance shape competition for iron in soil and freshwater Pseudomonas communities. *Nature Communications*, 8(1):414.

Carlson, J. M., Schaefer, M., Monaco, D. C., Batorsky, R., Claiborne, D. T., Prince, J., Deymier, M. J., Ende, Z. S., Klatt, N. R., DeZiel, C. E., Lin, T.-H., Peng, J., Seese, A. M., Shapiro, R., Frater, J., Ndung'u, T., Tang, J., Goepfert, P., Gilmour, J., Price, M. A., Kilembe, W., Heckerman, D., Goulder, P. J. R., Allen, T. M., Allen, S., and Hunter, E. (2014). Selection bias at the heterosexual HIV-1 transmission bottleneck. *Science*, 345(6193):1254031.

Castro-Gonzalez, S., Colomer-Lluch, M., and Serra-Moreno, R. (2018). Barriers for HIV cure: the latent reservoir. *AIDS Research and Human Retroviruses*, 34(9):739–759.

Chao, L. and Levin, B. R. (1981). Structured habitats and the evolution of anticompetitor toxins in bacteria. *Proceedings of the National Academy of Sciences*, 78(10):6324–6328.

Chomont, N., El-Far, M., Ancuta, P., Trautmann, L., Procopio, F. A., Yassine-Diab, B., Boucher, G., Boulassel, M.-R., Ghattas, G., Brenchley, J. M., Schacker, T. W., Hill, B. J., Douek, D. C., Routy, J.-P., Haddad, E. K., and Sékaly, R.-P. (2009). HIV reservoir size and persistence are driven by T cell survival and homeostatic proliferation. *Nature Medicine*, 15(8):893–900.

Chuang, J. S., Rivoire, O., and Leibler, S. (2009). Simpson's paradox in a synthetic microbial system. *Science*, 323(5911):272–275.

Chun, T. W., Carruth, L., Finzi, D., Shen, X., DiGiuseppe, J. A., Taylor, H., Hermankova, M., Chadwick, K., Margolick, J., Quinn, T. C., Kuo, Y. H., Brookmeyer, R., Zeiger, M. A., Barditch-Crovo, P., and Siliciano, R. F. (1997). Quantification of latent tissue reservoirs and total body viral load in HIV-1 infection. *Nature*, 387(6629):183–188.

Chun, T. W., Engel, D., Berrey, M. M., Shea, T., Corey, L., and Fauci, A. S. (1998a). Early establishment of a pool of latently infected, resting CD4(+) T cells during primary HIV-1 infection. *Proceedings of the National Academy of Sciences*, 95(15):8869–8873.

Chun, T. W., Engel, D., Mizell, S. B., Ehler, L. A., and Fauci, A. S. (1998b). Induction of HIV-1 replication in latently infected CD4+ T cells using a combination of cytokines. *The Journal of Experimental Medicine*, 188(1):83–91.

Chun, T.-W. and Fauci, A. S. (2012). HIV reservoirs: pathogenesis and obstacles to viral eradication and cure. *AIDS*, 26(10):1261–1268.

Claverys, J.-P. and Håvarstein, L. S. (2007). Cannibalism and fratricide: mechanisms and raisons d'être. *Nature Reviews Microbiology*, 5(3):219–229.

Cohn, L. B., Silva, I. T., Oliveira, T. Y., Rosales, R. A., Parrish, E. H., Learn, G. H., Hahn, B. H., Czartoski, J. L., McElrath, M. J., Lehmann, C., Klein, F., Caskey, M., Walker, B. D., Siliciano, J. D., Siliciano, R. F., Jankovic, M., and Nussenzweig, M. C. (2015). HIV-1 integration landscape during latent and active infection. *Cell*, 160(3):420–432.

Colizzi, E. S. and Hogeweg, P. (2016). High cost enhances cooperation through the interplay between evolution and self-organisation. *BMC Evolutionary Biology*, 16(1):31.

Coombs, D., Gilchrist, M. A., and Ball, C. L. (2007). Evaluating the importance of within- and between-host selection pressures on the evolution of chronic pathogens. *Theoretical Population Biology*, 72(4):576–591.

Cornforth, D. M. and Foster, K. R. (2013). Competition sensing: the social side of bacterial stress responses. *Nature Reviews Microbiology*, 11(4):285–293.

Cortes, M. G., Krog, J., and Balázsi, G. (2019). Optimality of the spontaneous prophage induction rate. *Journal of Theoretical Biology*, 483:110005.

Cressler, C. E., McLeod, D. V., Rozins, C., van den Hoogen, J., and Day, T. (2016). The adaptive evolution of virulence: a review of theoretical predictions and empirical tests. *Parasitology*, 143(7):915–930.

Cuevas, J. M., Geller, R., Garijo, R., López-Aldeguer, J., and Sanjuán, R. (2015). Extremely high mutation rate of HIV-1 in vivo. *PLoS Biology*, 13(9):e1002251.

Czárán, T. and Hoekstra, R. F. (2007). A spatial model of the evolution of quorum sensing regulating bacteriocin production. *Behavioral Ecology*, 18(5):866–873.

Czárán, T. and Hoekstra, R. F. (2009). Microbial communication, cooperation and cheating: Quorum Sensing drives the evolution of cooperation in bacteria. *PLoS ONE*, 4(8):e6655.

Czárán, T. L., Hoekstra, R. F., and Pagie, L. (2002). Chemical warfare between microbes promotes biodiversity. *Proceedings of the National Academy of Sciences*, 99(2):786–790.

Dal Co, A., van Vliet, S., Kiviet, D. J., Schlegel, S., and Ackermann, M. (2020). Short-range interactions govern the dynamics and functions of microbial communities. *Nature Ecology & Evolution*, 4(3):366–375.

Damuth, J. and Heisler, I. L. (1988). Alternative formulations of multilevel selection. *Biology and Philosophy*, 3(4):407–430.

Darch, S. E., West, S. A., Winzer, K., and Diggle, S. P. (2012). Density-dependent fitness benefits in quorum-sensing bacterial populations. *Proceedings of the National Academy of Sciences*, 109(21):8259–8263.

Day, T. and Bonduriansky, R. (2011). A unified approach to the evolutionary consequences of genetic and nongenetic inheritance. *The American Naturalist*, 178(2):E18–E36.

Díaz-Muñoz, S. L., Sanjuán, R., and West, S. (2017). Sociovirology: conflict, cooperation, and communication among viruses. *Cell Host & Microbe*, 22(4):437–441.

de Boer, R. J. and Perelson, A. S. (1998). Target cell limited and immune control models of HIV infection: a comparison. *Journal of Theoretical Biology*, 190(3):201–214.

de Paepe, M. and Taddei, F. (2006). Viruses' Life History: Towards a Mechanistic Basis of a Trade-Off between Survival and Reproduction among Phages. *PLOS Biology*, 4(7):e193.

de Roode, J. C., Pansini, R., Cheesman, S. J., Helinski, M. E. H., Huijben, S., Wargo, A. R., Bell, A. S., Chan, B. H. K., Walliker, D., and Read, A. F. (2005). Virulence and competitive ability in genetically diverse malaria infections. *Proceedings of the National Academy of Sciences*, 102(21):7624–7628.

de Vos, D., de Chial, M., Cochez, C., Jansen, S., Tümmler, B., Meyer, J.-M., and Cornelis, P. (2001). Study of pyoverdine type and production by Pseudomonas aeruginosa isolated from cystic fibrosis patients: prevalence of type II pyoverdine isolates and accumulation of pyoverdine-negative mutations. *Archives of Microbiology*, 175(5):384–388.

de Wolf, F., Spijkerman, I., Schellekens, P. T., Langendam, M., Kuiken, C., Bakker, M., Roos, M., Coutinho, R., Miedema, F., and Goudsmit, J. (1997). AIDS prognosis based on HIV-1 RNA, CD4+ T-cell count and function: markers with reciprocal predictive value over time after seroconversion. *AIDS*, 11(15):1799–1806.

Deymier, M. J., Ende, Z., Fenton-May, A. E., Dilernia, D. A., Kilembe, W., Allen, S. A., Borrow, P., and Hunter, E. (2015). Heterosexual transmission of subtype C HIV-1 selects consensus-like variants without increased replicative capacity or Interferon-alpha resistance. *PLoS Pathogens*, 11(9):e1005154.

Diekmann, O. and Heesterbeek, J. (2000). *Mathematical epidemiology of infectious diseases: model building, analysis and interpretation*. Wiley, Oxford, UK.

Diggle, S., Griffin, A., Campbell, G., and West, S. (2007). Cooperation and conflict in quorum-sensing bacterial populations. *Nature*, 450(7168):411–414.

Doekes, H. M., de Boer, R. J., and Hermsen, R. (2019). Toxin production spontaneously becomes regulated by local cell density in evolving bacterial populations. *PLOS Computational Biology*, 15(8):e1007333.

Doermann, A. H. (1948). Lysis and lysis inhibition with Escherichia coli bacteriophage. *Journal of Bacteriology*, 55(2):257–276.

Drescher, K., Nadell, C. D., Stone, H. A., Wingreen, N. S., and Bassler, B. L. (2014). Solutions to the public goods dilemma in bacterial biofilms. *Current Biology*, 24(1):50–55.

Durrett, R. and Levin, S. (1997). Allelopathy in spatially distributed populations. *Journal of Theoretical Biology*, 185(2):165–171.

Dykes, G. A. and Hastings, J. W. (1997). Selection and fitness in bacteriocin–producing bacteria. *Proceedings of the Royal Society of London. Series B: Biological Sciences*, 264(1382):683–687.

Eck, J. L., Stump, S. M., Delavaux, C. S., Mangan, S. A., and Comita, L. S. (2019). Evidence of within-species specialization by soil microbes and the implications for plant community diversity. *Proceedings of the National Academy of Sciences*, 116(15):7371–7376.

Eigen, M. (1971). Selforganization of matter and the evolution of biological macromolecules. *Die Naturwissenschaften*, 58(10):465–523.

Eisele, E. and Siliciano, R. F. (2012). Redefining the viral reservoirs that prevent HIV-1 eradication. *Immunity*, 37(3):377–388.

Erez, Z., Steinberger-Levy, I., Shamir, M., Doron, S., Stokar-Avihail, A., Peleg, Y., Melamed, S., Leavitt, A., Savidor, A., Albeck, S., Amitai, G., and Sorek, R. (2017). Communication between viruses guides lysis–lysogeny decisions. *Nature*, 541(7638):488–493.

Eriksson, S., Graf, E. H., Dahl, V., Strain, M. C., Yukl, S. A., Lysenko, E. S., Bosch, R. J., Lai, J., Chioma, S., Emad, F., Abdel-Mohsen, M., Hoh, R., Hecht, F., Hunt, P., Somsouk, M., Wong, J., Johnston, R., Siliciano, R. F., Richman, D. D., O'Doherty, U., Palmer, S., Deeks, S. G., and Siliciano, J. D. (2013). Comparative Analysis of Measures of Viral Reservoirs in HIV-1 Eradication Studies. *PLoS Pathogens*, 9(2):e1003174.

Esmail, H., Barry, C. E., Young, D. B., and Wilkinson, R. J. (2014). The ongoing challenge of latent tuberculosis. *Philosophical Transactions of the Royal Society B: Biological Sciences*, 369(1645):20130437.

Estrela, S., Libby, E., Van Cleve, J., Débarre, F., Deforet, M., Harcombe, W. R., Peña, J., Brown, S. P., and Hochberg, M. E. (2019). Environmentally Mediated Social Dilemmas. *Trends in Ecology & Evolution*, 34(1):6–18.

Finzi, D., Hermankova, M., Pierson, T., Carruth, L. M., Buck, C., Chaisson, R. E., Quinn, T. C., Chadwick, K., Margolick, J., Brookmeyer, R., Gallant, J., Markowitz, M., Ho, D. D., Richman, D. D., and Siliciano, R. F. (1997). Identification of a reservoir for HIV-1 in patients on highly active antiretroviral therapy. *Science*, 278(5341):1295–1300.

Fletcher, J. A. and Doebeli, M. (2009). A simple and general explanation for the evolution of altruism. *Proceedings of the Royal Society B: Biological Sciences*, 276(1654):13–19.

Frank, S. A. (2012). Natural selection. IV. The Price equation. *Journal of Evolutionary Biology*, 25(6):1002–1019.

Fraser, C., Hollingsworth, T. D., Chapman, R., de Wolf, F., and Hanage, W. P. (2007). Variation in HIV-1 set-point viral load: epidemiological analysis and an evolutionary hypothesis. *Proceedings of the National Academy of Sciences*, 104(44):17441–17446.

Fraser, C., Lythgoe, K., Leventhal, G. E., Shirreff, G., Hollingsworth, T. D., Alizon, S., and Bonhoeffer, S. (2014). Virulence and pathogenesis of HIV-1 infection: An evolutionary perspective. *Science*, 343(6177):1243727.

Frigo, M. and Johnson, S. (2005). The design and implementation of FFTW3. *Proceedings of the IEEE*, 93(2):216–231.

Gama, J. A., Reis, A. M., Domingues, I., Mendes-Soares, H., Matos, A. M., and Dionisio, F. (2013). Temperate bacterial viruses as double-edged swords in bacterial warfare. *PLOS ONE*, 8(3):e59043.

Gandon, S. (2016). Why be temperate: lessons from bacteriophage lambda. *Trends in Microbiology*, 24(5):356–365.

Ganusov, V. V., Goonetilleke, N., Liu, M. K. P., Ferrari, G., Shaw, G. M., McMichael, A. J., Borrow, P., Korber, B. T., and Perelson, A. S. (2011). Fitness costs and diversity of the cytotoxic T lymphocyte (CTL) response determine the rate of CTL escape during acute and chronic phases of HIV infection. *Journal of Virology*, 85(20):10518–10528.

Gao, F., Chen, Y., Levy, D. N., Conway, J. A., Kepler, T. B., and Hui, H. (2004). Unselected mutations in the Human Immunodeficiency Virus type 1 genome are mostly nonsynonymous and often deleterious. *Journal of Virology*, 78(5):2426–2433.

García-Bayona, L. and Comstock, L. E. (2018). Bacterial antagonism in host-associated microbial communities. *Science*, 361(6408):eaat2456.

Gardner, A. (2020). Price's equation made clear. *Philosophical Transactions of the Royal Society B: Biological Sciences*, 375(1797):20190361.

Gardner, A. and West, S. A. (2004). Spite and the scale of competition. *Journal of Evolutionary Biology*, 17(6):1195–1203.

Gardner, A., West, S. A., and Buckling, A. (2004). Bacteriocins, spite and virulence. *Proceedings of the Royal Society of London B: Biological Sciences*, 271(1547):1529–1535.

Ghazaryan, L., Soares, M. I. M., and Gillor, O. (2014). Auto-regulation of DNA degrading bacteriocins: molecular and ecological aspects. *Antonie van Leeuwenhoek*, 105(5):823–834.

Ghosh, D., Roy, K., Williamson, K. E., Srinivasiah, S., Wommack, K. E., and Radosevich, M. (2009). Acyl-homoserine lactones can induce virus production in lysogenic bacteria: an alternative paradigm for prophage induction. *Applied and Environmental Microbiology*, 75(22):7142–7152.

Ghoul, M. and Mitri, S. (2016). The ecology and evolution of microbial competition. *Trends in Microbiology*, 24(10):833–845.

Gilchrist, M. A. and Sasaki, A. (2002). Modeling host–parasite coevolution: a nested approach based on mechanistic models. *Journal of Theoretical Biology*, 218(3):289–308.

Golding, I., Coleman, S., Nguyen, T. V. P., and Yao, T. (2019). Decision making by temperate phages. In *Reference Module in Life Sciences*. Elsevier.

Gonzalez, D. and Mavridou, D. A. I. (2019). Making the best of aggression: the many dimensions of bacterial toxin regulation. *Trends in Microbiology*, 27(11):897–905.

Goodnight, C., Rauch, E., Sayama, H., Aguiar, M. A. M. D., Baranger, M., and Bar-Yam, Y. (2008). Evolution in spatial predator–prey models and the "prudent predator": The inadequacy of steady-state organism fitness and the concept of individual and group selection. *Complexity*, 13(5):23–44.

Granato, E. T., Meiller-Legrand, T. A., and Foster, K. R. (2019). The evolution and ecology of bacterial warfare. *Current Biology*, 29(11):R521–R537.

Griffin, A. S., West, S. A., and Buckling, A. (2004). Cooperation and competition in pathogenic bacteria. *Nature*, 430(7003):1024–1027.

Hamilton, W. D. (1964). The genetical evolution of social behaviour I & II. *Journal of Theoretical Biology*, 7(1):1–52.

Haraguchi, Y. and Sasaki, A. (2000). The evolution of parasite virulence and transmission rate in a spatially structured population. *Journal of Theoretical Biology*, 203(2):85–96.

Hatano, H., Yukl, S. A., Ferre, A. L., Graf, E. H., Somsouk, M., Sinclair, E., Abdel-Mohsen, M., Liegler, T., Harvill, K., Hoh, R., Palmer, S., Bacchetti, P., Hunt, P. W., Martin, J. N., McCune, J. M., Tracy, R. P., Busch, M. P., O'Doherty, U., Shacklett, B. L., Wong, J. K., and Deeks, S. G. (2013). Prospective antiretroviral treatment of asymptomatic, HIV-1 infected controllers. *PLoS Pathogens*, 9(10):e1003691.

Heilmann, S., Sneppen, K., and Krishna, S. (2010). Sustainability of virulence in a phage-bacterial ecosystem. *Journal of Virology*, 84(6):3016–3022.

Hense, B. A. and Schuster, M. (2015). Core Principles of Bacterial Autoinducer Systems. *Microbiology and Molecular Biology Reviews*, 79(1):153–169.

Herbeck, J. T., Rolland, M., Liu, Y., McLaughlin, S., McNevin, J., Zhao, H., Wong, K., Stoddard, J. N., Raugi, D., Sorensen, S., Genowati, I., Birditt, B., McKay, A., Diem, K., Maust, B. S., Deng, W., Collier, A. C., Stekler, J. D., McElrath, M. J., and Mullins, J. I. (2011). Demographic processes affect HIV-1 evolution in primary infection before the onset of selective processes. *Journal of Virology*, 85(15):7523–7534.

Hershey, A. D. (1946). Mutation of bacteriophage with respect to type of plaque. *Genetics*, 31(6):620–640.

Hibbing, M. E., Fuqua, C., Parsek, M. R., and Peterson, S. B. (2010). Bacterial competition: surviving and thriving in the microbial jungle. *Nature Reviews Microbiology*, 8(1):15–25.

Ho, Y.-C., Shan, L., Hosmane, N. N., Wang, J., Laskey, S. B., Rosenbloom, D. I. S., Lai, J., Blankson, J. N., Siliciano, J. D., and Siliciano, R. F. (2013). Replication-competent noninduced proviruses in the latent reservoir increase barrier to HIV-1 cure. *Cell*, 155(3):540–551.

Hogeweg, P. (1994). Multilevel evolution: replicators and the evolution of diversity. *Physica D: Nonlinear Phenomena*, 75(1):275–291.

Hutchison, C. A. and Sinsheimer, R. L. (1971). Requirement of protein synthesis for bacteriophage phiX174 superinfection exclusion. *Journal of Virology*, 8(1):121–124.

Hynes, A. P. and Moineau, S. (2017). Phagebook: The Social Network. *Molecular Cell*, 65(6):963–964.

Ibáñez, A., Puig, T., Elias, J., Clotet, B., Ruiz, L., and Martínez, M. A. (1999). Quantification of integrated and total HIV-1 DNA after long-term highly active antiretroviral therapy in HIV-1-infected patients. *AIDS*, 13(9):1045–1049.

Immonen, T. T., Conway, J. M., Romero-Severson, E. O., Perelson, A. S., and Leitner, T. (2015). Recombination enhances HIV-1 envelope diversity by facilitating the survival of latent genomic fragments in the plasma virus population. *PLoS Computational Biology*, 11(12):e1004625.

Immonen, T. T. and Leitner, T. (2014). Reduced evolutionary rates in HIV-1 reveal extensive latency periods among replicating lineages. *Retrovirology*, 11(1):81.

Inglis, R. F., Scanlan, P., and Buckling, A. (2016). Iron availability shapes the evolution of bacteriocin resistance in Pseudomonas aeruginosa. *The ISME Journal*, 10(8):2060–2066.

Jetzt, A. E., Yu, H., Klarmann, G. J., Ron, Y., Preston, B. D., and Dougherty, J. P. (2000). High rate of recombination throughout the human immunodeficiency virus type 1 genome. *Journal of Virology*, 74(3):1234–1240.

Jimenez, J. C. and Federle, M. J. (2014). Quorum sensing in group A Streptococcus. *Frontiers in Cellular and Infection Microbiology*, 4:127.

Johnson, C. R. and Boerlijst, M. C. (2002). Selection at the level of the community: the importance of spatial structure. *Trends in Ecology & Evolution*, 17(2):83–90.

Kawecki, T. J., Lenski, R. E., Ebert, D., Hollis, B., Olivieri, I., and Whitlock, M. C. (2012). Experimental evolution. *Trends in Ecology & Evolution*, 27(10):547–560.

Keele, B. F., Giorgi, E. E., Salazar-Gonzalez, J. F., Decker, J. M., Pham, K. T., Salazar, M. G., Sun, C., Grayson, T., Wang, S., Li, H., Wei, X., Jiang, C., Kirchherr, J. L., Gao, F., Anderson, J. A., Ping, L. ., Swanstrom, R., Tomaras, G. D., Blattner, W. A., Goepfert, P. A., Kilby, J. M., Saag, M. S., Delwart, E. L., Busch, M. P., Cohen, M. S., Montefiori, D. C., Haynes, B. F., Gaschen, B., Athreya, G. S., Lee, H. Y., Wood, N., Seoighe, C., Perelson, A. S., Bhattacharya, T., Korber, B. T., Hahn, B. H., and Shaw, G. M. (2008). Identification and characterization of transmitted and early founder virus envelopes in primary HIV-1 infection. *Proceedings of the National Academy of Sciences*, 105(21):7552–7557.

Kelly, J. K. (1996). Replication rate and evolution in the human immunodeficiency virus. *Journal of Theoretical Biology*, 180(4):359–364.

Kelly, J. K., Williamson, S., Orive, M. E., Smith, M. S., and Holt, R. D. (2003). Linking dynamical and population genetic models of persistent viral infection. *The American Naturalist*, 162(1):14–28.

Kerr, B., Neuhauser, C., Bohannan, B. J. M., and Dean, A. M. (2006). Local migration promotes competitive restraint in a host–pathogen 'tragedy of the commons'. *Nature*, 442(7098):75–78.

Kerr, B., Riley, M. A., Feldman, M. W., and Bohannan, B. J. M. (2002). Local dispersal promotes biodiversity in a real-life game of rock–paper–scissors. *Nature*, 418(6894):171–174.

Killingback, T., Doebeli, M., and Knowlton, N. (1999). Variable investment, the Continuous Prisoner's Dilemma, and the origin of cooperation. *Proceedings of the Royal Society B: Biological Sciences*, 266(1430):1723–1728.

Kim, H. and Perelson, A. S. (2006). Viral and latent reservoir persistence in HIV-1–infected patients on therapy. *PLoS Computational Biology*, 2(10):e135.

Kinchington, P. R., Leger, A. J. S., Guedon, J.-M. G., and Hendricks, R. L. (2012). Herpes simplex virus and varicella zoster virus, the house guests who never leave. *Herpesviridae*, 3(1):5.

Kirkup, B. C. and Riley, M. A. (2004). Antibiotic-mediated antagonism leads to a bacterial game of rock–paper–scissors *in vivo*. *Nature*, 428(6981):412–414.

Klaenhammer, T. R. (1988). Bacteriocins of lactic acid bacteria. *Biochimie*, 70(3):337–349.

Kleerebezem, M. and Quadri, L. E. (2001). Peptide pheromone-dependent regulation of antimicrobial peptide production in Gram-positive bacteria: a case of multicellular behavior. *Peptides*, 22(10):1579–1596.

Kliem, M. and Dreiseikelmann, B. (1989). The superimmunity gene sim of bacteriophage P1 causes superinfection exclusion. *Virology*, 171(2):350–355.

Kümmerli, R., Griffin, A. S., West, S. A., Buckling, A., and Harrison, F. (2009). Viscous medium promotes cooperation in the pathogenic bacterium Pseudomonas aeruginosa. *Proceedings of the Royal Society B: Biological Sciences*, 276(1672):3531–3538.

Koelsch, K. K., Liu, L., Haubrich, R., May, S., Havlir, D., Günthard, H. F., Ignacio, C. C., Campos-Soto, P., Little, S. J., Shafer, R., Robbins, G. K., D'Aquila, R. T., Kawano, Y., Young, K., Dao, P., Spina, C. A., Richman, D. D., and Wong, J. K. (2008). Dynamics of total, linear nonintegrated, and integrated HIV-1 DNA in vivo and in vitro. *The Journal of Infectious Diseases*, 197(3):411–419.

Korgaonkar, A. K. and Whiteley, M. (2011). Pseudomonas aeruginosa enhances production of an antimicrobial in response to N-acetylglucosamine and peptidoglycan. *Journal of Bacteriology*, 193(4):909–917.

Kourilsky, P. (1973). Lysogenization by bacteriophage lambda. *Molecular and General Genetics*, 122(2):183–195.

Kouyos, R. D., von Wyl, V., Hinkley, T., Petropoulos, C. J., Haddad, M., Whitcomb, J. M., Böni, J., Yerly, S., Cellerai, C., Klimkait, T., Günthard, H. F., Bonhoeffer, S., and Swiss HIV Cohort Study (2011). Assessing predicted HIV-1 replicative capacity in a clinical setting. *PLoS Pathogens*, 7(11):e1002321.

Kramer, J., Özkaya, z., and Kümmerli, R. (2020). Bacterial siderophores in community and host interactions. *Nature Reviews Microbiology*, 18(3):152–163.

Krin, E., Chakroun, N., Turlin, E., Givaudan, A., Gaboriau, F., Bonne, I., Rousselle, J.-C., Frangeul, L., Lacroix, C., Hullo, M.-F., Marisa, L., Danchin, A., and Derzelle, S. (2006). Pleiotropic role of Quorum-Sensing Autoinducer 2 in Photorhabdus luminescens. *Applied and Environmental Microbiology*, 72(10):6439–6451.

Laganenka, L., Sander, T., Lagonenko, A., Chen, Y., Link, H., and Sourjik, V. (2019). Quorum Sensing and metabolic state of the host control lysogeny-lysis switch of bacteriophage T1. *mBio*, 10(5):e01884–19.

Le Galliard, J.-F., Ferrière, R., and Dieckmann, U. (2003). The adaptive dynamics of altruism in spatially heterogeneous populations. *Evolution*, 57(1):1–17.

Lehmann, L. and Keller, L. (2006). The evolution of cooperation and altruism – a general framework and a classification of models. *Journal of Evolutionary Biology*, 19(5):1365–1376.

Lemey, P., Kosakovsky Pond, S. L., Drummond, A. J., Pybus, O. G., Shapiro, B., Barroso, H., Taveira, N., and Rambaut, A. (2007). Synonymous substitution rates predict HIV disease progression as a result of underlying replication dynamics. *PLoS Computational Biology*, 3(2):e29.

Lenski, R. E., Rose, M. R., Simpson, S. C., and Tadler, S. C. (1991). Long-term experimental evolution in Escherichia coli. I. Adaptation and divergence during 2,000 generations. *The American Naturalist*, 138(6):1315–1341.

LeRoux, M., Peterson, S. B., and Mougous, J. D. (2015). Bacterial danger sensing. *Journal of Molecular Biology*, 427(23):3744–3753.

Levin, B. R. and Bull, J. J. (1994). Short-sighted evolution and the virulence of pathogenic microorganisms. *Trends in Microbiology*, 2(3):76–81.

Levin, B. R., Perrot, V., and Walker, N. (2000). Compensatory mutations, antibiotic resistance and the population genetics of adaptive evolution in bacteria. *Genetics*, 154(3):985–997.

Lingappa, J. R., Hughes, J. P., Wang, R. S., Baeten, J. M., Celum, C., Gray, G. E., Stevens, W. S., Donnell, D., Campbell, M. S., Farquhar, C., Essex, M., Mullins, J. I., Coombs, R. W., Rees, H., Corey, L., Wald, A., and Partners in Prevention HSV/HIV Transmission Study Team (2010). Estimating the impact of plasma HIV-1 RNA reductions on heterosexual HIV-1 transmission risk. *PLoS One*, 5(9):e12598.

Lion, S., Jansen, V. A. A., and Day, T. (2011). Evolution in structured populations: beyond the kin versus group debate. *Trends in Ecology & Evolution*, 26(4):193–201.

Lion, S. and van Baalen, M. (2008). Self-structuring in spatial evolutionary ecology. *Ecology Letters*, 11(3):277–295.

Little, J. W., Shepley, D. P., and Wert, D. W. (1999). Robustness of a gene regulatory circuit. *The EMBO Journal*, 18(15):4299–4307.

Lories, B., Roberfroid, S., Dieltjens, L., De Coster, D., Foster, K. R., and Steenackers, H. P. (2020). Biofilm bacteria use stress responses to detect and respond to competitors. *Current Biology*, 30(7):1231–1244.e4.

Lythgoe, K. A., Blanquart, F., Pellis, L., and Fraser, C. (2016). Large variations in HIV-1 viral load explained by shifting-mosaic metapopulation dynamics. *PLoS Biology*, 14(10):e1002567.

Lythgoe, K. A. and Fraser, C. (2012). New insights into the evolutionary rate of HIV-1 at the within-host and epidemiological levels. *Proceedings of the Royal Society B: Biological Sciences*, 279(1741):3367–3375.

Lythgoe, K. A., Gardner, A., Pybus, O. G., and Grove, J. (2017). Short-sighted virus evolution and a germline hypothesis for chronic viral infections. *Trends in Microbiology*, 25(5):336–348.

Lythgoe, K. A., Pellis, L., and Fraser, C. (2013). Is HIV short-sighted? Insights from a multistrain nested model. *Evolution*, 67(10):2769–2782.

Makarova, K., Slesarev, A., Wolf, Y., Sorokin, A., Mirkin, B., Koonin, E., Pavlov, A., Pavlova, N., Karamychev, V., Polouchine, N., Shakhova, V., Grigoriev, I., Lou, Y., Rohksar, D., Lucas, S., Huang, K., Goodstein, D. M., Hawkins, T., Plengvidhya, V., Welker, D., Hughes, J., Goh, Y., Benson, A., Baldwin, K., Lee, J.-H., Díaz-Muñiz, I., Dosti, B., Smeianov, V., Wechter, W., Barabote, R., Lorca, G., Altermann, E., Barrangou, R., Ganesan, B., Xie, Y., Rawsthorne, H., Tamir, D., Parker, C., Breidt, F., Broadbent, J., Hutkins, R., O'Sullivan, D., Steele, J., Unlu, G., Saier, M., Klaenhammer, T., Richardson, P., Kozyavkin, S., Weimer, B., and Mills, D. (2006). Comparative genomics of the lactic acid bacteria. *Proceedings of the National Academy of Sciences*, 103(42):15611–15616.

Maldarelli, F., Kearney, M., Palmer, S., Stephens, R., Mican, J., Polis, M. A., Davey, R. T., Kovacs, J., Shao, W., Rock-Kress, D., Metcalf, J. A., Rehm, C., Greer, S. E., Lucey, D. L., Danley, K., Alter, H., Mellors, J. W., and Coffin, J. M. (2013). HIV populations are large and accumulate high genetic diversity in a nonlinear fashion. *Journal of Virology*, 87(18):10313–10323.

Maldarelli, F., Wu, X., Su, L., Simonetti, F. R., Shao, W., Hill, S., Spindler, J., Ferris, A. L., Mellors, J. W., Kearney, M. F., Coffin, J. M., and Hughes, S. H. (2014). HIV latency. Specific HIV integration sites are linked to clonal expansion and persistence of infected cells. *Science*, 345(6193):179–183.

Maldonado-Barragán, A. and West, S. A. (2020). The cost and benefit of quorum sensing-controlled bacteriocin production in Lactobacillus plantarum. *Journal of Evolutionary Biology*, 33(1):101–111.

Mansky, L. M. and Temin, H. M. (1995). Lower in vivo mutation rate of human immunodeficiency virus type 1 than that predicted from the fidelity of purified reverse transcriptase. *Journal of Virology*, 69(8):5087–5094.

Marshall, J. A. R. (2011). Group selection and kin selection: Formally equivalent approaches. *Trends in Ecology and Evolution*, 26(7):325–332.

Maslov, S. and Sneppen, K. (2015). Well-temperate phage: optimal bet-hedging against local environmental collapses. *Scientific Reports*, 5:10523.

Mavridou, D. A. I., Gonzalez, D., Kim, W., West, S. A., and Foster, K. R. (2018). Bacteria use collective behavior to generate diverse combat strategies. *Current Biology*, 28(3):345–355.e4.

McAllister, W. T. and Barrett, C. L. (1977). Superinfection exclusion by bacteriophage T7. *Journal of Virology*, 24(2):709–711.

Mellors, J. W., Rinaldo, C. R., Gupta, P., White, R. M., Todd, J. A., and Kingsley, L. A. (1996). Prognosis in HIV-1 infection predicted by the quantity of virus in plasma. *Science*, 272(5265):1167–1170.

Mens, H., Kearney, M., Wiegand, A., Shao, W., Schønning, K., Gerstoft, J., Obel, N., Maldarelli, F., Mellors, J. W., Benfield, T., and Coffin, J. M. (2010). HIV-1 continues to replicate and evolve in patients with natural control of HIV infection. *Journal of Virology*, 84(24):12971–12981.

Merritt, J., Kreth, J., Shi, W., and Qi, F. (2005). LuxS controls bacteriocin production in Streptococcus mutans through a novel regulatory component. *Molecular Microbiology*, 57(4):960–969.

Mideo, N., Alizon, S., and Day, T. (2008). Linking within- and between-host dynamics in the evolutionary epidemiology of infectious diseases. *Trends in Ecology and Evolution*, 23(9):511–517.

Miller, M. B. and Bassler, B. L. (2001). Quorum Sensing in bacteria. *Annual Review of Microbiology*, 55(1):165–199.

Millet, Y. A., Alvarez, D., Ringgaard, S., Andrian, U. H. v., Davis, B. M., and Waldor, M. K. (2014). Insights into Vibrio cholerae intestinal colonization from monitoring fluorescently labeled bacteria. *PLOS Pathogens*, 10(10):e1004405.

Mitri, S., Clarke, E., and Foster, K. R. (2016). Resource limitation drives spatial organization in microbial groups. *The ISME Journal*, 10(6):1471–1482.

Mittler, J. E. (1996). Evolution of the genetic switch in temperate bacteriophage. I. Basic theory. *Journal of Theoretical Biology*, 179(2):161–172.

Monod, J. (1949). The growth of bacterial cultures. *Annual Review of Microbiology*, 3(1):371–394.

Mukherjee, S. and Bassler, B. L. (2019). Bacterial quorum sensing in complex and dynamically changing environments. *Nature Reviews Microbiology*, 17:371–382.

Nadeem, A. and Wahl, L. M. (2017). Prophage as a genetic reservoir: Promoting diversity and driving innovation in the host community. *Evolution*, 71(8):2080–2089.

Nadell, C. D., Drescher, K., and Foster, K. R. (2016). Spatial structure, cooperation and competition in biofilms. *Nature Reviews Microbiology*, 14(9):589–600.

Nadell, C. D., Foster, K. R., and Xavier, J. B. (2010). Emergence of spatial structure in cell groups and the evolution of cooperation. *PLoS Computational Biology*, 6(3):e1000716.

Nadell, C. D., Xavier, J. B., and Foster, K. R. (2009). The sociobiology of biofilms. *FEMS Microbiology Reviews*, 33(1):206–224.

Nadell, C. D., Xavier, J. B., Levin, S. A., and Foster, K. R. (2008). The evolution of Quorum Sensing in bacterial biofilms. *PLOS Biology*, 6(1):e14.

Narisawa, N., Haruta, S., Arai, H., Ishii, M., and Igarashi, Y. (2008). Coexistence of antibiotic-producing and antibiotic-sensitive bacteria in biofilms is mediated by resistant bacteria. *Applied Environmental Microbiology*, 74(12):3887–3894.

Nealson, K. H., Platt, T., and Hastings, J. W. (1970). Cellular control of the synthesis and activity of the bacterial Luminescent System 1. *Journal of Bacteriology*, 104(1):313–322.

Ngo-Giang-Huong, N., Deveau, C., Da Silva, I., Pellegrin, I., Venet, A., Harzic, M., Sinet, M., Delfraissy, J. F., Meyer, L., Goujard, C., Rouzioux, C., and Frnech PRIMO Cohort Study Group (2001). Proviral HIV-1 DNA in subjects followed since primary HIV-1 infection who suppress plasma viral load after one year of highly active antiretroviral therapy. *AIDS*, 15(6):665–673.

Nowak, M. A. and May, R. M. (1992). Evolutionary games and spatial chaos. *Nature*, 359(6398):826–829.

Okasha, S. (2006). *Evolution and the Levels of Selection*. Oxford University Press.

Perelson, A. S., Neumann, A. U., Markowitz, M., Leonard, J. M., and Ho, D. D. (1996). HIV-1 dynamics in vivo: virion clearance rate, infected cell life-span, and viral generation time. *Science*, 271(5255):1582–1586.

Perelson, A. S. and Ribeiro, R. M. (2013). Modeling the within-host dynamics of HIV infection. *BMC Biology*, 11(1):96.

Picioreanu, C., Loosdrecht, M. C. M. V., and Heijnen, J. J. (2000). Effect of diffusive and convective substrate transport on biofilm structure formation: A two-dimensional modeling study. *Biotechnology and Bioengineering*, 69(5):504–515.

Platt, T. G. and Fuqua, C. (2010). What's in a name? The semantics of quorum sensing. *Trends in Microbiology*, 18(9):383–387.

Popat, R., Cornforth, D. M., McNally, L., and Brown, S. P. (2015). Collective sensing and collective responses in quorum-sensing bacteria. *Journal of The Royal Society Interface*, 12(103):20140882.

Price, G. R. (1970). Selection and covariance. *Nature*, 227:520–521.

Price, G. R. (1972). Extension of covariance selection mathematics. *Annals of Human Genetics*, 35:485–490.

Prince, J. L., Claiborne, D. T., Carlson, J. M., Schaefer, M., Yu, T., Lahki, S., Prentice, H. A., Yue, L., Vishwanathan, S. A., Kilembe, W., Goepfert, P., Price, M. A., Gilmour, J., Mulenga, J., Farmer, P., Derdeyn, C. A., Tang, J., Heckerman, D., Kaslow, R. A., Allen, S. A., and Hunter, E. (2012). Role of transmitted Gag CTL polymorphisms in defining replicative capacity and early HIV-1 pathogenesis. *PLoS Pathogens*, 8(11):e1003041.

Pugsley, A. P. (1983). Autoinduced synthesis of colicin E2. *Molecular and General Genetics*, 190(3):379–383.

Puigbò, P., Lobkovsky, A. E., Kristensen, D. M., Wolf, Y. I., and Koonin, E. V. (2014). Genomes in turmoil: quantification of genome dynamics in prokaryote supergenomes. *BMC Biology*, 12(1):66.

Pybus, O. G. and Rambaut, A. (2009). Evolutionary analysis of the dynamics of viral infectious disease. *Nature Reviews Genetics*, 10(8):540–550.

Qi, F., Merritt, J., Lux, R., and Shi, W. (2004). Inactivation of the ciaH gene in Streptococcus mutans diminishes mutacin production and competence development, alters sucrose-dependent biofilm formation, and reduces stress tolerance. *Infection and Immunity*, 72(8):4895–4899.

Queller, D. C. (1994). Genetic relatedness in viscous populations. *Evolutionary Ecology*, 8(1):70–73.

Quinn, T. C., Wawer, M. J., Sewankambo, N., Serwadda, D., Li, C., Wabwire-Mangen, F., Meehan, M. O., Lutalo, T., and Gray, R. H. (2000). Viral load and heterosexual transmission of human immunodeficiency virus type 1. Rakai Project Study Group. *The New England Journal of Medicine*, 342(13):921–929.

Quinones-Mateu, M. E., Ball, S. C., Marozsan, A. J., Torre, V. S., Albright, J. L., Vanham, G., van der Groen, G., Colebunders, R. L., and Arts, E. J. (2000). A dual infection/competition assay shows a correlation between Ex vivo human immunodeficiency virus type 1 fitness and disease progression. *Journal of Virology*, 74(19):9222–9233.

Rainey, P. B. and Travisano, M. (1998). Adaptive radiation in a heterogeneous environment. *Nature*, 394(6688):69–72.

Rand, D. A., Keeling, M., and Wilson, H. B. (1995). Invasion, stability and evolution to criticality in spatially extended, artificial host—pathogen ecologies. *Proceedings of the Royal Society of London. Series B: Biological Sciences*, 259(1354):55–63.

Read, A. F. and Taylor, L. H. (2001). The Ecology of Genetically Diverse Infections. *Science*, 292(5519):1099–1102.

Redd, A. D., Collinson-Streng, A. N., Chatziandreou, N., Mullis, C. E., Laeyendecker, O., Martens, C., Ricklefs, S., Kiwanuka, N., Nyein, P. H., Lutalo, T., Grabowski, M. K., Kong, X., Manucci, J., Sewankambo, N., Wawer, M. J., Gray, R. H., Porcella, S. F., Fauci, A. S., Sagar, M., Serwadda, D., and Quinn, T. C. (2012). Previously transmitted HIV-1 strains are preferentially selected during subsequent sexual transmissions. *The Journal of Infectious Diseases*, 206(9):1433–1442.

Reichenbach, T., Mobilia, M., and Frey, E. (2007). Mobility promotes and jeopardizes biodiversity in rock–paper–scissors games. *Nature*, 448(7157):1046–1049.

Ribeiro, R. M., Qin, L., Chavez, L. L., Li, D., Self, S. G., and Perelson, A. S. (2010). Estimation of the initial viral growth rate and basic reproductive number during acute HIV-1 infection. *Journal of Virology*, 84(12):6096–6102.

Rietkerk, M., Dekker, S. C., de Ruiter, P. C., and van de Koppel, J. (2004). Self-organized patchiness and catastrophic shifts in ecosystems. *Science*, 305(5692):1926–1929.

Riley, M. A. and Wertz, J. E. (2002a). Bacteriocin diversity: ecological and evolutionary perspectives. *Biochimie*, 84(5–6):357–364.

Riley, M. A. and Wertz, J. E. (2002b). Bacteriocins: evolution, ecology, and application. *Annual Review of Microbiology*, 56(1):117–137.

Roberts, H. E., Hurst, J., Robinson, N., Brown, H., Flanagan, P., Vass, L., Fidler, S., Weber, J., Babiker, A., Phillips, R. E., McLean, A. R., Frater, J., and SPARTAC trial investigators (2015). Structured observations reveal slow HIV-1 CTL escape. *PLoS Genetics*, 11(2):e1004914.

Rolfe, M. D., Rice, C. J., Lucchini, S., Pin, C., Thompson, A., Cameron, A. D. S., Alston, M., Stringer, M. F., Betts, R. P., Baranyi, J., Peck, M. W., and Hinton, J. C. D. (2012). Lag Phase is a distinct growth phase that prepares bacteria for exponential growth and involves transient metal accumulation. *Journal of Bacteriology*, 194(3):686–701.

Romani, B. and Allahbakhshi, E. (2017). Underlying mechanisms of HIV-1 latency. *Virus Genes*, 53(3):329–339.

Rong, L. and Perelson, A. S. (2009). Modeling latently infected cell activation: viral and latent reservoir persistence, and viral blips in HIV-infected patients on potent therapy. *PLoS Computational Biology*, 5(10).

Rossmann, F. S., Racek, T., Wobser, D., Puchalka, J., Rabener, E. M., Reiger, M., Hendrickx, A. P. A., Diederich, A.-K., Jung, K., Klein, C., and Huebner, J. (2015). Phage-mediated

dispersal of biofilm and distribution of bacterial virulence genes is induced by Quorum Sensing. *PLOS Pathogens*, 11(2):e1004653.

Sasaki, A. and Iwasa, Y. (1991). Optimal growth schedule of pathogens within a host: Switching between lytic and latent cycles. *Theoretical Population Biology*, 39(2):201–239.

Savill, N. J., Rohani, P., and Hogeweg, P. (1997). Self-reinforcing spatial patterns enslave evolution in a host-parasitoid system. *Journal of Theoretical Biology*, 188(1):11–20.

Schlub, T. E., Smyth, R. P., Grimm, A. J., Mak, J., and Davenport, M. P. (2010). Accurately measuring recombination between closely related HIV-1 genomes. *PLoS Computational Biology*, 6(4):e1000766.

Schluter, J., Schoech, A. P., Foster, K. R., and Mitri, S. (2016). The evolution of Quorum Sensing as a mechanism to infer kinship. *PLoS Computational Biology*, 12(4):e1004848.

Scott, J. R., West, B. W., and Laping, J. L. (1978). Superinfection immunity and prophage repression in phage P1 IV. The c1 repressor bypass function and the role of c4 repressor in immunity. *Virology*, 85(2):587–600.

Sedaghat, A. R., Rastegar, D. A., O'Connell, K. A., Dinoso, J. B., Wilke, C. O., and Blankson, J. N. (2009). T cell dynamics and the response to HAART in a cohort of HIV-1-infected elite suppressors. *Clinical Infectious Diseases*, 49(11):1763–1766.

Shao, Y. and Wang, I.-N. (2008). Bacteriophage adsorption rate and optimal lysis time. *Genetics*, 180(1):471–482.

Shirreff, G., Pellis, L., Laeyendecker, O., and Fraser, C. (2011). Transmission selects for HIV-1 strains of intermediate virulence: A modelling approach. *PLoS Computational Biology*, 7(10).

Siliciano, J. D., Kajdas, J., Finzi, D., Quinn, T. C., Chadwick, K., Margolick, J. B., Kovacs, C., Gange, S. J., and Siliciano, R. F. (2003). Long-term follow-up studies confirm the stability of the latent reservoir for HIV-1 in resting CD4+ T cells. *Nature Medicine*, 9(6):727–728.

Siliciano, R. F. and Greene, W. C. (2011). HIV latency. *Cold Spring Harbor Perspectives in Medicine*, 1(1):a007096.

Silpe, J. E. and Bassler, B. L. (2019). A host-produced Quorum-Sensing Autoinducer controls a phage lysis-lysogeny decision. *Cell*, 176(1):268–280.e13.

Sinha, V., Goyal, A., Svenningsen, S. L., Semsey, S., and Krishna, S. (2017). In silico evolution of lysis-lysogeny strategies reproduces observed lysogeny propensities in temperate bacteriophages. *Frontiers in Microbiology*, 8:1386.

Slager, J., Aprianto, R., and Veening, J.-W. (2019). Refining the Pneumococcal competence regulon by RNA sequencing. *Journal of Bacteriology*, 201(13):e00780–18.

Stacy, A., McNally, L., Darch, S. E., Brown, S. P., and Whiteley, M. (2016). The biogeography of polymicrobial infection. *Nature Reviews Microbiology*, 14(2):93–105.

Stewart, F. M. and Levin, B. R. (1984). The population biology of bacterial viruses: why be temperate. *Theoretical Population Biology*, 26(1):93–117.

Stokar-Avihail, A., Tal, N., Erez, Z., Lopatina, A., and Sorek, R. (2019). Widespread utilization of peptide communication in phages infecting soil and pathogenic bacteria. *Cell Host & Microbe*, 25(5):746–755.e5.

Susskind, M. M., Botstein, D., and Wright, A. (1974). Superinfection exclusion by P22 prophage in lysogens of Salmonella typhimurium: III. Failure of superinfecting phage DNA to enter sieA+ lysogens. *Virology*, 62(2):350–366.

Szolnoki, A., Mobilia, M., Jiang, L.-L., Szczesny, B., Rucklidge, A. M., and Perc, M. (2014). Cyclic dominance in evolutionary games: a review. *Journal of The Royal Society Interface*, 11(100):20140735.

Tait, K. and Sutherland, I. W. (2002). Antagonistic interactions amongst bacteriocin-producing enteric bacteria in dual species biofilms. *Journal of Applied Microbiology*, 93(2):345–352.

Tekwa, E. W., Gonzalez, A., and Loreau, M. (2015). Local densities connect spatial ecology to game, multilevel selection and inclusive fitness theories of cooperation. *Journal of Theoretical Biology*, 380:414–425.

Thiery, J. M., D'Herbes, J.-M., and Valentin, C. (1995). A model simulating the genesis of banded vegetation patterns in Niger. *Journal of Ecology*, 83(3):497–507.

Thingstad, T. F., Våge, S., Storesund, J. E., Sandaa, R.-A., and Giske, J. (2014). A theoretical analysis of how strain-specific viruses can control microbial species diversity. *Proceedings of the National Academy of Sciences*, 111(21):7813–7818.

Tolker-Nielsen, T. and Molin, S. (2000). Spatial organization of microbial biofilm communities. *Microbial Ecology*, 40(2):75–84.

Touchon, M., Bernheim, A., and Rocha, E. P. (2016). Genetic and life-history traits associated with the distribution of prophages in bacteria. *The ISME journal*, 10(11):2744–2754.

Troyer, R. M., Collins, K. R., Abraha, A., Fraundorf, E., Moore, D. M., Krizan, R. W., Toossi, Z., Colebunders, R. L., Jensen, M. A., Mullins, J. I., Vanham, G., and Arts, E. J. (2005). Changes in human immunodeficiency virus type 1 fitness and genetic diversity during disease progression. *Journal of Virology*, 79(14):9006–9018.

Tully, D. C., Ogilvie, C. B., Batorsky, R. E., Bean, D. J., Power, K. A., Ghebremichael, M., Bedard, H. E., Gladden, A. D., Seese, A. M., Amero, M. A., Lane, K., McGrath, G., Bazner, S. B., Tinsley, J., Lennon, N. J., Henn, M. R., Brumme, Z. L., Norris, P. J., Rosenberg, E. S., Mayer, K. H., Jessen, H., Kosakovsky Pond, S. L., Walker, B. D., Altfeld, M., Carlson, J. M., and Allen, T. M. (2016). Differences in the selection bottleneck between modes of sexual transmission influence the genetic composition of the HIV-1 founder virus. *PLoS Pathogens*, 12(5):e1005619.

Uppal, G. and Vural, D. C. (2020). Evolution of specialized microbial cooperation in dynamic fluids. *Journal of Evolutionary Biology*, 33(3):256–269.

van Baalen, M. and Sabelis, M. W. (1995). The milker-killer dilemma in spatially structured predator-prey interactions. *Oikos*, 74(3):391–400.

van Ballegooijen, W. M. v. and Boerlijst, M. C. (2004). Emergent trade-offs and selection for outbreak frequency in spatial epidemics. *Proceedings of the National Academy of Sciences*, 101(52):18246–18250.

van der Heijden, M. G. A., Bardgett, R. D., and van Straalen, N. M. (2008). The unseen majority: soil microbes as drivers of plant diversity and productivity in terrestrial ecosystems. *Ecology Letters*, 11:296–310.

van Dijk, B., Meijer, J., Cuypers, T. D., and Hogeweg, P. (2019). Trusting the hand that feeds: microbes evolve to anticipate a serial transfer protocol as individuals or collectives. *BMC Evolutionary Biology*, 19(1):201.

van Dorp, C. H., van Boven, M., and de Boer, R. J. (2014). Immuno-epidemiological modeling of HIV-1 predicts high heritability of the set-point virus load, while selection for CTL escape dominates virulence evolution. *PLoS Computational Biology*, 10(12).

van Dorp, C. H., van Boven, M., and de Boer, R. J. (2020). Modeling the immunological pre-adaptation of HIV-1. *bioRxiv*, page 2020.01.08.897983.

Velicer, G. J. and Yu, Y.-t. N. (2003). Evolution of novel cooperative swarming in the bacterium Myxococcus xanthus. *Nature*, 425(6953):75–78.

von Bronk, B., Götz, A., and Opitz, M. (2019). Locality of interactions in three-strain bacterial competition in E. coli. *Physical Biology*, 16(1):016002.

Vrancken, B., Rambaut, A., Suchard, M. A., Drummond, A., Baele, G., Derdelinckx, I., van Wijngaerden, E., Vandamme, A. ., van Laethem, K., and Lemey, P. (2014). The genealogical population dynamics of HIV-1 in a large transmission chain: bridging within- and among-host evolutionary rates. *PLoS Computational Biology*, 10(4):e1003505.

Wade, M. J. (1985). Soft selection, hard selection, kin selection, and group selection. *The American Naturalist*, 125(1):61–73.

Wagner, T. A., McLaughlin, S., Garg, K., Cheung, C. Y. K., Larsen, B. B., Styrchak, S., Huang, H. C., Edlefsen, P. T., Mullins, J. I., and Frenkel, L. M. (2014). HIV latency. Proliferation of cells with HIV integrated into cancer genes contributes to persistent infection. *Science*, 345(6196):570–573.

Wahl, L. M., Betti, M. I., Dick, D. W., Pattenden, T., and Puccini, A. J. (2019). Evolutionary stability of the lysis-lysogeny decision: Why be virulent? *Evolution*, 73(1):92–98.

Wakano, J. Y., Nowak, M. A., and Hauert, C. (2009). Spatial dynamics of ecological public goods. *Proceedings of the National Academy of Sciences*, 106(19):7910–7914.

Wang, I.-N. (2006). Lysis timing and bacteriophage fitness. *Genetics*, 172(1):17–26.

Ward, Z. and White, J. (2012). Impact of latently infected cells on strain archiving within HIV hosts. *Bulletin of Mathematical Biology*, 74(9):1985–2003.

Weber, M., Poxleitner, G., Hebisch, E., Frey, E., and Opitz, M. (2014). Chemical warfare and survival strategies in bacterial range expansions. *Journal of the Royal Society Interface*, 11(96):20140172.

West, S. A., Griffin, A. S., Gardner, A., and Diggle, S. P. (2006). Social evolution theory for microorganisms. *Nature Reviews Microbiology*, 4(8):597–607.

Westhoff, S., Otto, S. B., Swinkels, A., Bode, B., van Wezel, G. P., and Rozen, D. E. (2020). Spatial structure increases the benefits of antibiotic production in Streptomyces. *Evolution*, 74(1):179–187.

Whiteley, M., Diggle, S. P., and Greenberg, E. P. (2017). Progress in and promise of bacterial quorum sensing research. *Nature*, 551(7680):313–320.

Whitney, J. B., Hill, A. L., Sanisetty, S., Penaloza-MacMaster, P., Liu, J., Shetty, M., Parenteau, L., Cabral, C., Shields, J., Blackmore, S., Smith, J. Y., Brinkman, A. L., Peter, L. E., Mathew, S. I., Smith, K. M., Borducchi, E. N., Rosenbloom, D. I. S., Lewis, M. G., Hattersley, J., Li, B., Hesselgesser, J., Geleziunas, R., Robb, M. L., Kim, J. H., Michael, N. L., and Barouch, D. H. (2014). Rapid seeding of the viral reservoir prior to SIV viraemia in rhesus monkeys. *Nature*, 512(7512):74–77.

Wild, G., Gardner, A., and West, S. A. (2009). Adaptation and the evolution of parasite virulence in a connected world. *Nature*, 459(7249):983–986.

Wilson, D. S. (1975). A theory of group selection. *Proceedings of the National Academy of Sciences*, 72(1):143–146.

Xavier, J. B. and Foster, K. R. (2007). Cooperation and conflict in microbial biofilms. *Proceedings of the National Academy of Sciences*, 104(3):876–881.

Xavier, J. B., Kim, W., and Foster, K. R. (2011). A molecular mechanism that stabilizes cooperative secretions in Pseudomonas aeruginosa. *Molecular Microbiology*, 79(1):166–179.

Yanni, D., Márquez-Zacarías, P., Yunker, P. J., and Ratcliff, W. C. (2019). Drivers of spatial structure in social microbial communities. *Current Biology*, 29(11):R545–R550.

Zanini, F., Brodin, J., Thebo, L., Lanz, C., Bratt, G., Albert, J., and Neher, R. A. (2015). Population genomics of intrapatient HIV-1 evolution. *eLife*, 4:e11282.

Zinder, N. D. (1958). Lysogenization and superinfection immunity in Salmonella. *Virology*, 5(2):291–326.

Zong, C., So, L.-h., Sepúlveda, L. A., Skinner, S. O., and Golding, I. (2010). Lysogen stability is determined by the frequency of activity bursts from the fate-determining gene. *Molecular Systems Biology*, 6(1):440.

Samenvatting

Overal ter wereld leven microben: levensvormen die te klein zijn om met het blote oog te zien, zoals bacteriën en virussen. Microben zijn een onmisbaar onderdeel van ecosystemen. Zo breken zij bijvoorbeeld organisch materiaal af, waardoor biologische bouwstoffen weer beschikbaar komen voor andere organismen. Ook het menselijk leven wordt sterk beïnvloed door microben. De meeste infectieziekten worden veroorzaakt door bacteriën en virussen. Maar aan de andere kant worden bepaalde voedingsmiddelen, zoals yoghurt, geproduceerd met behulp van bacterieculturen, en helpen de microben in onze darmen bij het verteren van voedsel.

Onder de juiste omstandigheden planten veel microben zich meerdere keren per dag voort, en soms zelfs een paar keer per uur. Hun generatietijd is dus erg kort. Daarnaast bestaan microbiële populaties doorgaans uit erg grote aantallen organismen. In zo'n grote populatie ontstaat gemakkelijk genetische diversiteit door mutaties. Door overerving en natuurlijke selectie zullen vervolgens microben met de gunstigste eigenschappen de populatie gaan domineren. Vanwege de korte generatietijd van microben gaat deze evolutionaire aanpassing doorgaans erg snel. Dit maakt populaties van microben tot goede modelsystemen voor het bestuderen van evolutie, en evolutionaire experimenten in laboratoria hebben op dit vlak al tot veel nieuwe inzichten geleid. Het maakt echter ook duidelijk dat evolutie een cruciaal onderdeel is van de dynamica van populaties van microben. We kunnen pas echt begrijpen hoe een ziekteverwekker zich op lange termijn in een populatie van gastheren gedraagt, of hoe de interacties in een gemeenschap van bacteriën ontstaan en blijven bestaan, als we de evolutie van deze microben bestuderen.

Evolutie door middel van natuurlijke selectie zorgt ervoor dat een populatie van organismen zich aanpast aan de omgeving. Deze omgeving is echter vaak veranderlijk in de tijd en in de ruimte. Meerdere tijd- en ruimte-schalen kunnen dan een rol spelen in het evolutionaire aanpassingsproces. Neem bijvoorbeeld een virus dat een infectieziekte veroorzaakt. Wanneer dit virus een gastheer (bijvoorbeeld een mens) infecteert, zal het zich snel aanpassen aan zijn huidige omgeving: het lichaam van deze specifieke gastheer. Op korte termijn worden dus virusdeeltjes geselecteerd die zich het beste kunnen vermeerderen in de huidige gastheer. Echter, om op lange termijn succesvol te zijn zal het virus ook van gastheer op gastheer overgedragen moeten worden, zodat het zich kan verspreiden in de gastheerpopulatie. Er vindt dus op twee verschillende niveaus natuurlijke selectie plaats: op het binnen-gastheer en het tussen-gastheer-niveau. Deze niveaus komen overeen

met verschillende tijdschalen: aanpassingen op het binnen-gastheer-niveau vinden plaats op korte tijdschalen, aanpassingen op het tussen-gastheer-niveau op langere tijdschalen. De selectie op de twee niveaus kan verschillende aanpassingen van het virus vragen: een virusvariant die zo is aangepast dat hij zich snel vermenigvuldigt binnen het lichaam van een gastheer is niet noodzakelijkerwijs ook goed toegerust om zich te verspreiden van gastheer op gastheer. De uiteindelijke resultaten van het evolutieproces, en dus de eigenschappen van het virus, worden bepaald door de combinatie van selectiedrukken op de verschillende niveaus.

Het belang van verschillende tijd- en ruimteschalen voor evolutie komt ook naar voren in de structuur van populaties van microben. De afgelopen decennia is steeds duidelijker geworden dat de meeste microben niet afgezonderd leven, maar als onderdeel van complexe microbiële gemeenschappen. In deze gemeenschappen concurreren de microben om voedingsstoffen, maar wordt er ook samengewerkt. Zo produceren sommige microben signaalstoffen waarmee zij hun aanwezigheid communiceren aan anderen. Ook worden er zogeheten *public goods* geproduceerd: stoffen die niet alleen een voordeel opleveren voor degene die de stof produceert, maar voor alle microben in de buurt. Een voorbeeld hiervan zijn enzymen die voedingsstoffen vrij maken uit de omgeving, zodat die vervolgens opgenomen en verteerd kunnen worden. Hier tegenover staat dat veel microben ook gifstoffen produceren, waarmee zij naburige concurrenten aanvallen. Al deze interacties vinden plaats binnen een bepaalde, vaak beperkte, afstand. Uit de lokale interacties tussen microben komt een ruimtelijke structuur voort waarin bepaalde microben op bepaalde locaties goed kunnen gedijen, terwijl op andere locaties andere microben het beter doen. Deze ruimtelijke structuur, die afhangt van de ruimtelijke schalen waarop de onderliggende interacties plaatsvinden, bepaalt hoe de omgeving van microben eruitziet, en beïnvloedt zo hun evolutie.

De titel van dit proefschrift, “Evolutie van microben op verschillende schalen”, heeft een dubbele betekenis. Ten eerste beschrijft dit proefschrift meerdere studies waarin wordt gekeken hoe de evolutie van microben afhangt van processen op verschillende tijd- en ruimteschalen. Hiervoor worden wiskundige modellen en digitale simulatiemodellen gebruikt. We bekijken verschillende voorbeelden, zoals het effect van ruimtelijke structuur op de interacties tussen microben en het effect van selectie op binnen-gastheer- en tussen-gastheer-niveau op de evolutie van ziekteverwekkers. Ten tweede vertegenwoordigen de voorbeelden die we behandelen microben op verschillende “schalen”: we bestuderen de evolutie van een humaan virus (HIV; Hoofdstuk 2), virussen die bacteriën infecteren (Hoofdstuk 3) en bacteriën (Hoofdstuk 4).

Hoofdstuk 2 is een studie naar de evolutie van het humaan immunodeficiëntievirus (HIV), het virus dat de ziekte AIDS veroorzaakt, waarin we ons specifiek richten op de gevolgen van latente celinfectie. Wanneer HIV een cel infecteert, leidt

dit meestal tot een actieve infectie van die cel: het virus vermeerdert zich in de cel en na 1 tot 2 dagen wordt de cel opengebroken zodat de nieuwe virusdeeltjes vrijkomen. Naast deze actieve celinfectie komen er echter ook latent geïnfecteerde cellen voor, waarin het virus zich niet vermenigvuldigt. Deze cellen kunnen maanden en soms zelfs jaren een inactief virus met zich meedragen, totdat het virus gereactiveerd wordt en de cel alsnog actief geïnfecteerd raakt. Deze reservoirs van latent geïnfecteerde cellen zijn de belangrijkste reden waarom HIV-patiënten niet genezen kunnen worden: omdat het virus in de latent geïnfecteerde cellen niet actief is, is het onzichtbaar voor het immuunsysteem en voor medicijnen. De aanwezigheid van de latente reservoirs heeft echter mogelijk ook gevolgen voor de evolutie van het virus: omdat het virus zich niet voortplant in deze cellen, zijn de reservoirs een soort evolutionaire vriezers, waarin oude varianten van het virus bewaard blijven.

In hoofdstuk 2 gebruiken we een wiskundig model om te onderzoeken hoe groot het effect is van de latente reservoirs op de evolutie van HIV. We laten eerst zien dat een latent reservoir de evolutie van het virus binnen een gastheer flink kan vertragen. Hierdoor past het virus zich langzamer aan aan de huidige gastheer en blijft de virusvariant waarmee de gastheer oorspronkelijk geïnfecteerd is geraakt lange tijd aanwezig. Vervolgens bekijken we hoe deze vertraagde binnen-gastheer-evolutie doorspeelt op het tussen-gastheer niveau. Ook zonder behandeling leven mensen met HIV vaak lang voordat zij AIDS ontwikkelen en uiteindelijk sterven (2–20 jaar), en het virus veroorzaakt al die tijd actieve celinfecties die een levenscyclus hebben van 1–2 dagen. Dus zou je verwachten dat het virus zich in die tijd volledig aanpast aan zijn huidige gastheer, zelfs als deze aanpassingen ten koste gaan van het vermogen om van gastheer op gastheer overgedragen te worden. Dit zien we inderdaad gebeuren in het model wanneer we het latente reservoir buiten beschouwing laten; het virus blijkt zich dan nauwelijks aan te kunnen passen op het tussen-gastheer niveau. Maar wanneer we een latent reservoir meenemen in ons model, verandert dit: de vertraging in de binnen-gastheer-evolutie zorgt ervoor dat het virus zich beter aan kan passen op tussen-gastheer niveau, waardoor het virus op de lange termijn succesvoller is. Deze modelvoorspellingen zijn in lijn met observaties uit verschillende epidemiologische datasets, die suggereren dat HIV inderdaad aangepast lijkt om optimaal van mens op mens overgedragen te kunnen worden. Het wiskundige model helpt ons dus om de observaties uit de natuur te begrijpen.

Hoofdstuk 3 gaat ook over virussen, maar met een andere gastheer: bacteriën (deze bacterie-virussen worden *bacteriofagen* of *fagen* genoemd). In dit hoofdstuk onderzoeken we de evolutie van een recent ontdekt communicatiesysteem tussen bacteriofagen (Erez *et al.*, 2017). Deze fagen dragen de code voor een signaalmolecuul in hun genetische materiaal. Wanneer zo'n faag een bacterie infecteert, zet hij de bacterie aan tot de productie van dit signaalmolecuul. Dit signaal beïnvloedt vervolgens het gedrag van andere fagen in latere infecties. Steeds wanneer deze fa-

gen een bacterie infecteren, moeten zij "beslissen" om ofwel een actieve infectie te veroorzaken, waarin nieuwe virusdeeltjes worden geproduceerd en de bacterie wordt opgeblazen om deze vrij te laten (de *lytische* cyclus), of een latente infectie, waarin het virus-DNA bewaard blijft in de bacterie en alleen vermeerderd wordt wanneer de bacterie zich deelt (de *lysogene* cyclus). Deze beslissing wordt genomen op basis van biochemische interacties, en het signaalmolecuul wordt hierin gebruikt als bron van informatie. Als de concentratie van dit signaal laag is, "kiezen" de fagen vaak voor een actieve infectie, maar als de signaalconcentratie hoog is, "kiezen" ze juist vaak voor een latente infectie.

De ontdekking van dit virus-communicatiesysteem roept veel vragen op. Waarom produceren de fagen deze signaalmoleculen? Hoe heeft dit systeem kunnen evolueren? En welke communicatiestrategieën zijn evolutionair gezien het voordeligst? In hoofdstuk 3 beschrijven we een evolutionair wiskundig model waarmee we antwoord kunnen geven op deze vragen. We vergelijken de communicerende fagen met fagen die bij iedere infectie willekeurig kiezen tussen actieve of latente infectie, waarbij de kans op latente infectie wel kan evolueren (en dus geoptimaliseerd kan worden onder de omstandigheden die de fagen ervaren). De communicerende fagen blijken een evolutionair voordeel te hebben omdat zij zich tijdens een virusuitbraak kunnen aanpassen aan de beschikbaarheid van gastheercellen. Vroeg in een uitbraak zijn er veel gastheercellen beschikbaar omdat er nog maar weinig infecties hebben plaatsgevonden (de concentratie van het signaalmolecuul is dan dus laag). Het is dan voordelig om actieve infecties te veroorzaken, omdat de nieuw geproduceerde virusdeeltjes weer andere cellen kunnen infecteren. Later in de uitbraak, als een groot deel van de gastheercellen al geïnfecteerd is geraakt (en de concentratie van het signaalmolecuul hoog is), vervalt dit voordeel. Een latente infectie kan er dan juist voor zorgen dat de faag voor langere tijd bewaard blijft in de latent geïnfecteerde bacterie. Alhoewel deze uitleg hoe de communicatie tussen virussen kan evolueren al eerder was geopperd, is ons model het eerste dat deze verklaring in theorie heeft bevestigd. Maar nog belangrijker is dat het model inzicht geeft in de omstandigheden waaronder communicatie tussen virussen kan ontstaan (en wanneer dus niet): het communicatiesysteem is alleen evolutionair voordelig als het virus regelmatig grote uitbraken veroorzaakt in nieuwe, nog niet geïnfecteerde gastheerpopulaties. Onder deze omstandigheden voorspelt het model een optimale communicatiestrategie waarbij de virussen vroeg in een uitbraak uitsluitend actieve infecties veroorzaken, en omschakelen naar latente infecties wanneer de helft van de gastheerpopulatie geïnfecteerd is geraakt.

De concentratie van het door de fagen geproduceerde signaalmolecuul geeft informatie over het aantal bacteriën dat recent door een faag geïnfecteerd is, en is daarmee een maat van de "infectiedichtheid". Het gedrag van de fagen wordt vervolgens gereguleerd door deze dichtheidsmaat. Regulatie aan de hand van dichtheid

komt ook veel voor onder bacteriën. Een belangrijk voorbeeld hiervan is de productie van giftige stoffen (toxines) die gericht zijn tegen andere bacteriën. Veel bacteriën produceren deze toxines niet continu, maar alleen als er veel andere bacteriën in de buurt zijn (oftewel: als de lokale dichtheid van bacteriën hoog is). In **hoofdstuk 4** wordt een computersimulatiemodel beschreven dat wij ontwikkeld hebben om de evolutie van dit soort dichtheidsgereguleerde toxineproductie te bestuderen. In dit model wordt een groot aantal bacteriën gesimuleerd, die kunnen verschillen in een aantal "genetische" eigenschappen: of ze toxines produceren of niet, of ze resistent zijn tegen de toxines of niet, en of ze veranderingen in de lokale bacterie-dichtheid gebruiken om hun toxineproductie en -resistentie te reguleren. Het fenotype van de bacteriën – of ze toxine produceren of niet, en of ze resistent zijn of niet – hangt af van deze "genen" én de lokale bacterie-dichtheid. Op basis van dit fenotype, en de fenotypes van naburige bacteriën waarmee zij in competitie zijn, heeft elke bacterie in het model een bepaalde kans om zich voort te planten en om dood te gaan. Aan de hand van deze kansen simuleren we de populatiedynamica van honderden tot duizenden generaties bacteriën, en kijken vervolgens welke bacterie-eigenschappen succesvol zijn en welke niet. Zo kunnen we een evolutionair proces digitaal simuleren. In dit simulatiemodel wordt expliciet rekening gehouden met de ruimtelijke structuur van bacteriepopulaties: bacteriën in het model bevinden zich in een 2D ruimte en hebben alleen interacties met bacteriën in hun directe omgeving. Deze lokale interacties zorgen ervoor dat er ruimtelijke patronen kunnen ontstaan, waarin de omgeving van een bacterie (en dus de selectiedrukken op de eigenschappen van de bacterie) sterk afhangt van waar hij zich in het patroon bevindt.

In het model stellen we de bacteriepopulaties bloot aan twee verschillende omstandigheden: (1) een constante habitat, waarin de enige schommelingen in lokale dichtheid voortkomen uit de interacties tussen bacteriën (bijvoorbeeld doordat bacteriën worden gedood door de toxines van een ander), en (2) een regelmatig veranderende (fluctuerende) habitat, waarin regelmatig een klein deel van de populatie wordt geselecteerd en wordt overgebracht naar een nieuwe omgeving die vervolgens door de bacteriën wordt gekoloniseerd. Deze laatste situatie lijkt bijvoorbeeld op een ziekteverwekker die voortdurend wordt overgedragen op nieuwe gastheren. De simulaties laten zien dat dichtheidsafhankelijke toxineproductie kan ontstaan in beide habitats maar vaker voorkomt in de fluctuerende habitat (waarin de dichtheid veel sterker varieert over tijd en ruimte dan in de constante habitat). Bacteriën die in de fluctuerende habitat zijn geëvolueerd vormen kolonies met een heel specifieke ruimtelijke structuur (zoals te zien in Figuren 4.5c en 4.6a): aan de randen van de kolonie produceren deze bacteriën geen toxines, terwijl zij dat in het midden van de kolonie wel doen. Deze structuren zijn ontstaan omdat de bacteriekolonies bloot worden gesteld aan twee verschillende selectiedrukken. Aan de ene kant moeten de bacteriën regelmatig een nieuwe omgeving koloniseren, en dat gaat het snelst wanneer er niet in de productie van toxines hoeft te worden geïnvesteerd. Aan de

andere kant kan het produceren van toxines heel voordelig zijn wanneer de bacteriekolonie in contact komt met een andere kolonie, die mogelijk gevoelig is voor het toxine. Door de productie van toxines te reguleren op basis van de lokale dichtheid, kan een bacteriekolonie én snel groeien (omdat aan de randen, waar de lokale dichtheid laag is, geen toxines worden geproduceerd), én competitief zijn in het contact met anderen (omdat er bij hoge dichtheid wel toxines worden geproduceerd). Het simulatiemodel voorspelt dus dat bacteriën geselecteerd worden op een specifieke kolonie-structuur. De volgende stap is om te onderzoeken of bacteriekoloniën in de natuur ook daadwerkelijk zulke structuren vormen.

In hoofdstuk 4 hebben we gezien dat ruimtelijke structuur bepalend kan zijn voor evolutionaire processen. In **hoofdstuk 5** stellen we de algemene vraag of, en zo ja hoe, we het effect van verschillende ruimtelijke schalen op evolutie wiskundig kunnen definiëren. We richten ons hierbij op populaties met lokale interacties waaruit ruimtelijke patronen kunnen ontstaan (zoals de bacteriepopulaties van hoofdstuk 4), en ontwikkelen nieuwe wiskundige theorie om selectie op verschillende ruimteschalen in dit soort populaties te beschrijven. Als uitgangspunt nemen we de *selectie-differentiaal* uit de Price-vergelijking (Price, 1970). De selectie-differentiaal geeft weer welk gedeelte van de verandering in een eigenschap van organismen over een bepaalde tijd kan worden toegeschreven aan (natuurlijke) selectie. We laten zien dat we deze selectie-differentiaal kunnen opdelen in een lokale selectiecomponent, die het effect beschrijft van alle processen die op kleine schaal plaatsvinden, en een interlokale selectiecomponent, die het effect beschrijft van alle processen op grotere schaal. Hierbij kan bijvoorbeeld worden gedacht aan de evolutie van de productie van een *public good*: een product dat een competitief voordeel oplevert voor alle individuen in de buurt. Als we alleen de lokale competitie bekijken, is het voor een individu voordelig om minder *public good* te produceren dan zijn buren. Dit individu hoeft dan immers minder te investeren in de productie van *public good*, terwijl hij wel profiteert van het *public good* dat door zijn buren geproduceerd wordt, en daardoor kan hij zich sneller voortplanten dan zijn buren. Als we op een grotere schaal kijken, zien we echter het tegenovergestelde: individuen die zich in een omgeving bevinden waarin gemiddeld veel *public good* wordt geproduceerd, zijn beter af dan individuen in omgevingen waarin weinig *public good* geproduceerd wordt. Vanwege lokale reproductie zullen individuen die veel *public good* produceren vaker in de buurt zitten van anderen die ook veel *public good* produceren. Op de grotere schaal vinden we dus een voordeel voor individuen die meer *public good* produceren. De lokale en interlokale selectiecomponent vangen deze twee effecten, en laten zien hoe groot hun bijdrage is aan de uiteindelijke selectie op de productie van *public good*. Door de schaal waarop we "lokaal" en "interlokaal" definiëren te variëren, kunnen we vervolgens meten hoe verschillende ruimteschalen bijdragen aan de totale selectie op een eigenschap als *public-good*-productie. Dit stelt ons in staat om de voor natuurlijke selectie relevante ruimtelijke schalen te identificeren.

De studies in dit proefschrift geven nieuwe inzichten in de evolutie van microben, en laten zien hoe processen op verschillende tijd- en ruimteschalen hierin belangrijk zijn. Wiskundige modellen en computermodellen, zoals gebruikt in dit proefschrift, stellen ons in staat om specifieke hypotheses over microbiële evolutie te testen (zoals in hoofdstuk 3), maar kunnen ook worden gebruikt om te verkennen welke structuren kunnen voortkomen uit de interacties tussen microben (zoals in hoofdstuk 4). Door modellen te combineren met lab-experimenten en data uit de natuur, daarbij rekening houdend met de vele tijd- en ruimteschalen die een rol spelen, zullen we de evolutie van microben steeds beter begrijpen.

Curriculum Vitæ

Hilje Doekes was born in Utrecht, the Netherlands, on the 7$^{\text{th}}$ of May 1989. She grew up in Bennekom and received her pre-university secondary education at the Scholengemeenschap Pantarijn in Wageningen. During this time, her interest in biology was raised by the Biology Olympiad (a science competition for high school students) in which she competed at the national and international level, winning the Dutch Biology Olympiad in 2007. In the same year, she started her studies in Biology at Utrecht University, to which she added a second studies in Mathematics in 2008. Hilje obtained both Bachelor's degrees *cum laude* in 2011. She continued her education as a Master student in the Theoretical Biology and Bioinformatics group at Utrecht University. As part of her master's programme she conducted a research project under the supervision of prof. Paulien Hogeweg, modelling the evolution of early eusociality in insects, and an internship in evolutionary epidemiology with dr. Katrina Lythgoe and prof. Christophe Fraser at Imperial College London, which laid the foundation for chapter 2 of this thesis. After obtaining her Master's degree in 2014 (*cum laude*), Hilje stayed in the Theoretical Biology and Bioinformatics group at Utrecht University where in 2015 she started her PhD research under the supervision of dr. Rutger Hermsen and prof. Rob de Boer. The results of her PhD research are described in this thesis.

Currently, Hilje is an assistant professor in the Laboratory of Genetics at Wageningen University.

List of Publications

H.M. Doekes, R. Hermsen. Quantifying natural selection at different scales in spatially structured populations. *In preparation.*

H.M. Doekes, G.A. Mulder, R. Hermsen. Repeated outbreaks drive the evolution of communication between bacteriophages. *Under review.*

B. van Dijk, P. Hogeweg, **H.M. Doekes**, N. Takeuchi (2020). Slightly beneficial genes are retained by bacteria evolving DNA uptake despite selfish elements. *eLife* 9: e56801.

H.M. Doekes, R.J. de Boer, R. Hermsen (2019). Toxin production spontaneously becomes regulated by local cell density in evolving bacterial populations. *PLoS Computational Biology* 15(8): e1007333.

H.M. Doekes, C. Fraser, K.A. Lythgoe (2017). Effect of the latent reservoir on the evolution of HIV at the within- and between-host levels. *PLoS Computational Biology* 35(1): e1005228.

K. Saeki, **H.M. Doekes**, R.J. de Boer (2015). Optimal T cell cross-reactivity and the role of regulatory T cells. *Journal of Theoretical Biology* 375: 4–12.

Acknowledgements

There we are, the final pages of my thesis. While I suspect this might not be the last part of my thesis that you read, it is the last part that I have left to write. Here, I would like to thank the people without whom this thesis would not have existed.

Thirteen years ago, when I had just started my bachelor studies in biology, I wrote an essay about my study choices. In it, I explained why I had decided on biology, rather than mathematics, writing that "although I love mathematical puzzles and problem solving, I do not believe you can turn solving puzzles into your profession. A professional mathematician will more likely be involved with the development of mathematical models, a part of maths that I am less attracted to. Furthermore, I do not like work that requires you to sit behind a computer all the time." How could I have been so wrong about my future? For that, I owe a huge thank you to the amazing collective that is the Theoretical Biology and Bioinformatics group(s) of Utrecht University. When I got introduced to the world of TBB during the first-year course it was immediately clear to me that my previous ideas about modelling were deeply flawed, and after the Theoretical Ecology and Bioinformatic Processes courses I was completely sold. I am very happy to have had TBB as my scientific home for the past decade. Not only did I learn a great deal in this time, I also got to know many wonderful people. First and foremost, I thank all former and current group members for making TBB the inspiring, welcoming, fun, and sometimes pleasantly weird place it is. Additionally, I would like to mention some people individually.

First of all, my PhD advisors Rutger Hermsen and Rob de Boer. Rutger, I learned a lot from your different, more "physicy" look on things, as well as from your knowledge of good writing practices ("The elements of style" still sits on my desk, waiting to be returned to you). I have also highly appreciated your genuine interest in not just my scientific, but also my personal development and well-being. Rob, thank you for helping me get back on track when I was lost in the details, and for your personal support over the years. Whenever I was faced with a difficult (career) decision, I knew your door was open.

Secondly, I would like to thank the founders - not just of the group, but of bioinformatics (in its *original* meaning): Paulien Hogeweg and the late Ben Hesper. Paulien, your course is special because it does not just teach you new things, but new ways to think. Thank you for showing me how fascinating evolution really is,

and for introducing me to the fun of unexpected findings.

Thirdly, system administrator (and so much more) Jan Kees van Amerongen. Jan Kees, no work at TBB could be done without you. Thank you for making our lives so easy.

Then there are some other people I would like to name. “My” master students David and Glenn, thank you for your enthusiasm and hard work. I wish you the best in your careers. Reinder, thank you for being the early test pilot of the scales-of-selection project. Martijn and Laura van Schijndel, I very much enjoyed discussing the “scales of selection”-project with you. Thank you for helping me to further develop - and sometimes debug - my ideas. Berend, Bas, Juliane, Sandro, and Jeroen, thank you for the good conversations, scientific or otherwise.

Lastly, my dear paranymphs Laurens and Bram. Laurens, it is always a joy to see you explain whichever hard mathematical problem you are working on now. Your enthusiasm - for science and for music - is inspiring. Bram, you have been my TBB-buddy for many years. Thank you for your, sometimes blunt, honesty, and for showing your excitement about my work when I had temporarily lost mine.

Once this thesis was completed, it was scrutinised by the thesis assessment committee. Prof. Sylvain Gandon, prof. Joshua Weitz, prof. Lin Chao, prof. Franjo Weissing, and dr. Daniel Rozen, thank you for your time and effort, and the helpful comments.

Chapter 2 of this thesis started as an MSc internship at the Evolutionary Epidemiology group at Imperial College London. I would like to thank dr. Katrina Lythgoe and prof. Christophe Fraser (who are both now at the University of Oxford) for their supervision during my internship, and their continued input when we were finalising this project. I am also grateful to the Department of Infectious Disease Epidemiology at Imperial College for hosting me for six months.

During my PhD I had the opportunity to be part of the PhD council of the Graduate School of Life Sciences (GSLS), and chair this council for over two years. This was a great way of getting to know PhD candidates in very different fields. I also learned a lot about how the GSLS and the university in general is organised, what problems PhD candidates can run into, and what is being done to solve these issues. To all the council members I got to work with: thank you for caring (also about problems that might not be your own), and thanks for all the fun events we organised together! Special thanks to Saskia Ebeling and Kim van den Heuvel for their support of the council.

Als laatste wil ik mijn familie en vrienden bedanken voor hun steun de afgelopen vijf jaar. Susanne, David, Bram, Akke en Francine, dank jullie wel voor de geprekken over wetenschap, de wetenschappelijke wereld, programmeren en juist heel andere

dingen. Ik heb genoten van onze wandelingen, zelfgekookte of zelfafgehaalde etentjes, koppen thee en middernachtelijke bakavonturen. Daarnaast wil ik mijn vrienden van het Utrechts Studenten Koor en Orkest, van Collegium Musicum Traiectum, en mijn andere muzikale vrienden bedanken voor alle mooie momenten die we gedeeld hebben. Muziek maken, en dan vooral samen met anderen, is voor mij één van de beste manieren om te ontspannen. Een andere manier is sporten. Lieve korfbalteamgenootjes van Hebbes (inclusief natuurlijk de oma's) en HKC, dank jullie wel voor de sportiviteit en gezelligheid!

Harmen, mijn grote kleine broer, ik vind het heel leuk dat wij zoveel dingen delen: naast liefde voor korfbal, muziek en natuur nu zelfs onze promotiemaand! Dankjewel voor je vaste vertrouwen in je kleine grote zus, ook nu ik je wiskundige problemen lang niet allemaal meer op kan lossen. Ik heb er zin in om straks regelmatig als collega's te kunnen lunchen. Lieve papa en mama, jullie hebben ons altijd aangespoord om onze eigen interesses te ontwikkelen. Toch kunnen we denk ik wel stellen dat de liefde voor de natuur en de wetenschap Harmen en mij met de paplepel is ingegoten. Als je van iemand kan leren om kritisch te denken, een onmisbare vaardigheid als wetenschapper, dan is dat wel van papa. Dank jullie wel voor jullie liefde en ondersteuning, ik weet dat ik altijd bij jullie terecht kan.

Leo, jij hebt mijn hele PhD-proces van dichtbij meegemaakt. Ik ben blij en dankbaar dat jij er altijd voor mij bent, of ik nu een knuffel nodig heb of een proefkonijn voor mijn Nederlandse samenvatting. Ik kijk uit naar onze volgende avonturen samen!